NEW REACTIONS IN METAL-BASED AND ENZYMATIC CATALYSIS

Adriana Faraone

UNIVERSITAT
ROVIRA i VIRGILI

New Reactions in Metal-based and Enzymatic Catalysis

ADRIANA FARAONE

DOCTORAL THESIS
2022

Adriana Faraone

New Reactions in Metal-based and Enzymatic Catalysis

Doctoral Thesis

Supervised by Prof. Paolo Melchiorre

ICIQ – Institut Català d'Investigació Química

Tarragona

2022

Prof. Paolo Melchiorre, ICREA Research Professor & ICIQ Group Leader

I STATE that the present study, entitled "New Reactions in Metal-based and Enzymatic Catalysis", presented by ADRIANA FARAONE for the award of the degree of Doctor, has been carried out under my supervision at the Institut Català d'Investigació Química (ICIQ).

Tarragona, November the 23rd 2022

Doctoral Thesis Supervisor

Prof. Paolo Melchiorre

UNIVERSITAT ROVIRA I VIRGILI
NEW REACTIONS IN METAL-BASED AND ENZYMATIC CATALYSIS
Adriana Faraone

Acknowledgments

I would like to thank my supervisor Professor Paolo Melchiorre for giving me the opportunity to join his research group, for his support during these wonderful four years and for being a guide for me in this process of self-growth as a scientist and as a person.

I also want to thank all the current and past members of the Melchiorre group for the scientific and personal support and for all the beautiful moments spent together inside and outside the lab. I especially want to thank Eugenio and Giacomo for all the support they gave me during the first two years of my doctoral studies, for all the things they taught me and the funny moments we shared. I also want to thank Daniele, Riccardo and Yann, who I had the luck to work with even if for a short time and for all what I learnt from them. In the last period of my studies, I had the pleasure to join the team of the 'bio-guys' and I had a fantastic time working with Laura, Vasilis, Jan and Gianluca. I especially thank Laura for being such a close friend I can rely on and for standing me even during my worst times complaining and being stressed. I want to thank all the people visiting Tarragona that I shared amazing moments with, especially Pietro for the beautiful friendship we have and for being such a positive influence and very inspirational in my life. I take the chance to thank all the friends in ICIQ for the fantastic social life we have together.

I would like to thank Nuria Planella for all the help and the support she provided me during these four years and for being such a great person, as well as Noelia Flores and Lorena Tomás for the help with the fellowship. Lastly in ICIQ, I would like to thank all the research support units, especially the chromatographic unit, the NMR-staff, the spectroscopic, mass and X-ray units as well as the HTE lab.

I take the chance to thank also all the people that welcomed me during the short stay in Basel, Professor Thomas Ward and all the DrEAMers.

On a more personal point of view, I want to thank my family for all the support, especially my father and my sister, grazie papi per sopportare tutti i giorni le mie

lamentele al telefono e scusa per tutte le volte che ti ho causato ansie e preoccupazioni. I want to thank my friends in Italy, especially Ele and Vale for being always there since so many years. *Grazie!*

List of Publications

- Tseliou, V., **Faraone, A.**, Kqiku, L., Vilím, J., Simionato, G., Melchiorre, P. "Enantioselective Biocascade Catalysis With a Single Multifunctional Enzyme" *Angew. Chem. Int. Ed.* **2022**, *61*, e202212176.

- Crisenza, G. E. M., **Faraone, A.**, Gandolfo, E., Mazzarella, D., Melchiorre, P. "Catalytic asymmetric C-C cross-couplings enabled by photoexcitation" *Nat. Chem.* **2021**, *13*, 575-580.

A mio padre

Table of Contents

Chapter I

General Overview

1.1 Introduction

The main objective of this research thesis is to disclose novel reactivities to upgrade traditional strategies in enantioselective catalysis. Therefore, the definition of *catalysis* is here reminded. The term *catalysis* was proposed by Jöns Jakob Berzelius in 1835 and stems from the Greek words κατα (*kata*), meaning 'down' and λυειν (*lyein*), meaning 'loosen'.[1] By introducing this word, Berzelius suggested that catalysts have *"the property of exerting on other bodies an action which is very different from chemical affinity. By means of this action, they produce decomposition in bodies, and form new compounds into the composition of which they do not enter"*. Nowadays, we know that a catalyst is a compound that accelerates a process by lowering the energy barrier without affecting the thermodynamic driving force, i.e. without modifying the standard Gibbs energy change of the reaction.[2] As a consequence of the fact that it does not enter in the composition of the reaction products, it can be used in sub-stoichiometric amount and be recovered after the reaction and ideally recycled.

The increased demand of enantiopure chiral molecules in pharmaceutical and material manufacture led to the development of asymmetric catalysis, where a chiral catalyst is exploited to impart a high control on the three-dimensional arrangement of functionality-dense products.[3] The importance that asymmetric catalytic methodologies acquired for the synthesis of single enantiomer chiral compounds is testified by the assignation of the Nobel Prize in Chemistry in 2001 to K. Barry Sharpless, Ryoji Noyori and William S. Knowles for the development of "chirally catalysed hydrogenation and oxidation reactions".[4] On the same line, in 2018 F. Arnold was awarded the Nobel Prize in Chemistry for the "first directed evolution of enzymes, which are proteins that catalyze chemical reactions" and that allowed to expand the diversity of biocatalytic asymmetric processes that served to synthesize novel enantioenriched chiral molecules.[5]

---

[1] Wisniak, J. "The History of Catalysis. From the Beginning to Nobel Prizes" *Educ. Quím.* **2010**, *21*, 60-69.
[2] a) Anslyn, E. V., Dougherty, D. A. "Catalysis" Chapter 9, p. 489 in Modern Physical Organic Chemistry, 2006 University Science Books; b) Laider, K. J. "A Glossary of Terms Used in Chemical Kinetics, Including Reaction Dynamics (IUPAC Recommendations 1996)" *Pure and App. Chem.* **1996**, *68*, 149-192.
[3] Noyori, R. "Introduction" Chapter 1, p. 1 in "Asymmetric Catalysis in Organic Synthesis", 1994 Wiley.
[4] The Nobel Prize in Chemistry 2001. NobelPrize.org:
'https://www.nobelprize.org/prizes/chemistry/2001/summary'.
[5] The Nobel Prize in Chemistry 2018. NobelPrize.org:
'https://www.nobelprize.org/prizes/chemistry/2018/summary'.

By that time, the common understanding of asymmetric catalysis was the one recalled in the late 1990's by Sorensen and Nicolaou in their book '*Classics in Total Synthesis*', where they claimed that *"In a catalytic asymmetric reaction, a small amount of an enantiomerically pure catalyst, either an enzyme or a synthetic, soluble transition metal complex, is used to produce large quantities of an optically active compound from a precursor that may be chiral or achiral"*.[6] From this definition, transition metal catalysis and biocatalysis would have to be considered as the two pillars of asymmetric catalysis. And this concept also stemmed from the 1990's essay on the future of organic synthesis by Dieter Seebach, where he wrote that *"new synthetic methods are most likely to be encountered in the fields of biological and organometallic chemistry"*.[7] This view was significantly altered with the advent of organocatalysis.[8] In fact, this field was rapidly recognized as the third pillar of enantioselective catalysis[9] after the seminal reports from the early 2000's by MacMillan and List,[10] who were awarded the 2021 Nobel Prize in Chemistry for the "development of asymmetric organocatalysis".[11]

Over the last 60 years, the advances in enantioselective catalysis have led to the identification of a few privileged structures of synthetic chiral catalysts exerting generic catalytic modes of substrate activation and stereochemical induction.[12] These privileged scaffolds have the ability to induce the enantioselectivity for a broad class of substrates, a generality of scope which is uncommon in enzymatic catalysis. Selected examples are illustrated in Figure 1.1. As a common feature, these privileged structures are usually bio-inspired and bear some elements that impart rigidity, such as constrained rings, or symmetry, such as two-fold symmetry axes that create the chiral environment for the stereoinduction.

---

[6] Nicolaou, K. C., Sorensen, E. J. "Classics in Total Synthesis: Targets, Strategies, Methods", 1996 Wiley-VCH.

[7] Seebach, D. "Organic Synthesis-Where now?" *Angew. Chem Int. Ed. Engl.* **1990**, *29*, 1320-1367.

[8] MacMillan, D. W. C. "The advent and development of asymmetric organocatalysis" *Nature* **2008**, *455*, 304-308.

[9] List, B. "Introduction: Organocatalysis" *Chem. Rev.* **2007**, *107*, 5413-5415.

[10] (a) List, B., Lerner, R. A., Barbas, III, C. F. "Proline-Catalyzed Direct Asymmetric Aldol Reactions" *J. Am. Chem. Soc.* **2000**, *122*, 2395-2396; (b) Ahrendt, K. A., Borths, C. J., MacMillan, D. W. C. "New Strategies for Organic Catalysis: The First Highly Enantioselective Organocatalytic Diels-Alder Reaction" *J. Am. Chem. Soc.* **2000**, *122*, 4243-4244.

[11] The Nobel Prize in Chemistry 2021. NobelPrize.org:
'https://www.nobelprize.org/prizes/chemistry/2021/summary'.

[12] Yoon, T. P., Jacobsen, E. N. "Privileged chiral catalysts" *Science* **2003**, *299*, 1691-1693.

Examples of privileged chiral catalysts or ligands in asymmetric catalysis
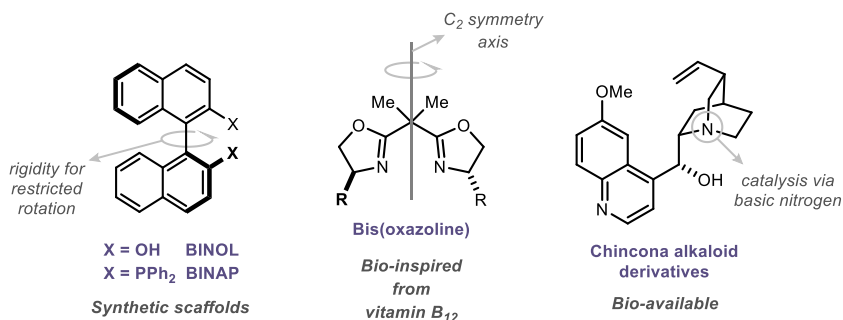
Figure 1.1. Selected examples of privileged chiral scaffolds employed in asymmetric transition metal and organocatalysis.

An intrinsic limitation of such established structures with general applicability in small-molecule enantioselective catalysis is that they allow the design of novel enantioselective processes but they exploit always the same mechanism of substrate activation and stereoinduction, therefore limiting the variety of their chemical potential. On the other hand, biocatalytic strategies usually offer a narrow range of applicability due to the fact that enzymes naturally evolved to catalyze a very specific reaction, accepting and activating selected substrates.[13]

On these premises, a useful strategy in asymmetric catalysis would aim at the upgrade of well-established catalytic functions of traditional chiral structures or natural enzymes by disclosing mechanistically unrelated modes of substrate activation (Figure 1.2). Two potential approaches are envisaged to unlock novel catalytic functions from established chiral catalysts: *i)* the synthetic modification of functionalities present in the structure of the catalyst, for example a chiral ligand on a transition metal complex, a functional group on a small organocatalyst, one or multiple amino acid residues in an enzyme sequence; *ii)* the manipulation of the reaction conditions, that change the environment where the catalyst operates.

---

[13] Drauz, K., Gröger, H., May, O. (Eds.) "Enzyme Catalysis in Organic Synthesis" Wiley-VCH, Weinheim, 2012.
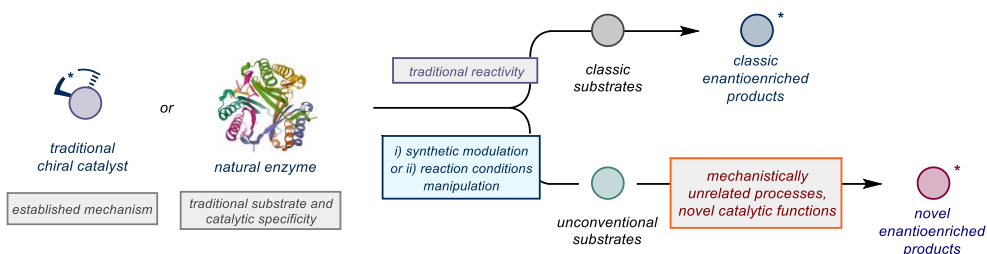
Figure 1.2. Disclosing novel catalytic functions from well-established tools in asymmetric catalysis.

A classic example of approach *i)* was provided in the field of asymmetric organocatalysis by the Cinchona alkaloid scaffolds illustrated in Figure 1.1. Structural conversion of the hydroxy functionality of naturally occurring Cinchona alkaloids into a primary amino group upgraded their catalytic functions as general bases and hydrogen-bonding catalysts[14] into primary amine-based catalysts for the covalent activation of carbonyl compounds *via* enamine and iminium ion intermediates[15] (Figure 1.3).
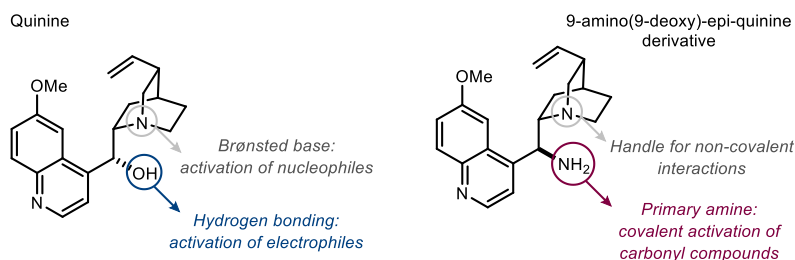
Figure 1.3. Functionality group interconversion turns natural Cinchona alkaloids into primary amine-based catalysts for the covalent activation of carbonyl substrates.

A more recent example of approach *i)* is provided by the technology known as directed evolution[16] of naturally occurring enzymes. Laboratory evolution of enzymes exploits the manipulation of their amino acid sequence (the primary structure) to unlock novel catalytic

---

[14] Wynberg, H. "Asymmetric Catalysis by Alkaloids" *Top. Stereochem.* **1986**, *16*, 87-129.

[15] Melchiorre, P. "Cinchona-based Primary Amine Catalysis in the Asymmetric Functionalization of Carbonyl Compounds" *Angew. Chem. Int. Ed.* **2012**, *51*, 9748-9770.

[16] a) Arnold, F. H. "Innovation by Evolution: Bringing New Chemistry to Life (Nobel Lecture)" *Angew. Chem. Int. Ed.* **2019**, *58*, 14420-14426; b) Bornscheuer, U. T.; Hauer, B., Jaeger, K. E., Schwaneberg, U. "Directed Evolution Empowered Redesign of Natural Proteins for the Sustainable Production of Chemicals and Pharmaceuticals" *Angew. Chem. Int. Ed.* **2019**, *58*, 36-40; c) Wang, Y., Xue, P., Cao, M., Yu, T., Lane, S. T., Zhao, H. "Directed Evolution: Methodologies and Applications" *Chem. Rev.* **2021**, *121*, 12384-12444.

functions or expand their traditional substrate specificity.[17] This technology recently served to prepare synthetically challenging enantioenriched chiral molecules with applications in pharmaceutical manufacture.[18] The laboratory-evolved structural changes in the enzymatic scaffolds can promote mechanistically novel transformations that are often inspired by established methodologies in organic synthesis but are unprecedented in the biological setting.[19] As an example, in 2013 the Arnold group reported engineered variants of cytochrome P450 enzymes with a novel catalytic function. These enzymes traditionally catalyze the monooxygenation of double bonds and C-H bonds into epoxides **3** and alcohols **4**, respectively (Scheme 1.1, left panel). The novel variants could promote the cyclopropanation of olefins **2** in the presence of the diazoester **5** and a reducing agent such as $Na_2S_2O_4$ to selectively deliver highly enantioenriched *cis* or *trans* cyclopropanes **6** or **7** (Scheme 1.1, right panel).[20] An Fe^{IV}-carbene complex, formed inside the active site in the presence of **5**, was proposed as the catalytic intermediate capable of transferring the carbene moiety to the double bond of substrate **2**. This mechanism diverged from the traditional reactivity of cytochrome P450 enzymes, which formed an Fe^{IV}-oxo complex as the crucial catalytic intermediate in the presence of *in situ* generated hydrogen peroxide.
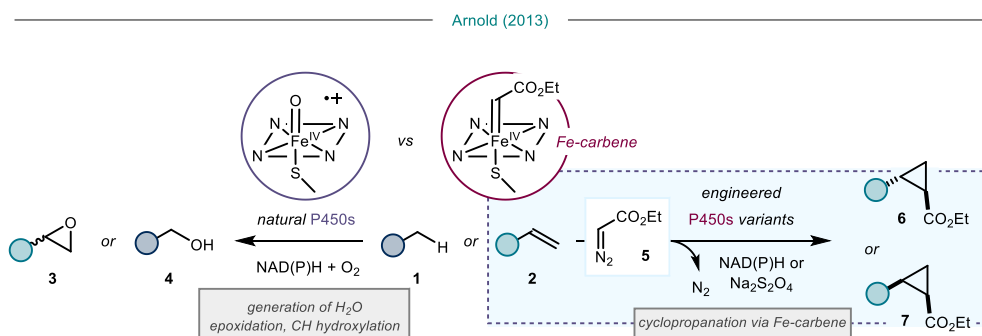
Scheme 1.1. Laboratory modification of the structure of an enzyme upgrades its traditional catalytic function from monooxygenation of double bonds and C-H bonds to stereoselective cyclopropanation of olefins.

[17] Renata, H., Wang, Z. J., Arnold, F. H. "Expanding the Enzyme Universe: Accessing Non Natural Reactions by Mechanism-Guided Directed Evolution" *Angew. Chem. Int. Ed.* **2015**, *54*, 3351-3367.

[18] For a seminal example, see: Savile, C. K., Janey, J. M., Mundorff, E. C., Moore, J. C., Tam, S., Jarvis, W. R., Colbeck, J. C., Krebber, A., Fleitz, F. J., Brands, J., Devine, P. N., Huisman, G. W., Hughes, G. J. "Biocatalytic Asymmetric Synthesis of Chiral Amines from Ketones Applied to Sitagliptin Manufacture" *Science* **2010**, *329*, 305-310. For a review, see: Bornscheuer, U. T., Huisman, G. W., Kazlauskas, R. J., Lutz, S., Moore, J. C., Robins, K. "Engineering the third wave of biocatalysis" *Nature* **2012**, *485*, 185-194.

[19] a) Reetz, M. "Making Enzymes Suitable for Organic Chemistry by Rational Protein Design" *ChemBioChem* **2022**, *23*, DOI: 10.1002/cbic.202200049; b) Brustad, E. M., Arnold, F. H. "Optimizing non-natural protein function with directed evolution" *Curr Opin Chem Biol.* **2011**, *15*, 201-210.

[20] Coelho, P. S., Brustad, E. M., Kannan, A., Arnold, F. H. "Olefin Cyclopropanation via Carbene Transfer Catalyzed by Engineered Cytochrome P450 Enzymes" *Science* **2013**, *339*, 307-310.

The examples discussed above demonstrated that synthetic manipulation of the structure of a chiral catalyst is a valuable strategy to upgrade its traditional reactivity unlocking unconventional catalytic functions towards mechanistically divergent novel stereoselective transformations.

Altering the reaction conditions in which a chiral catalyst with well-established functions traditionally operates can be an alternative strategy to discover novel reactivities (approach *ii)* in Figure 1.2). Recently, visible light irradiation of a reaction mixture emerged as a valuable tool to demonstrate that certain chiral catalytic intermediates with a well-established reactivity in their ground state are able to absorb light and reach a high energy excited state, from which they can access completely novel catalytic functions.[21] This photochemical approach can trigger energetically more demanding reaction pathways inaccessible in the dark, usually based on unconventional radical mechanisms.[22] For example, our group explored the photochemical behavior of a certain class of chiral organocatalytic intermediates with a well-established reactivity in the thermal domain.[23] In 2015, our group reported that light irradiation by a compact fluorescent lamp (CFL) enabled the photoactivation of a chiral enamine intermediate **I** generated *in situ* upon the condensation of butanal **8** with the diphenylprolinol trimethylsilyl ether organocatalyst (*R*)-**A** (Scheme 1.2).[24] Upon reaching the excited state, intermediate **I** became a good reductant and could transfer one electron to an electron-poor substrate such as the bromomalonate **9**, delivering a radical **II**. This event initiated a chain propagation mechanism in which radical **II** could be trapped by the enamine intermediate **I** in the ground state and deliver the open-shell intermediate **III**. A second single electron transfer (SET) reduction of radical precursor **9** or **11** from intermediate **III** generated radical **II** and the iminium ion intermediate **IV**, which upon hydrolysis released product **10** or **12** and the organocatalysts for the next catalytic cycle. These findings demonstrated how light irradiation could disclose a novel reactivity of the chiral enamine intermediate **I** which is characterized by a well-established nucleophilic character in the ground-state but became a strong SET reductant in the excited state. This allowed the implementation of a mechanistically novel radical-based enantioselective α-alkylation of linear aliphatic aldehydes using electrophilic reagents that would not react in the polar domain.

---

[21] Meggers, E. "Asymmetric catalysis activated by visible light" *Chem. Commun* **2015**, *51*, 3290-3301.

[22] See the examples in the presence of light irradiation discussed in the review: Mondal, S., Dumur, F., Gigmes, D., Sibi, M. P., Bertrand, M. P., Nechab, M. "Enantioselective Radical Reactions Using Chiral Catalysts" *Chem. Rev.* **2022**, *122*, 5842-5976.

[23] Silvi, M., Melchiorre, P. "Enhancing the Potential of Enantioselective Organocatalysis with Light", *Nature* **2018**, *554*, 41-49.

[24] Silvi, M., Arceo, E., Jurberg, I. D., Cassani, C., Melchiorre, P. "Enantioselective Organocatalytic Alkylation of Aldehydes and Enals Driven by the Direct Photoexcitation of Enamines" *J. Am. Chem. Soc.* **2015**, *137*, 6120-6123.
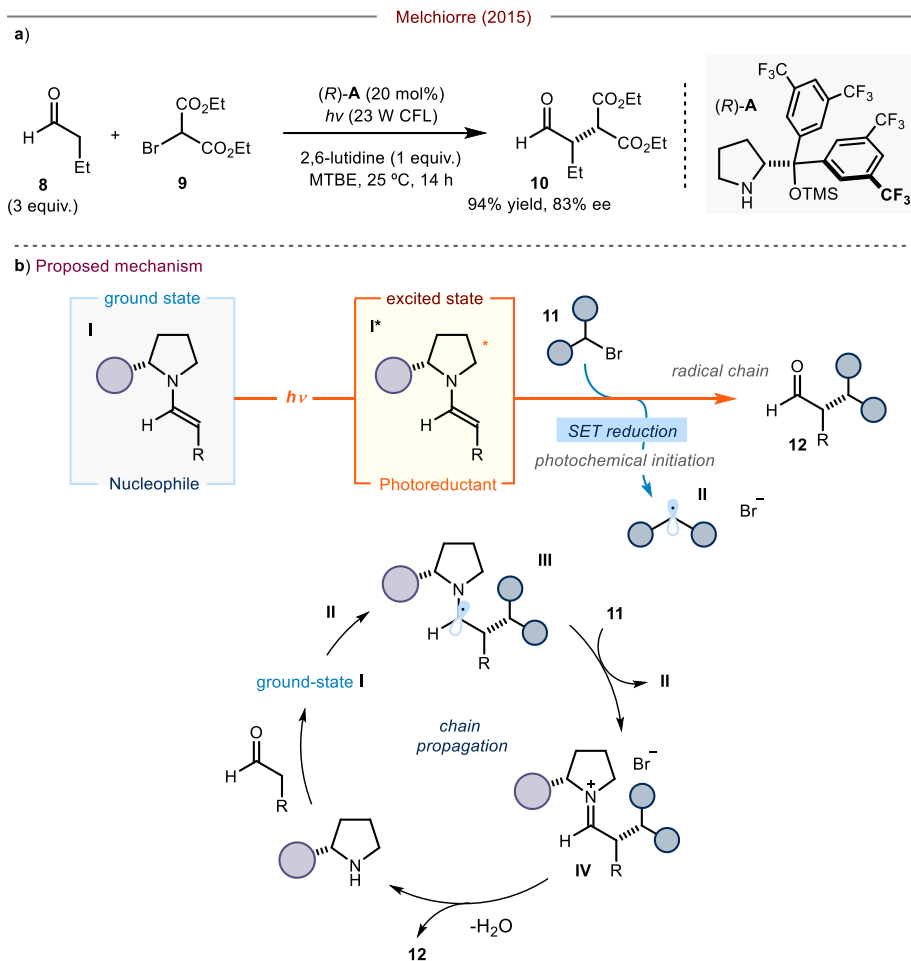
Scheme 1.2. a) Light irradiation turns a chiral enamine intermediate **I**, which is a nucleophile in the ground state, into a photoreductant in the excited state; b) proposed mechanism. CFL = compact fluorescent light; MTBE = methyl tertbutyl ether; TMS = trimethyl silyl; SET = single electron transfer.

In 2017, our group disclosed the photoactivity of another traditional organocatalytic intermediate in polar chemistry: the eneiminium ion of type **V** (Scheme 1.3).[25] Visible light irradiation of the reaction mixture promoted the enantioselective β-alkylation of enals, such as cinnamaldehyde **13**, with benzyl trimethylsilane **14** as the radical precursor in the presence of the aminocatalyst (S)-**B** and an acidic promoter to deliver product **15** in high yield and enantiomeric excess. Upon reaching the excited state, the eneiminium ion intermediate **V** became a strong oxidant and triggered the SET oxidation of the radical precursor **16**

[25] Silvi, M., Verrier, C., Rey, Y. P., Buzzetti, L, Melchiorre, P. "Visible-light Excitation of Iminium Ions Enables the Enantioselective Catalytic β-Alkylation of Enals" *Nat. Chem.*, **2017**, *9*, 868-873.

containing the trimethylsilyl (TMS) group, which acted as a suitable redox auxiliary (RA). Solvent-assisted fragmentation generated the radical **IV** in close proximity to the open-shell intermediate **VI**. A radical recombination delivered the enamine intermediate **VII**, which upon hydrolysis released the chiral product **17** and the aminocatalyst for turnover. This study demonstrated that a traditional organocatalytic intermediate such as the eneiminium ion **V**, which behaved as an electrophile in polar chemistry, could be turned into a photooxidant by visible light activation, thus unlocking new reactivities by altering the reaction conditions. This enabled a mechanistically novel radical-based enantioselective β-alkylation of enals *via* the SET activation of unconventional non-nucleophilic substrates **14**, which would not react in the polar domain.
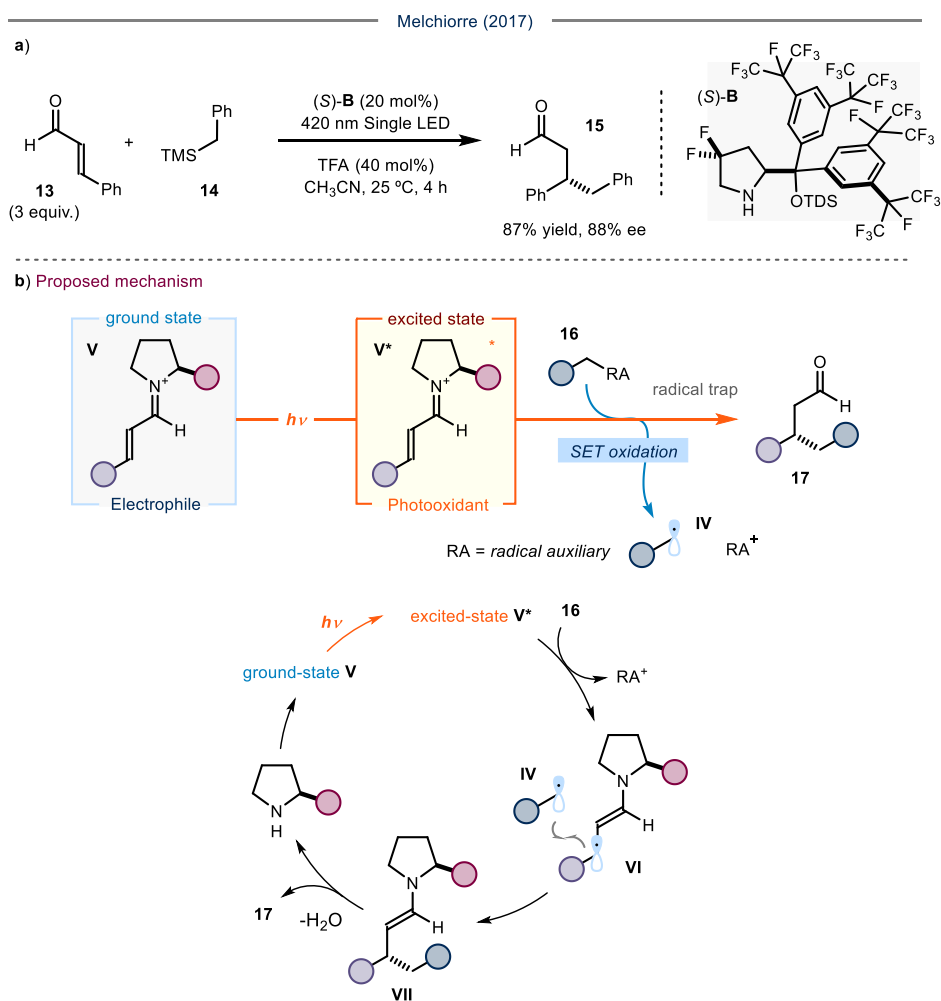
Scheme 1.3. a) Visible Light irradiation turns a chiral iminium ion intermediate **III** known as an electrophilic species in the ground state into a photooxidant in the excited state; b) proposed

mechanism. TMS = trimethyl silyl; LED = light emitting diode; TFA = trifluoroacetic acid; TDS = thexyl dimethyl silyl; SET = single electron transfer.

The photoactivation strategy proved valuable to disclose novel functions of traditional catalysts also in other fields of asymmetric catalysis, for example biocatalysis.[26] In 2016, Hyster reported a novel reactivity of naturally-occurring ketoreductase (KRED) enzymes enabled by visible light irradiation.[27] KREDs are NAD(P)$^+$ (nicotinamide adenine dinucleotide (phosphate)) cofactor-dependent enzymes which in Nature catalyze the enantioselective reduction of ketones *via* a hydride transfer mechanism from the reduced form NAD(P)H of the cofactor (Scheme 1.4a, left panel). They discovered that the reduced NAD(P)H cofactor could generate an electron-donor acceptor (EDA) complex **VIII** with bromolactones of type **20** inside the active site of the enzyme. Upon formation of the EDA complex **VIII** and absorption of the visible light, a charge transfer event promoted the reduction of bromolactone **20** and the generation of the radical couple **IX** after mesolytic cleavage of the bromide anion. A subsequent stereoselective hydrogen atom transfer (HAT) from the radical cation of the cofactor in **IX** to the alkyl radical deriving from **20** delivered the enantioenriched chiral product **21** and the oxidized form of the cofactor NAD(P)$^+$. The regeneration of NAD(P)H in the reaction mixture was operated by a sacrificial reductant or the biocatalytic oxidation of glucose in the presence of the NAD(P)$^+$-dependent enzyme GHD (gluconolactone dehydrogenase). This study demonstrated that a traditional biocatalyst with a well-established reactivity in Nature, such as a ketoreductase, could switch on new catalytic functions and act as a photoreductant and HAT agent upon visible light irradiation, thus promoting a mechanistically novel enantioselective reduction of α-bromolactones. These substrates could be accepted by the enzyme but would not be reduced in the dark.

The examples discussed demonstrated that photoexcitation is a promising direction in the future of asymmetric catalysis, with potential to unlock novel reactivities useful to access synthetically challenging chiral compounds.

[26] Hyster, T. K. "Radical Biocatalysis: Using Non-Natural Single Electron Transfer Mechanisms to Access New Enzymatic Functions" *Synlett* **2020**, *31*, 248-254.
[27] Emmanuel, M. A., Greenberg, N. R., Oblinsky, D. G., Hyster, T. K. "Accessing Non-Natural Reactivity by Irradiating Nicotinamide-Dependent Enzymes with Light" *Nature* **2016**, *540*, 414-417.
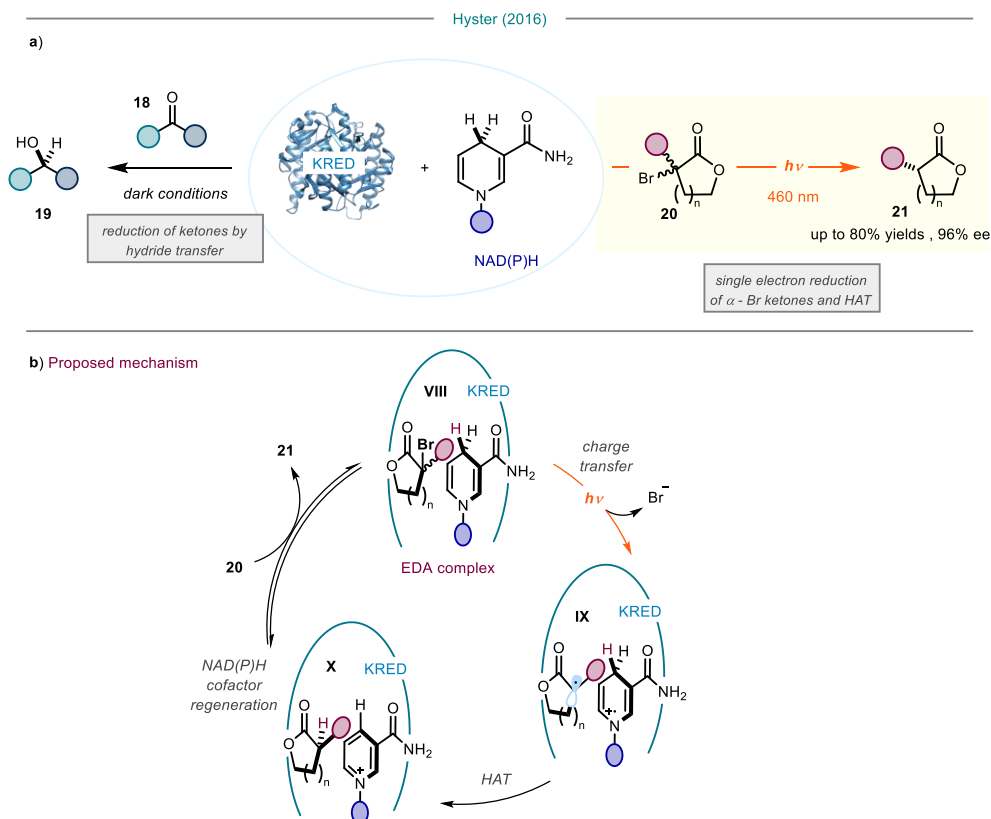
Scheme 1.4. a) Visible light irradiation turns a naturally occurring ketoreductase into a photoenzyme that promotes the single electron reduction of α-bromo ketones; b) proposed mechanism. KRED = ketoreductase; NAD(P)H = nicotinamide adenine dinucleotide (phosphate); HAT = hydrogen atom transfer; EDA = electron donor acceptor complex.

1.2 General Objectives and Summary

The main objective of the present doctoral studies was the development of mechanistically novel stereoselective transformations by employing general catalysts with well-established reactivities in traditional asymmetric catalysis. The aims was to find strategies to unlock novel and unconventional catalytic functions. Specifically, we altered the reaction conditions or the structure of the catalysts to enable mechanistically novel asymmetric processes. In the first project, a chiral iridium-based organometallic complex, with a well-established electrophilic profile in traditional polar chemistry, was exploited as a photooxidant in the excited state to activate via an SET oxidation unconventional non-nucleophilic substrates upon visible light irradiation. The iridium complex showed a dual function, serving as a photoactive SET oxidant and transition metal catalytic intermediate. This approach served to realize a radical-based enantioselective alkyl-alkyl cross-coupling reaction unattainable in the thermal domain.

In the second project, the structural modification of naturally-occurring tautomerase enzymes, which were known to activate aldehydes or enals *via* generation of enamine or eneiminium ion intermediates, respectively, enabled the development of mechanistically novel biocascade reactions where these two activation modes were operated by the same enzyme in a sequential fashion and in a single step. These single-enzyme biocascade processes were inspired by classic organocatalytic cascade reactions reported by Dieter Enders.[28] The biocatalytic methods matched and even surpassed the traditional organocatalytic approaches in terms of efficiency and stereoselectivity.

1.2.1 Catalytic Asymmetric C-C Cross-Couplings Enabled by Photoexcitation

In chapter II, light excitation proved to divert the well-established polar reactivity of the chiral organo-iridium complex **Ir-III**, switching on novel catalytic functions and enabling mechanistically new radical-based enantioselective pathways (Scheme 1.5). The **Ir-III** complex is a classic intermediate in asymmetric catalysis that was traditionally used to promote enantioselective allylic substitution processes, acting as a chiral electrophile.[29] The photoactivation of this chiral (η^3-allyl)iridium(III) complex disclosed its ability to oxidize by SET the 4-alkyl-dihydropyridine (DHP) radical precursors **23**, generating radicals **XI**. The dual function as photooxidant and transition metal complex was exploited to promote an enantioselective alkyl-alkyl radical cross-coupling reaction between allylic alcohols **22** and 4-alkyl-1,4-dihyropyridines **23** affording enantioenriched cross-coupled products **24**. Photophysical, electrochemical and other mechanistic studies provided evidence for the proposed radical pathway.
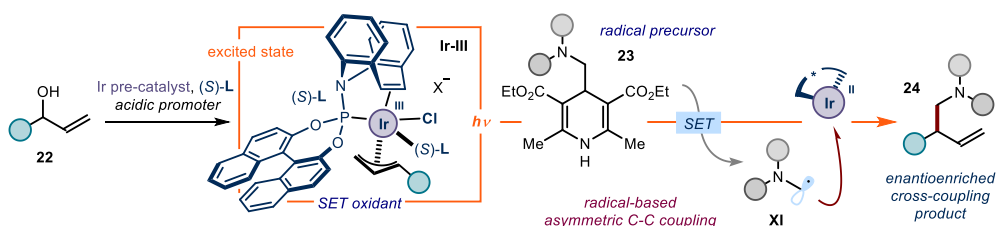
Scheme 1.5. The photoactivity of complex **Ir-III** was exploited to activate non-nucleophilic substrates **22** via SET oxidation and generate open-shell species **XI**, subsequently engaged in asymmetric radical cross-coupling reactions.

[28] a) Enders, D., Hüttl, M. R. M., Grondal, C., Raabe, G. "Control of Four Stereocentres in a Triple Cascade Organocatalytic Reaction" *Nature* **2006**, *441*, 861-863; b) Enders, D., Jeanty, M., Bats, J. W. "Organocatalytic Asymmetric Triple Domino Reactions of Nitromethane with α,β-Unsaturated Aldehydes" *Synlett* **2009**, *19*, 3175-3178.
[29] Rössler, S. L., Petrone, D. A., Carreira, E. M. "Iridium-Catalyzed Asymmetric Synthesis of Functionally Rich Molecules Enabled by (Phosphoramidite, Olefin) Ligands" *Acc. Chem. Res.* **2019**, *52*, 2657-2672.

1.2.2 Enantioselective Biocascade Catalysis Using a Single Multifunctional Enzyme

In chapter III, modification of the structure of 4-oxalocrotonate tautomerase (4-OT) enzymes allowed us to identify two variants that promoted mechanistically novel single-enzyme biocascade reactions. Biocatalytic cascade reactions traditionally rely on the combination of multiple enzymes, each catalyzing a single step of the sequence. Our cascade processes exploited the use of a single multifunctional enzyme capable of catalyzing each of the multiple steps of the transformation imparting high stereocontrol. The identified 4-OT variants could drive the enzymatic versions of the two- and three-component cascade reactions reported by Enders, which are the most sophisticated examples of cascade reactions developed in organocatalysis[28] (Scheme 1.6). The implementation of the more complex Enders triple cascade using a single enzyme required the identification of a 4-OT variant that could master both the enamine activation of aldehydes **25** and the iminium ion activation of enals **26** in a sequential fashion under the same reaction conditions (Scheme 1.6a). The two-component Enders cascade reaction enabled by a single enzyme required the identification of a 4-OT variant capable of driving an iminium ion-iminium ion-enamine activation sequence in the presence of enals **26** and nitromethane **29** (Scheme 1.6b). The cyclohexene carbaldehydes cascade products **28** and **30** were obtained with high yields, diastereomeric ratio and enantiomeric excess, matching the potential of the traditional organocatalytic strategies or, in some cases, even surpassing them in efficiency and stereoselectivity.
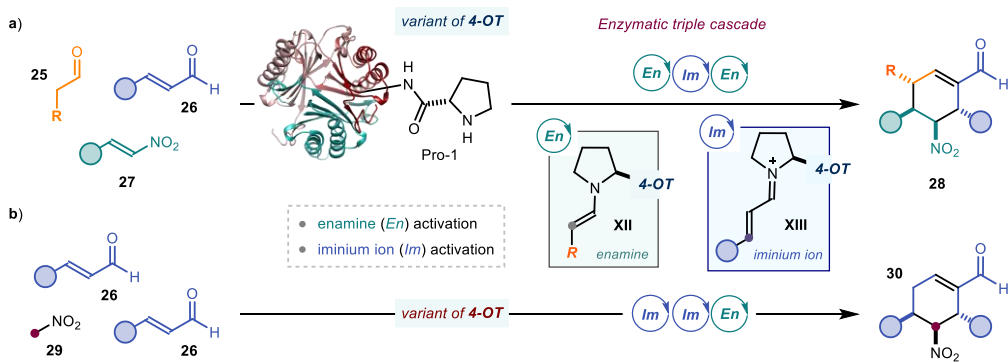
Scheme 1.6. A multifunctional variant of a **4-OT** (4-oxalocrotonate tautomerase) enzyme capable of activating substrates **25** and **26** *via* enamine and iminium ion formation in a sequential fashion was exploited to develop a novel single-enzyme triple biocascade reaction, specifically the enzymatic version of the classic organocatalyzed Enders triple cascade.

Chapter II

Catalytic Asymmetric C-C Cross-Couplings Enabled by Photoexcitation

Target

Developing an enantioselective radical C(sp^3)-C(sp^3) cross-coupling between secondary allylic alcohols and α-amino alkyl

radical precursors driven by the photoexcitation of a chiral iridium-π-allyl complex.
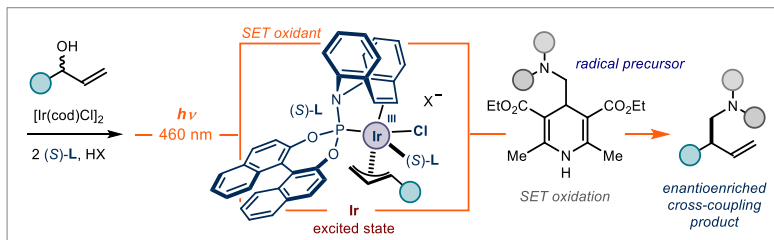
Tools

Exploiting the capacity of a photoexcited allyl-iridium complex to perform single electron transfer oxidation of suitable radical precursors, such as 4-alkyl-1,4-dihydropyridines.[1]

2.1 Introduction

Asymmetric iridium-catalyzed allylic substitutions have emerged since the late 1990's as efficient methods for the synthesis of enantioenriched chiral allylic compounds (Scheme 2.1a).[2] In contrast to traditional palladium-based methods, including the venerable Tsuji-Trost reaction reported in the 1960's,[3] iridium-catalyzed processes display a distinct regioselectivity in favor of the branched (over the linear) regioisomers of the allylic products. A major contribution in the field was reported by Carreira in 2007 (Scheme 2.1b).[4] The design of a

---

[1] The project discussed in this Chapter has been conducted in collaboration with Dr Giacomo E. M. Crisenza, Dr Eugenio Gandolfo, and Dr Daniele Mazzarella. Part of the work has been published in: Crisenza, G. E. M., Faraone, A., Gandolfo, E., Mazzarella, D., Melchiorre, P. "Catalytic Asymmetric C-C cross-couplings Enabled by Photoexcitation" *Nat. Chem.* **2021**, *13*, 575-581.

[2] (a) Dahnz, A., Dubon, P., Schelwies, M., Weihofen, R., Helmchen, G. "Iridium-catalysed asymmetric allylic substitutions" *Chem. Commun.* **2007**, *7*, 675-691; (b) Cheng, Q., Tu, H. F., Zheng, C., Qu, J. P., Helmchen, G. You, S. L. "Iridium-Catalyzed Asymmetric Allylic Substitution Reactions" *Chem. Rev.* **2019**, *119*, 1855-1969.

[3] Tsuji, J. "Palladium-Catalyzed Nucleophilic Substitution Involving Allylpalladium, Propargylpalladium, and Related Derivatives" *Handbook of Organopalladium Chemistry for Organic Synthesis*, John Wiley & Sons, Inc., 2002, pp 1669-1687.

[4] Defieber, C., Ariger, M. A., Moriel, P., Carreira, E. M. "Iridium- Catalyzed Synthesis of Primary Allylic Amines from Allylic Alcohols: Sulfamic Acid as Ammonia Equivalent" *Angew. Chem. Int. Ed.* **2007**, *46*, 3139-3143.

new hybrid chiral phosphoramidite-olefin ligand (*S*)-**L** led to the generation of a highly electrophilic (η^3-allyl)iridium(III) organometallic complex (**Ir-III**), which allowed to expand the scope of the traditional Tsuji-Trost chemistry to a broad panel of carbon-based nucleophiles.[5]
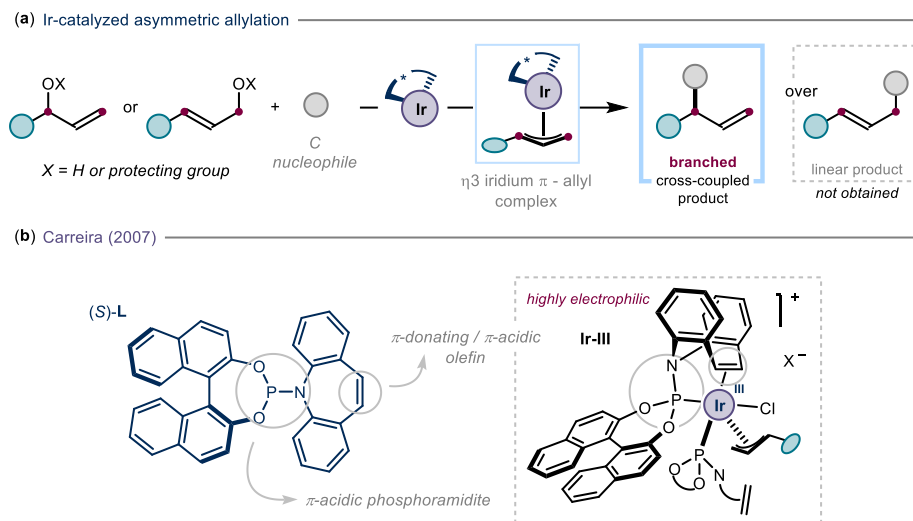
Scheme 2.1. (a) Asymmetric iridium-catalyzed allylic substitutions; (b) novel phosphoramidite-olefin ligand and electrophilic (η3-allyl)iridium(III) complex reported by Carreira in 2007.

Recently, the visible light photoexcitation of chiral catalytic intermediates has proved valuable to expand the potential of traditional catalytic intermediates beyond their established thermal reactivity. This was because light excitation disclosed mechanistically unrelated reactivity patterns in the excited state.[6] This photochemical approach was used to develop new asymmetric catalytic processes based on radical mechanisms.[7] For example, our group has demonstrated that photoexcitation of the colored iminium ion **I**, generated upon condensation of an aromatic α,β-unsaturated aldehyde with a chiral secondary amine catalyst, changes its reactivity completely (Scheme 2.2a). In fact, excitation turns this intermediate, which is electrophilic in the ground-state, into a strong photo-oxidant, which is capable to trigger single electron transfer (SET) events with suitable radical precursors **1** to generate radicals **II**.[8] A

[5] Rössler, S. L., Petrone, D. A., Carreira, E. M. "Iridium-Catalyzed Asymmetric Synthesis of Functionally Rich Molecules Enabled by (Phosphoramidite, Olefin) Ligands" *Acc. Chem. Res.* **2019**, *52*, 2657-2672.
[6] Meggers, E. "Asymmetric catalysis activated by visible light" *Chem. Commun* **2015**, *51*, 3290-3301.
[7] Silvi, M., Melchiorre, P. "Enhancing the Potential of Enantioselective Organocatalysis with Light", *Nature* **2018**, *554*, 41-49.
[8] Silvi, M., Verrier, C., Rey, Y. P., Buzzetti, L, Melchiorre, P. "Visible-light Excitation of Iminium Ions Enables the Enantioselective Catalytic β-Alkylation of Enals" *Nat. Chem.*, **2017**, *9*, 868-873.

subsequent stereocontrolled radical trap delivers enantioenriched β-functionalized aldehydes **2** that are not achievable by ground-state iminium ion catalysis.
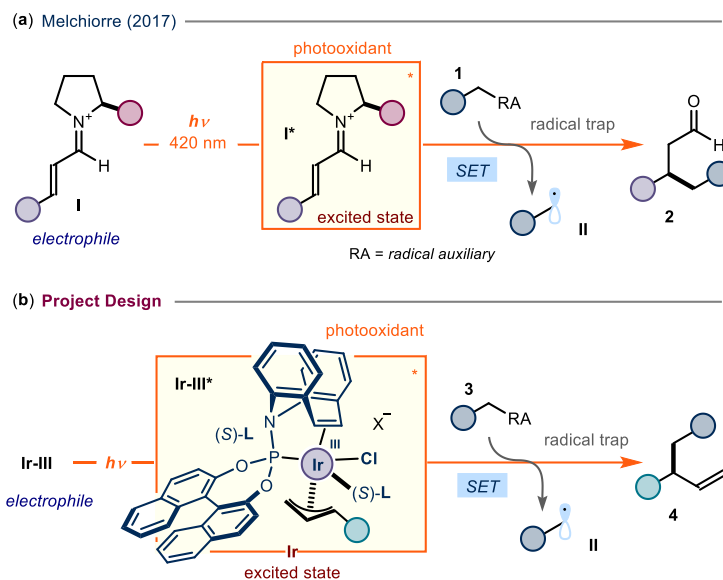
Scheme 2.2. (a) A chiral organocatalytic intermediate that becomes a strong oxidant in its excited state; (b) our project design: a chiral iridium organometallic complex becomes a strong oxidant in the excited state and triggers a SET event to generate an open-shell intermediate for subsequent radical cross-coupling.

We wondered if the strategy of drawing out new reactivity from classical chiral intermediates using photoexcitation could be expanded beyond organocatalysis to include other fields of asymmetric catalysis, such as transition metal catalysis. To date, only few examples of photoexcited chiral organometallic intermediates have been reported.[9] Our studies demonstrated that visible light excitation of a chiral organometallic intermediate, with a well-established reactivity in the ground state, can switch on completely new functions in the excited state. Specifically, we disclosed that the chiral organometallic iridium complex **Ir-III** introduced by Carreira, which has found extensive applications as a chiral electrophile in polar chemistry, could be activated upon visible light irradiation. In analogy to the iminium ion **I** photochemistry, the iridium complex **Ir-III** became a strong oxidant in the excited state and triggered SET oxidation of suitable radical precursors **3** (Scheme 2.2b). This SET event generated radicals that could be trapped by the iridium complex to form chiral allylic products **4**, thus resulting in a mechanistically novel radical C-C cross coupling process.

---

[9] Hossain, A., Bhattacharyya, A., Reiser, O. "Copper's Rapid Ascent in Visible-Light Photoredox Catalysis" *Science* **2019**, *364*, 1-11.

The first part of the chapter will provide an overview of the well-established ground-state electrophilic reactivity of iridium catalysts in enantioselective allylic substitutions. After this first section, the discussion will be focused on the strategy of the photoexcitation applied to organometallic intermediates, followed by our approach to disclose a novel function in the excited state of a chiral iridium organometallic complex.

2.2 Iridium-Catalyzed Asymmetric Allylic Alkylations

This section will provide an overview of the traditional ground-state reactivity of iridium catalysts in asymmetric allylic substitutions. Transition-metal-catalyzed asymmetric allylic substitutions[10] are useful reactions for the construction of C-C bonds in an enantioselective way (Scheme 2.3a).[11] Typically, an allyl substrate (linear **5** or branched **6**) is activated by a chiral metal catalyst **7** through oxidative addition, generating an electrophilic metal-π-allyl complex **IV** that engages with a variety of carbon nucleophiles. There are two possible mechanistic scenarios depending on the nature of the nucleophile. The first scenario occurs when a *hard* nucleophile (characterized by a pK_a of the conjugated acid higher than 25, typically an organometallic reagent) participates in the reaction. In this case, the chemistry follows an inner sphere mechanism (*path A*). In this path, the oxidative addition of the allyl precursor to the metal catalyst is followed by a transmetalation of the *hard* nucleophile with the η^3-electrophilic π-allyl complex (Scheme 2.3b, left panel). The ensuing complex **V** undergoes reductive elimination to generate the cross-coupling product **8** or **9**. Conversely, the second mechanistic scenario occurs when a *soft* nucleophile (characterized by a pK_a of the conjugated acid lower than 25) participates in the reaction, which happens *via* an outer sphere mechanism (*path B*). Here, the oxidative addition that generates the π-allyl complex **IV** is followed by the addition of the nucleophile to the allyl moiety from an opposite side to the metal center (Scheme 2.3b, right panel). The resulting η^2 complex **VI** or **VII** undergoes dissociation of the olefin product **8** or **9** to regenerate the catalyst and ensure the turnover of the cycle.

[10] Van Vranken, D. L., Trost, B. M. "Asymmetric Transition Metal-Catalyzed Allylic Alkylations" *Chem. Rev.* **1996**, *96*, 395-422.

[11] Cherney, A. H., Kadunce, N. T., Reisman, S. E. "Enantioselective and Enantiospecific Transition-Metal-Catalyzed Cross-Coupling Reactions of Organometallic Reagents To Construct C-C Bonds" *Chem. Rev.* **2015**, *115*, 9587-9652.
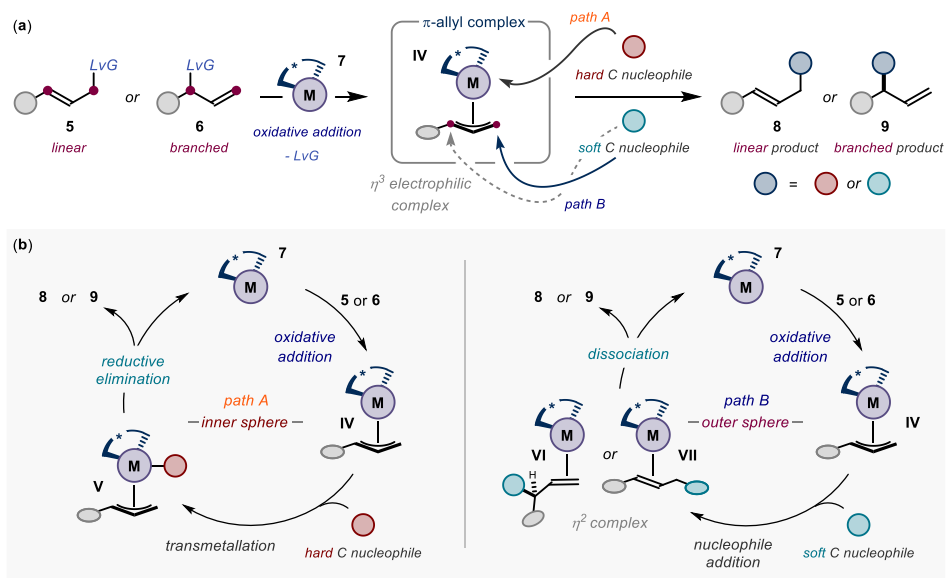
Scheme 2.3. (a) General features of asymmetric allylic substitution reactions; (b) inner sphere mechanism operative with *hard* nucleophiles (left panel) and the outer sphere mechanism taking place with *soft* nucleophiles (right panel). LvG = leaving group.

In both the inner and the outer sphere mechanisms (*path A and B*), the oxidative addition of the metal complex to a chiral allylic substrate **6** to give the chiral intermediate **IV** occurs in an *anti* disposition with respect to the leaving group. This stereospecific pathway results in an inversion of the absolute configuration with respect to substrate **6** (Scheme 2.4). The second step of the inner sphere mechanism (the reductive elimination in *path A*) occurs with retention of the absolute configuration of the allyl moiety, since the nucleophile addition occurs on the side that is bound to the metal center. Thus, for a reaction producing selectively the branched chiral product **9**, the inner sphere mechanism features an inversion-retention sequence, resulting in an overall inversion of the initial absolute configuration of the chiral allylic substrate **6**. In the outer sphere mechanism (*path B*), the addition of the nucleophile to the allyl moiety in complex **IV** occurs from the opposite side with respect to the metal center. Thus, for a reaction leading to the chiral product **9**, the outer sphere mechanism features an inversion-inversion sequence, resulting in an overall retention of the initial absolute configuration of the chiral allylic substrate **6**.
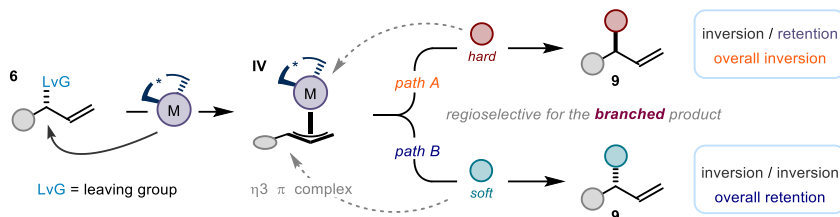
Scheme 2.4. Stereochemical outcome of the inner and outer sphere mechanisms.

Earliest studies in the field of asymmetric allylic substitutions focused on the use of palladium catalysts, which featured a wide substrate scope (the Tsuji-Trost reaction[12]).[3] In 1997 Kashio and Takeuchi reported the first iridium-catalyzed allylic substitution reaction between aliphatic and aromatic allylic acetates or carbonates **10** and sodium diethyl malonate **11** in the presence of an achiral phosphite ligand (Scheme 2.5). The process afforded the branched racemic allylic malonates **12** in high yields.[13] This seminal report opened up the research field of iridium-catalyzed Tsuji-Trost-type reactions,[2] a class of transformations which found many applications in the synthesis of natural products and bioactive compounds.[5,14]
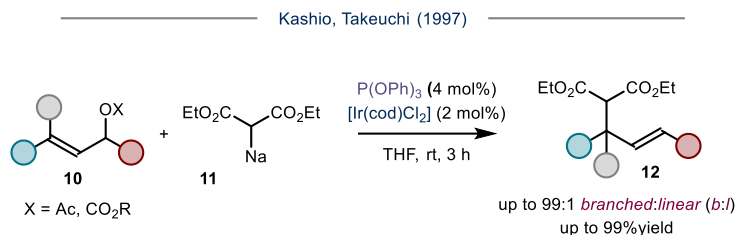
Scheme 2.5. The first example of an iridium-catalyzed Tsuji-Trost reaction.

Unlike palladium catalysts, which are selective for linear products **8**, iridium complexes induce high regioselectivity for the branched products **9**, arising from the addition of the nucleophile to the more substituted carbon of the allyl moiety in complex **IV** (see Scheme 2.3). Chiral iridium π-allyl complexes usually react with nucleophiles leading to the alkylated chiral products **9** with high enantiocontrol. A broad panel of chiral ligands, allyl precursors

[12] (a) Tsuji, J., Takahashi, H., Morikawa, M. "Organic syntheses by means of noble metal compounds XVII. Reaction of π-allylpalladium chloride with nucleophiles" *Tetrahedron Lett.* **1965**, 4387-4388; (b) Trost, B. M. "Organopalladium intermediates in organic synthesis" *Tetrahedron* **1977**, *33*, 2615-2649.
[13] Takeuchi, R., Kashio, M. "Highly Selective Allylic Alkylation with a Carbon Nucleophile at the More Substituted Allylic Terminus Catalyzed by an Iridium Complex: An Efficient Method for Constructing Quaternary Carbon Centers" *Angew. Chem. Int. Ed. Engl.* **1997**, *36*, 263-265.
[14] Qu, J., Helmchen, G. "Applications of Iridium-Catalyzed Asymmetric Allylic Substitution Reactions in Target-Oriented Synthesis" *Acc. Chem. Res.* **2017**, *50*, 2539-2555.

and both *hard* and *soft* nucleophiles can be successfully used in asymmetric iridium-catalyzed allylic substitutions.[2] The first enantioselective iridium-catalyzed allylic alkylation was reported by Helmchen and Janssen in 1997 (Scheme 2.6).[15] The reaction between linear allylic acetates **13** and sodium dimethyl malonate **14** delivered highly enantioenriched branched products **15** in the presence of an iridium (I) pre-catalyst and the chiral ligand Phox (phosphinooxazoline).
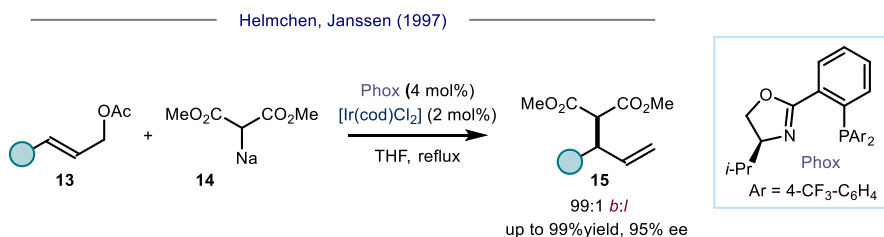
Scheme 2.6. The first example of an enantioselective iridium-catalyzed allylic substitution.

Phosphoramidite ligands, introduced by Feringa for copper-catalyzed enantioselective conjugate additions,[16] were used by Alexakis in 2004,[17] followed by Hartwig in 2005,[18] in iridium enantioselective allylations (Scheme 2.7). In the first report, enantioselective alkylation of allylic acetates and carbonates of type **16** with sodium dimethyl malonate **14** proceeded under iridium catalysis in the presence of the chiral ligand **L₂** to afford enantioenriched products **15** as the only regioisomers (Scheme 2.7a). In the Hartwig report, linear allylic carbonates **17** reacted with nucleophilic silyl enol ethers **18** in the presence of fluoride sources, an iridium (I) pre-catalyst, and chiral phosphoramidite ligand **L₁**, affording β-allyl ketones **19** in high yields, regioselectivity, and stereocontrol (Scheme 2.7b).

---

[15] Janssen, J. P., Helmchen, G. "First Enantioselective Alkylations of Monosubstituted Allylic Acetates Catalyzed by Chiral Iridium Complexes" *Tetrahedron Lett.* **1997**, *38,* 8025-8026.

[16] de Vries, A. H. M., Meetsma, A., Feringa, B. L. "Enantioselective Conjugate Addition of Dialkylzinc Reagents to Cyclic and Acyclic Enones Catalyzed by Chiral Copper Complexes of New Phosphorus Amidites" *Angew. Chem. Int. Ed. Engl.* **1996**, *35*, 2374-2376.

[17] Alexakis, A., Polet, D. "Very Efficient Phosphoramidite Ligand for Asymmetric Iridium-Catalyzed Allylic Alkylation" *Org. Lett.* **2004**, *6*, 3529-3532.

[18] Graening, T., Hartwig, J. F. "Iridium-Catalyzed Regio- and Enantioselective Allylation of Ketone Enolates" *J. Am. Chem. Soc.* **2005**, *127*, 17192-17193.
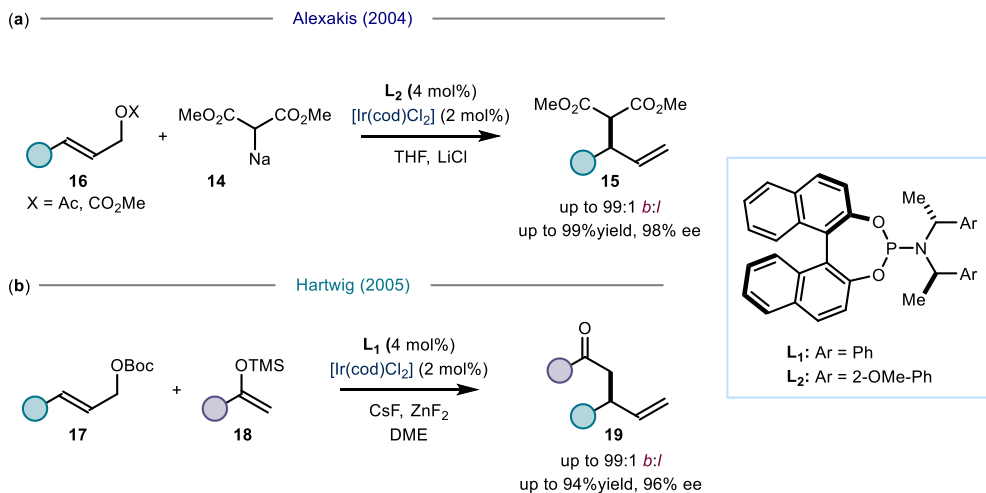
Scheme 2.7. Seminal examples of an asymmetric iridium-catalyzed allylic alkylation exploiting a chiral phosphoramidite ligand as source of stereoinduction.

In both reports, the authors proposed the in situ formation of an iridium π-allyl complex **IX** (Scheme 2.8), which was isolated later and characterized by X-ray crystallographic analysis.[19] The general features of this catalytic system, known as *type I*,[14] are summarized in Scheme 2.8. The formation of cationic complex **IX** required the use of a base to enable the formation of the metallacyclic iridium species by C-H activation at one of the methyl groups of the ligands **L₁** or **L₂**. The complex was moderately electrophilic and usually reacted with strong nucleophiles. This *type I* iridium catalysis generally worked under basic conditions and activated mostly linear substrates such as **16** and **17** in Scheme 2.7, selectively delivering branched products of type **9** in Scheme 2.3 with high enantiomeric excess.[20]

---

[19] (a) Madrahimov, S. T., Markovic, D., Hartwig, J. F. "The Allyl Intermediate in Regioselective and Enantioselective Iridium-Catalyzed Asymmetric Allylic Substitution Reactions" *J. Am. Chem. Soc.* **2009**, *131*, 7228-7229; (b) Spiess, S., Raskatov, J. A., Gnamm, C., Brödner, K., Helmchen, G. "Ir-Catalyzed Asymmetric Allylic Substitutions with (Phosphoramidite) Ir Complexes-Resting States, Synthesis, and Characterization of Catalytically Active (π-Allyl)Ir Complexes" *Chem. - Eur. J.* **2009**, *15*, 11087-11090.
[20] Madrahimov, S. T., Hartwig, J. F. "Origins of Enantioselectivity during Allylic Substitution Reactions Catalyzed by Metallacyclic Iridium Complexes" *J. Am. Chem. Soc.* **2012**, *134*, 8136-8147.
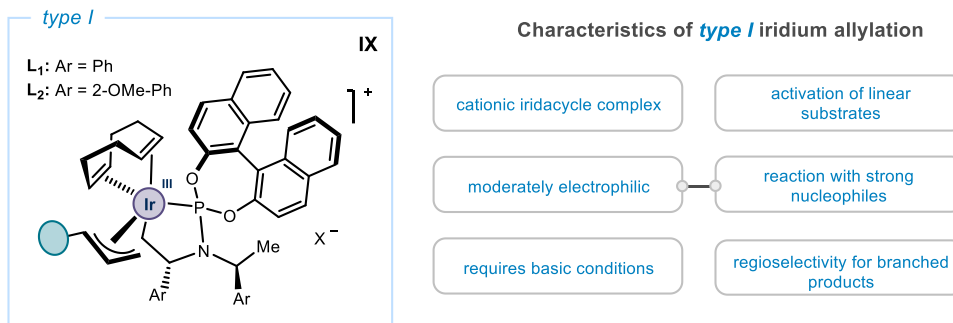
Scheme 2.8. Features of the *type I* catalysis by iridacycle complexes bearing phosphoramidite-type ligands.

In 2007, Carreira and co-workers introduced a new phosphoramidite ligand (*S*)-**L**, for enantioselective iridium catalytic allylations, which bore a dibenzazepine ring at the phosphorus atom capable of coordination to the metal center through its olefin moiety (Scheme 2.9).[4] The novel phosphoramidite-olefin structure proved an excellent ligand in an iridium-catalyzed enantioselective allylic vinylation reported by the group of Carreira in 2013 (Scheme 2.9).[21] Free branched allylic alcohols **20** could be engaged in the reaction with vinylic potassium trifluoroborate salts **21** under acidic conditions, delivering alkenes **22** in high yields, regio-, and enantio-selectivity. The reactive (η^3-allyl)iridium(III) complex (**Ir-III** in Scheme 2.10) was formed in situ by coordination of two molecules of the ligand (*S*)-**L** to the iridium center and subsequent oxidative addition of the free allylic alcohols under the activation by a strong acid.
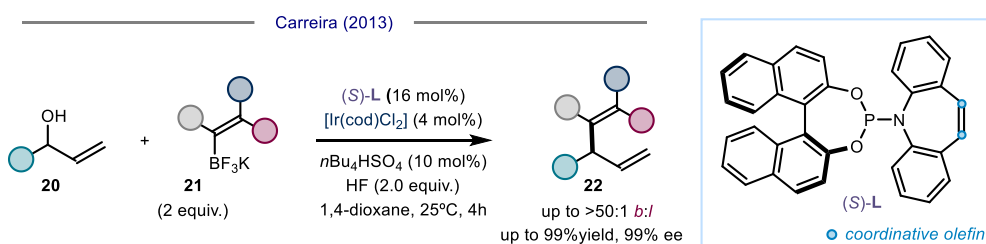
Scheme 2.9. First enantioselective iridium-catalyzed allylic vinylation enabled by a chiral phosphoramidite-olefin ligand.

[21] Hamilton, J. Y., Sarlah, D., Carreira, E. M. "Iridium-Catalyzed Enantioselective Allylic Vinylation" *J. Am. Chem. Soc.* **2013**, *135*, 994-997.

Several other weak nucleophiles, including alkynyl potassium trifluoroborate salts,[22] simple olefins,[23] allyl silanes,[24] and carbonyl species,[25] among others,[5] successfully participated in the reaction with free allylic alcohols using (*S*)-**L** as the chiral ligand. The mechanistic aspects of this catalytic system, known as *type II*,[14] are summarized in Scheme 2.10. The structure of the iridium π-allyl complex **Ir-III**, which is the reactive intermediate in the catalytic cycle, was elucidated by X-ray crystallographic analysis of the isolated major *exo* diastereomer.[26] Complex **Ir-III** adopts a distorted octahedral geometry, with one of the phosphoramidite-olefin ligands chelating the metal center through the coordination of both the phosphorus atom and the olefin moiety at the axial and equatorial positions, respectively. The second molecule of the ligand coordinates the metal center only through the phosphorus atom, which occupies another equatorial position. Finally, the allyl moiety coordinates iridium at the equatorial position while exposing preferentially one of the prochiral faces to the nucleophile, which is typically *soft* and approaches from the outer sphere (mechanistic scenario illustrated as *path B* in Scheme 2.3). The more substituted carbon atom of the allyl moiety C(1) is subjected to the *trans* effect exerted by the P atom of the chelating ligand, whereas C(3) lies in the *trans* position with respect to the coordinating olefin. The different *trans* effects of the phosphorus atom and the olefin, together with the steric effect of the sterically encumbered azepine moieties of the two ligands, have been accounted for the difference between the two Ir-C bond distances in the allyl group, with Ir-C(1) that is 0.35 Å longer than Ir-C(3). This difference makes the Ir-C(1) bond more labile and, therefore, it could explain the high regioselectivity of the reactions for the branched products.[27] Complex **Ir-III** is more electrophilic than **IX** in the *type I* system due to the presence of two π-acidic phosphine ligands. It therefore reacts under acidic conditions with weak nucleophiles.

[22] Hamilton, J. Y., Sarlah, D., Carreira, E. M. "Iridium-Catalyzed Enantioselective Allylic Alkynylation" *Angew. Chem. Int. Ed.* **2013**, *52*, 7532-7535.

[23] Hamilton, J. Y., Sarlah, D., Carreira, E. M. "Iridium-Catalyzed Enantioselective Allyl-Alkene Coupling" *J. Am. Chem. Soc.* **2014**, *136*, 3006-3009.

[24] Hamilton, J. Y., Hauser, N., Sarlah, D., Carreira, E. M. "Iridium-Catalyzed Enantioselective Allyl-Allylsilane Cross-Coupling" *Angew. Chem. Int. Ed.* **2014**, *53*, 10759-10762.

[25] (a) Krautwald, S., Sarlah, D., Schafroth, M. A., Carreira, E. M. "Enantio- and Diastereodivergent Dual Catalysis: a-Allylation of Branched Aldehydes" *Science* **2013**, *340*, 1065-1068; (b) Krautwald, S., Schafroth, M. A., Sarlah, D., Carreira, E. M. "Stereodivergent α-Allylation of Linear Aldehydes with Dual Iridium and Amine Catalysis" *J. Am. Chem. Soc.* **2014**, *136*, 3020-3023.

[26] Rössler, S. L., Krautwald, S., Carreira, E. M. "Study of Intermediates in Iridium-(Phosphoramidite,Olefin)-Catalyzed Enantioselective Allylic Substitution" *J. Am. Chem. Soc.* **2017**, *139*, 3603-3606.

[27] This might be true for *type II* iridium catalysis, however previous studies on other iridium-allyl complexes disproved the correlation between the regioselectivity of the reaction and the Ir-C bond distances in the allyl moiety. See: Madrahimov, S. T., Li, Q., Sharma, A., Hartwig, J. F. "Origins of Regioselectivity in Iridium Catalyzed Allylic Substitution" *J. Am. Chem. Soc.* **2015**, *137*, 14968-14981.
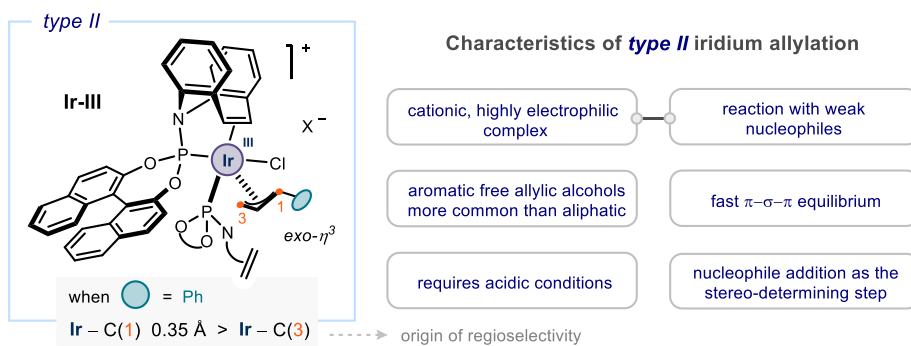
Scheme 2.10. General features of the *type II* iridium catalysis with phosphoramidite-olefin-type ligands.

Carreira and co-workers found that the formation of the π-allyl complex was moderately to highly diastereoselective depending on the aromatic substituent on the allylic alcohol. The *exo* diastereomer was formed as the major complex, in some cases in up to 20:1 dr, regardless of the absolute configuration of the starting allylic alcohol (Scheme 2.11a, left panel).[26] This diastereoconvergence was suggested to occur *via* a fast equilibration between the *exo* and *endo* π-allyl diastereomers (π−σ−π equilibrium, Scheme 2.11b), which would initially arise stereospecifically from the *R* and *S* enantiomers of the allylic alcohol, respectively. This resulted in the stereochemical information of the starting allylic alcohol being completely lost. However, if an outer sphere mechanism was operative, the enantiomeric outcome of the reaction could only be rationalized by the addition of the *soft* nucleophile to the minor *endo* diastereomeric complex (Scheme 2.11a, right panel). This would suggest that the stereodetermining addition of the nucleophile to the *endo* diastereomer was significantly faster than addition to the *exo* complex and that the fast π−σ−π equilibration between the *exo* and *endo* complexes was key to the overall enantioconvergent process.
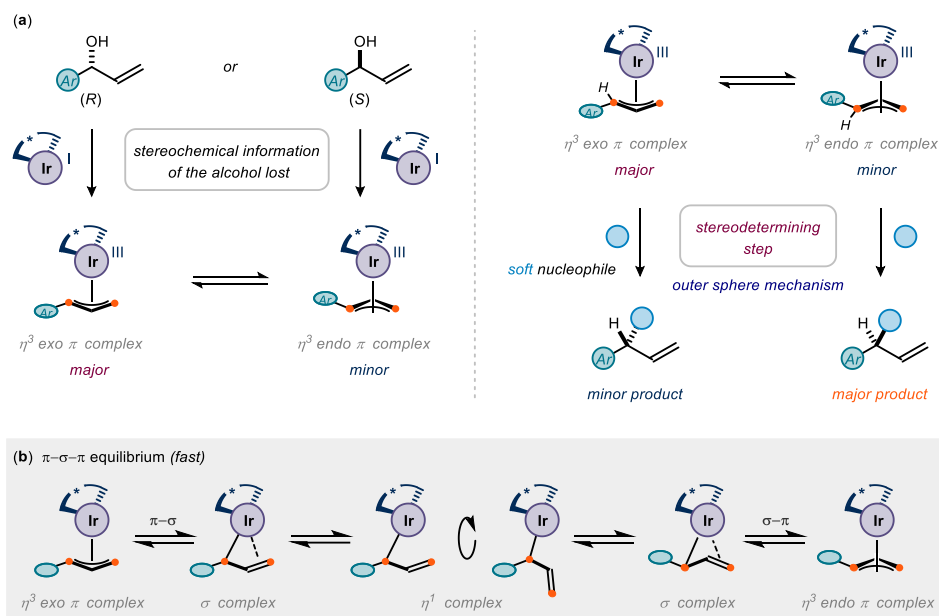
Scheme 2.11. (a) Formation of a diastereomeric mixture of iridium π-allyl complex Ir-III starting from enantioenriched chiral allylic alcohols and stereochemical outcome of the reaction; (b) rationalization of the stereochemical outcome of the reaction on the basis of the occurrence of a fast π−σ−π equilibrium.

Recently, Krische and co-workers reported a third general iridium-based catalytic system for enantioselective allylic substitutions, known as *type III*,[28] which was previously introduced for nucleophilic carbonyl allylations.[29] The catalyst was prepared from simple allylic acetate and an electron-poor benzoic acid to generate, under basic conditions, a neutral iridium π-allyl C,O-benzoate complex **X** adorned with a chiral diphosphine ligand, such as Tol-BINAP or SEGPHOS (Scheme 2.12). This complex displayed a unique amphiphilic character that allowed allylations of electrophilic carbonyl species as well as allylic substitutions of amines and carbon-based nucleophiles. The addition of the nucleophile to the π-allyl was proposed to occur following the outer sphere mechanism described as *path B* in Scheme 2.3 and Scheme 2.4 and to be the stereo-determining step of the transformation.[30]

[28] Stivala, C. E., Zbieg, J. R., Liu, P., Krische, M. J. "Chiral Amines via Enantioselective π-Allyliridium-C,O-Benzoate-Catalyzed Allylic Alkylation: Student Training via Industrial-Academic Collaboration" *Acc. Chem. Res.* **2022**, *55*, 2138-2147.

[29] Kim, S. W., Zhang, W., Krische, M. J. "Catalytic Enantioselective Carbonyl Allylation and Propargylation via Alcohol-Mediated Hydrogen Transfer: Merging the Chemistry of Grignard and Sabatier" *Acc. Chem. Res.* **2017**, *50*, 2371-2380.

[30] (a) Kim, S. W., Schempp, T. T., Zbieg, J. R., Stivala, C. E., Krische, M. J. "Regio- and Enantioselective Iridium-Catalyzed N-Allylation of Indoles and Related Azoles with Racemic Branched Alkyl-Substituted Allylic Acetates" *Angew. Chem. Int. Ed.* **2019**, *58*, 7762-7766; (b) Kim, S. W., Schwartz, L. A., Zbieg, J. R., Stivala, C. E., Krische, M. J. "Regio- and Enantioselective Iridium-Catalyzed Amination of Racemic
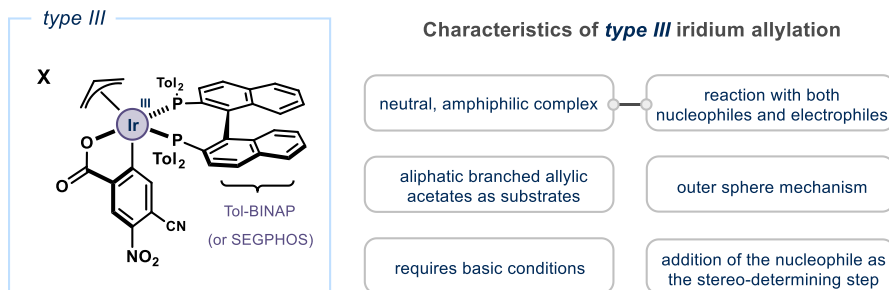
Scheme 2.12. General features of the *type III* iridium catalysis.

In 2021, the group of Krische reported the synthesis of highly enantioenriched quaternary nitroalkanes **25** starting from of α,α-disubstituted nitroalkanes **24** and aliphatic branched allylic acetates **23** in the presence of the Tol-BINAP-adorned complex **X** (Scheme 2.13).[31] Products **25** could be further reduced to deliver highly enantioenriched α-quaternary primary amines. The synthesis of these valuable scaffolds *via* asymmetric allylic substitution of unactivated, sterically encumbered nitroalkanes and subsequent reduction was unprecedented in *type I* and *type II* iridium catalysis.
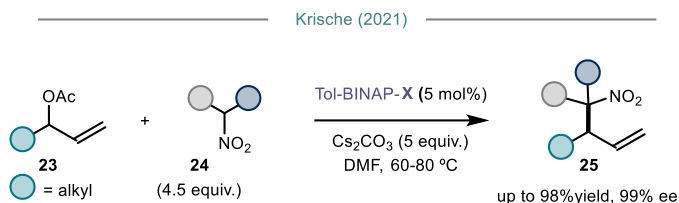
Scheme 2.13. Enantioselective allylic alkylation enabled by a C,O-benzoate iridium π-allyl complex.

A common feature of the three systems (*type I*, *II* and *III*) discussed in this paragraph is the high stability of the corresponding iridium π-allyl complex, which, in some cases, was identified as the resting state of the catalyst in the reaction mixture.[32] Sometimes, these complexes could be even isolated by silica gel chromatography since they are extremely

Branched Alkyl-Substituted Allylic Acetates with Primary and Secondary Aromatic and Heteroaromatic Amines" *J. Am. Chem. Soc.* **2019**, *141*, 671-676.

[31] Jung, W.-O., Mai, B. K., Spinello, B. J., Dubey, Z. J., Kim, S. W., Stivala, C. E., Zbieg, J. R., Liu, P., Krische, M. J. "Enantioselective Iridium-Catalyzed Allylation of Nitroalkanes: Entry to β-Stereogenic α-Quaternary Primary Amines" *J. Am. Chem. Soc.* **2021**, *143*, 9343-9349.

[32] Raskatov, J. A., Spiess, S., Gnamm, C., Brödner, K., Rominger, F., Helmchen, G. "Ir-Catalysed Asymmetric Allylic Substitutions with Cyclometalated (Phosphoramidite)Ir Complexes-Resting States, Catalytically Active (π-Allyl)Ir Complexes and Computational Exploration" *Chem. Eur. J.* **2010**, *16*, 6601-6615.

tolerant to oxygen and moisture and could be used as competent pre-formed catalysts as an alternative to their preparation in situ.

2.3 Photoexcitation of Chiral Organometallic Complexes in Asymmetric Catalysis

The chiral organometallic iridium complexes discussed in the previous section have been extensively used in the polar domain by exploiting their ground-state reactivity. The target of this project was to expand the traditional polar reactivity of a chiral iridium organometallic complex by disclosing a novel catalytic function in the excited state. In this section, an overview of the few examples reported to date that exploit the photoactivation of chiral organometallic complexes is provided.

Following the increasing interest in the field of photochemistry, recent studies have shown that the direct photoexcitation of chiral catalytic intermediates is a powerful strategy to disclose novel reactivities in the excited state, which are not attainable in the ground-state domain.[6,33] For example, this approach was recently exploited in the field of asymmetric organocatalysis, with the seminal contributions of our group on the photoexcitation of enamine and iminium ion intermediates **XI** and **XII**, respectively (Scheme 2.14a).[34] This photochemical strategy was also successfully applied in the field of biocatalysis, with the contributions from the Hyster group on photoactive ene-reductase (ERED) enzymes (Scheme 2.14b),[35] and in the field of Lewis-acid (LA) catalysis, with major contributions from the groups of Bach, Meggers, Yoon, and Gong (structure of the LA-substrate complex in Scheme 2.14c).[36]

---

[33] (a) Genzink, M. J., Kidd, J. B., Swords, W. B., Yoon, T. P. "Chiral Photocatalyst Structures in Asymmetric Photochemical Synthesis" *Chem. Rev.* **2022**, *122*, 1654-1716; (b) Mondal, S., Dumur, F., Gigmes, D., Sibi, M. P., Bertrand, M. P., Nechab, M. "Enantioselective Radical Reactions Using Chiral Catalysts" *Chem. Rev.* **2022**, *122*, 5842-5976.

[34] Silvi, M., Melchiorre, P. "Enhancing the Potential of Enantioselective Organocatalysis with Light" *Nature* **2018**, *554*, 41-49.

[35] For a selected example: Black, M. J., Biegasiewicz, K. F., Meichan, A. J., Oblinsky, D. G., Kudisch, B., Scholes, G. D., Hyster, T. K. "Asymmetric redox-neutral radical cyclization catalysed by flavin-dependent 'ene'-reductases" *Nat. Chem.* **2020**, *12*, 71-75.

[36] Selected examples: (a) Brimioulle, R., Bach, T. "Enantioselective Lewis Acid Catalysis of Intramolecular Enone [2+2] Photocycloaddition Reactions" *Science* **2013**, *342*, 840-843; (b) Huo, H., Shen, X., Wang, C., Zhang, L., Röse, P., Chen, L.-A., Harms, K., Marsch, M., Hilt, G., Meggers, E., "Asymmetric Photoredox Transition-Metal Catalysis Activated by Visible Light" *Nature* **2014**, *515*, 100-103; (c) Skubi, K. L., Kidd, J. B., Jung, H., Guzei, I. A., Baik, M. H., Yoon, T. P. "Enantioselective Excited-State Photoreactions Controlled by a Chiral Hydrogen-Bonding Iridium Sensitizer" *J. Am. Chem. Soc.* **2017**, *139*, 17186-17192; (d) Li, Y., Zhou, K., Wen, Z., Cao, S., Shen, X., Lei, M., Gong, L. "Copper(II)-Catalyzed Asymmetric Photoredox Reactions: Enantioselective Alkylation of Imines Driven by Visible Light" *J. Am. Chem. Soc.* **2018**, *140*, 15850-15858; (e) Zhang, K., Lu, L. Q., Jia, Y., Wang, Y., Lu, F. D., Pan, F., Xiao, W. J. "Exploration of a Chiral Cobalt Catalyst for Visible-Light-Induced Enantioselective Radical Conjugate Addition" *Angew. Chemie Int. Ed.* **2019**, *58*, 13375-13379.

Excited State Chiral Catalytic Intermediates

(**a**) Organocatalysis   (**b**) Biocatalysis   (**c**) Lewis acid catalysis
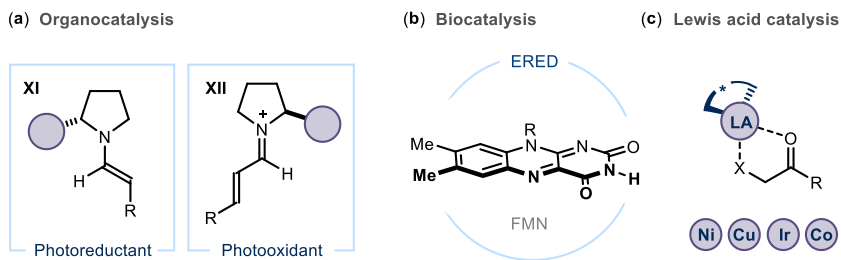
Scheme 2.14. Examples of photoactive chiral catalytic intermediates in: (a) organocatalysis; (b) biocatalysis; (c) Lewis-acid (LA) catalysis. ERED = ene-reductase.

In contrast, asymmetric organometallic photocatalysis has been far less explored. A general approach would require the activation of a substrate by association to a chiral metal catalyst, generating a chiral organometallic intermediate which is capable to absorb visible light and trigger mechanistically new transformations compared to its traditional ground-state reactivity (Scheme 2.15).
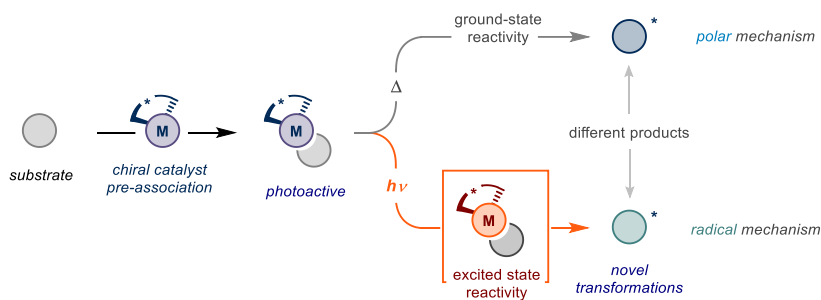
Scheme 2.15. General strategy to unlock novel reactivities by photoexcitation of a chiral organometallic catalytic intermediate.

Recently, this photochemical strategy has been brought to fruition.[37] The reaction mechanisms in the excited state available to metal catalysts are illustrated in Scheme 2.16. The generation

[37] For reviews on the topic, see: (a) Cheng, W. M., Shang, R. "Transition Metal-Catalyzed Organic Reactions under Visible Light: Recent Developments and Future Perspectives" *ACS Catal.* **2020**, *10*, 9170-9196; (b) Kancherla, R., Muralirajan, K., Sagadevan, A., Rueping, M. "Visible Light-Induced Excited-State Transition-Metal Catalysis" *Trends in Chemistry* **2019**, *1*, 510-523; (c) Lunic, D., Bergamaschi, E., Teskey, C. J. "Using Light to Modify Selectivity of Transition Metal Catalysed Transformations" *Angew. Chem. Int. Ed.* **2021**, *60*, 20594-20605; (d) Cheung, K. P. S., Sarkar, S., Gevorgyan, V. "Visible Light-Induced Transition Metal Catalysis" *Chem. Rev.* **2022**, *122*, 1543-1625.

of radicals can occur *via* SET events (*path i*) or bond homolysis (*path ii*).[38] Alternatively, the visible light excitation can facilitate elementary steps such as oxidative addition (OA) and/or reductive elimination (RE) by bringing the metal catalyst to a high energy excited state (*path iii*).[39]
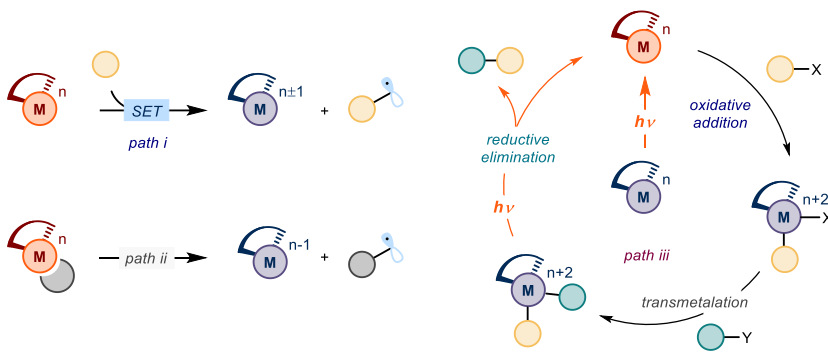
Scheme 2.16. Mechanisms of radical generation from metal catalysts in their excited state.

So far, the direct excitation of organometallic intermediates was applied mainly to non-asymmetric transformations.[37] Only few reports have shown that photoactive chiral organometallic complexes can successfully catalyze novel asymmetric transformations under light irradiation. Here, copper-based complexes have played a central role.[9] In 2016, Peters and Fu reported a radical copper-catalyzed enantioconvergent cross-coupling to forge carbon-nitrogen bonds under visible light excitation (Scheme 2.17).[40] Racemic tertiary α-chloro amides **26** were coupled with substituted indoles or carbazoles **27** under blue LED (Light Emitting Diode) irradiation to afford α-amino amides **28** in high yields and enantioselectivity. The photoactive copper complex **XIII** was formed in situ by coordination of the commercially available chiral phosphine ligand (*S*)-SITCP and the substrate **27** to a copper(I) pre-catalyst under basic conditions. Mechanistic studies elucidated some aspects of the catalytic cycle, particularly regarding the C-N bond formation which was identified as the stereo-determining

[38] Abderrazak, Y., Bhattacharyya, A., Reiser, O. "Visible-Light-Induced Homolysis of Earth-Abundant Metal-Substrate Complexes: A Complementary Activation Strategy in Photoredox Catalysis" *Angew. Chem. Int. Ed.* **2021**, *60*, 21100-21115.
[39] For seminal examples of *path iii* mechanism: (a) Welin, E. R., Le, C., Arias-Rotondo, D. M., McCusker, J. K., MacMillan, D. W. C. "Photosensitized, energy transfer-mediated organometallic catalysis through electronically excited nickel(II)" *Science* **2017**, *355*, 380-385; (b) Torres, G. M., Liu, Y., Arndtsen, B. A. "A Dual Light-Driven Palladium Catalyst: Breaking the Barriers in Carbonylation Reactions" *Science* **2020**, *368*, 318-323.
[40] Kainz, Q. M., Matier, C. D., Bartoszewicz, A., Zultanski, S. L., Peters, J. C., Fu, G. C. "Asymmetric copper-catalyzed C-N cross-couplings induced by visible light" *Science* **2016**, *351*, 681-684.

step.[41] Upon formation of the photoactive species **XIII** and visible light absorption, a SET reduction of substrate **26** delivered the radical intermediate **XIV** and a Cu(II) complex, which subsequently coordinated a second molecule of **27**. This intermediate collapsed with radical **XIV** to intermediate **XV** *via* coordination of the carbonyl group and generated product **28** by radical recombination, releasing at the same time the photoactive Cu(I) complex for turnover. This photoactive copper(I)-amido complex did not have previous application in polar enantioselective catalysis since it required the identification of a tailored chiral phosphine ligand that ensured the reactivity in the excited state and the stereocontrol of the transformation.
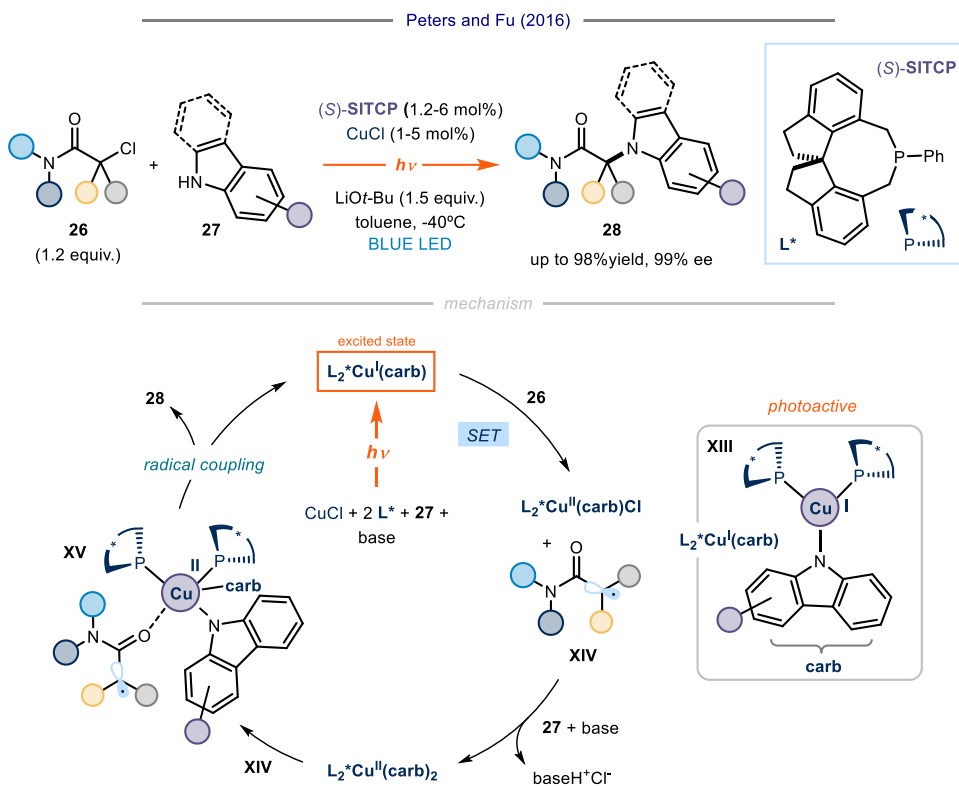
Scheme 2.17. Seminal report of a C-N cross coupling enabled by visible light excitation of a chiral copper complex.

---

[41] Lee, H., Ahn, J. M., Oyala, P. H., Citek, C., Yin, H., Fu, G. C., Peters, J. C. "Investigation of the C-N Bond-Forming Step in a Photoinduced, Copper-Catalyzed Enantioconvergent N-Alkylation: Characterization and Application of a Stabilized Organic Radical as a Mechanistic Probe" *J. Am. Chem. Soc.* **2022**, *144*, 4114-4123.

Recently, the method was expanded to Csp-Csp³ and Csp²-Csp³ enantioselective cross couplings.[42,43] For example, Zhang and co-workers reported that benzoxazoles **29** could be coupled with racemic secondary benzyl bromides **30** in the presence of a Cu(I) pre-catalyst, the chiral tridentate ligand *t*BuCbzbox and visible light irradiation under basic conditions and low temperature, affording alkylated benzoxazoles **31** in high yields and enantioselectivity (Scheme 2.18).[43] The photoactive complex **XVI** was obtained in situ by deprotonation and coordination of substrate **29** to the chiral Cu(I)-bis(oxazoline) catalyst. Upon photoexcitation of **XVI**, a SET reduction of benzyl bromide **30** delivered a Cu(II) intermediate and the benzyl radical **XVII**, which recombined to the Cu(II) complex through a radical-metal crossover event[44] generating **XVIII**. A final reductive elimination from the Cu(III) intermediate **XVIII** delivered product **31** in a highly stereo-controlled way and the Cu(I) catalyst for turnover.

---

[42] (a) Zhang, Y., Sun, Y., Chen, B., Xu, M., Li, C., Zhang, D., Zhang, G. "Copper-Catalyzed Photoinduced Enantioselective Dual Carbofunctionalization of Alkenes" *Org. Lett.* **2020**, *22*, 1490-1494; (b) Xia, H. D., Li, Z. L., Gu, Q. S., Dong, X. Y., Fang, J. H., Du, X. Y., Wang, L. L., Liu, X. Y. "Photoinduced Copper-Catalyzed Asymmetric Decarboxylative Alkynylation with Terminal Alkynes" *Angew. Chemie Int. Ed.* **2020**, *59*, 16926-16932.
[43] Li, C., Chen, B., Ma, X., Mo, X., Zhang, G. "Light-Promoted Copper-Catalyzed Enantioselective Alkylation of Azoles" *Angew. Chemie Int. Ed.* **2021**, *60*, 2130-2134.
[44] Leifert, D., Studer, A. "The Persistent Radical Effect in Organic Synthesis" *Angew. Chemie Int. Ed.* **2020**, *59*, 74-108.
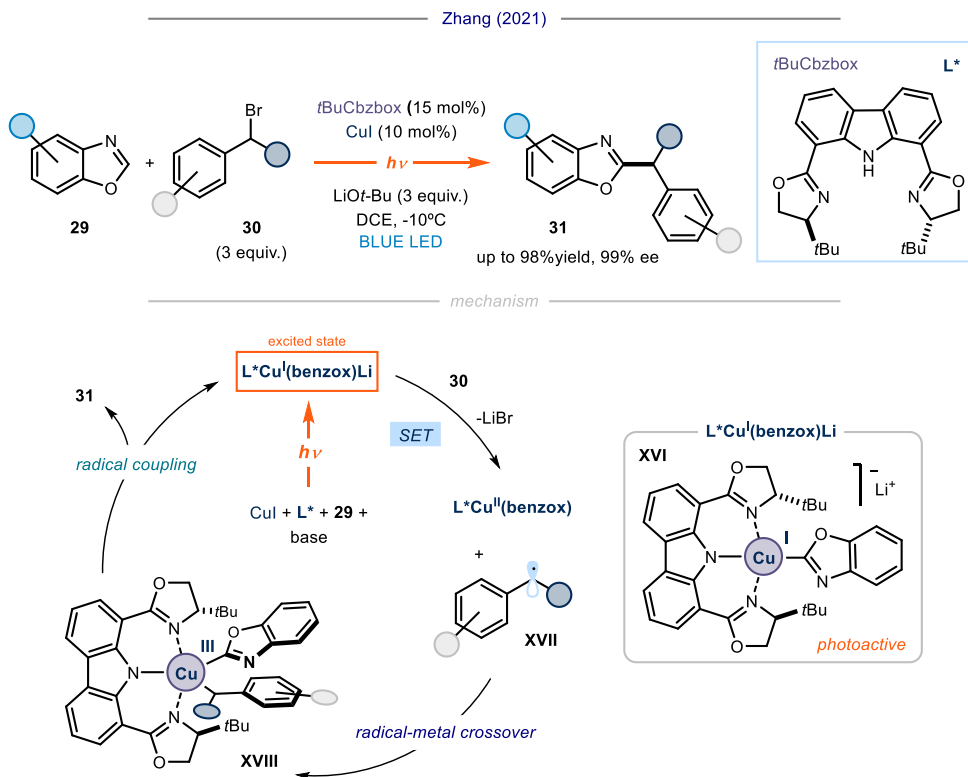
Scheme 2.18. Example of a C-C cross coupling enabled by the visible light excitation of a chiral copper complex.

Examples of enantioselective copper-catalyzed cyanation reactions that exploit the photoactivation of chiral copper intermediates under visible light irradiation were also reported.[45]

2.4 Target of the Project

Considering the successful applications of the photoexcitation strategy in asymmetric catalysis, we recognized that asymmetric organometallic photocatalysis is a research field with great potential but still in its infancy. The chiral organometallic copper complexes discussed in the previous section were specifically designed to be photoactive and did not have an established reactivity in polar chemistry. For example, the photocatalyzed C-N cross coupling reported in 2016 by Peters and Fu required the identification of a specifically

---

[45] (a) Li, J., Zhang, Z., Wu, L., Zhang, W., Chen, P., Lin, Z., Liu, G. "Site-Specific Allylic C-H Bond Functionalization with a Copper-Bound N-Centred Radical" *Nature* **2019**, *574*, 516-521; (b) Guo, Q., Wang, M., Peng, Q., Huo, Y., Liu, Q., Wang, R., Xu, Z. "Dual-Functional Chiral Cu-Catalyst-Induced Photoredox Asymmetric Cyanofluoroalkylation of Alkenes" *ACS Catal.* **2019**, *9*, 4470-4476.

designed phosphine-based copper(I)-amido complex to disclose the novel reactivity in the excited state and its use was not documented previously in ground-state catalysis.[40]

The aim of this project was to demonstrate that the strategy of the photoexcitation of a chiral organometallic complex could divert its well-established reactivity in the ground-state and disclose completely novel catalytic functions in the excited state. Specifically, we showed that the chiral (η^3-allyl)iridium(III) complex **Ir-III** reported by Carreira in 2007, which is a well-established electrophile in ground-state catalysis,[4] could be activated upon visible light irradiation and become a strong oxidant in the excited state, thus upgrading its catalytic functions beyond traditional polar chemistry and diverging from mechanistically known and broadly exploited reactivity (Scheme 2.19). The idea of exploring the photoactivity of the (η^3-allyl)iridium(III) complex was informed by the observation that **Ir-III** is highly colored and highly electrophilic and absorbs in the visible light region, in analogy with a photoactive chiral iminium ion intermediate reported by our group (see Scheme 2.2a in the *Introduction*).[8] In analogy to iminium ion photochemistry, we envisaged that complex **Ir-III** in the excited state could generate open-shell species by SET oxidation of suitable radical precursors, thus upgrading the traditional reactivity and disclosing a novel function, and promote a mechanistically novel radical-based enantioselective allylic substitution.
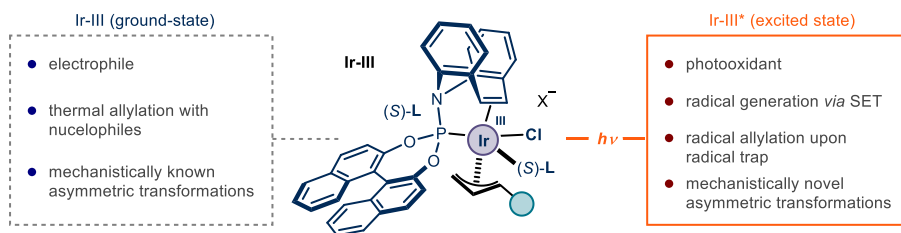
Scheme 2.19. Our hypothesis: photoexcitation of the chiral electrophilic organoiridium complex **Ir-III** discloses its potential role as photooxidant.

By exploiting the photoactivity of complex **Ir-III**, we developed a mechanistically novel radical enantioselective allylic substitution starting from the free allylic alcohol **20** and a non-nucleophilic radical precursor **3** that would not react in traditional polar allylation chemistry, to ultimately deliver highly enantioenriched cross-coupled products **4** (Scheme 2.20a). The process started with the visible light excitation of **Ir-III** to generate the photooxidant **Ir-III*** (Scheme 2.20b). Upon SET oxidation of a suitable radical precursor **3** and mesolytic cleavage of the redox auxiliary (RA), a radical species **II** was generated, together with the reduced complex **Ir(II)**. We envisaged that a subsequent radical-metal crossover event[44] would allow the recombination of radical **II** with **Ir(II)**, affording the **Ir(III)** intermediate **XXV**. This complex released the cross-coupled product **4** by reductive elimination and generated again catalyst **Ir(I)**, which would be prone to intercept a second molecule of allylic alcohol **20** by

oxidative addition and start a second catalytic cycle. Overall, the strategy allowed the mild generation of reactive radical species and enabled the development of a novel radical-based enantioselective alkyl-alkyl cross-coupling reaction, a highly valuable but difficult-to-realize process for making chiral molecules.
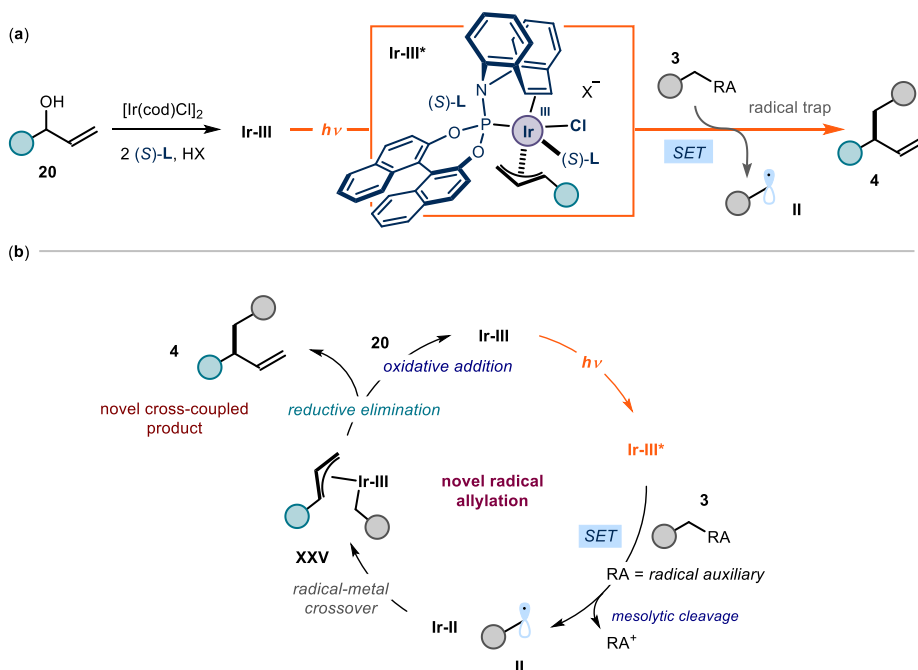
Scheme 2.20. (a) Our reaction design: enantioselective photocatalyzed allylic substitution using **Ir-III** as a single metal catalyst; (b) mechanistic proposal for the novel radical allylic substitution enabled by the photoexcitation of **Ir-III**.

Sparse examples of enantioselective transition-metal-catalyzed radical allylations that were previously reported will be discussed in the next section. Importantly, these methods all required the use of an external photoredox catalyst for the radical generation, and therefore, on a mechanistic level, they significantly diverged from our photochemical protocol, which exploited the photoactivity of the chiral organometallic iridium-based catalyst.

## 2.5 Precedents in photoredox enantioselective radical allylations

Few examples of enantioselective transition-metal catalyzed allylic substitutions operating through a radical mechanism were reported, but these reactions all required an external

photoredox catalyst for the generation of radical intermediates.[46] For example, the group of Yu disclosed an asymmetric radical allylic substitution starting from aromatic branched allylic acetates **32** and 4-alkyl-1,4-dihydropyridines (DHP) **33** as radical precursors and alkylating agents to afford allylic compounds **34** in high yields and enantioselectivity (Scheme 2.21).[46b] The reaction proceeded in the presence of a palladium(0) pre-catalyst and the chiral ligand GARPHOS, in combination with an iridium-based photoredox catalyst (**PC**) and visible light irradiation. The mechanism proposed for this radical C-C coupling reaction envisaged a synergistic interplay between two catalytic cycles: the one operated by the palladium complex **XXI** in its ground-state and the one of the photoredox catalyst **PC** in its excited state. Upon visible light excitation, the photocatalyst **PC** could oxidize *via* SET the radical precursor **33**, generating the reduced intermediate **PC·⁻** and the fleeting radical cation of the DHP that released radical **XXIII** upon mesolytic cleavage. The ground-state Pd(0) complex **XXI** underwent oxidative addition (OA) to the allylic acetate **32** and generated the Pd(II) intermediate **XXII**, which could trap radical **XXIII** to form the Pd(III) species **XXIV**. This intermediate released the cross-coupled product **34** and Pd(I) upon reductive elimination (RE). The oxidation state of the palladium complex was modulated by the photoredox catalyst, which could reduce Pd(I) to Pd(0), thus securing the turnover of the two interconnected catalytic cycles. Alternative mechanistic pathways, such as the generation of allylic radicals and Pd(0) *via* SET reduction of complex **XXII** or the reduction of Pd(III) to Pd(II) prior to reductive elimination, were not completely ruled out. In a following report, Yu and co-workers showed that other radical precursors prone to SET oxidation such as anilines could be coupled with allylic acetates **32** under the same reaction conditions and comparable efficiency.[46c]

---

[46] (a) Lang, S. B., O'Nele, K. M., Douglas, J. T., Tunge, J. A. "Dual Catalytic Decarboxylative Allylations of α-Amino Acids and Their Divergent Mechanisms" *Chem. Eur. J.* **2015**, *21*, 18589-18593; (b) Zhang, H. H., Zhao, J. J., Yu, S. "Enantioselective Allylic Alkylation with 4-Alkyl-1,4-Dihydro-Pyridines Enabled by Photoredox/Palladium Cocatalysis" *J. Am. Chem. Soc.* **2018**, *140*, 16914-16919; (c) Zhang, H. H., Zhao, J. J., Yu, S. "Enantioselective α-Allylation of Anilines Enabled by a Combined Palladium and Photoredox Catalytic System" *ACS Catal.* **2020**, *10*, 4710-4716. After our studies, few other examples of asymmetric photoredox catalyzed allylic alkylations were reported: (d) Zheng, J., Nikbakht, A., Breit, B. "Dual Palladium/Photoredox-Catalyzed Enantioselective and Regioselective Decarboxylative Hydroaminoalkylation of Allenes" *ACS Catal.* **2021**, *11*, 3343-3350; (e) Xue, S., Limburg, B., Ghorai, D., Benet-Buchholz, J., Kleij, A. W. "Asymmetric Synthesis of Homoallylic Alcohols Featuring Vicinal Tetrasubstituted Carbon Centers via Dual Pd/Photoredox Catalysis" *Org. Lett.* **2021**, *23*, 4447-4451; (f) Song, C., Zhang, H. H., Yu, S. "Regio- and Enantioselective Decarboxylative Allylic Benzylation Enabled by Dual Palladium/Photoredox Catalysis" *ACS Catal.* **2022**, *12*, 1428-1432.
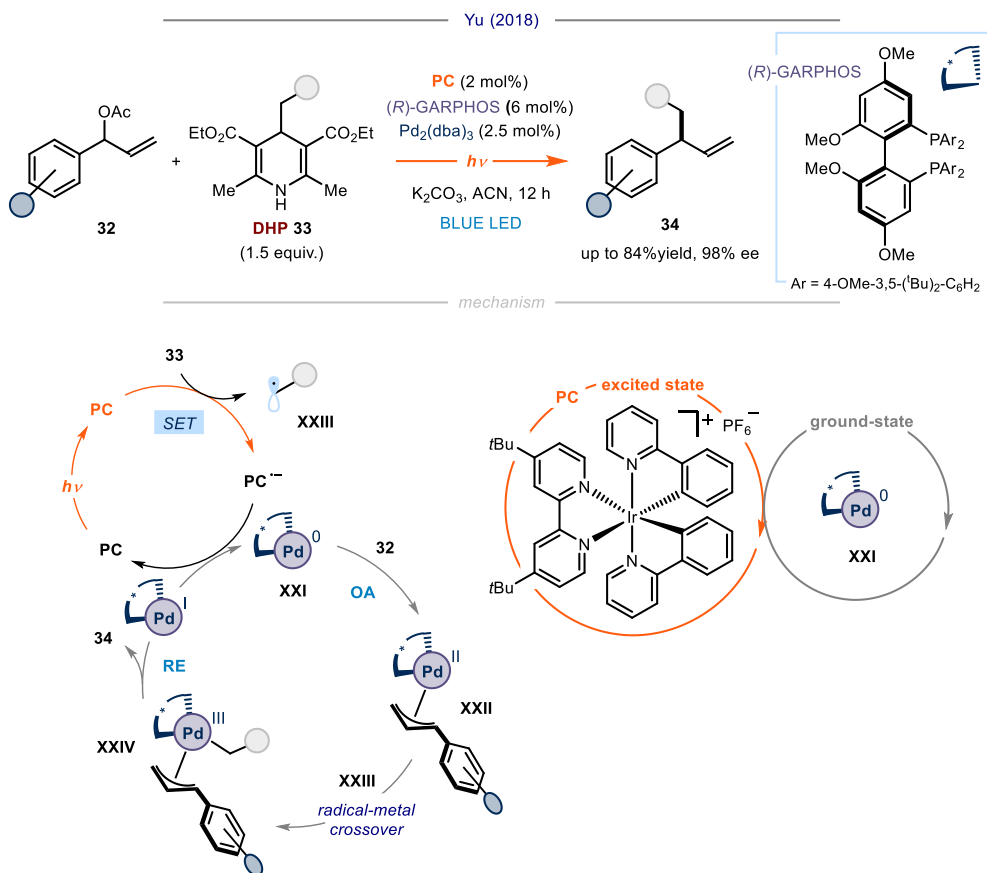
Scheme 2.21. Example of an enantioselective photocatalyzed radical allylic substitution enabled by the interplay of a palladium complex and a photoredox catalyst. OA = oxidative addition; RE = reductive elimination.

The examples discussed so far significantly diverged from our target strategy since in all the cases, the transition-metal catalyst involved was not photoactive and an external photoredox catalyst was required for the radical generation.

2.6 Results and Discussion

2.6.1 Synthesis and studies of complex Ir-III

We started our investigation by synthesizing the chiral phosphoramidite-olefin ligand (*S*)-**L** and the corresponding (η^3-allyl)iridium(III) complex **Ph-Ir-III** from the allylic alcohol **37**, according to a reported procedures (Scheme 2.22).[4,26]

(a)

1. PCl$_3$ (10 equiv.)
   DMF (10 mol%), 50 ºC, 1 h

2. **36**, n-BuLi (1 equiv.)
   THF, -78 ºC, 18 h

(S)-**L**

35

36
(1.05 equiv.)

(b)

Ph-Ir-III

OH

Ph

37
(3 equiv.)

(S)-**L**
(2 equiv.)

[Ir(cod)Cl]$_2$ (1 equiv.)

TfOH (1 equiv.)
CHCl$_3$
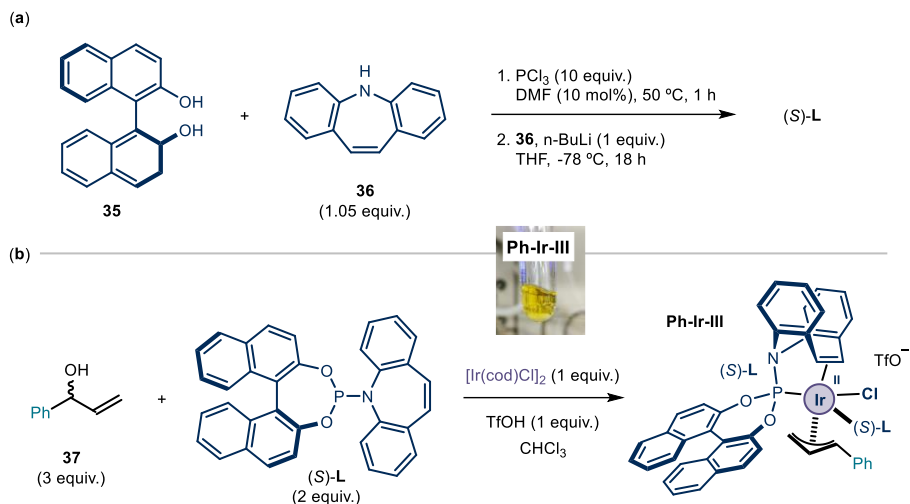
Ph-Ir-III

Scheme 2.22. (a) Synthesis of the phosphoramidite-olefin ligand (S)-**L**; (b) synthesis of the iridium π-allyl complex **Ph-Ir-III** of interest in these studies.

We noticed that complex **Ph-Ir-III** was a dark orange solid after filtration and showed a bright yellow color in chloroform or acetone solution. We therefore recorded the UV-vis absorption spectra of several chloroform solutions of **Ph-Ir-III** at different concentrations (Figure 2.1). In the selected range of concentrations, the absorption spectrum of the complex showed a tail wavelength at around 480 nm, confirming the ability of **Ph-Ir-III** to absorb visible light. An extinction coefficient ε of 930 M^{-1} cm^{-1} was estimated at 460 nm.
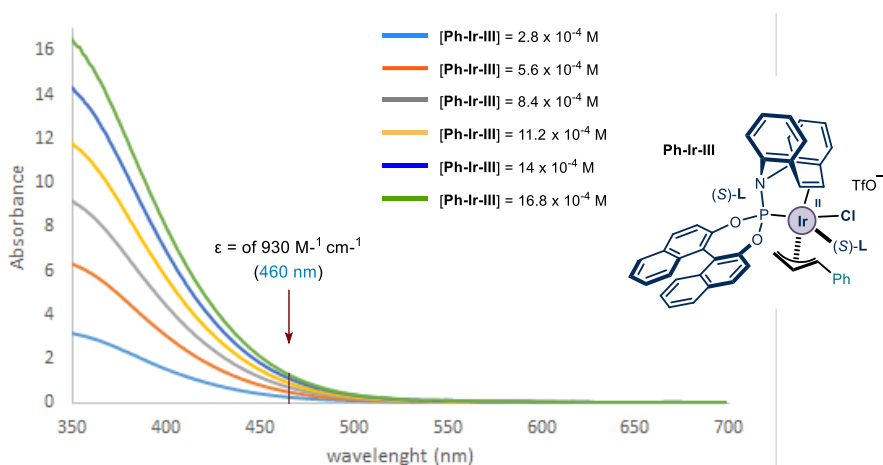
Figure 2.1. UV-vis absorption spectra of **Ph-Ir-III**, recorded at different concentrations in anhydrous CHCl$_3$.

We then evaluated the electrochemical properties of complex **Ph-Ir-III** by performing the differential pulse voltammetry (DPV) analysis under reductive potentials and inert atmosphere (see the *Experimental Section* for details).[47] An irreversible reductive process from Ir(III) to Ir(II) took place with a peak of the maximum cathodic current occurring at a potential of -1.34 V vs Ag/AgNO₃ as reference electrode (Figure 2.2).
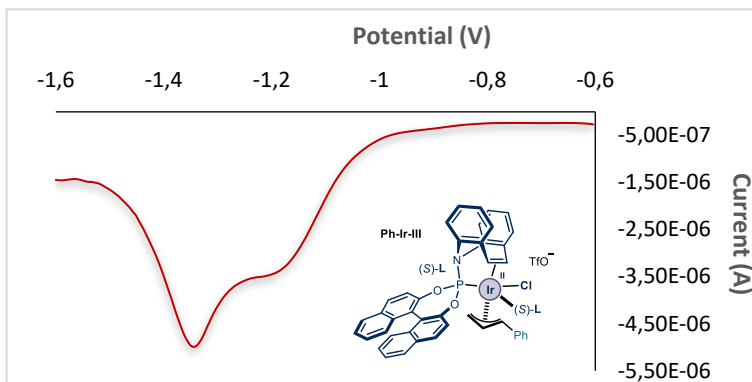
Figure 2.2. Differential pulse voltammogram of 0.005M of **Ph-Ir-III** in DCM in the presence of 0.1 M of TBAPF6. Glassy carbon as working electrode; Ag/AgNO3 (in Et2O) as reference electrode; Pt wire as auxiliary electrode. DCM = dichloromethane; TBAPF6 = tetrabutylammonium hexafluorophosphate.

According to the Rehm-Weller theory,[48] the reduction potential E* of a certain species **X** in its excited state can be calculated using the following approximation:

$$E^{*}(X^{*}/X^{-})=E\ (X/X^{-})+ E_{00}\ (X^{*}/X) \tag{1},$$

where E (X/X^-) is the reduction potential of the species **X** in the ground-state, whereas E_{00} (X^{*}/X) is the energy gap between the excited state and the ground-state. The E_{00} can be approximated with the energy value of the tail of the absorption spectrum. Alternatively, it is estimated as the crossing point of the normalized absorption and emission spectra of species **X** under the same experimental conditions. We used the energy value of 2.58 eV, corresponding to the absorption tail set at 480 nm, and the reduction potential of **Ph-Ir-III** in the ground state, approximated with the potential of -1.34 V corresponding to the peak of the cathodic current. Substituting these parameters in equation (1), the reduction potential of complex **Ph-Ir-III** in the excited state could be estimated as +1.24 V vs Ag/AgNO₃:

$$E^{*}(Ir_{III}^{*}/ Ir_{II})=-1.34\ V+ 2.58\ V= +1.24\ V\ (vs\ Ag/Ag^{+}\ in\ CH_{2}Cl_{2}) \tag{2}$$

---

[47] We thank Prof. A. Llobet and Dr. J. Holub for assistance with differential pulse voltammetry.
[48] Rehm, D., Weller, A., "Kinetics of Fluorescence Quenching by Electron and H-Atom Transfer" *Isr. J. Chem.* **1970**, *8*, 259-262.

This value suggested the ability of complex **Ph-Ir-III** to act as a good SET oxidant in the excited state. The SET oxidation of a redox active radical precursor (substrate **3** in Scheme 2.20a) would be thermodynamically favored when the oxidation potential of this precursor is below the value +1.24 V.

### 2.6.2 Evaluation of the suitable radical precursors

To probe the ability of the (η^3-allyl)iridium(III) complex **Ph-Ir-III** to trigger a SET oxidation of a suitable reaction partner upon visible light photoexcitation, we first tested trimethylsilyl substrates **38** as a class of radical precursors that might engage in the SET oxidation based on previous studies from our group (Scheme 2.23a).[7] These radical precursors generally display moderately low oxidation potentials and the ability to release alkyl radicals upon fragmentation of the trimethylsilyl (TMS) redox auxiliary.[49] Specifically, we identified the carbazolyl-based TMS substrate **39** as a good candidate based on the low redox potential of +1.13 V vs Ag/Ag$^+$ in acetonitrile, corresponding to the first anodic peak in the cyclic voltammetry curve of the redox couple **39$^{\bullet+}$/39** (Scheme 2.23b). Upon oxidation of **39** and mesolytic cleavage of the TMS$^+$ auxiliary, the α-amino alkyl radical **XXVI** would be generated, which is stabilized by the vicinal electron-donating nitrogen atom. We also evaluated different redox active radical precursors delivering radical **XXVI**, such as the potassium trifluoroborate salt[50] **40** and the 4-alkyl-1,4-dihydropyridine (DHP)[51] **41**, which showed lower potentials of +0.98 V and +0.96 V vs Ag/Ag$^+$ in acetonitrile, respectively (Scheme 2.23c). Since 4-alkyl-1,4-dihydropyridines are known to be photoactive alkylating reagents,[52] the absorption spectrum of the DHP substrate **41** was also recorded to evaluate potential filtering effects during visible-light irradiation of **Ph-Ir-III** or interference by photoexcitation of the radical precursor. In this case, substrate **41** bearing the DHP redox auxiliary showed a UV-vis absorption profile at wavelengths below 400 nm in anhydrous dichloromethane (Figure 2.3). Thus, in the range of frequencies used in this study (between 400 nm and 480 nm), the absorption of the DHP precursor **41** did not interfere with the photoexcitation of complex **Ph-Ir-III**.

---

[49] Dockery, K. P., Dinnocenzo, J. P., Farid, S., Goodman, J. L., Gould, I. R., Todd, W. P. "Nucleophile-Assisted Cleavage of Benzyltrialkylsilane Cation Radicals" *J. Am. Chem. Soc.* **1997**, *119*, 1876-1883.

[50] Molander, G. A., Sandrock, D. L. "Potassium trifluoroborate salts as convenient, stable reagents for difficult alkyl transfers" *Curr. Opin. Drug Discov. Devel.* **2009**, *12*, 811-823.

[51] Wang, P. Z., Chen, J. R., Xiao, W. J. "Hantzsch Esters: An Emerging Versatile Class of Reagents in Photoredox Catalyzed Organic Synthesis" *Org. Biomol. Chem.* **2019**, *17*, 6936-6951.

[52] Buzzetti, L., Prieto, A., Roy, S. R., Melchiorre, P. "Radical-Based C–C Bond-Forming Processes Enabled by the Photoexcitation of 4-Alkyl-1,4-Dihydropyridines", *Angew. Chem. Int. Ed.* **2017**, *56*, 15039-15043.
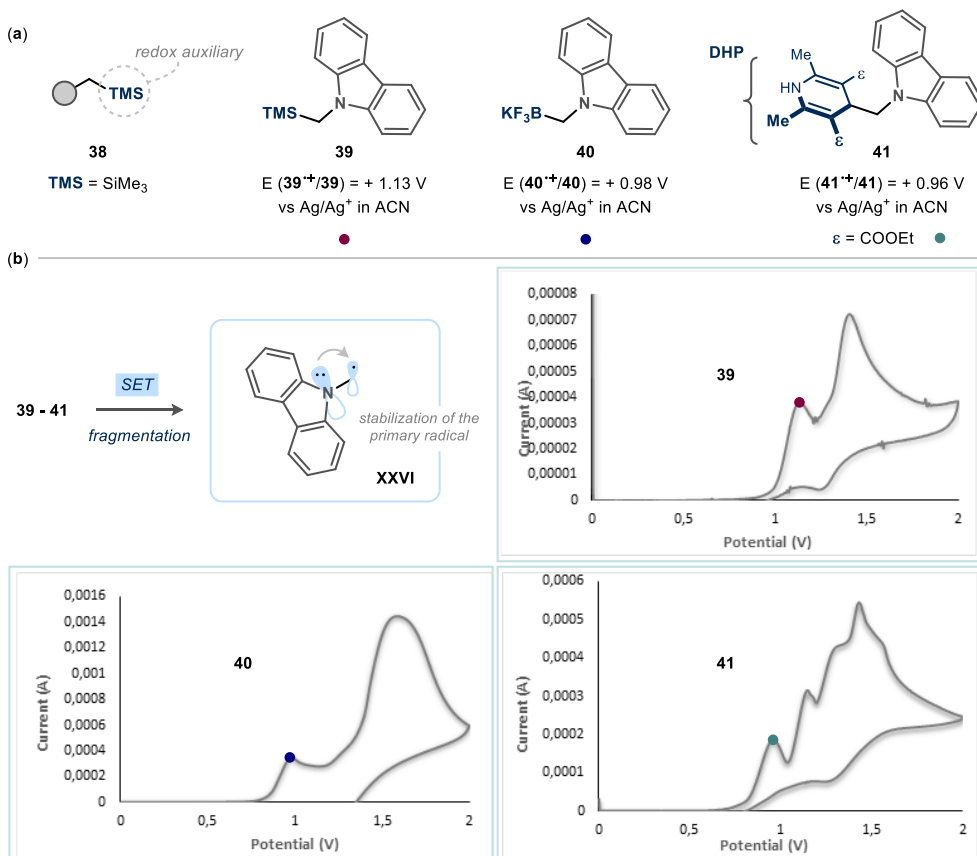
Scheme 2.23. (a) Selection of radical precursors; (b) cyclic voltammograms in 0.1 M TBAPF$_6$ in ACN of: **39** (0.001 M); **40** (0.02 M); **41** (0.02 M). Glassy carbon or platinum as working electrodes; Ag/AgCl (KCl saturated) as reference electrode; Pt wire as auxiliary electrode. ACN = acetonitrile.
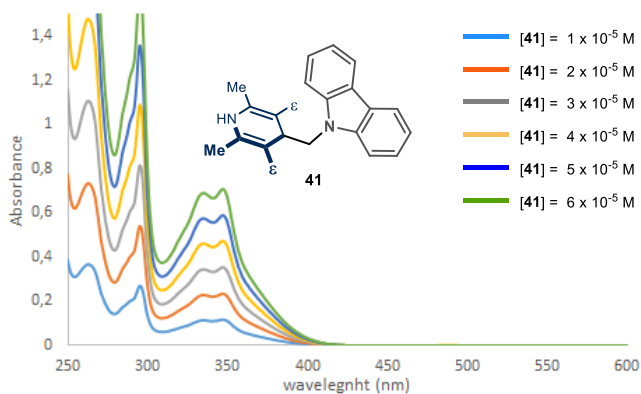
Figure 2.3. UV-vis absorption spectra of 1,4-dihydropyridine **41** recorded at different concentrations in anhydrous DCM. DHP = dihydropyridine.

All the substrates evaluated showed an oxidation potential lower than the E^* of complex **Ph-Ir-III**, thus rendering their SET oxidation by the excited state of **Ph-Ir-III** thermodynamically favored. Therefore, they were tested in the reaction under visible light irradiation (460 nm HP LED - High Power LED -, see the *Experimental Section* for details of the reaction setup) in the presence of racemic 1-phenylprop-2-en-1-ol **37** (2 equiv.), [Ir(cod)Cl]$_2$ as the Ir(I) pre-catalyst (2.5 mol%), the phosphoramidite-olefin ligand (*S*)-**L** (11 mol%) and TFA (trifluoroacetic acid, 1 equiv.) under the reaction conditions detailed in Table 2.1. Gratifyingly, when using the TMS substrate **39**, the cross coupled product **42** was obtained with 58% yield and 86% enantiomeric excess as the sole branched regioisomer (entry 1), in accordance with the traditional selectivity displayed by iridium-based catalysts in asymmetric allylic substitutions (see *Section 2.2*). In a control experiment under dark conditions, product **42** was obtained only in traces, confirming the necessity of visible light irradiation to trigger the transformation (entry 2). The potassium trifluoroborate substrate **40** delivered product **42** in a lower yield of 44% (entry 3), whereas the DHP substrate **41** increased the efficiency of the process delivering product **42** in 81% yield and 88% ee (entry 4). The reaction between the racemic alcohol **37** and the DHP substrate **41** in the presence of the ligand (*R*)-**L** was scaled up to 1 mmol of **41** and, in this case, product (*R*)-**42** was obtained in slightly lower yield and comparable enantiomeric excess (entry 5, see the *Experimental Section* for the details of the setup on a larger scale).

Table 2.1. Evaluation of the best radical precursor among the selected substrates.
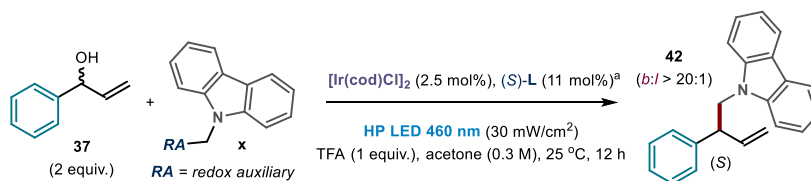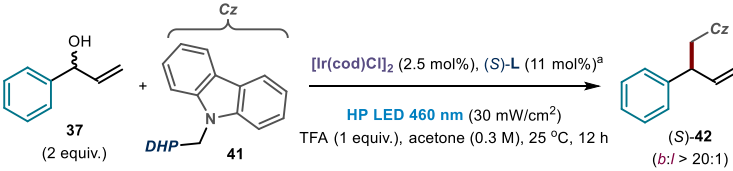
entry	x	deviation	yield **42** (%)	*ee* **42** (%)
1	**39**	none	58	86
2	**39**	dark conditions, 60 ºC	<5	nd
3	**40**	none	44	82
4	**41**	none	81	88
5	**41**	1 mmol scale, (*R*)-**L** as ligand	68	-92

[a]Reactions performed on a 100 µmol scale (300 mM) at 25 °C, pre-treating [Ir(cod)Cl]$_2$ with ligand (*S*)-**L** for 15 minutes before the addition of the other reagents. Yields of **42** are given for the isolated product **42** after silica gel chromatography. HP LED = high power single LED; TFA = trifluoroacetic acid; b:l = branched:linear; n.d. = not determined.

2.6.3 Experiments to probe the photoactivity of complex Ir-III

In the experiments detailed in Table 2.1, the active (η^3-allyl)iridium(III) complex **Ph-Ir-III** was generated in situ. To further confirm the role of **Ph-Ir-III** as the photoactive species, the reaction between the allylic alcohol **37** (2 equiv.) and the DHP substrate **41** (100 µmol) was performed using the pre-formed and isolated π-allyl complex **Ph-Ir-III** (5 mol%) and one equivalent of TFA under 460 nm HP LED irradiation (Table 2.2, entry 1). In this case, product **42** was obtained in 75% yield and 88% enantiomeric excess in accordance with the result obtained upon in situ generation of the active complex. Furthermore, the reaction worked under green light irradiation (525 nm HP LED), delivering product **42** in 57% yield and 84% enantiomeric excess (Table 2.2, entry 2).

Table 2.2. Experiments to confirm the role of the iridium-π-allyl complex as the photoactive species.

entry	deviation	yield **42** (%)	ee **42** (%)
1	**Ph-Ir-III** (5 mol%) instead of Ir(I) and (*S*)-**L**	75	88
2	GREEN LED, 525 nm	57	84
3	**L₁** (5 mol%) instead of (*S*)-**L**	-	nd
4	without iridium catalyst	-	nd
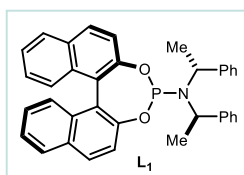
[a]Reactions performed on a 100 µmol scale (300 mM) at 25 °C. Yields of **42** are given for the isolated product after silica gel chromatography. DHP = dihydropyridine; HP LED = high power single LED; TFA = trifluoroacetic acid; b:l = branched:linear; nd = not determined.

This result suggested that the reaction was driven by the sole photoexcitation of **Ph-Ir-III**, which was the only chromophore absorbing at a wavelength close to 525 nm, as confirmed by UV-vis studies (Figure 2.4). The UV-vis spectrum of the reaction mixture was recorded in anhydrous acetone and compared to the UV-vis spectra of the iridium complex **Ph-Ir-III** and of the DHP substrate **41**, both analyzed at a concentration corresponding to the one obtained in the reaction mixture. The absorption of the reaction mixture above 460 nm is mostly given by the absorption of the pre-formed **Ph-Ir-III** complex.
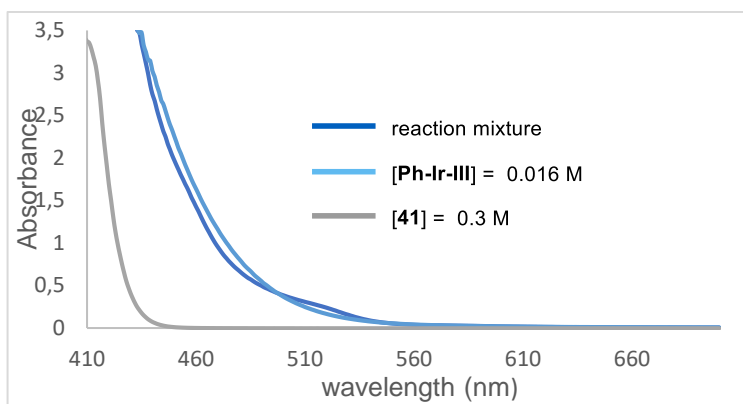
Figure 2.4. UV-vis absorption spectra of **41** (0.3 M), the in situ formed **Ph-Ir-III** (0.016M), and the reaction mixture (0.3 M in **41**) recorded in anhydrous acetone.

The chiral phosphoramidite ligand **L₁**, that is typically used in *type I* iridium-catalyzed allylic substitutions (see *Section 2.2*), did not favor the formation of product **42** when replacing the phosphoramidite-olefin-type ligand (*S*)-**L** (Table 2.2, entry 3). Finally, a control experiment in the absence of the iridium pre-catalyst did not deliver any product (Table 2.2, entry 4).

To further prove the role of complex **Ph-Ir-III** in the radical generation, we performed luminescence quenching studies to evaluate the ability of the excited **Ph-Ir-III** to interact with the carbazolyl-based radical precursor **39** and form the radical by SET oxidation. The following discussion will provide the theoretical background and the details of these experiments.

2.6.3.1 Stern-Volmer Experiments

The emission quenching studies are known as Stern-Volmer quenching experiments.[53] The principles of the excited-state emission quenching and the details of the Stern-Volmer equations and plots are illustrated in Scheme 2.24. The emission of a fluorophore from its excited state **S₁** is usually observed at a higher wavelength than the excitation wavelength (Stokes shift) due to internal vibrational relaxation (Scheme 2.24a). Non-radiative events can also take place, causing a decrease of the fluorescence efficiency. The quenching phenomenon occurs when a quencher **Q** undergoes collisional events with the molecule of the fluorophore in the excited state **S₁** and deactivate the fluorescence emission *via* single electron transfer (SET), energy transfer (EnT), or formation of an exciplex (excited-state complex) and subsequent charge transfer (*dynamic quenching*). Alternatively, a pre-association of the fluorophore and the quencher in the ground state brings to the formation of a non-emitting

---

[53] (a) Lakowicz, J. R. "Principles of Fluorescence Spectroscopy" New York: Springer, 2006; (b) Balzani, V., Ceroni, P., Juris, A. "Photochemistry and Photophysics: Concept, Research and Applications" Weinheim, Wiley-VCH, 2014.

complex that causes a decrease in the number of molecules that populate the excited state S_1 (*static quenching*). In both cases, a decrease of the emission intensity (***I***) is observed (Scheme 2.24b) and the Stern-Volmer plots show a linear correlation between ***I*** and the quencher concentration [**Q**] (Scheme 2.24c). In the case of a static quenching, the Stern-Volmer constant K_S is the equilibrium constant for the pre-association of the two molecules in the ground-state S_0. In a dynamic quenching mechanism, the Stern-Volmer constant k_D has the contribution of the excited-state lifetime τ_0 in the absence of quencher **Q** and of the bimolecular quenching constant k_q, which depends on the collisional frequency (diffusion control) and the efficiency of the quenching event. To distinguish between the two possible mechanisms of quenching, a Stern-Volmer experiment measuring the fluorescence lifetimes should be performed. In fact, the lifetime of the excited state has a linear correlation with the increasing concentration of **Q** in the case of the dynamic quenching, whereas it remains constant in the case of a static quenching. Alternatively, recording the absorption spectra of the fluorophore with and without quencher can give an indication of the mechanism taking place, since a ground-state pre-association of the fluorophore with **Q** that is typical in the static quenching scenario produces a new species which normally displays different absorption properties.
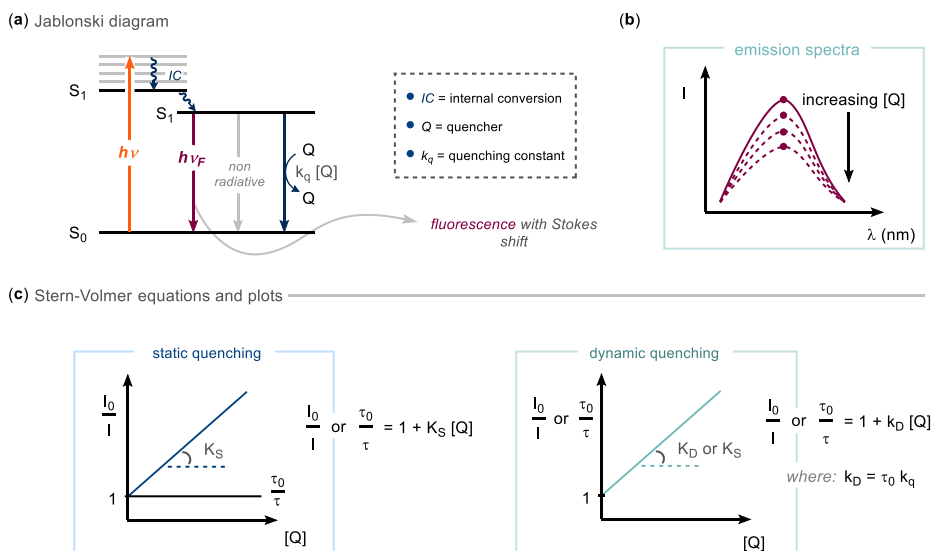
Scheme 2.24. (a) Modified Jablonski diagram showing the non-radiative interaction of a quencher **Q** with the excited state S_1 of a fluorophore; (b) emission spectra of a fluorophore in the presence of increasing amount of a quencher **Q**; (c) Stern-Volmer equations and plots in the two cases of a static or a dynamic quenching. k_q = bimolecular quenching constant; I = emission intensity; I_0 = emission intensity in the absence of **Q**; τ = excited state lifetime; τ_0 = excited state lifetime in the absence of **Q**; K_S = ground-state association constant; k_D = dynamic Stern-Volmer constant.

The emission quenching studies were performed in anhydrous and deaerated chloroform using the isolated complex **Ph-Ir-III** in a concentration as low as 0.1 mM and increasing concentrations of the TMS substrate **39**, which proved competent in the model reaction (Table 2.1, entry 1), as quencher (Figure 2.9, see the *Experimental Section* for more details of the experiment). The emission of complex **Ph-Ir-III** was recorded under the excitation wavelength of 480 nm and showed a maximum around 535 nm. Increasing concentrations of **39** caused a decrease in the emission intensity of complex **Ph-Ir-III** and the Stern-Volmer plot revealed a linear correlation between the ratio I_0/I and the concentration of **39**, with a Stern-Volmer quenching constant K_{SV} of 134 M^{-1}, which was further corrected to 102.8 M^{-1} according to the application of a dilution factor (see the *Experimental Section* for more details).
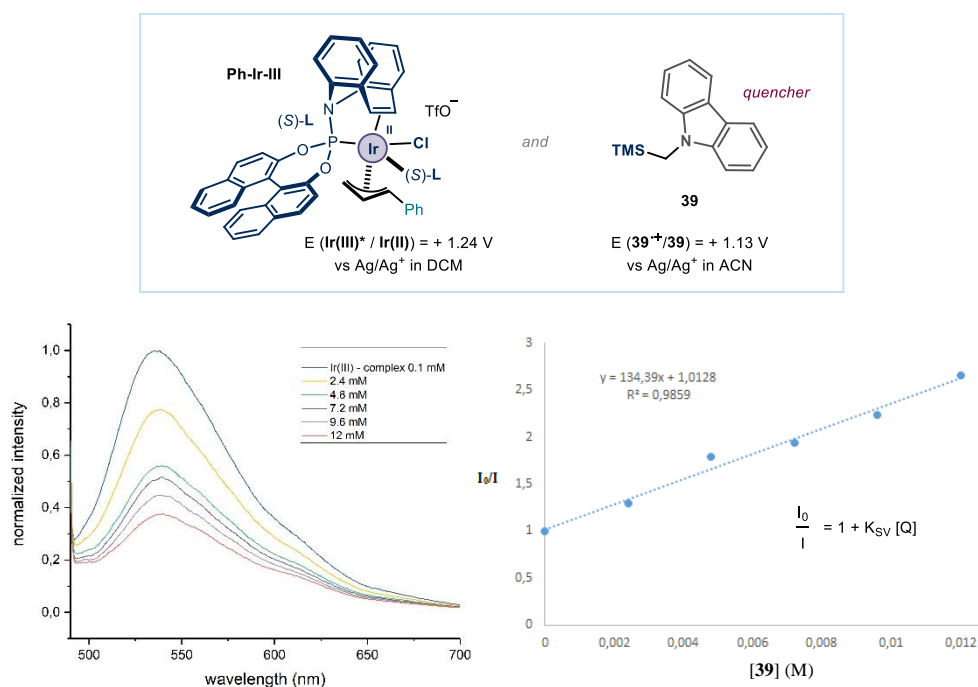
Figure 2.5. Stern-Volmer quenching studies of complex **Ph-Ir-III** (0.1 mM in chloroform) in the presence of substrate **39** as quencher. I_0 = emission intensity in the absence of quencher; I = emission intensity in the presence of quencher; K_{SV} = Stern-Volmer quenching constant.

Based on the observation that the absorbance spectra were not affected by the presence of increasing concentrations of the quencher **39** (see the *Experimental Section*), we excluded the formation of a ground-state pre-associated complex and, therefore, a mechanism based on a dynamic quenching was hypothesized. The quenching event was congruent with the proposed

SET oxidation of the redox active TMS substrate **39** from the excited state of complex **Ph-Ir-III**.

2.6.4 Further optimization studies

Based on the results shown in Table 2.1, we selected the DHP substrate **41** as the best radical precursor for further optimization studies. First, the nature and amount of the allylic precursor employed in the reaction with the DHP substrate **41** were evaluated under the best experimental conditions (Table 2.3). The best result was obtained with 2 equivalents of the allylic alcohol **37** (81% yield of product **42**, entry 4 in Table 2.1 and entry 2 in Table 2.3), whereas the yield of product **42** decreased to 44% yield when only 1 equivalent of **37** was employed (entry 1). Increasing the equivalents of **37** to 3 delivered product **42** in lower yield (entry 3). Finally, the allylic carbonate **38** used in combination with the Lewis acid activation by Sc(OTf)$_3$[54] delivered product **42** in a lower yield of 30% and low enantiomeric excess of 66% (entry 4).

Table 2.3. Optimization of the allylic precursor.

| entry	allylic precursor	y (equiv.)	deviation	yield **42** (%)	ee **42** (%)
1	**37**	**1**	none	44	82
2	**37**	**2**	none	81	88
3	**37**	**3**	none	66	88
4	**38**	**2**	Sc(OTf)$_3$ (10 mol%), no TFA	30	66

[a]Reactions performed on a 100 μmol scale (300 mM) at 25 °C. Yields of **42** are given for the isolated product after silica gel chromatography. DHP = dihydropyridine; HP LED = high power single LED; TFA = trifluoroacetic acid; b:l = branched:linear.

2.6.5 Scope of the method

Having identified the best reaction conditions (Table 2.3, entry 2), the generality of the method was investigated. Different DHP radical precursors were evaluated in the reaction with allylic alcohol **37** (Figure 2.5). Diversely substituted carbazolyl scaffolds bearing an alkyl group (product **43**), halogen atoms (products **44**-**45**, **47**-**49**), or a boronic ester (product **46**) could be

[54] Breitler, S., Carreira, E. M. "Formaldehyde N,N-Dialkylhydrazones as Neutral Formyl Anion Equivalents in Iridium-Catalyzed Asymmetric Allylic Substitution" *J. Am. Chem. Soc.* **2015**, *137*, 5296-5299.

installed on the allylic moiety with good yields (in the range 50-81%) and good enantiomeric excess (in the range of 78-94%). Radical precursors bearing an indole and an oxindole core afforded products **50** and **51**, respectively, both in 51% yield and a high enantiomeric excess of 98%. Other α-amino radical precursors reacted smoothly, allowing the installation of *N*-heterocyclic fragments of pharmaceutical interest, including a quinolone (product **52**) and a 3,4-dihydroquinolone moiety (product **53**), and the scaffold of the antipsychotic *aripiprazole* drug (product **55**), with high enantiomeric excess in all cases. Other biologically active molecules could be coupled with allylic alcohol **37**, such as *N*-protected tryptamine (product **54**), the antiviral *efavirenz* drug (products **56** and **57**), and the scaffold of the pesticide *carbaryl* (product **59**).
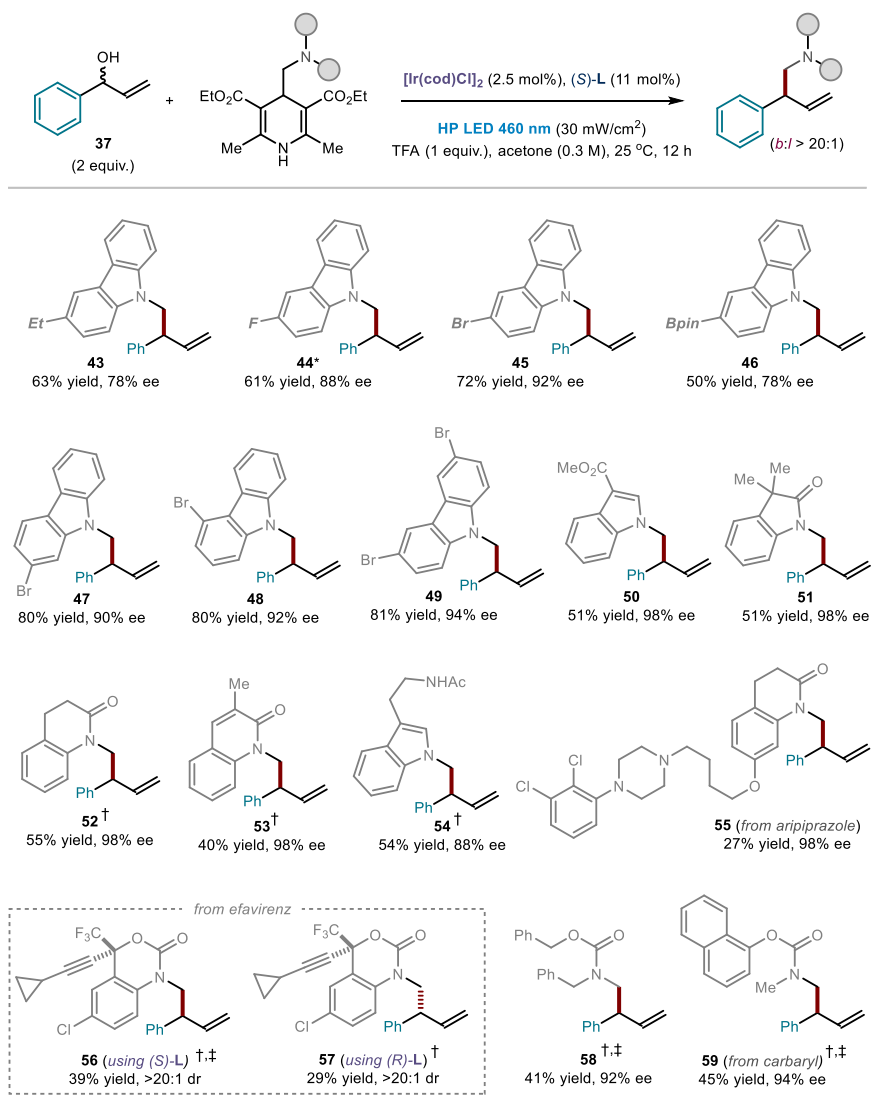
Figure 2.6. Scope of the radical precursors. Reactions performed on a 100 μmol scale. Yields are given for the isolated products as an average of two runs. *Reaction performed with the trimethylsilane radical precursor. †Reaction performed in CHCl₃. ‡Reaction performed using the pre-formed complex **Ph-Ir-III** as the catalyst (5 mol%).

The scope of the allylic alcohols was also investigated using the carbazolyl DHP radical precursor **41** as the model substrate (Figure 2.6). Several aromatic allylic alcohols with alkyl and alkynyl substituents on the phenyl ring were tolerated well under the reaction conditions (products **60-62**, **73**). Also halogen substituents (products **66-68**, **74**), silicon (product **64**) and boron-based groups (product **65**) could be used. Importantly, both electron-donating groups (products **69** and **72**) and electron-withdrawing substituents (product **71**) could be installed in

meta position on the aryl moiety and be tolerated in the reaction. Finally, an extended aromatic system and a 5-membered aromatic ring reacted smoothly, affording products **63** and **70**, respectively.

Figure 2.7. Scope of the allylic precursors. Reactions performed on a 100 μmol scale. Yields are given for the isolated products as an average of two runs. ‡Reaction performed using the pre-formed complex **Ph-Ir-III** as the catalyst (5 mol%). Cz = carbazolyl moiety.

X-ray crystallographic analysis allowed us to unambiguously assign the absolute configuration of products **66** and **67**.

2.6.6 Limitations of the method

Radical precursors that failed delivering the cross-coupled products or offered poor yields are listed in Figure 2.7. A limitation of the method is that secondary alkyl radical precursors proved completely unreactive or, in some cases, low yielding but only when stabilized by an adjacent heteroatom. Benzyl radical precursor **75** proved also unreactive under the optimal experimental conditions. Considering a previous report on the generation of the benzyl radical by direct photoexcitation of substrate **75**,[52] the reaction was repeated under 405 nm irradiation wavelength (Figure 2.7b). Also in this case, the desired cross-coupled product **76** was not observed, whereas complete degradation of substrate **75** resulted in the formation of byproducts **77** and **78**. Other classes of radical precursors, suitable for activation via an SET oxidation, including anilines,[46c] potassium trifluoroborate salts,[50] or tetrahydroisoquinolines,[55] proved unreactive under the optimal experimental conditions.
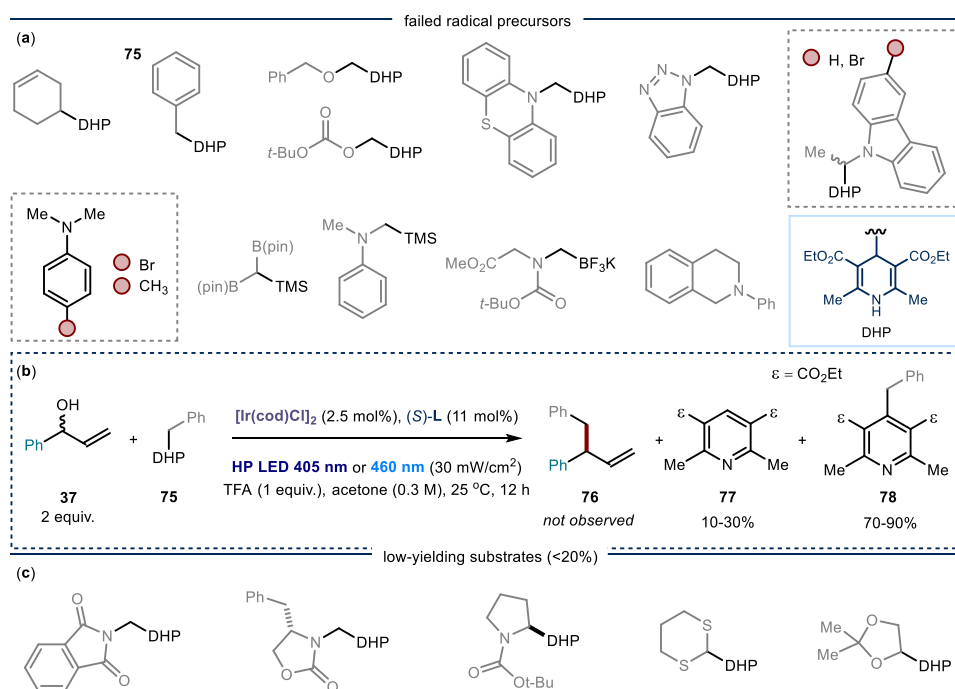
Figure 2.8. Survey of failed and low yielding radical precursors. DHP = dihydropyridine; TMS = trimethylsilyl; pin = pinacol.

[55] Xuan, J., Zeng, T. T., Feng, Z. J., Deng, Q. H., Chen, J. R., Lu, L. Q., Xiao, W. J., Alper, H. "Redox-Neutral α-Allylation of Amines by Combining Palladium Catalysis and Visible-Light Photoredox Catalysis" *Angew. Chem. Int. Ed.* **2015**, *54*, 1625-1628.

Allylic alcohols that failed or proved poorly reactive are listed in Figure 2.8. The major limitations of the method are related to the complete lack of reactivity observed for linear substrates, such as cinnamyl alcohol, allylic alcohols bearing two substituents on the olefin, tertiary alcohols, or conjugated systems. Aliphatic systems can be engaged in thermal iridium-catalyzed allylic substitutions[56] but proved unreactive in the photochemical process based on a radical-reaction mechanism. Finally, allylic alcohols bearing heteroaromatic rings, such as the indole core or *para*-substituted phenyl rings accommodating both electron-donating and electron-withdrawing groups, proved poorly reactive under the experimental conditions.
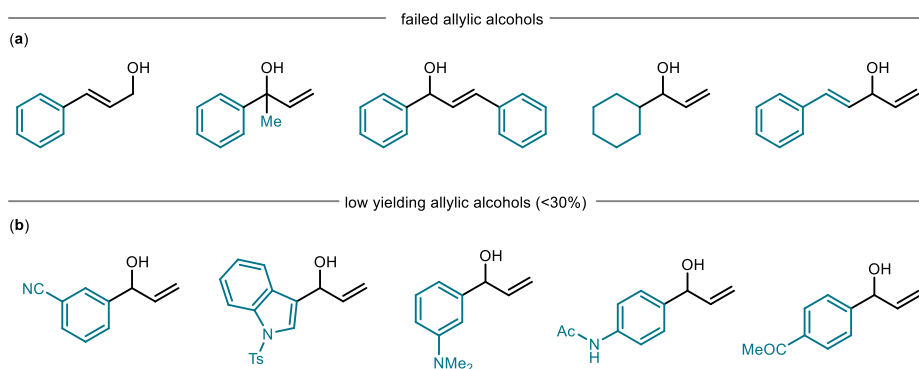
Figure 2.9. Survey of failed and low yielding allylic precursors. Ts = *para*-toluensulfonyl; Ac = acetyl.

2.6.7 Mechanistic Investigations

2.6.7.1 Origin of the Stereoselectivity

To understand the origin of the stereoselectivity, the enantiopure allylic alcohol (*S*)-**37** was reacted with the DHP model substrate **41** in the presence of both *S* and *R*-configured phosphoramidite-olefin ligand **L** under the optimal experimental conditions (Scheme 2.25). The cross-coupled product **42** was obtained with similar yields and enantiomeric excess in the two cases, but opposite absolute configuration. The results indicated that the three-dimensional information inherent to the enantiopure substrate **37** was completely erased during the reaction and that the stereoselectivity of the process was completely dictated by the sole phosphoramidite-olefin chiral ligand. These findings were comparable with the previous studies reported by Carreira for the ground-state reactivity of complex **Ir-III** and discussed in Scheme 2.11 of *Section 2.2*.[26]

[56] Roggen, M., Carreira, E. M. "Enantioselective Allylic Etherification: Selective Coupling of Two Unactivated Alcohols" *Angew. Chem. Int. Ed.* **2011**, *50*, 5568-5571.
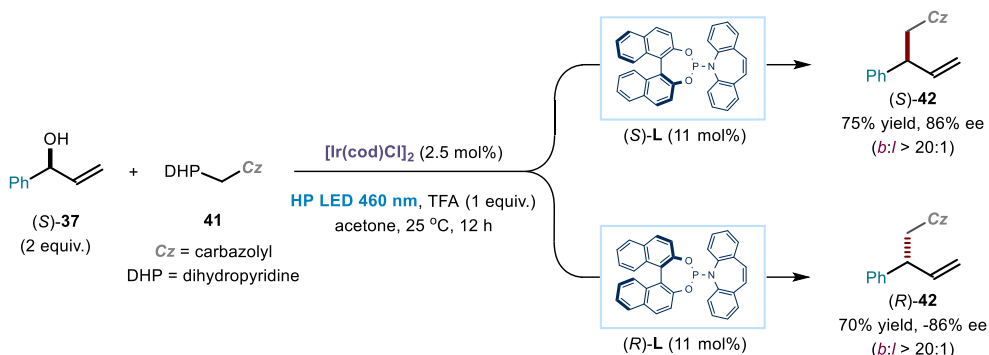
Scheme 2.25. Experiments to probe the origin of the stereoselectivity of the model reaction.

2.6.7.2 Radical Generation and Quantum Yield determination

An indication of the participation of radical species in our process was obtained by conducting the model reaction in the presence of the radical scavenger 2,2,6,6-tetramethylpiperidin-1-yl)oxyl (TEMPO, Scheme 2.26). Product **42** was not observed in the presence of 3 equivalents of TEMPO, and only the TEMPO adduct **79** was isolated in 79% yield, indicating the formation of the carbazolyl radical from substrate **41** and its trapping by the radical scavenger.
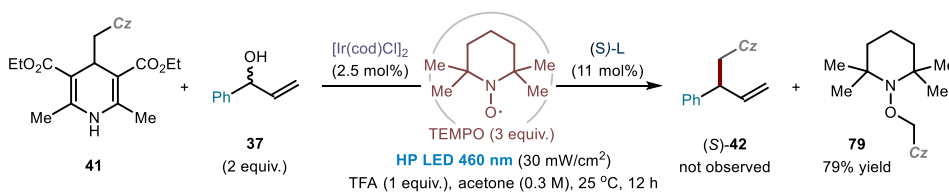
Scheme 2.26. Experiment in the presence of the radical scavenger TEMPO.

To prove the ability of the Ir(III)-π-allyl complex to generate radicals in the excited state by SET oxidation of the DHP substrate **41**, we performed an experiment using the pre-formed complex **Ph-Ir-III** as a photoredox initiator in the presence of substrate **41** and the allyl sulfone **80** as a radical trap (1 equiv.) under visible light irradiation (Scheme 2.27a). Product **81**, resulting from a radical addition-desulfonylation process,[57] was isolated in 47% yield. The reaction required the addition of tris(*para*-bromophenyl)amine (TBPA, E (TBPA[.+]/TBPA) = +1.10 V vs Ag/Ag^{+} in ACN) as a redox mediator to sustain the reactivity[58] due to the
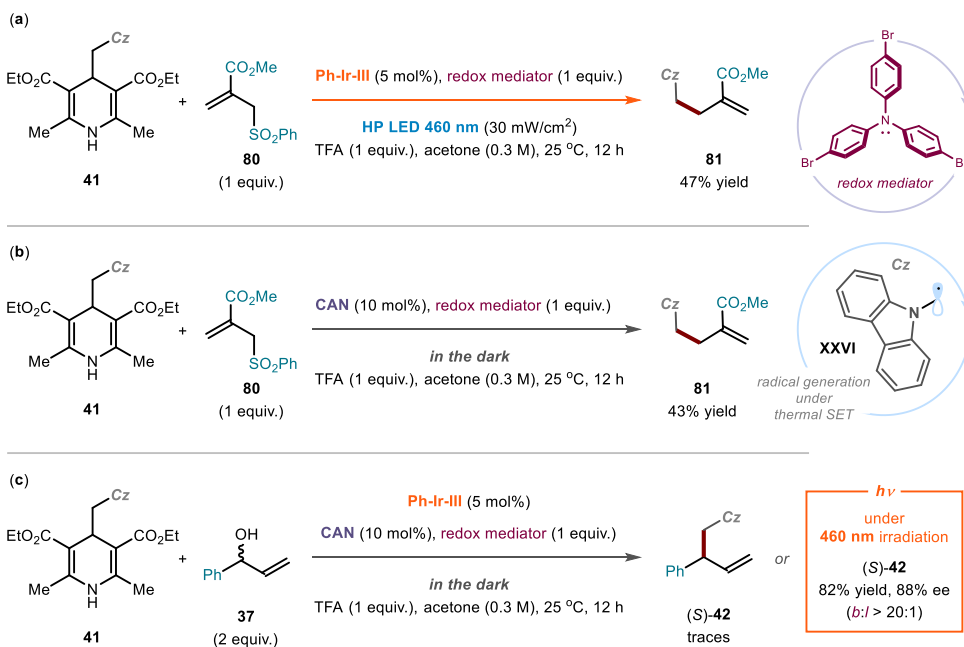
---

[57] Bertrand, F., Le Guyader, F., Liguori, L., Ouvry, G., Quiclet-Sire, B., Seguin, S. & Zard, S. Z. "α-Scission of sulfonyl radicals: a versatile process for organic synthesis" C. R. *Acad. Sci. Ser. IIc* **2001**, *4*, 547-555.

[58] Herath, A. C., Becker, J. Y. "Kinetics of Redox Mediator Tris(4-Bromophenyl) Amine in Acetonitrile and Ionic Liquid [Bmim][PF$_6$]: Oxidation of Benzyl and Cyclohexyl Alcohols" J. *Electroanal. Chem.* **2008**, *619–620*, 98-104.

consumption of **Ph-Ir-III** (the iridium complex was added in catalytic amount). Importantly, product **81** was not observed in control experiments that excluded the iridium catalyst or that were performed under dark conditions.

Importantly, we also generated radical **XXVI** from substrate **41** under thermal conditions and in the dark using a combination of the oxidant CAN (cerium ammonium nitrate) and TBPA as redox mediator. Under these conditions, substrate **41** reacted with the radical trap **80** affording product **81** with a similar yield of 43% (Scheme 2.27b).

Having identified a method to generate radical **XXVI** from DHP **41** (a competent substrate in our cross-coupling protocol) under dark conditions, we investigated if a radical addition to the ground-state electrophilic complex **Ph-Ir-III** could be the key C-C bond forming step of the model reaction. In this case, substrate **41** was allowed to react with allylic alcohol **37** in the presence of the pre-formed iridium complex **Ph-Ir-III** and the CAN/TBPA system for the generation of radical **XXVI** *under dark conditions* (Scheme 2.27c).

Scheme 2.27. (a) Experiment with a radical trap to prove the radical generation from substrate **41** by complex **Ph-Ir-III** used as photo-initiator; (b) alternative generation of radical **XXVI** under thermal conditions; (c) experiments to prove the ability of complex **Ph-Ir-III** to trap radical **XXVI**.

We wanted to check that once radical **XXVI** was generated upon SET oxidation of **41** induced by the CAN/TBPA system and in the dark, the Ir(III)-π-allyl complex, which could operate only via its ground-state reactivity, might serve as a trap for **XXVI** and liberate product **42** and an Ir(II) intermediate (Scheme 2.28). For this step to be the key process in our

photochemical system, the ensuing Ir(II) complex, generated together with product **42**, should be capable of oxidizing substrate **41** and thus regenerate the Ir(I) pre-catalyst together with radical **XXVI**. This mechanism would result in a self-propagation radical process where the photoactivation of complex **Ph-Ir-III** would serve only as an initiation step.
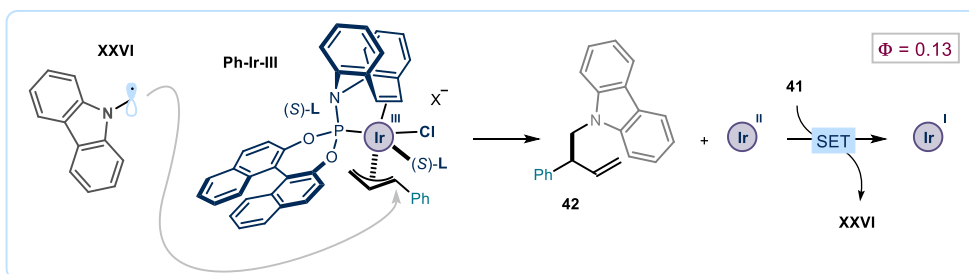
Scheme 2.28. Evaluation of a possible chain mechanism starting from the addition of the open-shell species **XXVI** to the ground-state of the Ir(III) complex **Ph-Ir-III**.

We used the CAN/TBPA to mimic the radical initiation in the absence of visible light. However, the reaction between allylic alcohol **37** (2 equiv.) and DHP **41** conducted in the presence of a catalytic amount of **Ph-Ir-III** and the initiation system CAN/TBPA under dark conditions afforded only traces of product **42** (Scheme 2.27c). This result indicated that, even if radical **XXVI** might add to the ground-state complex **Ph-Ir-III**, this event did not generate an organometallic species suitable for sustaining a radical chain propagation. To prove the compatibility between the iridium catalyst and the CAN/TBPA system, we repeated the same experiment under 460 nm light irradiation and we found that product **42** was formed, this time, in 82% yield and 88% enantiomeric excess.

To further disprove the occurrence of a radical chain mechanism, the quantum yield of the reaction between alcohol **37** and both the TMS substrates **39** and the DHP substrate **41** was measured according to a reported procedure (see the *Experimental Section* for details of the experiments).[59]

The quantum yield (Φ) of a photochemical reaction is a dimensionless value which indicates the number of molecules of product generated in each process that is triggered by the absorption of a single photon by the chromophore. Φ can be expressed with the following ratio:

$$\Phi = \frac{\text{molecules of product}}{\text{number of photons absorbed}}$$

---

[59] Murov, S. L. Ed. "Handbook of Photochemistry" Marcel Dekker, New York, 1973.

If the value of Φ is higher than 1, a chain mechanism is taking place, since more than one molecule of product are generated upon the absorption of each photon. If Φ is lower than 1, a chain mechanism might not take place or, alternatively, a very short or inefficient chain mechanism is taking place.[60]

We measured a value of Φ of 0.13 in the experiment with substrate **39** and 0.8 with substrate **41**. In both cases, Φ was lower than 1, which suggested that a chain mechanism was unlikely.

2.6.8 Mechanistic Proposal

A mechanistic proposal based on the studies described in the previous section is illustrated in Scheme 2.29.
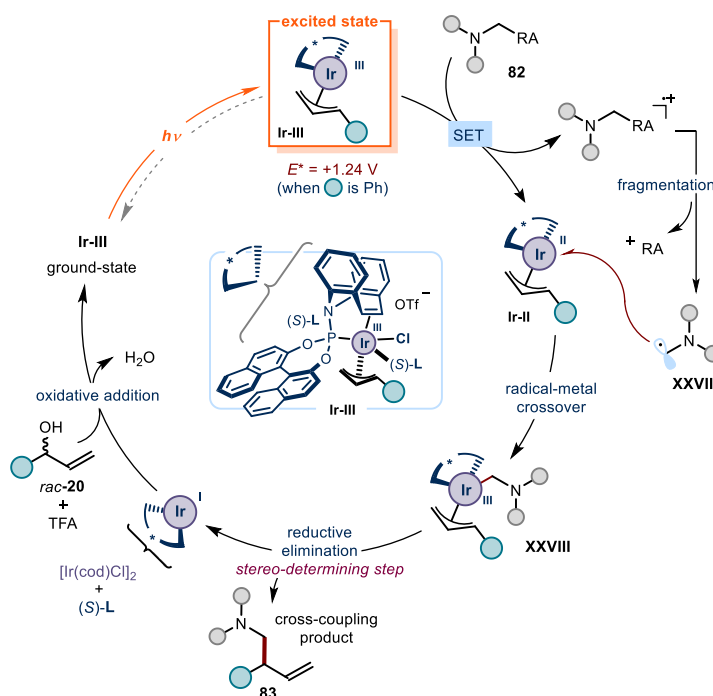
Scheme 2.29. Mechanistic proposal.

The Ir(I) intermediate was generated upon complexation of two molecules of ligand (*S*)-**L** to the metal center deriving from the dissociation of the iridium dimer [Ir(cod)Cl]₂ used as pre-

---

[60] A value of Φ<1 does not completely exclude a radical chain mechanism, since the measured quantum yield does not account for non-productive energy-wasting processes that quench the excited state of the key photoactive species and affect the efficiency of the photo-initiation for a possible chain process. For a review detailing the key aspects of mechanistic studies in photocatalysis, see: Buzzetti, L., Crisenza, G. E. M., Melchiorre, P. "Mechanistic Studies in Photocatalysis" *Angew. Chem. Int. Ed.* **2019**, *58*, 3730-3747.

catalyst. Subsequent oxidative addition of the allylic alcohol **20** promoted by the acid generated complex **Ir-III** and released water. The electrophilic complex **Ir-III** reached the excited state upon visible light absorption and turned into a good SET oxidant. Therefore, it triggered a SET oxidation of a suitable radical precursor **82**, which upon fragmentation delivered the reactive radical **XXVII**. The ensuing **Ir-II** intermediate underwent a radical-metal crossover[44] event recombining with radical **XXVII** to generate the Ir(III) intermediate **XXVIII**. The latter released back the Ir(I) complex and the cross-coupled product **83** upon reductive elimination, which was the stereo-determining step of the transformation. The last step also secured the turnover of the iridium catalyst.

2.7 Conclusion

This project demonstrated that simple visible light irradiation of chiral organometallic intermediates with an established ground-state reactivity can unlock novel catalytic functions to trigger mechanistically different enantioselective processes in the excited state. Specifically, we found that the (η^3-allyl)iridium(III) organometallic complex **Ir-III**, which has been studied thoroughly as a strong electrophile in the thermal domain, becomes a good oxidant in the excited state and promotes a mechanistically novel radical allylic substitution by SET activation of unconventional non-nucleophilic reaction partners. The method allows the preparation of several homoallylic amines with good efficiency and enantioselectivity, including biologically relevant *N*-heterocycles and drug derivatives. Mechanistic investigations were conducted to elucidate the key aspects of the radical generation and subsequent allylation towards the formation of the enantioenriched cross-coupled products.

2.8 Experimental Section

2.8.1 General Information

Copies of the NMR spectra are available in the published manuscript[1] and are not reported in the present dissertation.

The NMR spectra were recorded at 300 MHz, 400 MHz and 500 MHz for ^{1}H, at 75 MHz, 101 MHz and 125 MHz for ^{13}C, at 376 MHz for ^{19}F and at 162 and 202 MHz for ^{31}P. The chemical shifts (δ) for ^{1}H and ^{13}C are given in ppm relative to residual signals of the solvents (CHCl$_3$ @ 7.26 ppm ^{1}H NMR, 77.16 ppm ^{13}C NMR; DMSO @ 2.54 ppm ^{1}H NMR, 40.45 ppm ^{13}C NMR). Coupling constants (*J*) are given in Hz, and are quoted to the nearest 0.5 Hz. The following abbreviations are used to indicate the multiplicity: s, singlet; d, doublet; t, triplet; q, quartet; sext, sextet; hept, heptuplet; m, multiplet. Additionally, signals can be described as broad (br) and apparent (app).

High-resolution mass spectra (HRMS) were obtained from the ICIQ High Resolution Mass Spectrometry Unit on MicroTOF Focus and Maxis Impact (Bruker Daltonics) with

electrospray ionization. Optical rotations were measured on a Polarimeter Jasco P-1030 and are reported as follows: $[\alpha]_D^T$ (c in g per 100 mL, solvent).

UV-vis measurements were carried out on a UV-Vis cary60-TR0 spectrophotometer equipped with photomultiplier detector, double beam optics and D2 and W light sources. Emission spectra were recorded on a Fluorolog Horiba Jobin Yvon spectrofluorimeter, equipped with a photomultiplier detector, a double monochromator, and a 350W xenon light source.

Cyclic voltammetry studies were carried out on a Princeton Applied Research PARSTAT 2273 potentiostat offering compliance voltage up to $\pm$ 100 V (available at the counter electrode), $\pm$ 10 V scan range and $\pm$ 2 A current range. Cyclic voltammetry and differential pulse voltammetry (DPV) analyses, performed on air-sensitive compounds, were obtained using a CH Instruments CHI660C electrochemical workstation installed inside a glovebox, in order to secure measurements under inert atmosphere. The latter experimental set-up was courtesy of the Llobet group at ICIQ.

General Procedures. All reactions were set up under an argon atmosphere in oven-dried glassware using standard Schlenk techniques, unless otherwise stated. Synthesis and HPLC grade solvents were used as purchased. Anhydrous solvents were taken from a commercial SPS solvent dispenser. Chromatographic purification of products was accomplished using force-flow chromatography (FC) on silica gel (35-70 mesh). When required, neutralization of silica gel was accomplished adding 3-4 mL of triethylamine per 150 g of silica powder. For thin layer chromatography (TLC) analyses throughout this work, Merck precoated TLC plates (silica gel 60 GF_{254}, 0.25 mm) were employed. UV light was used as the visualizing agent, and either an ethanol solution of phosphomolybdic acid or basic aqueous potassium permanganate ($KMnO_4$), and heat served as developing agents. Organic solutions were concentrated under reduced pressure on a Büchi rotary evaporator (in vacuo at 40 ºC, ~5 mbar).

Determination of Enantiomeric Purity: HPLC analyses on chiral stationary phase were performed on an Agilent 1200 series HPLC, using a Daicel Chiralpak IC-3 column. UPC^2 analyses on chiral stationary phases were performed on a Waters ACQUITY® UPC^2 instrument, using either Daicel Chiralpak IB-3 and IG-3 columns, or a CHIRALCEL® OJ-3 chiral column. For each compound, the exact conditions for the analysis are specified within the characterization section. HPLC/UPC^2 traces were compared to racemic samples prepared by running the reactions under the conditions specified in *Section 2.8.2*.

Materials: Commercial grade reagents and solvents were purchased at the highest commercial quality from Sigma Aldrich, Fluka, Acros Organics, Fluorochem or Alfa Aesar and used as received, unless otherwise stated. The $[Ir(cod)Cl]_2$ dimer pre-catalyst was purchased from Strem Chemicals. Both the iridium catalyst and the chiral ligands were stored

at -20 ℃, and in the dark, prior to use. Allylic alcohol **37**, also in its enantiopure form, is commercially available and has been purchased from Sigma Aldrich. The synthetic procedures for the preparation of allylic alcohols **20** and DHP (dihydropyridine) substrates are reported in the published manuscript[1] and are not provided in the present dissertation.

2.8.2 General Experimental Procedures

GP1 – General Procedure for the Synthesis of Phosphoramidite-Olefin Ligands
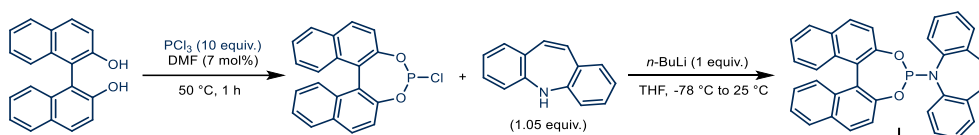
Chiral phosphoramidite-olefin ligands **L** were synthesized according to a modified literature procedure.[4] A 50 mL two-necked flask, equipped with a fractionating column fitted with a distillation apparatus, was sequentially charged with the appropriate enantiomer of 1,1′-bi-2-naphthol (1 equiv.), PCl_3 (10 equiv.) and anhydrous DMF (0.07 equiv.), under argon atmosphere and at ambient temperature. The resulting brown suspension was heated to 50 °C for 1 h forming a brown solution. The mixture was stirred at 80 °C to secure the removal of the excess PCl_3 through a short-path distillation into a flask cooled to –78 °C (*PCl_3 was later quenched by cautious addition of sat. aq. $NaHCO_3$*). Anhydrous toluene (3 × 1 mL) was then added, in three portions, to the remaining residue: each time the solvent was removed under reduced pressure (for 10 min, 10 min and 30 min, respectively). The flask was allowed to cool to ambient temperature and the residue was dissolved in anhydrous THF (0.5 M). In a separate, single-necked 100 mL round-bottomed flask a solution of 5*H*-dibenzo[*b,f*]azepine (1.05 equiv.) in anhydrous THF (0.5 M), at –78 °C, was treated with a 2.5 M solution of *n*-BuLi in hexanes (1 equiv.). The resulting dark violet mixture was stirred at –78 °C for 2 h. Then, a solution of phosphorochloridite in THF was added to the flask by slow dropwise addition. The resulting dark green mixture was slowly allowed to warm up to 15 °C, and stirred for 18 hours. The now orange solution was concentrated to give an orange gum. The crude product was suspended in a mixture of hexane/toluene 2:1 containing 0.5% Et_3N. Celite® (2 g/mmol) was added and the volatiles were removed under reduced pressure. The solid was loaded onto a column and the corresponding chiral phosphoramidite ligand **L** was obtained after flash column chromatography on silica gel (isocratic hexane/toluene 2:1 with 0.5% Et_3N). The title compounds were transferred into argon filled Schlenk vessels and stored at –20 °C.

### 5-((11b*S*)-dinaphtho[2,1-*d*:1',2'-*f*][1,3,2]dioxaphosphepin-4-yl)-5*H*-dibenzo[*b,f*]azepine
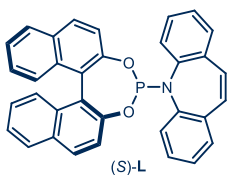
Prepared according to *GP1*, using (*S*)-(–)-1,1′-bi-2-naphthol (1.43 g, 5 mmol), in the presence of PCl$_3$ (4.36 mL, 50 mmol), DMF (25.0 μL, 0.33 mmol), *n*-BuLi (2.00 mL, 5 mmol) and 5H-dibenzo[*b,f*]azepine (1.02 g, 5.25 mmol) in THF (10.0 mL). The reaction afforded phosphoramidite (*S*)-**L** (1.30 g, 51% yield) as a colorless solid. The characterization of this compound was consistent with the data available in the literature.[4]

^{1}H NMR (500 MHz, CDCl$_3$): δ 7.97 (d, *J* = 9.0 Hz, 1H), 7.89 (dd, *J* = 8.5, 1.0 Hz, 1H), 7.74 (dd, *J* = 8.5, 1.0 Hz, 1H), 7.60 (dd, *J* = 9.0, 1.0 Hz, 1H), 7.42 (d, *J* = 9.0 Hz, 1H), 7.41 – 7.31 (m, 2H), 7.29 – 7.12 (m, 9H), 7.11 – 7.06 (m, 1H), 6.98 (d, *J* = 11.5 Hz, 1H), 6.95 – 6.88 (m, 2H), 6.86 – 6.81 (m, 1H), 6.52 (ddd, *J* = 7.5, 1.5 Hz, 1H).

^{13}C NMR (126 MHz, CDCl$_3$): δ 150.0 (d, $^2J_{P-C}$ = 8.0 Hz), 148.9, 143.1 (d, $^2J_{P-C}$ = 24.0 Hz), 142.7, 136.6 (d, $^3J_{P-C}$ = 3.5 Hz), 135.3, 133.0, 132.3, 131.7, 131.6, 131.5, 130.5, 130.3, 129.3, 129.2 (d, $^3J_{P-C}$ = 2.0 Hz), 129.1 (d, $^3J_{P-C}$ = 4.0 Hz), 129.0, 128.7, 128.5, 128.4 (*2 signals*), 128.00, 127.2, 126.9, 126.8, 126.30, 126.2, 125.8, 125.0, 124.4, 124.4 (d, $^3J_{P-C}$ = 5.0 Hz), 122.3 (d, $^3J_{P-C}$ = 1.5 Hz), 121.6, 121.3 (d, $^3J_{P-C}$ = 2.5 Hz).

^{31}P NMR (202 MHz, CDCl$_3$): δ 140.9.

5-((11b*R*)-dinaphtho[2,1-*d*:1',2'-*f*][1,3,2]dioxaphosphepin-4-yl)-5*H*-dibenzo[*b,f*]azepine
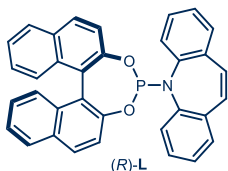
Prepared according to *GP1*, using (*R*)-(+)-1,1′-bi-2-naphthol (1.43 g, 5 mmol), in the presence of PCl$_3$ (4.36 mL, 50.0 mmol), DMF (25.0 μL, 0.33 mmol), *n*-BuLi (2.00 mL, 5 mmol) and 5H-dibenzo[*b,f*]azepine (1.02 g, 5.25 mmol) in THF (10.0 mL). The reaction afforded phosphoramidite (*R*)-**L** (960 mg, 36% yield) as a colorless solid. The characterization of this compound was consistent with the data available in the literature.[4]

Synthesis and Characterization of complex Ph-Ir-III
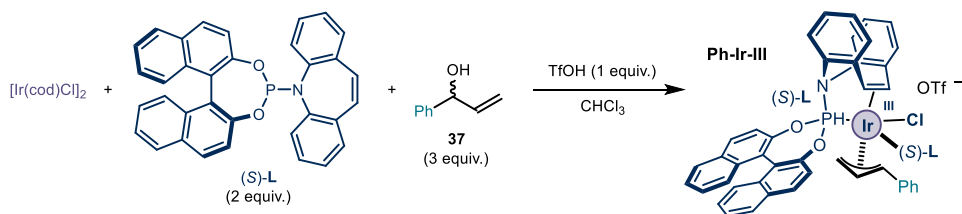
Complex **Ph-Ir-III** was synthesized according to a reported literature procedure.[26] A 10 mL Schlenk flask was charged with [Ir(cod)Cl]$_2$ (67.2 mg, 100 μmol) and ligand (*S*)-**L** (203 mg, 400 μmol), under an argon atmosphere. Allylic alcohol **37** (79.0 μL, 600 μmol) and anhydrous

CHCl$_3$ (5 mL) were sequentially added to the vessel, and the resulting solution was stirred at room temperature for 2 hours. A freshly prepared 1 M solution of trifluoromethanesulfonic acid in anhydrous Et$_2$O (200 μL, 200 μmol) was added to the mixture, dropwise, and the reaction was stirred for additional 15 minutes. The reaction mixture was concentrated under reduced pressure to a third of its volume and treated with anhydrous Et$_2$O (2 mL), affording an ochre precipitate. The supernatant solution was removed via syringe. The solid residue was washed with anhydrous Et$_2$O (3 x 5 mL) and dried under high vacuum to deliver complex **Ph-Ir-III** (300 mg, 99% yield) as an ochre solid. The title compound was transferred into an argon filled Schlenk vessel and stored at –20 °C. The characterization of this compound was consistent with the data available in the literature.[26] Due to its complexity, the ^{1}H NMR spectrum for **Ph-Ir-III** is not detailed, although the characteristic signals of the complex match the ones previously reported in the literature.[26]

^{31}P NMR (162 MHz, CDCl$_3$): δ 108.52 (d, *J* = 31.5 Hz, *major isomer*), 104.99 (d, *J* = 25.0 Hz, *minor isomer*), 72.98 (d, *J* = 24.0 Hz, *minor isomer*), 69.65 (d, *J* = 31.5 Hz, *major isomer*). ^{19}F NMR (376 MHz, CDCl$_3$): δ -78.07.

GP2 - General Procedure for the Asymmetric Photochemical Ir-Catalyzed Cross-Coupling
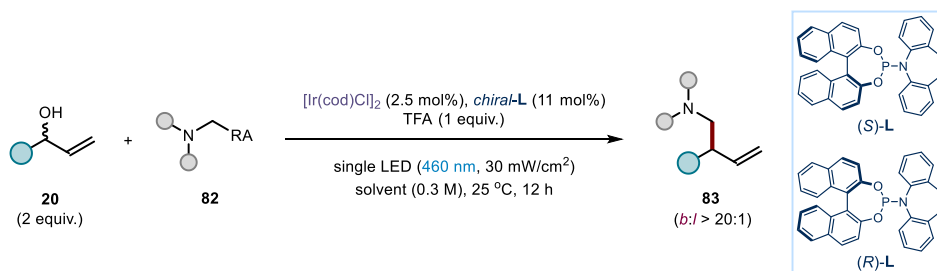
A screw-capped vial, fitted with a rubber septum, was charged with [Ir(cod)Cl]$_2$ (1.7 mg, 2.50 μmol, 2.5 mol%), the appropriate enantiomer of chiral ligand **L** (5.6 mg, 11.0 μmol, 11 mol%) and anhydrous, argon-purged reaction solvent (300 μL), under an argon atmosphere. The resulting solution was vigorously stirred for 15 minutes and then transferred to a Schlenk tube containing the allylic alcohol **20** (200 μmol, 2 equiv.) and the radical precursor **82** (100 μmol, 1 equiv.), affording a yellow solution. TFA (7.7 μL, 100 μmol, 1 equiv.) was added to this solution and the Schlenk tube was sealed with a screw-cap. The vessel was placed into a 3D-printed plastic support mounted on an aluminum block fitted with a 460 nm high-power single LED (λ = 460 nm, irradiance = 30 mW/cm^2 as controlled by an external power supply; a detailed representation of the set-up is depicted in Figure 2.10). This set-up secured a reliable irradiation while keeping a constant distance of 1 cm between the bottom of the reaction vessel and the light source. The reaction was stirred under visible light irradiation at ambient temperature for 12 hours, prior to removal of the solvent under reduced pressure. Purification

of the crude mixture by flash column chromatography on silica gel gave the corresponding products **83** in the stated yield and enantiomeric purity. All of the obtained cross-coupled products were previously unknown.

When pre-formed complex **Ph-Ir-III** was used as the catalyst, a solution of the latter (7.6 mg, 5 mol%) in 300 μL of the appropriate solvent was directly charged into the reaction vessel, containing **20** and **82**.
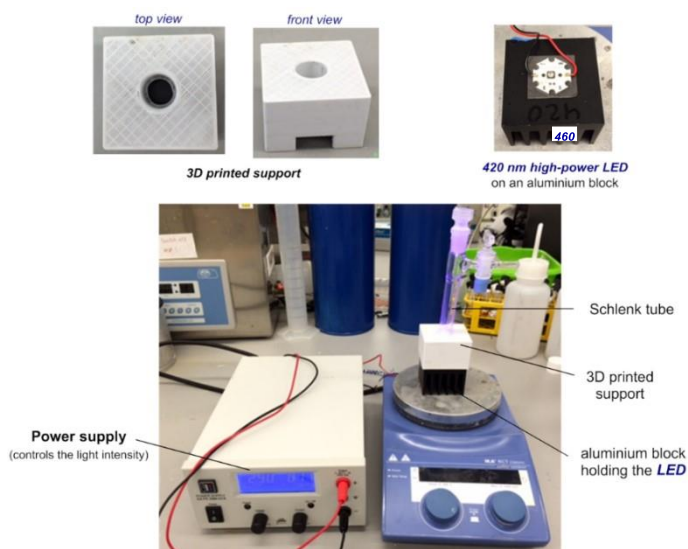
Figure 2.10. Reaction set-up. The light source for illuminating the reaction vessel consisted in a 460 nm high-power single LED (LZ1-00DB00) purchased from OSA OPTO.

GP3 – General Procedure for the Synthesis of the Racemic Samples
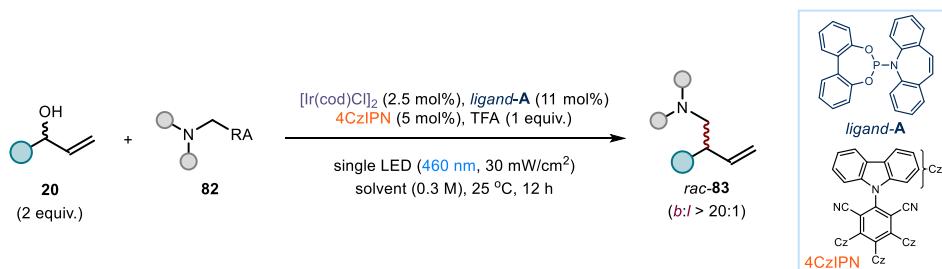
The synthesis of the racemic products **83**, needed for enantiomeric excess determination, was initially attempted performing protocol *GP2* in the presence of 11 mol% of an equimolar mixture of ligands (*S*)-**L** and (*R*)-**L**. However, the resulting racemic (η^3-allyl)iridium(III) complex was insoluble in the reaction solvents, thwarting the efficiency of the photochemical method. To overcome this issue, a different procedure was developed (depicted in the diagram

above): the reaction was carried out in the presence of ligand **A** and photocatalyst 4CzIPN, both of which were synthesized according to reported procedures.[4,61] In all cases, this protocol delivered the corresponding racemic products **83** with decreased chemical yield compared to our asymmetric photochemical method (*GP2*).

Procedure for the Asymmetric Photochemical Ir-Catalyzed Cross-Coupling in Large Scale
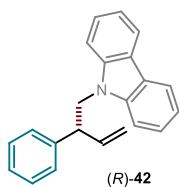
A screw-capped vial, fitted with a rubber septum, was charged with [Ir(cod)Cl]$_2$ (17.0 mg, 25.0 µmol), chiral ligand (*R*)-**L** (56.0 mg, 110.0 µmol) and anhydrous, argon-sparged acetone (3 mL), under an argon atmosphere. The resulting solution was vigorously stirred for 15 minutes and, then, transferred to a 20 mL Schlenk tube containing 1,4-dihydropyridine **41** (1.00 mmol) and allylic alcohol **37** (2.00 mmol), affording a yellow solution. TFA (78.0 µL, 1.00 mmol) was added to this solution and the vial was sealed with a glass stopper. The vessel was placed into a HepatoChem PhotoRedox TC photoreactor, fitted with an EvoluChem™ lamp (λ = 450-455 nm), and connected to a programmable chiller, securing the temperature to be kept at 25 ºC (Figure 2.11). The reaction was stirred under visible light irradiation for 18 hours, prior to removal of the solvent under reduced pressure. Purification of the crude mixture by flash column chromatography on silica gel (isocratic 5% PhMe in hexane) afforded product (*R*)-**42** (200 mg, 68% yield, 88% ee) as a colorless oil. The enantiomeric ratio was determined by UPC^2 analysis on a Daicel Chiralpak IB-3 column: gradient CO$_2$/CH$_3$CN from 100% CO$_2$ to 60:40 over 9 minutes, curve 6, flow rate 2 mL/min, λ = 260 nm: τ$_{minor}$ = 4.1 min, τ$_{major}$ = 4.3 min. ; [α]$_D^{26}$ = -6.9 (c = 0.23, CH$_2$Cl$_2$, 88% ee). The spectra obtained for compound (*R*)-**42** were identical to those obtained for (*S*)-**42**, detailed below.

[61] Luo, J., Zhang, J. "Donor-acceptor fluorophores for visible-light-promoted organic synthesis: photoredox/Ni dual catalytic C(sp$_3$)–C(sp$_2$) cross-coupling" *ACS Catal.* **2016**, *6*, 873-877.
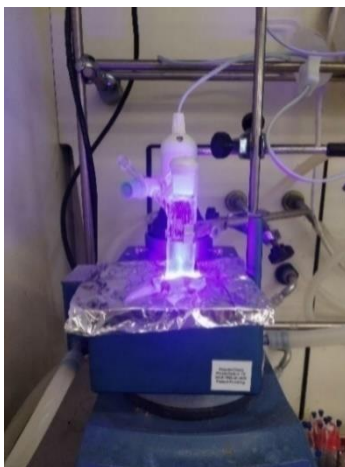
Figure 2.11. Large scale reaction set-up. The light source for illuminating the reaction vessel consisted in a 450-455 nm EvoluChemTM lamp.

2.8.3 Characterization of Products

(*S*)-9-(2-phenylbut-3-en-1-yl)-9*H*-carbazole (42)
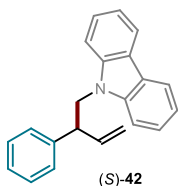
Prepared according to *GP2*, using [Ir(cod)Cl]$_2$/(*S*)-**L** as the catalytic system, diethyl 4-((9*H*-carbazol-9-yl)methyl)-2,6-dimethyl-1,4-dihydropyridine-3,5-dicarboxylate **41** (43 mg, 100 µmol) and 1-phenylprop-2-en-1-ol **37** (26 µL, 200 µmol) as the substrates, and performing the reaction in acetone. The crude mixture was purified by flash column chromatography (isocratic 5% PhMe in hexane) to afford product (*S*)-**42** (24 mg, 80% yield, 88% ee) as a colorless oil. The enantiomeric excess was determined by UPC^2 analysis on a Daicel Chiralpak IB-3 column: gradient CO$_2$/CH$_3$CN from 100% CO$_2$ to 60:40 over 4 minutes, curve 6, flow rate 2 mL/min, λ = 260 nm: τ$_{major}$ = 4.1 min, τ$_{minor}$ = 4.3 min; [α]$_D^{26}$ = +2.0 (c = 1.00, CH$_2$Cl$_2$, 88% ee).

^{1}H NMR (500 MHz, CDCl$_3$): δ 8.06 (dt, *J* = 7.5, 1.0 Hz, 2H), 7.38 (ddd, *J* = 8.5, 7.0, 1.0 Hz, 2H), 7.27 – 7.21 (m, 4H), 7.22 – 7.14 (m, 5H), 6.13 (ddd, *J* = 17.0, 10.5, 7.5 Hz, 1H), 5.01 (dt, *J* = 10.5, 1.0 Hz, 1H), 4.95 (dt, *J* = 17.0, 1.5 Hz, 1H), 4.61 (dd, *J* = 14.5, 8.0 Hz, 1H), 4.48 (dd, *J* = 14.5, 7.0 Hz, 1H), 4.02 (app q, *J* = 7.5 Hz, 1H).

^{13}C NMR (126 MHz, CDCl$_3$): δ 141.4, 140.7, 138.4, 128.8, 127.9, 127.2, 125.6, 123.0, 120.4, 119.0, 117.0, 109.1, 49.4, 49.1.

HRMS (ESI) Exact mass calculated for C$_{22}$H$_{20}$N [M+H]$^+$: 298.1590, found: 298.1592.

(*S*)-3-ethyl-9-(2-phenylbut-3-en-1-yl)-9*H*-carbazole (43)
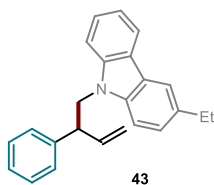
Prepared according to *GP2*, using [Ir(cod)Cl]$_2$/(*S*)-**L** as the catalytic system, diethyl 4-((3-ethyl-9*H*-carbazol-9-yl)methyl)-2,6-dimethyl-1,4-dihydropyridine-3,5-dicarboxylate (46 mg, 100 µmol) and 1-phenylprop-2-en-1-ol **37** (26 µL, 200 µmol) as the substrates, and performing the reaction in acetone. The crude mixture was purified by flash column chromatography (isocratic 5% PhMe in hexane) to afford product **43** (20.5 mg, 63% yield, 78% ee) as a pale yellow oil. The enantiomeric excess was determined by UPC^2 analysis on a Daicel Chiralpak IB-3 column: gradient CO$_2$/CH$_3$CN from 100% CO$_2$ to 60:40 over 4 minutes, curve 6, flow rate 2 mL/min, λ = 260 nm: τ_{major} = 5.0 min, τ_{minor} = 5.4 min; $[\alpha]_D^{26}$ = +0.9 (c = 0.22, CHCl$_3$, 78% ee). The absolute configuration for the title compound was assigned in comparison to compounds **66** and **67**.

<u>^{1}H NMR</u> (400 MHz, CDCl$_3$): δ 8.08 (dt, *J* = 7.5, 1.0 Hz, 1H), 7.93 (t, *J* = 1.0 Hz, 1H), 7.40 (ddd, *J* = 8.5, 7.0, 1.0 Hz, 1H), 7.36 – 7.17 (m, 9H), 6.18 (ddd, *J* = 17.5, 10.5, 7.5 Hz, 1H), 5.06 (dt, *J* = 10.5, 1.0 Hz, 1H), 4.99 (dt, *J* = 17.5, 1.0 Hz, 1H), 4.64 (dd, *J* = 14.5, 8.0 Hz, 1H), 4.51 (dd, *J* = 14.5, 6.5 Hz, 1H), 4.07 (q, *J* = 7.5 Hz, 1H), 2.87 (q, *J* = 7.5 Hz, 2H), 1.38 (t, *J* = 7.5 Hz, 3H).

<u>^{13}C NMR</u> (101 MHz, CDCl$_3$): δ 141.5, 141.0, 139.2, 138.5, 135.0, 128.8, 127.9, 127.1, 126.0, 125.4, 123.1, 122.9, 120.2, 119.1, 118.7, 117.0, 109.0, 108.8, 49.5, 49.2, 29.0, 16.6.

<u>HRMS (ESI)</u> Exact mass calculated for C$_{24}$H$_{23}$N [M+H]$^+$: 326.1903, found: 326.1903.

(*S*)-3-fluoro-9-(2-phenylbut-3-en-1-yl)-9*H*-carbazole (44)
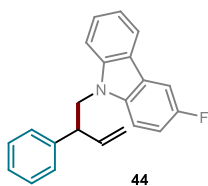
Prepared according to *GP2*, using [Ir(cod)Cl]$_2$/(*S*)-**L** as the catalytic system, 3-fluoro-9-((trimethylsilyl)methyl)-9*H*-carbazole (27 mg, 100 µmol) and 1-phenylprop-2-en-1-ol **37** (26 µL, 200 µmol) as the substrates, and performing the reaction in acetone. The crude mixture was purified by flash column chromatography (isocratic 5% PhMe in hexane) to afford product **44** (19.5 mg, 61% yield, 88% ee) as a colorless wax. The enantiomeric excess was determined by UPC^2 analysis on a Daicel Chiralpak IB-3 column: gradient CO$_2$/CH$_3$CN from 100% CO$_2$ to 60:40 over 4 minutes, curve 6, flow rate 2 mL/min, λ = 260 nm: τ_{major} = 3.4 min, τ_{minor} = 3.5 min; $[\alpha]_D^{26}$ = -13.3 (c = 0.21, CHCl$_3$, 88% ee). The absolute configuration for the title compound was assigned in comparison to compounds **66** and **67**.

<u>^{1}H NMR</u> (400 MHz, CDCl$_3$): δ 8.01 (d, *J* = 8.0 Hz, 1H), 7.74 – 7.67 (m, 1H), 7.42 (ddd, *J* = 8.5, 7.0, 1.0 Hz, 1H), 7.30 – 7.05 (m, 9H), 6.15 (ddd, *J* = 17.5, 10.5, 7.5 Hz, 1H), 5.06 (dd, J = 10.5, 1.0 Hz, 1H), 5.00 (dt, J = 17.0, 1.0 Hz, 1H), 4.61 (dd, *J* = 14.5, 8.0 Hz, 1H), 4.48 (dd, *J* = 14.5, 7.0 Hz, 1H), 4.00 (q, *J* = 7.5 Hz, 1H).

^{13}C NMR (101 MHz, CDCl$_3$): δ δ 157.3 (d, [1]J_{C-F} = 235.2 Hz), 141.5, 141.2, 138.3, 137.1, 128.8, 127.9, 127.2, 126.2, 123.3 (d, [3]J_{C-F} = 9.4 Hz), 122.5 (d, J = 4.1 Hz), 120.6, 119.0, 117.1, 113.3 (d, [2]J_{C-F} = 25.5 Hz), 109.6 (d, [3]J_{C-F} = 9.0 Hz), 109.3, 106.0 (d, [2]J_{C-F} = 23.7 Hz), 49.4, 49.3.

^{19}F NMR (376 MHz, CDCl$_3$) δ -125.39 – -125.47 (m, 1F).

HRMS (ESI) Exact mass calculated for C$_{22}$H$_{18}$FN [M+H]$^+$: 316.1496, found: 316.1494.

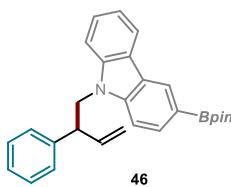### (*S*)-3-bromo-9-(2-phenylbut-3-en-1-yl)-9*H*-carbazole (45)
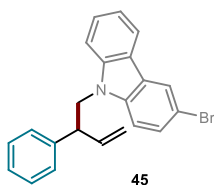
Prepared according to *GP2*, using [Ir(cod)Cl]$_2$/(*S*)-**L** as the catalytic system, diethyl 4-((3-bromo-9*H*-carbazol-9-yl)methyl)-2,6-dimethyl-1,4-dihydropyridine-3,5-dicarboxylate (51 mg, 100 µmol) and 1-phenylprop-2-en-1-ol **37** (26 µL, 200 µmol) as the substrates, and performing the reaction in acetone. The crude mixture was purified by flash column chromatography (isocratic 5% PhMe in hexane) to afford product **45** (27.5 mg, 72% yield, 92% ee) as a colorless wax. The enantiomeric excess was determined by UPC^2 analysis on a Daicel Chiralpak IB-3 column: gradient CO$_2$/CH$_3$CN from 100% CO$_2$ to 60:40 over 9 minutes, curve 6, flow rate 2 mL/min, λ = 260 nm: τ$_{major}$ = 4.9 min, τ$_{minor}$ = 5.1 min; [α]$_D^{26}$ = -6.8 (c = 0.31, CHCl$_3$, 92% ee). The absolute configuration for the title compound was assigned in comparison to compounds **66** and **67**.

^{1}H NMR (400 MHz, CDCl$_3$): δ 8.19 (d, J = 2.0 Hz, 1H), 8.04 (dt, J = 8.0, 1.0 Hz, 1H), 7.51 – 7.41 (m, 2H), 7.34 – 7.21 (m, 5H), 7.20 – 7.14 (m, 2H), 7.11 (d, J = 8.5 Hz, 1H), 6.13 (ddd, J = 17.0, 10.5, 7.5 Hz, 1H), 5.09 (dt, J = 10.5, 1.0 Hz, 1H), 5.02 (dt, J = 17.0, 1.0 Hz, 1H), 4.63 (dd, J = 14.5, 8.0 Hz, 1H), 4.50 (dd, J = 14.5, 7.0 Hz, 1H), 4.02 (q, J = 7.5 Hz, 1H).

^{13}C NMR (101 MHz, CDCl$_3$): δ 141.1, 140.9, 139.3, 138.2, 128.9, 128.2, 127.8, 127.3, 126.4, 124.6, 123.1, 122.0, 120.6, 119.5, 117.2, 111.8, 110.5, 109.3, 49.3, 49.2.

HRMS (ESI) Exact mass calculated for C$_{22}$H$_{18}$BrN [M+H]$^+$: 376.0695, found: 376.0679.

(*S*)- 9-(2-phenylbut-3-en-1-yl)-3-(4,4,5,5-tetramethyl-1,3,2-dioxaborolan-2-yl)-9*H*-carbazole (46)

Prepared according to *GP2*, using [Ir(cod)Cl]$_2$/(*S*)-**L** as the catalytic system, 3-(4,4,5,5-tetramethyl-1,3,2-dioxaborolan-2-yl)-9-((trimethyl -silyl)methyl)-9*H*-carbazole (38. mg, 100 µmol) and 1-phenylprop-2-en-1-ol **37** (26 µL, 200 µmol) as the substrates, and performing the reaction in acetone. The crude mixture was purified by flash column chromatography (isocratic 5% PhMe in hexane) to afford product **46** (21 mg, 50% yield, 78% ee) as an off-white wax. The enantiomeric excess was determined by UPC^2 analysis on a Daicel Chiralpak IB-3 column: gradient CO$_2$/CH$_3$CN from 100% CO$_2$ to 60:40

over 4 minutes, curve 6, flow rate 2 mL/min, λ = 260 nm: τ_{major} = 3.8 min, τ_{minor} = 4.00 min; $[\alpha]_D^{26}$ = -11.5 (c = 0.23, CHCl$_3$, 78% ee). The absolute configuration for the title compound was assigned in comparison to compounds **66** and **67**.

^{1}H NMR (400 MHz CDCl$_3$): δ 8.57 (t, J = 1.0 Hz, 1H), 8.12 – 8.09 (m, 1H), 7.85 (dd, J = 8.0, 1.0 Hz, 1H), 7.39 (ddd, J = 8.5, 7.0, 1.0 Hz, 1H), 7.29 – 7.17 (m, 8H), 6.13 (ddd, J = 17.0, 10.5, 7.5 Hz, 1H), 5.01 (dt, J = 10.5, 1.0 Hz, 1H), 4.94 (dt, J = 17.0, 1.0 Hz, 1H), 4.51 (dd, J = 14.5, 7.0 Hz, 1H), 6.13 (ddd, J = 17.0, 10.5, 7.5 Hz, 1H), 4.03 (q, J = 7.5 Hz, 1H), 1.40 (s, 12H).

^{13}C NMR (101 MHz, CDCl$_3$): δ δ 142.8, 141.2, 140.7, 138.3, 132.2, 128.9, 128.8, 128.8, 127.9, 127.8, 127.7, 127.2, 125.7, 123.2, 122.7, 120.6, 119.4, 117.1, 109.1, 108.5, 83.7, 49.3, 49.0, 25.1, 25.1.

HRMS (ESI) Exact mass calculated for C$_{28}$H$_{30}$BNO$_2$ [M+H]$^+$: 423.2479, found: 423.2471.

(*S*)-2-bromo-9-(2-phenylbut-3-en-1-yl)-9*H*-carbazole (47)
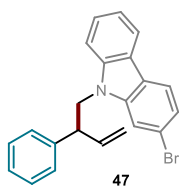
Prepared according to *GP2*, using [Ir(cod)Cl]$_2$/(*S*)-**L** as the catalytic system, diethyl 4-((2-bromo-9*H*-carbazol-9-yl)methyl)-2,6-dimethyl-1,4-dihydro pyridine-3,5-dicarboxylate (51 mg, 100 µmol) and 1-phenylprop-2-en-1-ol **37** (26 µL, 200 µmol) as the substrates, and performing the reaction in acetone. The crude mixture was purified by flash column chromatography (isocratic 5% PhMe in hexane) to afford product **47** (30 mg, 80% yield, 90% ee) as a colorless wax. The enantiomeric excess was determined by UPC^2 analysis on a Daicel Chiralpak IB-3 column: gradient CO$_2$/CH$_3$CN from 100% CO$_2$ to 60:40 over 4 minutes, curve 6, flow rate 2 mL/min, λ = 260 nm: τ_{major} = 5.0 min, τ_{minor} = 4.6 min; $[\alpha]_D^{26}$ = +12.5 (c = 0.34, CHCl$_3$, 90% ee). The absolute configuration for the title compound was assigned in comparison to compounds **66** and **67**.

^{1}H NMR (400 MHz, CDCl$_3$): δ 8.05 (d, J = 8.0 Hz, 1H), 7.91 (d, J = 8.0 Hz, 1H), 7.45 (ddd, J = 8.5, 7.0, 1.0 Hz, 1H), 7.35 – 7.21 (m, 7H), 7.22 – 7.13 (m, 2H), 6.16 (ddd, J = 17.0, 10.5, 7.5 Hz, 1H), 5.11 (dt, J = 10.5, 1.0 Hz, 1H), 5.04 (dt, J = 17.0, 1.0 Hz, 1H), 4.61 (dd, J = 14.5, 7.5 Hz, 1H), 4.47 (dd, J = 14.5, 7.5 Hz, 1H), 4.01 (q, J = 7.5 Hz, 1H).

^{13}C NMR (101 MHz, CDCl$_3$): δ 141.5, 141.1, 140.8, 138.1, 128.9, 127.9, 127.4, 126.1, 122.5, 122.1, 121.8, 121.4, 120.4, 119.6, 119.2, 117.2, 112.2, 109.3, 49.2.

HRMS (ESI) Exact mass calculated for C$_{22}$H$_{18}$BrN [M+H]$^+$: 398.0515, found: 398.0502.

(*S*)-4-bromo-9-(2-phenylbut-3-en-1-yl)-9*H*-carbazole (48)
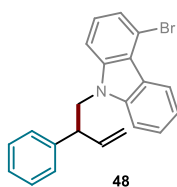
Prepared according to *GP2*, using [Ir(cod)Cl]$_2$/(*S*)-**L** as the catalytic system, diethyl 4-((4-bromo-9*H*-carbazol-9-yl)methyl)-2,6-dimethyl-1,4-dihydropyridine-3,5-dicarboxylate (51 mg, 100 µmol) and 1-phenylprop-2-en-1-ol **37** (26 µL, 200 µmol) as the substrates, and performing the reaction in acetone. The crude mixture was purified by flash column chromatography (isocratic 5% PhMe in hexane) to afford product **48** (30 mg, 80% yield, 92% ee) as a colorless wax. The enantiomeric excess was determined by UPC^2 analysis on a Daicel Chiralpak IG-3 column: gradient CO_2/CH_3CN from 100% CO_2 to 60:40 over 4 minutes, curve 6, flow rate 2 mL/min, λ = 260 nm: τ_{major} = 3.3 min, τ_{minor} = 3.2 min; $[\alpha]_D^{26}$ = -17.5 (c = 0.33, CHCl$_3$, 92% ee). The absolute configuration for the title compound was assigned in comparison to compounds **66** and **67**.

^{1}H NMR (400 MHz, CDCl$_3$): δ 8.85 – 8.77 (m, 1H), 7.50 (ddd, *J* = 8.5, 6.5, 1.0 Hz, 1H), 7.40 (dd, *J* = 6.5, 2.0 Hz, 1H), 7.35 – 7.15 (m, 9H), 6.24 – 6.10 (m, 1H), 5.08 (dt, *J* = 10.5, 1.0 Hz, 1H), 5.02 (dt, *J* = 17.0, 1.0 Hz, 1H), 4.65 (dd, *J* = 14.5, 8.0 Hz, 1H), 4.52 (dd, *J* = 14.5, 7.0 Hz, 1H), 4.04 (q, *J* = 7.5 Hz, 1H).

^{13}C NMR (101 MHz, CDCl$_3$): δ 141.8, 141.1, 140.8, 138.1, 128.9, 127.9, 127.3, 126.3, 126.0, 123.2, 122.8, 122.6, 121.6, 119.2, 117.2, 116.8, 108.9, 108.0, 49.2, 49.1.

HRMS (ESI) Exact mass calculated for C$_{22}$H$_{18}$BrN [M+H]$^+$: 376.0695, found: 376.0688.

(*S*)-3,6-dibromo-9-(2-phenylbut-3-en-1-yl)-9*H*-carbazole (49)
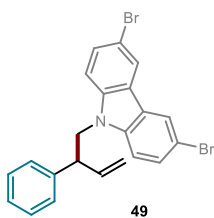
Prepared according to *GP2*, using [Ir(cod)Cl]$_2$/(*S*)-**L** as the catalytic system, diethyl 4-((3,6-dibromo-9*H*-carbazol-9-yl)methyl)-2,6-dimethyl-1,4-dihydropyridine-3,5-dicarboxylate (59 mg, 100 µmol) and 1-phenylprop-2-en-1-ol **37** (26 µL, 200 µmol) as the substrates, and performing the reaction in acetone. The crude mixture was purified by flash column chromatography (isocratic 5% PhMe in hexane) to afford product **49** (37 mg, 81% yield, 94% ee) as a colorless wax. The enantiomeric excess was determined by UPC^2 analysis on a Daicel Chiralpak IB-3 column: gradient CO_2/CH_3CN from 100% CO_2 to 60:40 over 4 minutes, curve 6, flow rate 2 mL/min, λ = 260 nm: τ_{major} = 4.3 min, τ_{minor} = 4.2 min; $[\alpha]_D^{26}$ = -30.4 (c = 0.41, CHCl$_3$, 94% ee). The absolute configuration for the title compound was assigned in comparison to compounds **66** and **67**.

^{1}H NMR (400 MHz, CDCl$_3$): δ 8.10 (d, *J* = 2.0 Hz, 2H), 7.49 (dd, *J* = 8.5, 2.0 Hz, 2H), 7.35 – 7.18 (m, 4H), 7.16 – 7.05 (m, 3H), 6.13 (ddd, *J* = 17.0, 10.5, 7.5 Hz, 1H), 5.09 (dt, *J* = 10.5, 1.0 Hz, 1H), 5.03 (dt, *J* = 17.0, 1.5 Hz, 1H), 4.57 (dd, *J* = 14.5, 7.5 Hz, 1H), 4.43 (dd, *J* = 14.5, 7.5 Hz, 1H), 3.95 (q, *J* = 7.5 Hz, 1H).

^{13}C NMR (101 MHz, CDCl$_3$): δ 140.8, 139.5, 137.9, 129.2, 129.0, 128.9, 128.4, 127.8, 127.4, 125.4, 123.5, 123.3, 117.3, 112.2, 110.8, 49.3, 49.2.

HRMS (ESI) Exact mass calculated for C$_{22}$H$_{17}$Br$_2$N [M+H]$^+$: 453.9801, found: 453.9801.

methyl (*S*)-1-(2-phenylbut-3-en-1-yl)-1*H*-indole-3-carboxylate (50)
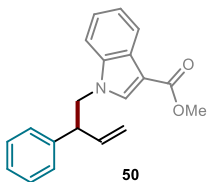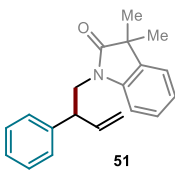
Prepared according to *GP2*, using [Ir(cod)Cl]$_2$/(*S*)-**L** as the catalytic system, diethyl 4-((3-(methoxycarbonyl)-1*H*-indol-1-yl)methyl)-2,6-dimethyl-1,4-dihydropyridine-3,5-dicarboxylate (44 mg, 100 µmol) and 1-phenylprop-2-en-1-ol **37** (26 µL, 200 µmol) as the substrates, and performing the reaction in acetone. The crude mixture was purified by flash column chromatography (gradient from hexane to 5% EtOAc in hexane) to afford product **50** (16 mg, 52% yield, 98% ee) as a colorless wax. The enantiomeric excess was determined by HPLC analysis on a Daicel Chiralpak IC-3 column: isocratic hexane/*i*-PrOH 95:5, flow rate 1 mL/min, λ = 230 nm: τ$_{major}$ = 31.4 min, τ$_{minor}$ = 36.8 min; [α]$_D^{26}$ = -12.7 (c = 0.18, CHCl$_3$, 98% ee). The absolute configuration for the title compound was assigned in comparison to compounds **66** and **67**.

^{1}H NMR (400 MHz, CDCl$_3$): δ 8.19 – 8.12 (m, 1H), 7.57 (s, 1H), 7.39 – 7.22 (m, 6H), 7.17 – 7.10 (m, 2H), 6.06 (ddd, *J* = 17.0, 10.5, 7.5 Hz, 1H), 5.13 (dt, *J* = 10.5, 1.0 Hz, 1H), 5.00 (dt, *J* = 17.0, 1.0 Hz, 1H), 4.40 (qd, *J* = 14.0, 7.5 Hz, 2H), 3.94 – 3.84 (m, 4H).

^{13}C NMR (101 MHz, CDCl$_3$): δ 165.6, 140.4, 137.6, 136.6, 135.0, 129.1, 127.7, 127.5, 126.8, 122.8, 122.0, 121.9, 117.7, 110.1, 107.0, 52.4, 51.1, 50.0.

HRMS (ESI) Exact mass calculated for C$_{20}$H$_{19}$NaNO$_2$ [M+Na]$^+$: 328.1308, found: 328.1306.

**(*S*)- 3,3-dimethyl-1-(2-phenylbut-3-en-1-yl)indolin-2-one (51)**

Prepared according to *GP2*, using [Ir(cod)Cl]$_2$/(*S*)-**L** as the catalytic system, diethyl 4-((3,3-dimethyl-2-oxoindolin-1-yl)methyl)-2,6-dimethyl-1,4-dihydropyridine-3,5-dicarboxylate (43 mg, 100 µmol) and 1-phenylprop-2-en-1-ol **37** (26 µL, 200 µmol) as the substrates, and performing the reaction in acetone. The crude mixture was purified by flash column chromatography (isocratic 5% EtOAc in hexane) to afford product **51** (15 mg, 51% yield, 98% ee) as a colorless oil. The enantiomeric excess was determined by HPLC analysis on a Daicel Chiralpak IC-3 column: isocratic hexane/*i*-PrOH 90:10, flow rate 1 mL/min, λ = 254 nm: τ$_{major}$ = 8.2 min, τ$_{minor}$ = 8.7 min; [α]$_D^{26}$ = +2.5 (c = 0.59, CHCl$_3$, 98% ee). The absolute configuration for the title compound was assigned in comparison to compounds **66** and **67**.

^{1}H NMR (400 MHz, CDCl₃): δ 7.35 – 7.14 (m, 7H), 7.04 (td, J = 7.5, 1.0 Hz, 1H), 6.87 (d, J = 8.0 Hz, 1H), 6.15 – 5.99 (m, 1H), 5.11 – 4.98 (m, 2H), 4.15 – 4.02 (m, 1H), 3.97 – 3.82 (m, 2H), 1.32 (s, 3H), 1.20 (s, 3H).

^{13}C NMR (101 MHz, CDCl₃): δ 181.4, 141.9, 140.8, 138.5, 136.0, 128.8, 128.0, 127.6, 127.2, 122.5, 122.4, 116.8, 108.5, 47.9, 44.4, 44.1, 24.6, 24.4.

HRMS (ESI) Exact mass calculated for $C_{20}H_{22}NO$ [M+H]⁺: 292.1696, found: 292.1706.

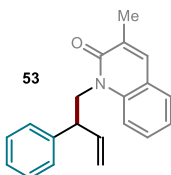### (*S*)- 1-(2-phenylbut-3-en-1-yl)-3,4-dihydroquinolin-2(1*H*)-one (52)
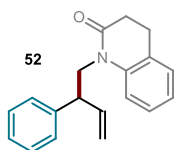
Prepared according to *GP2*, using [Ir(cod)Cl]₂/(*S*)-**L** as the catalytic system, diethyl 2,6-dimethyl-4-((2-oxo-3,4-dihydroquinolin-1(2*H*)-yl)methyl)-1,4-dihydropyridine-3,5-dicarboxylate (41 mg, 100 µmol) and 1-phenylprop-2-en-1-ol **37** (26 µL, 200 µmol) as the substrates, and performing the reaction in CHCl₃. The crude mixture was purified by flash column chromatography (isocratic 5% EtOAc in hexane) to afford product **52** (15 mg, 55% yield, 98% ee) as an off-white wax. The enantiomeric excess was determined by UPC² analysis on a CHIRALCEL® OJ-3 column: gradient CO₂/EtOH from 100% CO₂ to 60:40 over 4 minutes, curve 6, flow rate 2 mL/min, λ = 260 nm: τ_{major} = 2.8 min, τ_{minor} = 3.1 min; $[\alpha]_D^{26}$ = +53.0 (c = 0.12, CH₂Cl₂, 98% ee). The absolute configuration for the title compound was assigned in comparison to compounds **66** and **67**.

^{1}H NMR (500 MHz, CDCl₃): δ 7.30 – 7.22 (m, 3H), 7.22 – 7.15 (m, 3H), 7.13 (dd, J = 7.5, 1.5 Hz, 1H), 7.05 – 6.98 (m, 2H), 6.02 (ddd, J = 17.0, 10.0, 8.0 Hz, 1H), 5.03 (d, J = 10.0 Hz, 1H), 4.94 (d, J = 17.0 Hz, 1H), 4.53 – 4.41 (m, 1H), 4.22 – 4.11 (m, 1H), 3.70 (q, J = 8.0 Hz, 1H), 2.79 – 2.69 (m, 1H), 2.63 – 2.45 (m, 3H).

^{13}C NMR (126 MHz, CDCl₃): δ 170.6, 141.1, 139.2, 138.8, 128.7, 128.1, 127.9, 127.7, 127.4, 127.0, 123.0, 116.3, 115.6, 47.7, 45.0, 32.2, 25.4.

HRMS (ESI) Exact mass calculated for $C_{19}H_{19}NNaO$ [M+Na]⁺: 300.1359, found: 300.1359.

(*S*)-3-methyl-1-(2-phenylbut-3-en-1-yl)quinolin-2(1*H*)-one (53)

Prepared according to *GP2*, using [Ir(cod)Cl]₂/(*S*)-**L** as the catalytic system, diethyl 2,6-dimethyl-4-((3-methyl-2-oxoquinolin-1(2H)-yl)methyl)-1,4-di hydropyridine-3,5-dicarboxylate (42 mg, 100 µmol) and 1-phenylprop-2-en-1-ol **37** (26 µL, 200 µmol) as the substrates, and performing the reaction in CHCl₃. The crude mixture was purified by flash column chromatography (isocratic 2% EtOAc in CH₂Cl₂) to afford product **53** (12 mg, 40% yield, 98% ee) as an off-white wax. The enantiomeric excess was determined by HPLC analysis on a Daicel Chiralpak IC-3 column: isocratic hexane/*i*-PrOH 95:5, flow rate 1 mL/min, λ = 230 nm: τ_{major} = 44.2 min, τ_{minor} = 38.0 min; $[\alpha]_D^{26}$ = +40.4 (c = 0.07, CH₂Cl₂,

98% ee). The absolute configuration for the title compound was assigned in comparison to compounds **66** and **67**.

^{1}H NMR (500 MHz, CDCl$_3$): δ 7.52 (s, 1H), 7.51 – 7.43 (m, 2H), 7.36 – 7.29 (m, 5H), 7.28 – 7.22 (m, 1H), 7.18 (ddd, J = 7.5, 7.5, 1.0 Hz, 1H), 6.15 (ddd, J = 17.0, 10.0, 8.5 Hz, 1H), 5.06 – 4.97 (m, 1H), 4.95 (ddd, J = 10.0, 1.5, 1.0 Hz, 1H), 4.84 (ddd, J = 17.0, 1.5, 1.0 Hz, 1H), 4.39 – 4.26 (m, 1H), 3.93 (td, J = 9.5, 6.0 Hz, 1H), 2.24 (d, J = 1.5 Hz, 3H).

^{13}C NMR (126 MHz, CDCl$_3$): δ 163.1, 141.4, 138.6, 138.5, 135.9, 130.1, 129.2, 128.9, 128.2, 127.9, 127.1, 121.9, 121.1, 116.5, 114.3, 48.7, 47.0, 17.8.

HRMS (ESI) Exact mass calculated for C$_{20}$H$_{19}$NNaO [M+Na]$^+$: 312.1359, found: 312.1346.

(S)-N-(2-(1-(2-phenylbut-3-en-1-yl)-1H-indol-3-yl)ethyl)acetamide (54)
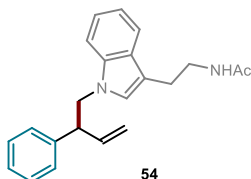
Prepared according to *GP2*, using [Ir(cod)Cl]$_2$/(S)-**L** as the catalytic system, diethyl 4-((3-(2-acetamidoethyl)-1H-indol-1-yl)methyl)-2,6-dimethyl-1,4-dihydropyridine-3,5-dicarboxylate (47 mg, 100 μmol) and 1-phenylprop-2-en-1-ol **37** (26 μL, 200 μmol) as the substrates, and performing 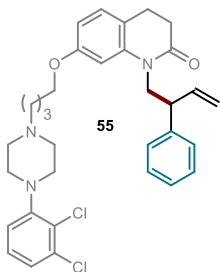the reaction in chloroform, reaction time 4h. The crude mixture was purified by flash column chromatography (gradient from hexane:EtOAc 50% to 80% EtOAc in hexane) to afford product **54** (19.5 mg, 58% yield, 88% ee) as a yellow wax. The enantiomeric excess was determined by UPC^2 analysis on a Daicel Chiralpak IB-3 column: isocratic CO$_2$/MeOH 10% MeOH, curve 6, flow rate 2 mL/min, λ = 220 nm: τ$_{minor}$ = 7.7 min, τ$_{major}$ = 8.2 min; $[α]_D^{26}$ = -49.3 (c = 0.9, CHCl$_3$, 88% ee). The absolute configuration for the title compound was assigned in comparison to compounds **66** and **67**.

^{1}H NMR (400 MHz, CDCl$_3$) δ 7.58 (dt, J = 7.9, 1.0 Hz, 1H), 7.40 – 7.21 (m, 5H), 7.17 – 7.09 (m, 3H), 6.65 (s, 1H), 6.10 (ddd, J = 17.2, 10.4, 7.5 Hz, 1H), 5.48 – 5.36 (bs, 1H), 5.14 (dt, J = 10.4, 1.2 Hz, 1H), 5.06 (dt, J = 17.2, 1.3 Hz, 1H), 4.44 (dd, J = 14.2, 7.5 Hz, 1H), 4.32 (dd, J = 14.2, 7.5 Hz, 1H), 3.89 (q, J = 7.5 Hz, 1H), 3.51 (q, J = 6.4 Hz, 2H), 2.94 – 2.82 (m, 2H), 1.91 (s, 3H).

^{13}C NMR (101 MHz, CDCl$_3$) δ 170.0, 141.1, 138.4, 136.4, 128.7, 128.0, 127.8, 127.1, 126.4, 121.8, 119.1, 118.9, 116.8, 111.2, 109.6, 51.7, 50.2, 39.8, 25.0, 23.4.

HRMS (ESI) Exact mass calculated for C$_{22}$H$_{24}$N$_2$O [M+Na]$^+$: 355.1888, found: 355.1781.

(S)-7-(4-(4-(2,3-dichlorophenyl)piperazin-1-yl)butoxy)-1-(2-phenylbut-3-en-1-yl)-3,4-dihydroquinolin-2(1H)-one (55)

Prepared according to *GP2*, using [Ir(cod)Cl]₂/(*S*)-**L** as the catalytic system, diethyl 4-((7-(4-(4-(2,3-dichlorophenyl)piperazin-1-yl)butoxy)-2-oxo-3,4-dihydroquinolin-1(2H)-yl)methyl)-2,6-dimethyl-1,4-dihydropyridine-3,5-dicarboxylate (71 mg, 100 μmol) and 1-phenylprop-2-en-1-ol **37** (26 μL, 200 μmol) as the substrates, trifluoroacetic acid (23 μL, 300 μmol), and performing the reaction in acetone or CHCl₃. The crude mixture was purified by flash column chromatography (isocratic 50% EtOAc in hexane) to afford product **55** (16 mg, 27% yield, 98% ee) as a yellow oil. The enantiomeric excess was determined by HPLC analysis on a Daicel Chiralpak IC-3 column: isocratic hexane/*i*-PrOH 90:10, flow rate 1.2 mL/min, λ = 225 nm: τ_{major} = 41.5 min, τ_{minor} = 43.9 min; $[\alpha]_D^{26}$ = +9.2 (c = 0.61, CHCl₃, 96% ee). The absolute configuration for the title compound was assigned in comparison to compounds **66** and **67**.

<u>¹H NMR</u> (400 MHz, CDCl₃, *isolated as a 5:1 mixture of rotamers* A *and* B): δ 7.47 – 7.10 (m, 7H, A + 7H, B), 7.02 (d, *J* = 8.0 Hz, 1H, A), 6.99 – 6.91 (m, 1H, A + 2H, B). 6.77 (dd, *J* = 8.5, 2.0 Hz, 1H, B), 6.72 (d, *J* = 2.0 Hz, 1H, B), 6.60 (d, *J* = 2.5 Hz, 1H, A), 6.54 (dd, *J* = 8.0, 2.5 Hz, 1H, A), 6.16 (ddd, *J* = 17.0, 10.0, 8.0 Hz, 1H, B), 6.03 (ddd, *J* = 17.0, 10.0, 8.0 Hz, 1H, A), 5.10 – 4.91 (m, 2H, A), 5.02 – 4.81 (m, 3H, B), 4.52 – 4.35 (m, 1H, A), 4.29 – 4.07 (m, 1H, A + 1H, B), 4.04 (t, *J* = 6.0 Hz, 2H, B), 3.99 (t, *J* = 6.0 Hz, 2H, A), 3.93 (q, *J* = 8.5 Hz, 1H, B), 3.75 (q, *J* = 8.0 Hz, 1H, A), 3.13 (br s, 4H, A + 4H, B), 2.87 – 2.40 (m, 10H, A + 10H, B), 1.95 – 1.66 (m, 4H, A + 4H, B).

<u>¹³C NMR</u> (101 MHz, CDCl₃): δ 170.8, 160.1, 158.6, 141.1, 140.2, 140.0, 138.8, 138.7, 135.8, 134.2, 129.4, 128.9, 128.7, 128.5, 128.0, 127.9, 127.7, 127.6, 127.1, 127.0, 124.9, 119.8, 118.8, 116.5, 116.3, 115.2, 110.0, 107.6, 103.7, 99.6, 68.0, 64.6, 58.3, 53.3, 51.0, 48.5, 47.6, 45.2, 32.5, 29.8, 27.4, 25.5, 24.7.

The experiment DOSY2DLEDBP at 400 MHz in CDCl₃ confirmed the presence of a single species in solution with a diffusion coefficient of $6.3 \cdot 10^{-10}$ m²/s.

<u>HRMS (ESI)</u> Exact mass calculated for C₃₃H₃₈Cl₂N₃O₂ [M+H]⁺: 578.2336, found: 578.2325.

(S)-6-chloro-4-(cyclopropylethynyl)-1-((S)-2-phenylbut-3-en-1-yl)-4-(trifluoromethyl)-1,4-dihydro-2H-benzo[d][1,3]oxazin-2-one (56)
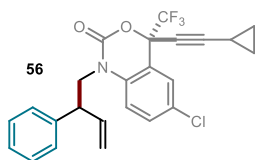
Prepared according to *GP2*, using pre-formed complex **Ph-Ir-III** as the catalyst, diethyl (*S*)-4-((6-chloro-4-(cyclopropylethynyl)-2-oxo-4-(trifluoromethyl)-2H-benzo[d][1,3]oxazin-1(4H)-yl)methyl)-2,6-dimethyl-1,4-dihydropyridine-3,5-dicarboxylate (58 mg, 100 μmol) and 1-phenylprop-2-en-1-ol **37** (26 μL, 200 μmol) as the substrates, and performing the reaction in CHCl₃. The crude mixture was purified

by flash column chromatography (isocratic 5% Et_2O in hexane) to afford product **56** (17 mg, 39% yield, >20:1 dr) as a colorless wax. This compound was obtained as a single diastereoisomer, as inferred by ^{1}H NMR analyses on both the crude mixture and the isolated compound; $[\alpha]_D^{26}$ = -61.5 (c = 0.12, CH_2Cl_2). The absolute configuration for the title compound was assigned in comparison to compounds **66** and **67**.

When the reaction was carried out using [Ir(cod)Cl]$_2$/(S)-**L** as the catalytic system, product **56** (12.3 mg, >20:1 dr) was obtained in 28% yield, as a single diastereoisomer.

^{1}H NMR (500 MHz, CDCl$_3$): δ 7.51 (d, J = 2.5 Hz, 1H), 7.37 – 7.28 (m, 3H), 7.28 – 7.22 (m, 3H), 6.81 (d, J = 9.0 Hz, 1H), 6.06 (ddd, J = 17.0, 10.0, 8.0 Hz, 1H), 5.10 (ddd, J = 10.0, 1.0, 1.0 Hz, 1H), 5.05 (dt, J = 17.0, 1.0, 1.0 Hz, 1H), 4.28 (dd, J = 14.5, 8.0 Hz, 1H), 4.16 (dd, J = 14.5, 7.0 Hz, 1H), 3.82 (q, J = 8.0 Hz, 1H), 1.37 (tt, J = 8.0, 5.0 Hz, 1H), 0.94 – 0.87 (m, 2H), 0.87 – 0.81 (m, 2H).

^{13}C NMR (126 MHz, CDCl$_3$): δ 148.2, 140.3, 138.0, 135.4, 131.3, 129.0, 128.8, 128.2, 127.9, 127.4, 122.2 (q, $^1J_{C-F}$ = 287.5 Hz), 117.7, 117.1, 115.3, 95.5, 77.8 – 76.6 (m), 66.7, 49.1, 48.0, 8.9, 8.8, -0.5.

^{19}F NMR (471 MHz, CDCl$_3$) δ -80.6 (s, 3F).

HRMS (ESI) Exact mass calculated for $C_{24}H_{19}ClF_3NNaO_2$ [M+Na]$^+$: 468.0949, found: 468.0943.

(*S*)-6-chloro-4-(cyclopropylethynyl)-1-((*R*)-2-phenylbut-3-en-1-yl)-4-(trifluoromethyl)-1,4-dihydro-2*H*-benzo[*d*][1,3]oxazin-2-one (57)
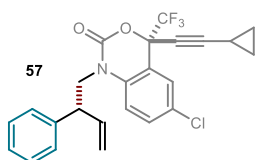
Prepared according to *GP2*, using [Ir(cod)Cl]$_2$/(R)-**L** as the catalytic system, diethyl (*S*)-4-((6-chloro-4-(cyclopropylethynyl)-2-oxo-4-(trifluoromethyl)-2*H*-benzo[*d*][1,3]oxazin-1(4*H*)-yl)methyl)-2,6-dimethyl-1,4-dihydropyridine-3,5-dicarboxylate (58 mg, 100 µmol) and 1-phenylprop-2-en-1-ol **37** (26 µL, 200 µmol) as the substrates, and performing the reaction in CHCl$_3$. The crude mixture was purified by flash column chromatography (isocratic 5% Et_2O in hexane) to afford product **57** (12.5 mg, 28% yield, 1:>20 dr) as a colorless wax. This compound was obtained as a single diastereoisomer, as inferred by ^{1}H NMR analyses on both the crude mixture and the isolated compound; $[\alpha]_D^{26}$ = -64.2 (c = 0.10, CH_2Cl_2). The absolute configuration for the title compound was assigned in comparison to compounds **66** and **67**.

^{1}H NMR (500 MHz, CDCl$_3$): δ 7.54 (d, J = 2.5 Hz, 1H), 7.39 (dd, J = 9.0, 2.5 Hz, 1H), 7.38 – 7.31 (m, 2H), 7.29 – 7.24 (m, 3H), 6.87 (d, J = 9.0 Hz, 1H), 6.04 (ddd, J = 17.0, 10.0, 8.0 Hz, 1H), 5.08 (dt, J = 10.0, 1.0, 1.0 Hz, 1H), 5.01 (dd, J = 17.0, 1.0, 1.0 Hz, 1H), 4.62 (dd, J = 14.5, 9.5 Hz, 1H), 3.85 (dd, J = 14.5, 5.0 Hz, 1H), 3.71 (ddd, J = 9.5, 8.0, 5.0 Hz, 1H), 1.38 (tt, J = 8.5, 5.0 Hz, 1H), 0.94 – 0.88 (m, 2H), 0.88 – 0.81 (m, 2H).

^{13}C NMR (126 MHz, CDCl$_3$): δ 148.2, 140.8, 137.6, 135.1, 131.4, 129.1, 128.9, 128.6, 127.7, 127.4, 122.3 (q, J = 287.5 Hz), 117.6 (*2 signals*), 115.2, 95.5, 77.8 – 76.4 (m), 66.8, 48.7, 47.8, 8.9 (*2 signals*), -0.5.

^{19}F NMR (471 MHz, CDCl$_3$) δ -80.5 (s, 3F).

HRMS (ESI) Exact mass calculated for C$_{24}$H$_{19}$ClF$_3$NNaO$_2$ [M+Na]$^+$: 468.0949, found: 468.0950.

benzyl (*S*)-benzyl(2-phenylbut-3-en-1-yl)carbamate (58)
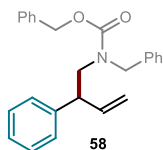
Prepared according to *GP2*, using pre-formed complex **Ph-Ir-III** as the catalyst, diethyl 4-((benzyl((benzyloxy)carbonyl)amino)methyl)-2,6-dimethyl-1,4-dihydropyridine-3,5 dicarboxylate (51 mg, 100 µmol) and 1-phenylprop-2-en-1-ol **37** (26 µL, 200 µmol) as the substrates, and performing the reaction in CHCl$_3$. The crude mixture was purified by flash column chromatography (isocratic PhMe) to afford product **58** (15 mg, 41% yield, 92% ee) as a colorless oil. The enantiomeric excess was determined by UPC^2 analysis on a CHIRALCEL$^®$ OJ-3 column: gradient CO$_2$/EtOH from 100% CO$_2$ to 60:40 over 4 minutes, curve 6, flow rate 2 mL/min, λ = 220 nm: τ$_{major}$ = 3.0 min, τ$_{minor}$ = 4.1 min; [α]$_D^{26}$ = +11.5 (c = 0.17, CH$_2$Cl$_2$, 92% ee). The absolute configuration for the title compund was assigned in comparison to compounds **66** and **67**.

^{1}H NMR (500 MHz, CDCl$_3$, *isolated as a 1:1 mixture of rotamers* A *and* B): δ 7.43 – 7.02 (m, 15H, A+B), 6.06 – 5.95 (m, 1H, A), 5.97 – 5.87 (m, 1H, B), 5.22 – 4.93 (m, 4H, A+B), 4.52 (d, J = 15.5 Hz, 1H, A), 4.47 (d, J = 16.0 Hz, 1H, B), 4.08 (d, J = 15.5 Hz, 1H, A), 4.02 (d, J = 16.0 Hz, 1H, B), 3.80 – 3.66 (m, 2H, A), 3.65 – 3.51 (m, 2H, B), 3.41 – 3.29 (m, 1H, A+B).

^{13}C NMR (126 MHz, CDCl$_3$, *isolated as a 1:1 mixture of rotamers* A *and* B): δ 156.8, 156.5, 141.7, 141.6, 139.1, 138.9, 137.8, 137.7, 136.9, 136.8, 129.0, 128.9, 128.74, 128.69, 128.66, 128.61, 128.54, 128.50, 128.2, 128.04, 128.02, 127.9, 127.8, 127.5, 127.41, 127.35, 126.94, 126.90, 116.5, 116.4, 67.5, 67.3, 52.3, 51.5, 51.03, 50.96, 49.2, 48.6.

HRMS (ESI) Exact mass calculated for C$_{25}$H$_{25}$NNaO$_2$ [M+Na]$^+$: 394.1777, found: 394.1762.

naphthalen-1-yl (S)-methyl(2-phenylbut-3-en-1-yl)carbamate (59)
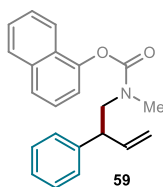
Prepared according to *GP2*, using pre-formed complex **Ph-Ir-III** as the catalyst, diethyl 2,6-dimethyl-4-((methyl((naphthalen-1-yloxy)carbonyl)amino)methyl)-1,4-dihydropyridine-3,5-dicarboxylate (47 mg, 100 µmol) and 1-phenylprop-2-en-1-ol **37** (26 µL, 200 µmol) as the substrates, and performing the reaction in CHCl$_3$. The crude mixture was purified by flash column chromatography (isocratic PhMe) to afford product **59** (15 mg, 45% yield, 94% ee) as a colorless oil. The enantiomeric excess was determined by HPLC analysis on a Daicel Chiralpak IC-3 column: isocratic hexane/*i*-PrOH 90:10, flow rate 1 mL/min, λ =

225 nm: τ_{minor} = 25.8 min, τ_{major} = 28.9 min; $[\alpha]_D^{26}$ = -0.11 (c = 0.17, CH_2Cl_2, 94% ee). The absolute configuration for the title compound was assigned in comparison to compounds **66** and **67**.

^{1}H NMR (400 MHz, CDCl$_3$, *isolated as a 1.2:1 mixture of rotamers* A *and* B): δ 7.91 – 7.68 (m, 3H, A+B), 7.53 – 7.41 (m, 3H, A+B), 7.40 – 7.27 (m, 5H, A+B), 7.21 (dd, *J* = 7.5, 1.0 Hz, 1H, A), 7.12 (dd, *J* = 7.5, 1.0 Hz, 1H, B), 6.25 – 6.00 (m, 1H, A+B), 5.28 – 5.14 (m, 2H, A+B), 4.05 – 3.92 (m, 1H, B), 3.93 – 3.77 (m, 2H, A+B), 3.67 – 3.53 (m, 1H, A), 3.13 (s, 3H, A), 2.99 (s, 3H, B).

^{13}C NMR (101 MHz, CDCl$_3$, *isolated as a 1.2:1 mixture of rotamers* A *and* B): δ 155.1, 154.9, 147.5, 147.4, 141.3, 139.1, 138.9, 134.8, 129.0, 128.8, 128.1, 127.60, 127.55, 127.2, 127.0, 126.4, 126.3, 125.6, 121.6, 121.4, 118.4, 118.1, 116.9, 116.5, 54.8, 54.7, 49.2, 48.7, 35.7.

HRMS (ESI) Exact mass calculated for $C_{22}H_{21}NNaO_2$ [M+Na]$^+$: 354.1464, found: 354.1457.

(S)-9-(2-(4-isopropylphenyl)but-3-en-1-yl)-9*H*-carbazole (60)
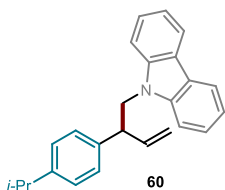
Prepared according to *GP2*, using [Ir(cod)Cl]$_2$/(*S*)-**L** as the catalytic system, diethyl 4-((9*H*-carbazol-9-yl)methyl)-2,6-dimethyl-1,4-dihydro pyridine-3,5-dicarboxylate **41** (43 mg, 100 µmol) and 1-(4-isopropylphenyl)prop-2-en-1-ol (35 mg, 200 µmol) as the substrates, and performing the reaction in acetone. The crude mixture was purified by flash column chromatography (isocratic 5% PhMe in hexane) to afford product **60** (20 mg, 58% yield, 86% ee) as a colorless oil. The enantiomeric excess was determined by UPC^2 analysis on a Daicel Chiralpak IB-3 column: gradient CO_2/CH$_3$CN from 100% CO_2 to 60:40 over 4 minutes, curve 6, flow rate 2 mL/min, λ = 260 nm: τ_{major} = 4.1 min, τ_{minor} = 4.3 min; $[\alpha]_D^{26}$ = +6.6 (c = 0.56, CH_2Cl_2, 86% ee). The absolute configuration for the title compound was assigned in comparison to compounds **66** and **67**.

^{1}H NMR (400 MHz, CDCl$_3$): δ 8.08 (dt, *J* = 7.5, 1.0 Hz, 2H), 7.39 (ddd, *J* = 8.5, 7.0, 1.0 Hz, 2H), 7.29 – 7.24 (m, 2H), 7.21 (ddd, *J* = 8.0, 7.0, 1.0 Hz, 2H), 7.12 (s, 4H), 6.15 (ddd, *J* = 17.0, 10.5, 7.6 Hz, 1H), 5.01 (dt, *J* = 10.5, 1.0 Hz, 1H), 4.96 (dt, *J* = 17.0, 1.5 Hz, 1H), 4.63 (dd, *J* = 14.5, 8.0 Hz, 1H), 4.48 (dd, *J* = 14.5, 6.5 Hz, 1H), 4.05 – 3.95 (m, 1H), 2.86 (hept, *J* = 7.0 Hz, 1H), 1.23 (d, *J* = 7.0 Hz, 6H).

^{13}C NMR (101 MHz, CDCl$_3$): δ 147.9, 140.7, 138.8, 138.6, 127.8, 126.9, 125.6, 122.9, 120.3, 118.9, 116.9, 109.1, 49.2, 49.1, 33.9, 24.17, 24.16.

HRMS (ESI) Exact mass calculated for $C_{25}H_{26}N$ [M+H]$^+$: 340.2060, found: 340.2056.

(*S*)-9-(2-(4-(*tert*-butyl)phenyl)but-3-en-1-yl)-9*H*-carbazole (61)
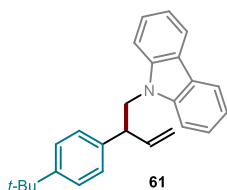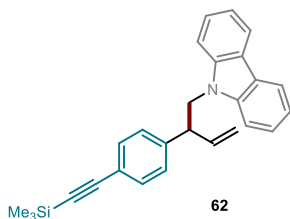
Prepared according to *GP2*, using [Ir(cod)Cl]$_2$/(*S*)-**L** as the catalytic system, diethyl 4-((9*H*-carbazol-9-yl)methyl)-2,6-dimethyl-1,4-dihydro pyridine-3,5-dicarboxylate **41** (43 mg, 100 µmol) and 1-(4-(*tert*-butyl)phenyl)prop-2-en-1-ol (38 mg, 200 µmol) as the substrates, and performing the reaction in acetone. The crude mixture was purified by flash column chromatography (isocratic 5% PhMe in hexane) to afford product **61** (21 mg, 60% yield, 84% ee) as a colorless solid. The enantiomeric excess was determined by UPC^2 analysis on a Daicel Chiralpak IB-3 column: gradient CO$_2$/CH$_3$CN from 100% CO$_2$ to 60:40 over 4 minutes, curve 6, flow rate 2 mL/min, λ = 260 nm: τ_{major} = 4.2 min, τ_{minor} = 4.3 min; $[\alpha]_D^{26}$ = +5.4 (c = 0.71, CH$_2$Cl$_2$, 86% ee). The absolute configuration for the title compound was assigned in comparison to compounds **66** and **67**.

^{1}H NMR (400 MHz, CDCl$_3$): δ 8.09 (dt, *J* = 7.5, 1.0 Hz, 2H), 7.39 (ddd, *J* = 8.5, 7.0, 1.0 Hz, 2H), 7.31 – 7.24 (m, 4H), 7.21 (ddd, *J* = 8.0, 7.0, 1.0 Hz, 2H), 7.15 – 7.09 (m, 2H), 6.16 (ddd, *J* = 17.0, 10.5, 7.5 Hz, 1H), 5.02 (dt, *J* = 10.5, 1.0 Hz, 1H), 4.97 (dt, *J* = 17.0, 1.5 Hz, 1H), 4.64 (dd, *J* = 14.5, 8.0 Hz, 1H), 4.49 (dd, *J* = 14.5, 6.5 Hz, 1H), 4.01 (app q, *J* = 7.5 Hz, 1H), 1.30 (s, 9H).

^{13}C NMR (101 MHz, CDCl$_3$): δ 150.1, 140.7, 138.5, 138.4, 127.5, 125.7, 125.6, 122.9, 120.3, 118.9, 116.9, 109.1, 49.2, 49.0, 34.6, 31.5.

HRMS (ESI) Exact mass calculated for C$_{26}$H$_{28}$N [M+H]$^+$: 354.2216, found: 354.2206.

(*S*)-9-(2-(4-((trimethylsilyl)ethynyl)phenyl)but-3-en-1-yl)-9*H*-carbazole (62)

Prepared according to *GP2*, using [Ir(cod)Cl]$_2$/(*S*)-**L** as the catalytic system, diethyl 4-((9*H*-carbazol-9-yl)methyl)-2,6-dimethyl-1,4-dihydro pyridine-3,5-dicarboxylate **41** (43 mg, 100 µmol) and 1-(4-((trimethylsilyl)ethynyl)phenyl)prop-2-en-1-ol (46 mg, 200 µmol) as the substrates, and performing the reaction in acetone. The crude mixture was purified by flash column chromatography (isocratic 10% PhMe in hexane) to afford product **62** (16.5 mg, 40% yield, 72% ee) as a colorless oil. The enantiomeric excess was determined by UPC^2 analysis on a Daicel Chiralpak IB-3 column: gradient CO$_2$/CH$_3$CN from 100% CO$_2$ to 60:40 over 4 minutes, curve 6, flow rate 2 mL/min, λ = 260 nm: τ_{major} = 4.3 min, τ_{minor} = 4.5 min; $[\alpha]_D^{26}$ = -41.7 (c = 0.72, CH$_2$Cl$_2$, 72% ee). The absolute configuration for the title compound was assigned in comparison to compounds **66** and **67**.

^{1}H NMR (400 MHz, CDCl$_3$): δ 8.07 (dt, *J* = 8.0, 1.0 Hz, 2H), 7.45 – 7.33 (m, 4H), 7.26 (dt, *J* = 8.0, 1.0 Hz, 2H), 7.22 (ddd, *J* = 8.0, 7.0, 1.0 Hz, 2H), 7.16 – 7.10 (m, 2H), 6.11 (ddd, *J* = 17.0, 10.5, 7.5 Hz, 1H), 5.05 (dt, *J* = 10.5, 1.0 Hz, 1H), 4.97 (dt, *J* = 17.0, 1.5 Hz, 1H), 4.61
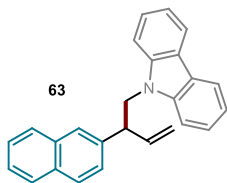
(dd, J = 14.5, 8.0 Hz, 1H), 4.49 (dd, J = 14.5, 7.0 Hz, 1H), 4.04 (app q, J = 7.5 Hz, 1H), 0.25 (s, 9H).

<u>13C NMR</u> (101 MHz, CDCl$_3$): δ 141.9, 140.6, 138.0, 132.4, 127.9, 125.7, 123.0, 122.0, 120.4, 119.1, 117.4, 109.0, 105.0, 94.3, 49.2, 48.9, 0.1.

<u>HRMS (ESI)</u> Exact mass calculated for C$_{27}$H$_{28}$NSi [M+H]$^+$: 394.1986, found: 394.1984.

(*S*)-9-(2-(naphthalen-2-yl)but-3-en-1-yl)-9*H*-carbazole (63)

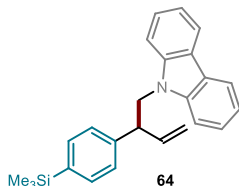Prepared according to *GP2*, using [Ir(cod)Cl]$_2$/(*S*)-**L** as the catalytic system, diethyl 4-((9*H*-carbazol-9-yl)methyl)-2,6-dimethyl-1,4-dihydro pyridine-3,5-dicarboxylate **41** (43.3 mg, 100 µmol) and 1-(naphthalen-2-yl)prop-2-en-1-ol (37 mg, 200 µmol) as the substrates, and performing the reaction in acetone. The crude mixture was purified by flash column chromatography (isocratic 5% PhMe in hexane) to afford product **63** (16 mg, 46% yield, 72% ee) as a yellow oil. The enantiomeric excess was determined by UPC^2 analysis on a Daicel Chiralpak IB-3 column: gradient CO$_2$/ CH$_3$CN from 100% CO$_2$ to 60:40 over 4 minutes, curve 6, flow rate 2 mL/min, λ = 260 nm: τ_{major} = 5.1 min, τ_{minor} = 5.4 min; $[\alpha]_D^{26}$ = -10.9 (c = 0.65, CH$_2$Cl$_2$, 72% ee). The absolute configuration for the title compound was assigned in comparison to compounds **66** and **67**.

<u>1H NMR</u> (400 MHz, CDCl$_3$): δ 8.08 (dt, J = 8.0, 1.0 Hz, 2H), 7.84 – 7.72 (m, 3H), 7.68 (d, J = 2.0 Hz, 1H), 7.50 – 7.42 (m, 2H), 7.41 – 7.31 (m, 5H), 7.20 (ddd, J = 8.0, 7.0, 1.0 Hz, 2H), 6.21 (ddd, J = 17.0, 10.5, 7.5 Hz, 1H), 5.04 (dt, J = 10.5, 1.0 Hz, 1H), 4.97 (dt, J = 17.0, 1.5 Hz, 1H), 4.74 (dd, J = 14.5, 8.5 Hz, 1H), 4.61 (dd, J = 14.5, 6.5 Hz, 1H), 4.22 (q, J = 7.5 Hz, 1H).

<u>13C NMR</u> (101 MHz, CDCl$_3$): δ 140.7, 138.8, 138.4, 133.7, 132.7, 128.6, 127.80, 127.77, 126.6, 126.3, 126.2, 125.9, 125.7, 123.0, 120.4, 119.0, 117.3, 109.1, 49.5, 49.0.

<u>HRMS (ESI)</u> Exact mass calculated for C$_{26}$H$_{22}$N [M+H]$^+$: 348.1747, found: 348.1756.

(*S*)-9-(2-(4-(trimethylsilyl)phenyl)but-3-en-1-yl)-9*H*-carbazole (64)

Prepared according to *GP2*, using [Ir(cod)Cl]$_2$/(*S*)-**L** as the catalytic system, diethyl 4-((9*H*-carbazol-9-yl)methyl)-2,6-dimethyl-1,4-dihydro pyridine-3,5-dicarboxylate **41** (43 mg, 100 µmol) and 1-(4-(trimethylsilyl)phenyl)prop-2-en-1-ol (41 mg, 200 µmol) as the substrates, and performing the reaction in acetone. The crude mixture was purified by flash column chromatography (isocratic 5% PhMe in hexane) to afford product **64** (25 mg, 66% yield, 82% ee) as a colorless oil. The enantiomeric excess was determined by UPC^2 analysis on a Daicel Chiralpak IB-3 column: gradient CO$_2$/CH$_3$CN from 100% CO$_2$ to 60:40 over 4 minutes, curve 6, flow rate 2 mL/min, λ = 260 nm: τ_{major} = 3.9 min,

τ_{minor} = 4.1 min; $[\alpha]_D^{26}$ = +7.8 (c = 1.32, CH$_2$Cl$_2$, 82% ee). The absolute configuration for the title compound was assigned in comparison to compounds **66** and **67**.

^{1}H NMR (400 MHz, CDCl$_3$): δ 8.07 (ddd, J = 8.0, 1.0, 1.0 Hz, 2H), 7.42 (d, J = 8.0 Hz, 2H), 7.38 (ddd, J = 8.5, 7.0, 1.0 Hz, 2H), 7.26 (dt, J = 8.0, 1.0 Hz, 2H), 7.23 – 7.17 (m, 4H), 6.14 (ddd, J = 17.0, 10.5, 7.5 Hz, 1H), 5.00 (dt, J = 10.5, 1.0 Hz, 1H), 4.94 (dt, J = 17.0, 1.5 Hz, 1H), 4.64 (dd, J = 14.5, 8.5 Hz, 1H), 4.49 (dd, J = 14.5, 6.5 Hz, 1H), 4.01 (app q, J = 7.5 Hz, 1H), 0.25 (s, 9H).

^{13}C NMR (101 MHz, CDCl$_3$): δ 142.0, 140.7, 139.3, 138.3, 133.9, 127.3, 125.6, 123.0, 120.3, 119.0, 117.2, 109.1, 49.5, 49.1, -1.0.

HRMS (ESI) Exact mass calculated for C$_{25}$H$_{27}$NNaSi [M+Na]$^+$: 392.1805, found: 392.1795.

(*S*)-9-(2-(4-(4,4,5,5-tetramethyl-1,3,2-dioxaborolan-2-yl)phenyl)but-3-en-1-yl)-9*H*-carbazole (65)
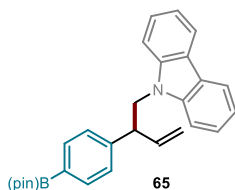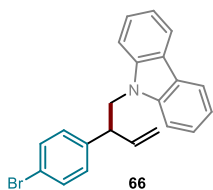

Prepared according to *GP2*, using pre-formed complex **Ph-Ir-III** as the catalyst, diethyl 4-((9*H*-carbazol-9-yl)methyl)-2,6-dimethyl-1,4-dihydro pyridine-3,5-dicarboxylate **41** (43 mg, 100 µmol) and 1-(4-(4,4,5,5-tetramethyl-1,3,2-dioxaborolan-2-yl)phenyl)prop-2-en-1-ol (52 mg, 200 µmol) as the substrates, and performing the reaction in acetone. The crude mixture was purified by rapid filtration on a short pad of silica gel (*eluting with* PhMe), in order to prevent product decomposition, to afford product **65** (26 mg, 58% yield, 76% ee) as a yellow oil. The enantiomeric excess was determined by UPC^2 analysis on a Daicel Chiralpak IB-3 column: gradient CO$_2$/EtOH from 100% CO$_2$ to 60:40 over 4 minutes, curve 6, flow rate 2 mL/min, λ = 260 nm: τ_{major} = 3.9 min, τ_{minor} = 4.0 min; $[\alpha]_D^{26}$ = +52.5 (c = 1.04, CH$_2$Cl$_2$, 76% ee). The absolute configuration for the title compound was assigned in comparison to compounds **66** and **67**.

^{1}H NMR (400 MHz, CDCl$_3$): δ 8.08 (dt, J = 8.0, 1.0 Hz, 2H), 7.79 – 7.73 (m, 2H), 7.42 (ddd, J = 8.5, 7.0, 1.0 Hz, 2H), 7.34 – 7.26 (m, 4H), 7.22 (ddd, J = 8.0, 7.0, 1.0 Hz, 2H), 6.11 (ddd, J = 17.0, 10.5, 7.5 Hz, 1H), 4.98 (dt, J = 10.5, 1.0 Hz, 1H), 4.89 (dt, J = 17.0, 1.5 Hz, 1H), 4.64 (dd, J = 14.5, 8.5 Hz, 1H), 4.51 (dd, J = 14.5, 6.5 Hz, 1H), 4.06 (app q, J = 7.5 Hz, 1H), 1.36 (s, 12H).

^{13}C NMR (101 MHz, CDCl$_3$): δ 144.6, 140.7, 138.2, 135.4, 127.4, 125.7, 123.0, 120.4, 119.0, 117.3, 109.1, 83.9, 49.7, 48.9, 25.02, 24.98.

HRMS (ESI) Exact mass calculated for C$_{28}$H$_{31}$NO$_2$^{10}B [M+H]$^+$: 423.2479, found: 423.2489.

(S)-9-(2-(4-bromophenyl)but-3-en-1-yl)-9H-carbazole (66)

Prepared according to *GP2*, using [Ir(cod)Cl]$_2$/(*S*)-**L** as the catalytic system, diethyl 4-((9*H*-carbazol-9-yl)methyl)-2,6-dimethyl-1,4-dihydropyridine-3,5-dicarboxylate **41** (43 mg, 100 µmol) and 1-(4-bromophenyl)prop-2-en-1-ol (43 mg, 200 µmol) as the substrates, and performing the reaction in acetone. The crude mixture was purified by flash column chromatography (isocratic 10% PhMe in hexane) to afford product **66** (22 mg, 60% yield, 84% ee) as a colorless oil. The enantiomeric excess was determined by UPC^2 analysis on a Daicel Chiralpak IB-3 column: gradient CO$_2$/CH$_3$CN from 100% CO$_2$ to 60:40 over 4 minutes, curve 6, flow rate 2 mL/min, λ = 260 nm: τ$_{major}$ = 5.6 min, τ$_{minor}$ = 5.9 min; [α]$_D^{26}$ = -27.3 (c = 1.10, CH$_2$Cl$_2$, 84% ee). Crystals of derivative **66**, suitable for X-ray diffraction analysis, were obtained upon slow evaporation of a CH$_2$Cl$_2$ solution of the title compound. This enabled the unambiguous determination of the absolute stereochemical configuration for product **66**.

<u>^{1}H NMR</u> (400 MHz, CDCl$_3$): δ 8.08 (dt, *J* = 7.5, 1.0 Hz, 2H), 7.40 (ddd, *J* = 8.5, 7.0, 1.0 Hz, 2H), 7.38 – 7.33 (m, 2H), 7.27 – 7.18 (m, 4H), 7.06 – 7.00 (m, 2H), 6.11 (ddd, *J* = 17.5, 10.5, 7.5 Hz, 1H), 5.09 (dt, *J* = 10.5, 1.0 Hz, 1H), 5.01 (dt, *J* = 17.0, 1.5 Hz, 1H), 4.61 (dd, *J* = 14.5, 7.5 Hz, 1H), 4.47 (dd, *J* = 14.5, 7.0 Hz, 1H), 4.01 (app q, *J* = 7.5 Hz, 1H).

<u>^{13}C NMR</u> (101 MHz, CDCl$_3$): δ 140.6, 140.3, 137.9, 131.9, 129.7, 125.7, 123.0, 121.0, 120.4, 119.1, 117.4, 109.0, 48.9, 48.7.

<u>HRMS (ESI)</u> Exact mass calculated for C$_{22}$H$_{19}$BrN [M+H]$^+$: 376.0695, found: 376.0688.

(S)-9-(2-(4-chlorophenyl)but-3-en-1-yl)-9H-carbazole (67)
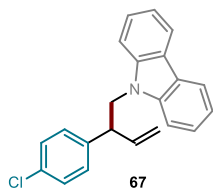
Prepared according to *GP2*, using [Ir(cod)Cl]$_2$/(*S*)-**L** as the catalytic system, diethyl 4-((9*H*-carbazol-9-yl)methyl)-2,6-dimethyl-1,4-dihydro pyridine-3,5-dicarboxylate **41** (43 mg, 100 µmol) and 1-(4-chlorophenyl)prop-2-en-1-ol (34 mg, 200 µmol) as the substrates, and performing the reaction in acetone. The crude mixture was purified by flash column chromatography (isocratic 5% PhMe in hexane) to afford product **67** (21 mg, 61% yield, 84% ee) as a colorless solid. The enantiomeric excess was determined by UPC^2 analysis on a Daicel Chiralpak IB-3 column: gradient CO$_2$/CH$_3$CN from 100% CO$_2$ to 60:40 over 4 minutes, curve 6, flow rate 2 mL/min, λ = 260 nm: τ$_{major}$ = 4.4 min, τ$_{minor}$ = 4.6 min; [α]$_D^{26}$ = -23.9 (c = 0.12, CH$_2$Cl$_2$, 82% ee). Crystals of derivative **67**, suitable for X-ray diffraction analysis, were obtained upon slow evaporation of a CH$_2$Cl$_2$ solution of the title compound. This enabled the unambiguous determination of the absolute stereochemical configuration for product **67**.

^{1}H NMR (400 MHz, CDCl$_3$): δ 8.08 (dt, J = 7.5, 1.0 Hz, 2H), 7.41 (ddd, J = 8.5, 7.0, 1.0 Hz, 2H), 7.27 – 7.16 (m, 6H), 7.10 – 7.06 (m, 2H), 6.12 (ddd, J = 17.5, 10.5, 7.5 Hz, 1H), 5.09 (dt, J = 10.5, 1.0 Hz, 1H), 5.02 (dt, J = 17.0, 1.5 Hz, 1H), 4.61 (dd, J = 14.5, 7.5 Hz, 1H), 4.47 (dd, J = 14.5, 7.5 Hz, 1H), 4.02 (app q, J = 7.5 Hz, 1H).

^{13}C NMR (101 MHz, CDCl$_3$): δ 140.6, 139.8, 138.0, 133.0, 129.3, 128.9, 125.7, 123.0, 120.4, 119.1, 117.4, 109.0, 48.9, 48.6.

HRMS (ESI) Exact mass calculated for C$_{22}$H$_{19}$ClN [M+H]$^+$: 332.1201, found: 332.1201.

(*S*)-9-(2-(3-iodophenyl)but-3-en-1-yl)-9*H*-carbazole (68)
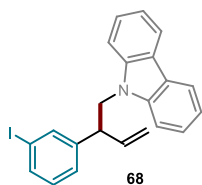
Prepared according to *GP2*, using [Ir(cod)Cl]$_2$/(*S*)-**L** as the catalytic system, diethyl 4-((9*H*-carbazol-9-yl)methyl)-2,6-dimethyl-1,4-dihydro pyridine-3,5-dicarboxylate **41** (43 mg, 100 µmol) and 1-(3-iodophenyl)prop-2-en-1-ol (52 mg, 200 µmol) as the substrates, and performing the reaction in acetone. The crude mixture was purified by flash column chromatography (isocratic 5% PhMe in hexane) to afford product **68** (14 mg, 33% yield, 70% ee) as a colorless oil. The enantiomeric ratio was determined by UPC^2 analysis on a Daicel Chiralpak IB-3 column: gradient CO$_2$/CH$_3$CN from 100% CO$_2$ to 60:40 over 4 minutes, curve 6, flow rate 2 mL/min, λ =260 nm: τ$_{major}$ = 4.7 min, τ$_{minor}$ = 4.8 min; [α]$_D^{26}$ = -14.1 (c = 0.89, CH$_2$Cl$_2$, 70% ee). The absolute configuration for the title compound was assigned in comparison to compounds **66** and **67**.

^{1}H NMR (400 MHz, CDCl$_3$): δ 8.08 (dt, J = 8.0, 1.0 Hz, 2H), 7.57 – 7.47 (m, 2H), 7.41 (ddd, J = 8.5, 7.0, 1.0 Hz, 2H), 7.28 – 7.18 (m, 4H), 7.06 (dt, J = 7.5, 1.5 Hz, 1H), 6.93 (t, J = 7.5 Hz, 1H), 6.10 (ddd, J = 17.0, 10.5, 7.5 Hz, 1H), 5.08 (dt, J = 10.5, 1.0 Hz, 1H), 5.00 (dt, J = 17.0, 1.0 Hz, 1H), 4.61 (dd, J = 14.5, 8.0 Hz, 1H), 4.48 (dd, J = 14.5, 7.0 Hz, 1H), 3.97 (app q, J = 7.5 Hz, 1H).

^{13}C NMR (101 MHz, CDCl$_3$): δ 143.7, 140.6, 137.6, 136.9, 136.2, 130.4, 127.4, 125.7, 123.0, 120.4, 119.1, 117.6, 109.0, 94.8, 48.8, 48.8.

HRMS (ESI) Exact mass calculated for C$_{22}$H$_{19}$IN [M+H]$^+$: 424.0557, found: 424.0557.

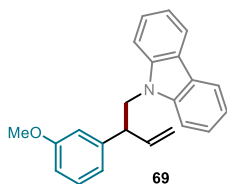### (*S*)-9-(2-(3-methoxyphenyl)but-3-en-1-yl)-9*H*-carbazole (69)

Prepared according to *GP2*, using [Ir(cod)Cl]$_2$/(*S*)-**L** as the catalytic system, diethyl 4-((9*H*-carbazol-9-yl)methyl)-2,6-dimethyl-1,4-dihydro pyridine-3,5-dicarboxylate **41** (43 mg, 100 µmol) and 1-(3-methoxyphenyl)prop-2-en-1-ol (33 mg, 200 µmol) as the substrates, and performing the reaction in acetone. The crude mixture was purified by flash column chromatography (isocratic 30% PhMe in hexane) to afford product **69** (23 mg, 68% yield, 84% ee) as a colorless oil. The enantiomeric excess was determined by
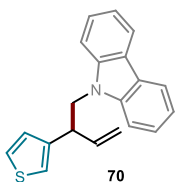
UPC^2 analysis on a Daicel Chiralpak IB-3 column: gradient CO_2/CH_3CN from 100% CO_2 to 60:40 over 4 minutes, curve 6, flow rate 2 mL/min, λ = 260 nm: τ_{major} = 4.3 min, τ_{minor} = 4.5 min; $[\alpha]_D^{26}$ = -0.6 (c = 0.87, CH_2Cl_2, 84% ee). The absolute configuration for the title compound was assigned in comparison to compounds **66** and **67**.

<u>^{1}H NMR</u> (400 MHz, CDCl$_3$): δ 8.09 (dt, *J* = 7.5, 1.0 Hz, 2H), 7.42 (ddd, *J* = 8.5, 7.0, 1.0 Hz, 2H), 7.29 (dt, *J* = 8.5, 1.0 Hz, 2H), 7.25 – 7.17 (m, 3H), 6.82 (dt, *J* = 7.5, 1.5 Hz, 1H), 6.76 (ddd, *J* = 8.0, 2.5, 1.0 Hz, 1H), 6.68 (dd, *J* = 2.5, 1.5 Hz, 1H), 6.15 (ddd, *J* = 17.0, 10.5, 7.5 Hz, 1H), 5.04 (dt, *J* = 10.5, 1.0 Hz, 1H), 4.99 (dt, *J* = 17.0, 1.5 Hz, 1H), 4.64 (dd, *J* = 14.5, 8.0 Hz, 1H), 4.51 (dd, *J* = 14.5, 7.0 Hz, 1H), 4.01 (app q, *J* = 7.5 Hz, 1H), 3.69 (s, 3H).

<u>^{13}C NMR</u> (101 MHz, CDCl$_3$): δ 160.0, 143.0, 140.7, 138.3, 129.8, 125.6, 123.0, 120.3, 120.2, 119.0, 117.1, 113.9, 112.5, 109.1, 55.3, 49.4, 49.0.

<u>HRMS (ESI)</u> Exact mass calculated for $C_{23}H_{22}NO$ [M+H]$^+$: 328.1696, found: 328.1699.

(*S*)-9-(2-(thiophen-3-yl)but-3-en-1-yl)-9*H*-carbazole (70)

Prepared according to *GP2*, using [Ir(cod)Cl]$_2$/(*S*)-**L** as the catalytic system, diethyl 4-((9*H*-carbazol-9-yl)methyl)-2,6-dimethyl-1,4-dihydropyridine-3,5-dicarboxylate **41** (43 mg, 100 µmol) and 1-(thiophen-3-yl)prop-2-en-1-ol (28 mg, 200 µmol) as the substrates, and performing the reaction in acetone. The crude mixture was purified by flash column chromatography (isocratic 10% PhMe in hexane) to afford product **70** (14 mg, 44% yield, 88% ee) as a colorless oil. The enantiomeric excess was determined by UPC^2 analysis on a Daicel Chiralpak IB-3 column: gradient CO_2/CH_3CN from 100% CO_2 to 60:40 over 4 minutes, curve 6, flow rate 2 mL/min, λ = 260 nm: τ_{major} = 4.4 min, τ_{minor} = 4.6 min; $[\alpha]_D^{26}$ = +24.7 (c = 0.43, CH_2Cl_2, 88% ee). The absolute configuration for the title compound was assigned in comparison to compounds **66** and **67**.

<u>^{1}H NMR</u> (400 MHz, CDCl$_3$): δ 8.08 (dt, *J* = 7.5, 1.0 Hz, 2H), 7.41 (ddd, *J* = 8.5, 7.0, 1.0 Hz, 2H), 7.32 – 7.12 (m, 5H), 6.92 (d, *J* = 4.0 Hz, 2H), 6.10 (ddd, *J* = 17.0, 10.5, 7.5 Hz, 1H), 5.07 – 4.96 (m, 2H), 4.63 – 4.47 (m, 2H), 4.17 (app q, *J* = 7.5 Hz, 1H).

<u>^{13}C NMR</u> (101 MHz, CDCl$_3$): δ 141.7, 140.7, 138.1, 127.1, 126.1, 125.7, 123.0, 121.4, 120.4, 119.0, 117.1, 109.0, 48.8, 44.8.

<u>HRMS (ESI)</u> Exact mass calculated for $C_{20}H_{18}NS$ [M+H]$^+$: 304.1154, found: 304.1156.

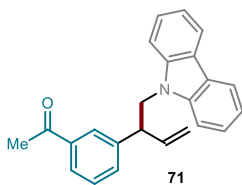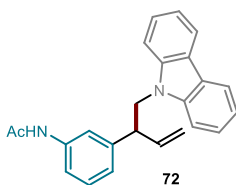### (S)-1-(3-(1-(9H-carbazol-9-yl)but-3-en-2-yl)phenyl)ethan-1-one (71)

Prepared according to *GP2*, using [Ir(cod)Cl]$_2$/(S)-**L** as the catalytic system, diethyl 4-((9H-carbazol-9-yl)methyl)-2,6-dimethyl-1,4-dihydropyridine-3,5-dicarboxylate **41** (43 mg, 100 µmol) and 1-(3-(1-hydroxyallyl)phenyl)ethan-1-one (35 mg, 200 µmol) as the substrates, and performing the reaction in acetone. The crude mixture was purified by flash column chromatography (isocratic PhMe) to afford product **71** (18 mg, 52% yield, 78% ee) as a colorless oil. The enantiomeric excess was determined by UPC^2 analysis on a Daicel Chiralpak IB-3 column: gradient CO$_2$/CH$_3$CN from 100% CO$_2$ to 60:40 over 4 minutes, curve 6, flow rate 2 mL/min, λ =260 nm: τ_{major} = 4.5 min, τ_{minor} = 4.6 min; $[\alpha]_D^{26}$ = -15.6 (c = 0.91, CH$_2$Cl$_2$, 78% ee). The absolute configuration for the title compound was assigned in comparison to compounds **66** and **67**.

^{1}H NMR (400 MHz, CDCl$_3$): δ 8.06 (dt, *J* = 8.0, 1.0 Hz, 2H), 7.73 (dt, *J* = 7.0, 2.0 Hz, 1H), 7.66 – 7.61 (m, 1H), 7.38 (ddd, *J* = 8.5, 7.0, 1.0 Hz, 2H), 7.34 – 7.27 (m, 2H), 7.25 – 7.16 (m, 4H), 6.19 (ddd, *J* = 17.0, 10.5, 7.5 Hz, 1H), 5.15 (dt, *J* = 10.5, 1.0 Hz, 1H), 5.08 (dt, *J* = 17.0, 1.5 Hz, 1H), 4.67 (dd, *J* = 14.5, 7.5 Hz, 1H), 4.51 (dd, *J* = 14.5, 7.5 Hz, 1H), 4.12 (app q, *J* = 7.5 Hz, 1H), 2.42 (s, 3H).

^{13}C NMR (101 MHz, CDCl$_3$): δ 198.1, 141.9, 140.5, 137.7, 137.5, 132.7, 129.0, 127.8, 127.2, 125.7, 123.0, 120.4, 119.1, 117.6, 109.0, 48.9, 48.8, 26.6.

HRMS (ESI) Exact mass calculated for C$_{24}$H$_{22}$NO [M+H]$^+$: 340.1696, found: 340.1692.

(S)-N-(3-(1-(9H-carbazol-9-yl)but-3-en-2-yl)phenyl)acetamide (72)

Prepared according to *GP2*, using [Ir(cod)Cl]$_2$/(S)-**L** as the catalytic system, diethyl 4-((9H-carbazol-9-yl)methyl)-2,6-dimethyl-1,4-dihydropyridine-3,5-dicarboxylate **41** (43 mg, 100 µmol) and N-(3-(1-hydroxyallyl)phenyl)acetamide (38 mg, 200 µmol) as the substrates, and performing the reaction in acetone. The crude mixture was purified by flash column chromatography (isocratic 30% PhMe in hexane) to afford product **72** (26 mg, 72% yield, 88% ee) as a colorless solid. The enantiomeric excess was determined by UPC^2 analysis on a Daicel Chiralpak IB-3 column: gradient CO$_2$/CH$_3$CN from 100% CO$_2$ to 60:40 over 4 minutes, curve 6, flow rate 2 mL/min, λ = 230 nm: τ_{major} = 5.6 min, τ_{minor} = 5.7 min; $[\alpha]_D^{26}$ = -18.4 (c = 0.96, CH$_2$Cl$_2$, 88% ee). The absolute configuration for the title compound was assigned in comparison to compounds **66** and **67**.

^{1}H NMR (400 MHz, CDCl$_3$): δ 8.06 (dt, *J* = 7.5, 1.0 Hz, 2H), 7.44 – 7.34 (m, 3H), 7.35 – 7.25 (m, 3H), 7.24 – 7.15 (m, 4H), 6.92 (d, *J* = 7.5 Hz, 1H), 6.12 (ddd, *J* = 17.5, 10.5, 7.5 Hz, 1H), 5.08 – 4.91 (m, 2H), 4.61 (dd, *J* = 14.5, 8.0 Hz, 1H), 4.50 (dd, *J* = 14.5, 7.0 Hz, 1H), 4.00 (app q, *J* = 7.5 Hz, 1H), 2.13 (s, 3H).

^{13}C NMR (101 MHz, CDCl$_3$): δ 168.4, 142.4, 140.6, 138.4, 138.1, 129.4, 125.7, 123.8, 122.9, 120.3, 119.4, 119.0, 118.6, 117.2, 109.1, 49.3, 49.0, 24.7.

HRMS (ESI) Exact mass calculated for C$_{24}$H$_{22}$N$_2$NaO [M+Na]$^+$: 377.1624, found: 377.1638.

(S)-9-(2-(o-tolyl)but-3-en-1-yl)-9H-carbazole (73)

Prepared according to *GP2*, using using pre-formed complex **Ph-Ir-III** as the catalyst, diethyl 4-((9H-carbazol-9-yl)methyl)-2,6-dimethyl-1,4-dihydro pyridine-3,5-dicarboxylate **41** (43 mg, 100 µmol) and 1-(o-tolyl)prop-2-en-1-ol (21 mg, 140 µmol) as the substrates, and performing the reaction in acetone. The crude mixture 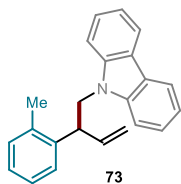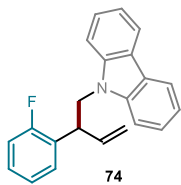was purified by flash column chromatography (isocratic 5% PhMe in hexane) to afford product **73** (20 mg, 61% yield, 70% ee) as a colorless oil. The enantiomeric excess was determined by UPC^2 analysis on a Daicel Chiralpak IB-3 column: gradient CO$_2$/CH$_3$CN from 100% CO$_2$ to 60:40 over 4 minutes, curve 6, flow rate 2 mL/min, λ = 260 nm: τ$_{major}$ = 5.1 min, τ$_{minor}$ = 5.4 min; [α]$_D^{26}$ = +14.4 (c = 0.20, CH$_2$Cl$_2$, 70% ee). The absolute configuration for the title compound was assigned in comparison to compounds **66** and **67**.

^{1}H NMR (400 MHz, CDCl$_3$): δ 8.08 (d, J = 8.0 Hz, 2H), 7.48 – 7.37 (m, 3H), 7.29 (d, J = 8.0 Hz, 3H), 7.25 – 7.19 (m, 2H), 7.14 (td, J = 7.5, 1.5 Hz, 1H), 7.05 (d, J = 7.5 Hz, 1H), 6.07 (ddd, J = 17.0, 10.5, 7.0 Hz, 1H), 4.99 (dt, J = 10.5, 1.5 Hz, 1H), 4.89 (dt, J = 17.0, 1.5 Hz, 1H), 4.72 (dd, J = 14.5, 8.5 Hz, 1H), 4.51 (dd, J = 14.5, 6.5 Hz, 1H), 4.29 (dt, J = 8.0, 6.5 Hz, 1H), 2.05 (s, 3H).

^{13}C NMR (101 MHz, CDCl$_3$): δ 140.7, 139.7, 138.8, 136.5, 130.8, 127.0, 126.9, 126.5, 125.7, 123.0, 120.4, 119.0, 116.6, 109.0, 48.7, 44.7, 19.6.

HRMS (ESI) Exact mass calculated for C$_{23}$H$_{22}$N [M+H]$^+$: 312.1747, found: 312.1745.

(S)-9-(2-(2-fluorophenyl)but-3-en-1-yl)-9H-carbazole (74)

Prepared according to *GP2*, using [Ir(cod)Cl]$_2$/(S)-**L** as the catalytic system, diethyl 4-((9H-carbazol-9-yl)methyl)-2,6-dimethyl-1,4-dihydropyridine-3,5-dicarboxylate **41** (43 mg, 100 µmol) and 1-(2-fluorophenyl)prop-2-en-1-ol (30 mg, 200 µmol) as the substrates, and performing the reaction in acetone. The crude mixture was purified by flash column chromatography (isocratic 5% PhMe in hexane) to afford product **74** (17 mg, 50% yield, 74% ee) as a colorless oil. The enantiomeric excess was determined by UPC^2 analysis on a Daicel Chiralpak IB-3 column: gradient CO$_2$/CH$_3$CN from 100% CO$_2$ to 60:40 over 4 minutes, curve 6, flow rate 2 mL/min, λ = 260 nm: τ$_{major}$ = 3.7 min, τ$_{minor}$ = 4.00 min; [α]$_D^{26}$ = +8.6 (c = 0.43, CH$_2$Cl$_2$, 74% ee). The absolute configuration for the title compound was assigned in comparison to compounds **66** and **67**.

<u>^{1}H NMR</u> (400 MHz, CDCl$_3$): δ 807 (d, J = 7.5 Hz, 2H), 7.47 – 7.35 (m, 4H), 7.26 – 7.17 (m, 4H), 7.10 – 6.99 (m, 2H), 6.19 (dddd, J = 17.0, 10.0, 8.0, 1.5 Hz, 1H), 5.03 – 4.89 (m, 2H), 4.71 – 4.53 (m, 2H), 4.31 (app q, J = 7.5 Hz, 1H).

<u>^{13}C NMR</u> (101 MHz, CDCl$_3$): δ 161.1 (d, $^1J_{C\text{-}F}$ = 245 Hz), 140.7, 136.8 (d, $^4J_{C\text{-}F}$ = 1.5 Hz), 129.6 (d, $^3J_{C\text{-}F}$ = 5.0 Hz), 128.8 (d, $^3J_{C\text{-}F}$ = 8.5 Hz), 128.2 (d, $^2J_{C\text{-}F}$ = 14.5 Hz), 125.7, 124.6 (d, $^4J_{C\text{-}F}$ = 3.5 Hz), 123.0, 120.4, 119.1, 117.8, 116.0 (d, $^2J_{C\text{-}F}$ = 22.5 Hz), 109.0, 47.7 (d, $^3J_{C\text{-}F}$ = 2.5 Hz), 44.6.

<u>^{19}F NMR</u> (376 MHz, CDCl$_3$): δ -117.0 (s, 1F).

<u>HRMS (ESI)</u> Exact mass calculated for C$_{22}$H$_{19}$FN [M+H]$^+$: 316.1496, found: 316.1500.

2.8.4 Mechanistic Studies

2.8.4.1 Electrochemical Studies

The following differential pulse voltammetry (DPV) analysis was performed on an electrochemical workstation installed inside a glovebox, in order to secure measurements under inert atmosphere.
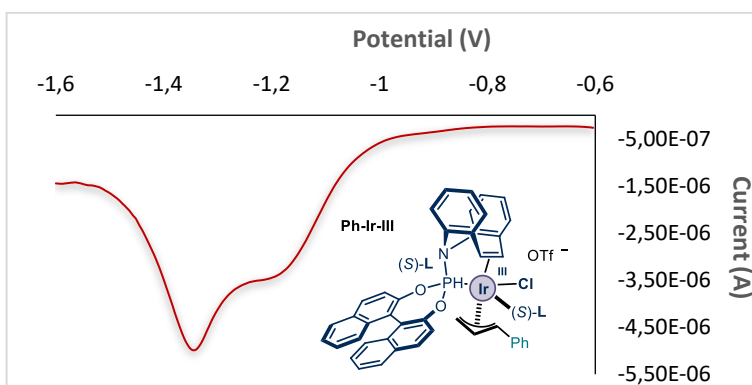
Figure 2.12. Differential pulse voltammogram for the pre-formed complex **Ph-Ir-III** [0.005M] in [0.1 M] TBAPF6 in CH2Cl2. Initial E: -0.6 V; final E: -1.6 V; amplitude: 0.05 V; pulse width: 0.05 sec; sample width: 0.017 sec; pulse period: 0.5 sec; quiet time: 2 sec. Glassy carbon electrode working electrode, Ag/AgNO3 (in Et2O) reference electrode, Pt wire auxiliary electrode. Irreversible reduction, EpC = E (**Ir(III)/Ir(II)**) = -1.34 V, EpC is the cathodic peak potential, while the E value describes the electrochemical properties of the ground-state complex **Ph-Ir-III**.
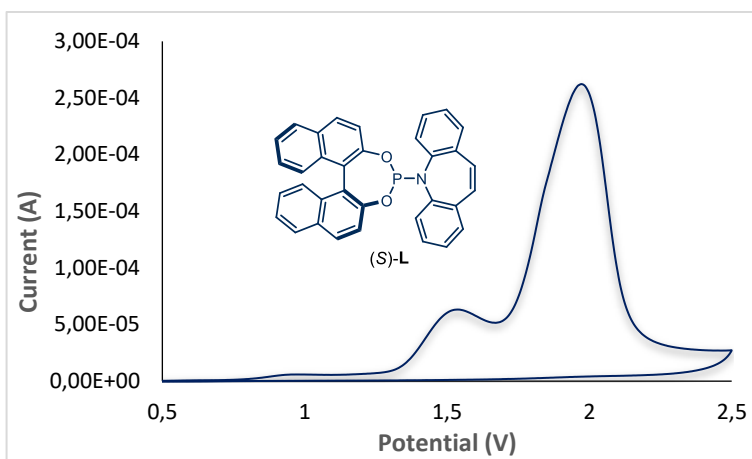
Figure 2.13. Cyclic voltammogram for the chiral ligand (S)-**L** [0.005M] in [0.1 M] TBAPF6 in CH3CN. Sweep rate: 50 mV/s. Pt electrode working electrode, Ag/AgCl (KCl saturated) reference electrode, Pt wire auxiliary electrode. Irreversible oxidation, EpA = E ((S)-**L**/(S)-**L·+**) = +1.53 V, EpA refers to the anodic peak potential, while the E value describes the electrochemical properties of (S)-**L**.
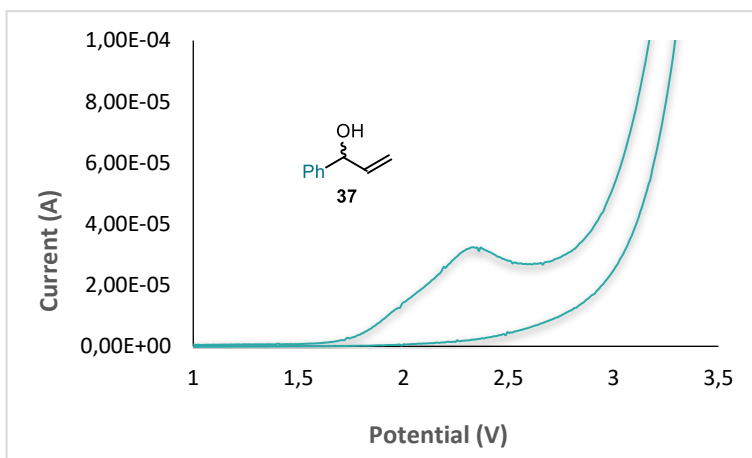
Figure 2.14. Cyclic voltammogram for allylic alcohol **37** [0.02M] in [0.1 M] TBAPF6 in CH3CN. Sweep rate: 30 mV/s. Pt electrode working electrode, Ag/AgCl (KCl saturated) reference electrode, Pt wire auxiliary electrode. Irreversible oxidation, EpA = E (**37**/**37·+**) = +2.36 V, EpA refers to the anodic peak potential, while the E value describes the electrochemical properties of **37**.
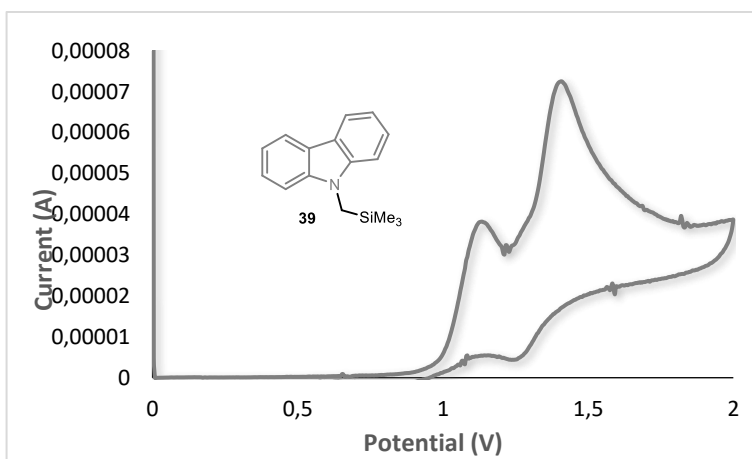
Figure 2.15. Cyclic voltammogram for silane **39** [0.001 M] in [0.1 M] TBAPF6 in CH3CN. Sweep rate: 100 mV/s. Glassy carbon working electrode, Ag/AgCl (KCl saturated) reference electrode, Pt wire auxiliary electrode. Irreversible oxidation, EpA = E (**39/39·+**) = +1.13 V, where EpA refers to the anodic peak potential, while the E value describes the electrochemical properties of **39**.
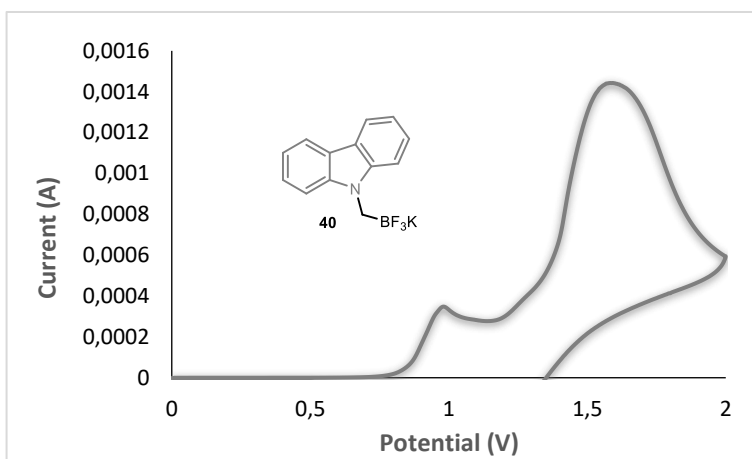
Figure 2.16. Cyclic voltammogram for trifluoroborate salt **40** [0.02 M] in [0.1 M] TBAPF6 in CH3CN. Sweep rate: 50 mV/s. Glassy carbon working electrode, Ag/AgCl (KCl saturated) reference electrode, Pt wire auxiliary electrode. Irreversible oxidation peaks, EpA = E (**40/40·+**) = +0.98 V, where EpA refers to the anodic peak potential, while the E value describes the electrochemical properties of **40**.
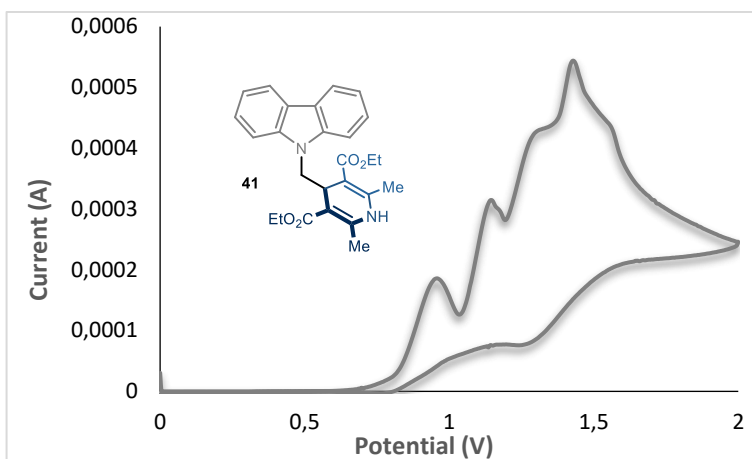
Figure 2.17. Cyclic voltammogram for 1,4-dihydropyridine **41** [0.02 M] in [0.1 M] TBAPF6 in CH3CN. Sweep rate: 50 mV/s. Platinum working electrode, Ag/AgCl (KCl saturated) reference electrode, Pt wire auxiliary electrode. Four irreversible oxidation peaks: EpA = E (**41**/**41**·+) = +0.96 V, where EpA refers to the anodic peak potential, while the E value describes the electrochemical properties of **41**.
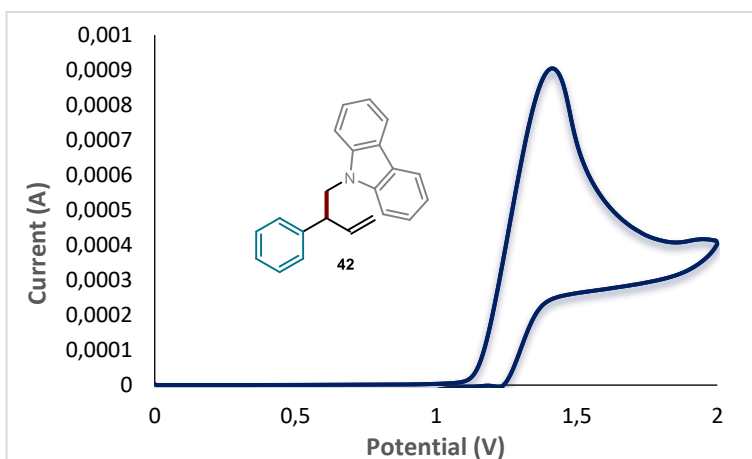
Figure 2.18. Cyclic voltammogram for product **42** [0.023 M] in [0.1 M] TBAPF6 in CH3CN. Sweep rate: 200 mV/s. Platinum working electrode, Ag/AgCl (KCl saturated) reference electrode, Pt wire auxiliary electrode. Irreversible oxidation peak, EpA = E (**42**/**42**·+) = +1.42 V, where EpA refers to the anodic peak potential, while the E value describes the electrochemical properties of **42**.

2.8.4.2 UV-vis Studies

Solutions at different concentrations of the analyte were introduced into a 1 cm path length quartz cuvette equipped with a Teflon® septum, under an argon atmosphere. Conversely, the UV-vis absorption profile of complex **Ph-Ir-III** was performed with a 0.1 cm path length quartz cuvette. All of the analyses were conducted using a UV-vis cary60-TR0

spectrophotometer. The absorbance show a typical Lambert-Beer linear correlation with respect to the concentration.
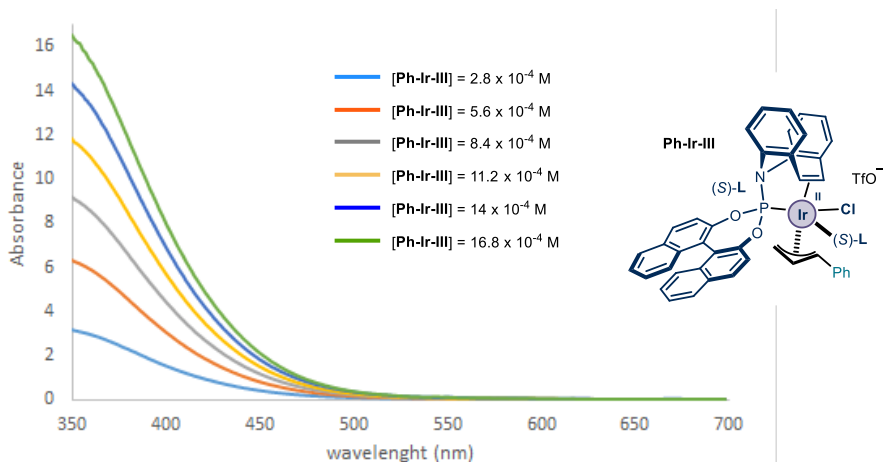
Figure 2.19. UV-vis absorption spectra for pre-formed complex **Ph-Ir-III**, recorded at different concentrations in anhydrous CHCl3. The spectrum profile does not present a discrete maximum of absorbance. The tail wavelength was considered to be at about 480 nm.
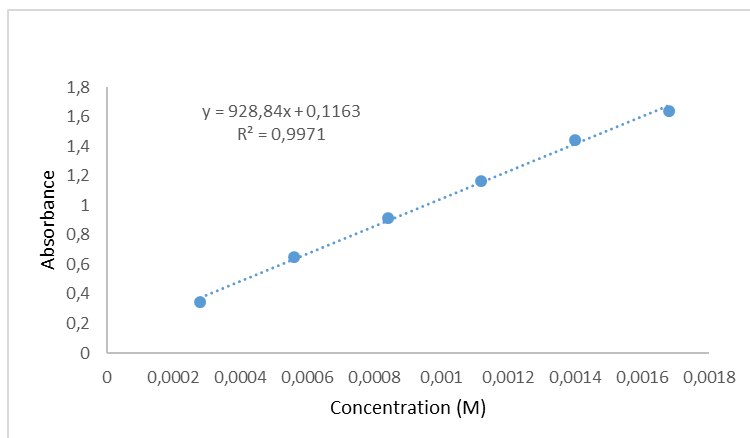
Figure 2.20. Lambert-Beer linear correlation between absorbance and concentration at 460 nm for complex **Ph-Ir-III**. A cuvette with an optical path length of 0.1 cm was used for the analyses. The slope of the line is the molar extinction coefficient ε at 460 nm (ε = 930 M-1 cm-1).
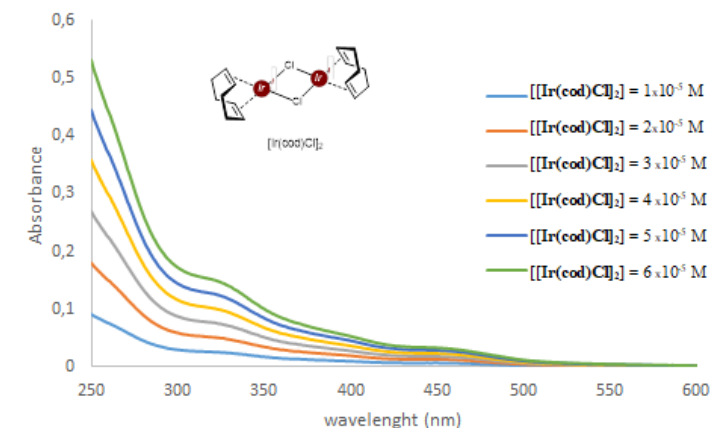
Figure 2.21. UV-vis absorption spectra for pre-catalyst [Ir(cod)Cl]2, recorded at different concentrations in anhydrous CH2Cl2.
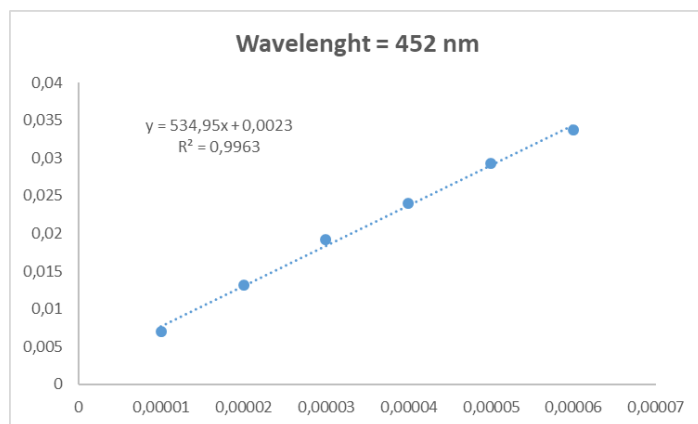
Figure 2.22. Lambert-Beer linear correlation between absorbance and concentration at 452 nm for [Ir(cod)Cl]2. The slope of the line is the molar extinction coefficient ε at 452 nm (ε = 535 M-1 cm-1).
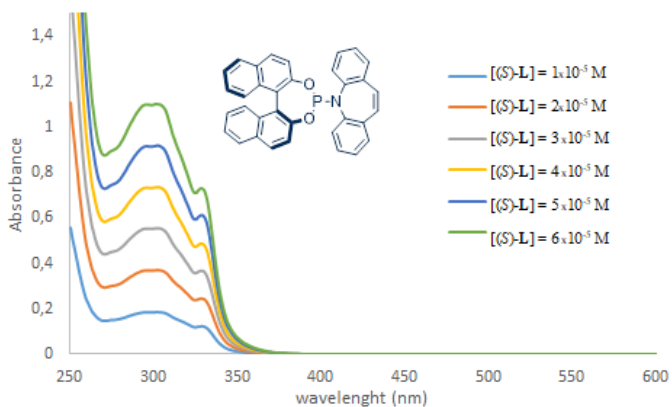
Figure 2.23. UV-vis absorption spectra for chiral ligand (S)-**L**, recorded at different concentrations in anhydrous CH2Cl2.
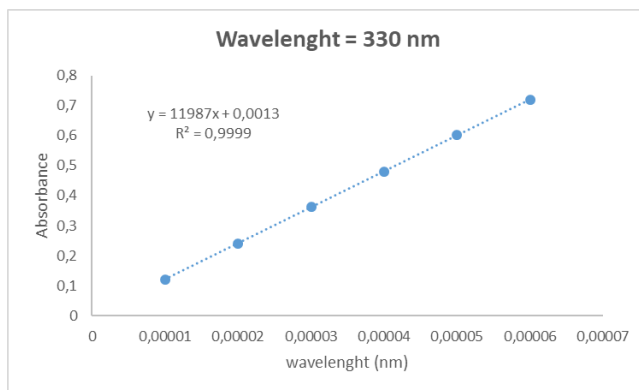
Figure 2.24. Lambert-Beer linear correlation between absorbance and concentration at 330 nm for ligand (S)-**L**. The slope of the line is the molar extinction coefficient ε at 330 nm (ε = 11987 M-1 cm-1).
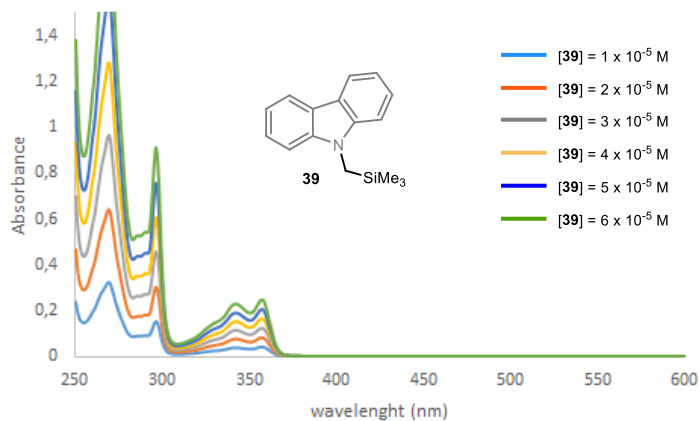
Figure 2.25. UV-vis absorption spectra of silane **39**, recorded at different concentrations in anhydrous CH2Cl2.
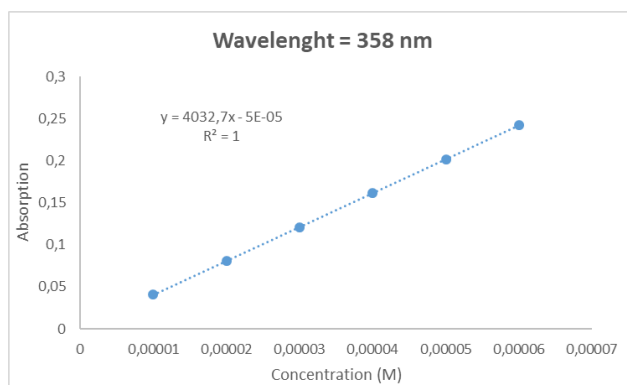
Figure 2.26. Lambert-Beer linear correlation between absorbance and concentration at 358 nm for silane **39**. The slope of the line is the molar extinction coefficient ε at 358 nm (ε = 4032 M-1 cm-1).
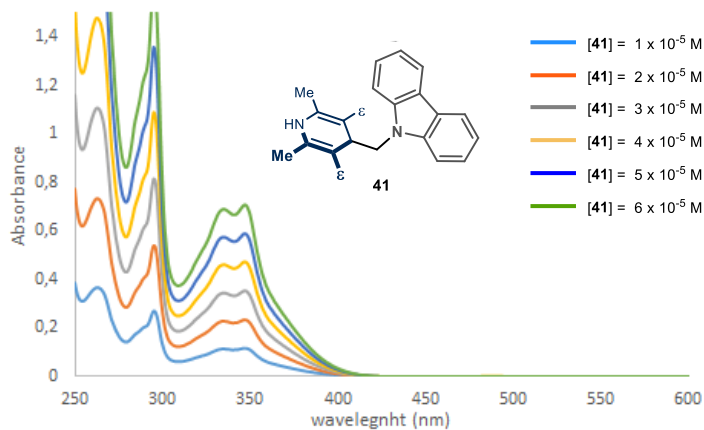
Figure 2.27. UV-vis absorption spectra of 1,4-dihydropyridine **41**, recorded at different concentrations in anhydrous CH2Cl2.
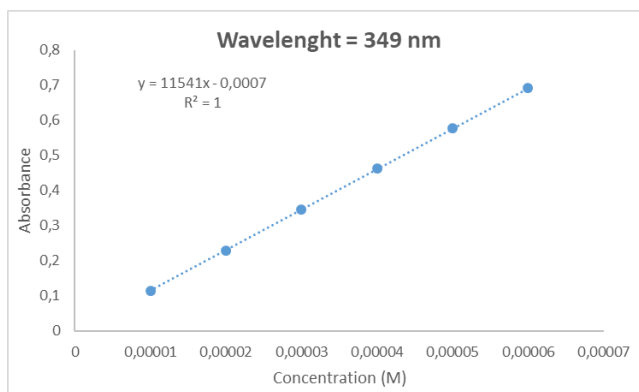
Figure 2.28. Lambert-Beer linear correlation between absorbance and concentration at 349 nm for substrate **41**. The slope of the line is the molar extinction coefficient ε at 349 nm (ε = 11541 M-1 cm-1).
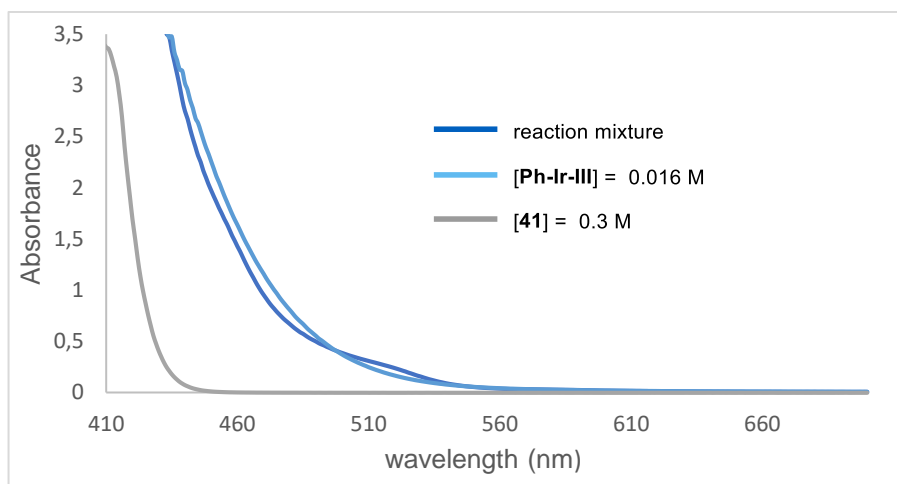
Figure 2.29. UV-vis absorption spectra of 1,4-dihydropyridine **41** (0.3 M), the in situ formed **Ph-Ir-III** complex (0.016M), and the reaction mixture (0.3 M with respect to **41**) recorded in degassed acetone. These studies, conducted under conditions that mirror the concentration of the model reaction, indicate that at 460 nm, which is the wavelength generally used in our experiments, the main absorbing species is the Ir(III)-π-allylic intermediate **Ph-Ir-III**, and that the direct excitation of substrates of type **41** does not play a relevant role.

2.8.4.3 Rehm-Weller approximation

Using the data collected from the differential pulse voltammetry (DPV) studies (*Section 2.8.4.1*) and from the absorption spectra (*Section 2.8.4.2*) of complex **Ph-Ir-III**, we could estimate the redox potential relative to its excited state **Ph-Ir-III***, by means of the following Equation 1:[62]

$$E(Ir(III)*/Ir(II)) = E(Ir(III)/Ir(II)) + E_{0-0}(Ir(III)*/Ir(III)) \qquad [Eq.\ 1]$$

Since the electrochemical oxidation of complex **Ph-Ir-III** was irreversible (Figure 2.12), the irreversible peak potential E_p^C was used for $E(Ir(III)/Ir(II))$. A direct spectroscopic evaluation of $E_{0-0}(Ir(III)*/Ir(III))$, deriving from the intersection point between the absorption and emission profiles for **Ph-Ir-III**, was not possible because of the overlap with the laser peak. Such evaluation was not feasible also when using diverse excitation wavelengths ($420 < \lambda < 480$ nm). Therefore, $E_{0-0}(Ir(III)*/Ir(III))$ was estimated spectroscopically from the position of the long wavelength tail of the absorption spectrum (480 nm, see Figure 2.19) recorded in anhydrous $CHCl_3$.

---

[62] Kavarnos, G. J. "Energetics of photoinduced electron transfer" in *Fundamentals of Photoinduced Electron Transfer*, VCH Publishers, 1993, pp 29-37.

For complex **Ph-Ir-III**, the $E_p{}^C$, which provides the E(Ir(III)/Ir(II)), is -1.34 V (Figure 2.12), while the position of the long wavelength tail of its absorption spectrum corresponds to 480 nm (Figure 2.19), which translates into an E_{0-0}(Ir(III)*/Ir(III)) of 2.58 eV.

$$E(Ir(III)^*/Ir(II)) = -1.34 \text{ V} + 2.58 \text{ V} = +1.24 \text{ V (vs Ag/Ag}^+ \text{ in CH}_2\text{Cl}_2)$$

2.8.4.4 Stern-Volmer Experiments

The emission spectra were recorded on a Fluorolog Horiba Jobin Yvon spectrofluorometer equipped with a photomultiplier detector, a double monochromator, and a 350W xenon light source. The absorption spectra were recorded in a UV-vis cary60-TR0 spectrophotometer.

Anhydrous $CHCl_3$ (2.5 mL), degassed by freeze pump thaw (5 cycles) and kept under argon sparging for 30 minutes prior of use, was placed into a 10 x 10 mm light path quartz fluorescence cuvette equipped with Silicone/PTFE 3.2 mm septum, under an argon atmosphere. 40 µL of a 6 mM solution of **Ph-Ir-III** in anhydrous $CHCl_3$ were added to the vessel, giving a final concentration of **Ph-Ir-III** of 0.1 mM. The excitation wavelength was fixed at 480 nm (incident light slit regulated to 6 mm), while the emission light was acquired from 490 nm to 700 nm (emission light slit regulated to 6 mm). A solvent blank was subtracted from the measurement.

N.B. In order to minimize detrimental effect of moisture and oxygen on complex **Ph-Ir-III**, this was weighted and handled into a nitrogen-filled glovebox. Conversely, the 6 mM stock solution and the solution inside the cuvette (0.1 mM) were prepared outside the glovebox, but always securing an inert atmosphere.
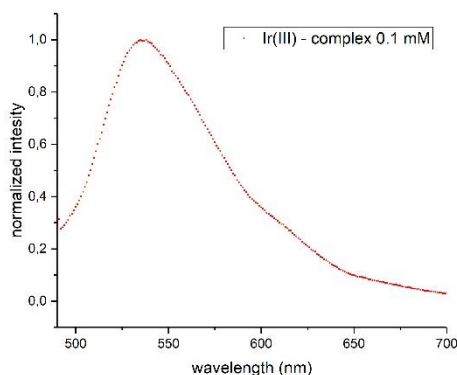
Figure 2.30. Emission spectrum of the preformed complex **Ph-Ir-III** (excitation wavelength at 480 nm).

A screw-capped vial, fitted with a rubber septum, was charged with 9-((trimethylsilyl)methyl)-9*H*-carbazole **39** (64 mg, 253 μmol), inside a nitrogen-filled glovebox. The vial was taken out from the glovebox and 0.5 mL of anhydrous, degassed CHCl$_3$ was added, delivering a 0.5 M solution with respect to **39**. 12 μL of this solution were added to a cuvette containing a 0.1 mM solution of complex **Ph-Ir-III**, prepared as previously described. The addition of **39** was repeated five consecutive times. After each addition, both an absorption spectrum and an emission spectrum of the title solution were recorded. The excitation wavelength was fixed at 480 nm (incident light slit regulated to 6 mm), the emission light was acquired from 490 nm to 700 nm (emission light slit regulated to 6 mm). A solvent blank was subtracted from all the measurements.

The excitation wavelength was chosen in order to avoid: 1) inner-filter effect of complex **Ph-Ir-III** (absorption at 480 nm < 0.1 a.u.), and 2) minimize the solvent scattering.

The results shown in Figure 2.31 indicate that silane **39** quenches the excited state of **Ph-Ir-III** and its emission.
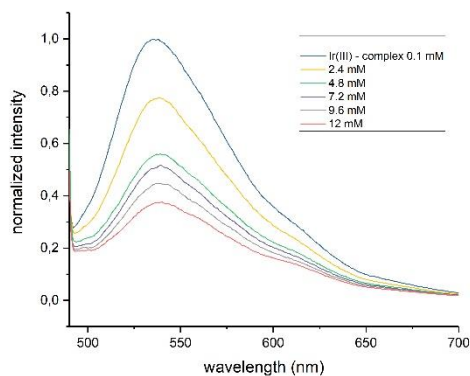
Figure 2.31. Quenching of the complex **Ph-Ir-III** emission (0.1 mM in CHCl3) in the presence of increasing amounts of silane radical precursor **39**.

The Stern-Volmer plot, reported in Figure 2.32, shows a linear correlation between the increasing amounts of **39** and the ratio I_0/I. Based on the following Equation 2, it is possible to calculate the Stern-Volmer constant K_{SV}.[53a]

$$I_0/I = 1 + K_{SV}[Q] \qquad [Eq.\ 2]$$

We calculated a Stern-Volmer quenching constant of 134 M^{-1}.
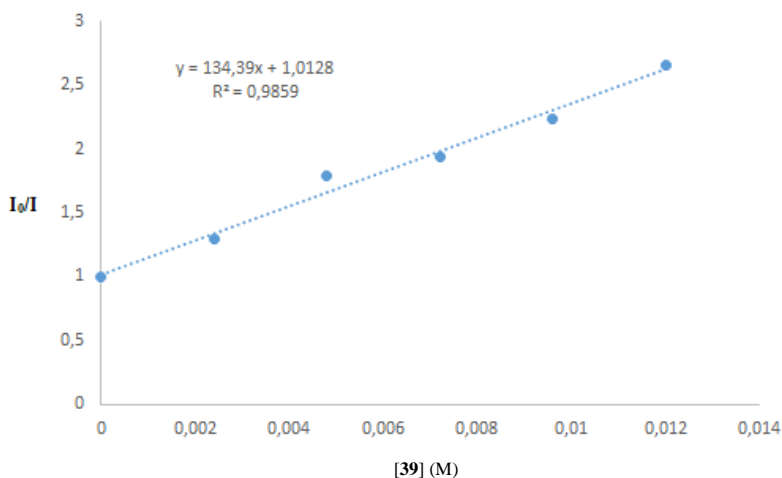
Figure 2.32. Stern-Volmer quenching plot.

During the addition of quencher **39**, a minimal decrease in absorption intensity was noticed. This can be ascribable to different factors: *e.g.* further dilution of the **Ph-Ir-III** solution upon sequential addition of the silane; minimal hydrolysis of the **Ph-Ir-III** over time etc.

The small change of normalized absorbance of complex **Ph-Ir-III** during the quenching experiment is shown in Figure 2.33:
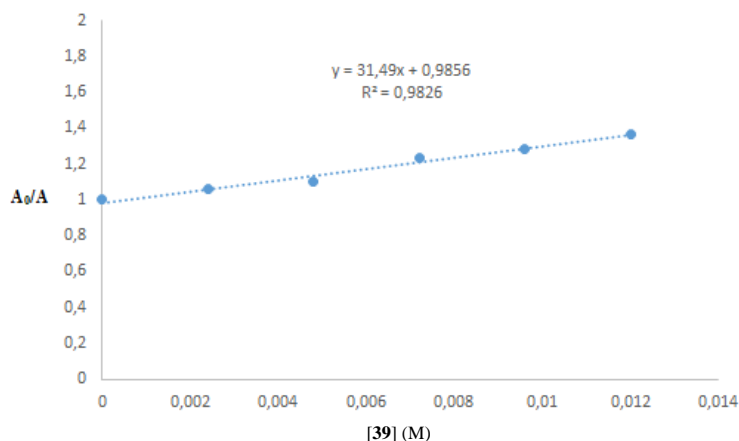
Figure 2.33. Slight decrease in absorption of **Ph-Ir-III** during the quenching experiment.

In order to account for this minimal variation of **Ph-Ir-III** concentration, we calculated the Stern-Volmer quenching constant, according to Eq. 2, but subtracting the value of the slope of the change in absorbance (31.4 M^{-1}), as deduced from Figure 2.33.

This correction provided a quenching constant of 102.8 M^{-1}.

A static quenching can occur if a complex is formed in the ground-state between **Ph-Ir-III** and silane **39**. A careful analysis of the absorption spectra of complex **Ph-Ir-III** in the presence of increasing amounts of silane **39** has been carried out, which excluded the possibility of any ground-state association between **Ph-Ir-III** and **39** (Figure 2.34).
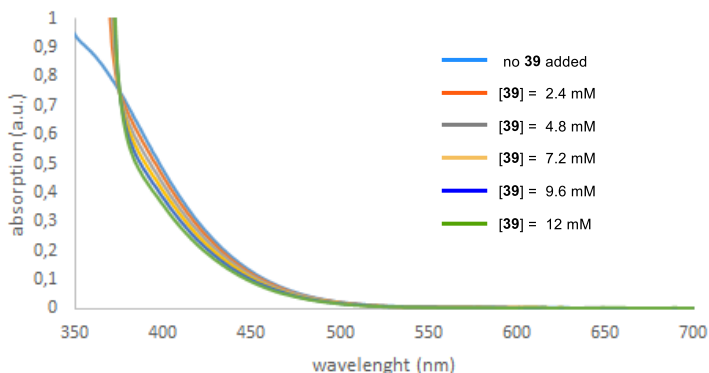
Figure 2.34. Absorption spectra of **Ph-Ir-III** with increasing amounts of quencher **39**.

Except for a minor decrease in absorption, no spectral variations were observed in the area between 350 nm – 700 nm, excluding any association in the ground-state. The absorption below 370 nm is due to the absorption profile of **39**.

2.8.4.5 Quantum Yield Determination

A ferrioxalate actinometer solution was prepared by following the Hammond variation of the Hatchard and Parker procedure outlined in the Handbook of Photochemistry.[59,63] The ferrioxalate actinometer solution measures the decomposition of ferric ions to ferrous ions, which are complexed by 1,10-phenanthroline and monitored by UV-vis absorbance at 510 nm. The moles of iron-phenanthroline complex formed are related to moles of photons absorbed.

The following solutions were prepared and stored in a dark laboratory (red light):

1. *Potassium ferrioxalate solution*: 294.8 mg of potassium ferrioxalate (commercially available from Alfa Aesar) and 139 μL of sulfuric acid (96%) were added to a 50 mL volumetric flask, and filled to the mark with water (HPLC grade).

2. *Phenanthroline solution*: 0.2% by weight of 1,10-phenanthroline in water (100 mg in 50 mL volumetric flask).

---

[63] Hatchard, C. G., Parker, C. A. "A new sensitive chemical actinometer. II. Potassium ferrioxalate as a standard chemical actinometer" *Proc. R. Soc. Lond. A* **1956**, *235*, 518-536.

3. *Buffer solution*: 2.47 g of NaOAc and 0.5 mL of sulfuric acid (96%) were added to a 50 mL volumetric flask, and filled to the mark with water (HPLC grade).

*Quantum Yield for the Reaction between Alcohol **37** and Silane **39***:

The actinometry measurements were done as follows:

1) 1 mL of the actinometer solution was added to a screw-cap vial and placed on a single HP LED 1.5 cm away from the light source. The solution was irradiated at 460 nm (irradiance 30 mW/cm^2). This procedure was repeated 5 times, quenching the solutions after different time intervals: 5 sec, 10 sec, 15 sec, 20 sec, and 25 sec.

2) After irradiation, the actinometer solutions were removed and placed in a 10 mL volumetric flask containing 0.5 mL of 1,10-phenanthroline solution and 2 mL of buffer solution. These flasks were filled to the mark with water (HPLC grade).

3) The UV-vis spectra of the complexed actinometer samples were recorded for each time interval. The absorbance of the complexed actinometer solution was monitored at 510 nm.
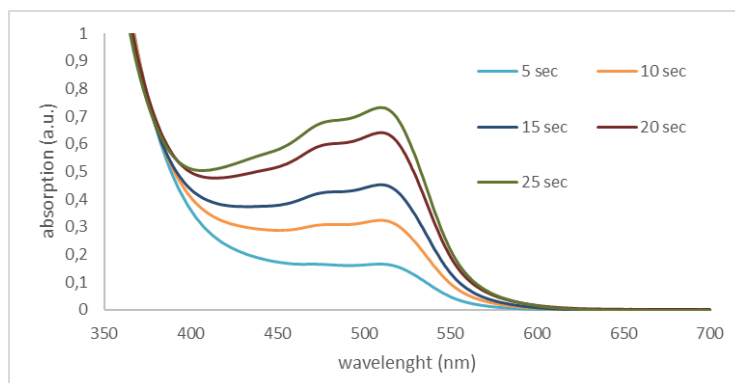
Figure 2.35. Absorbance of the complexed actinometer solutions.

The moles of Fe^{2+} formed for each sample is determined using Beers' Law (Equation 3):

$$Mols\ of\ Fe(II) = V_1{\times}V_3{\times}\ \Delta A(510\ nm)/10^3{\times}V_2{\times}l{\times}\varepsilon(510\ nm) \qquad [Eq.\ 3]$$

where V_1 is the irradiated volume (1 mL), V_2 is the aliquot of the irradiated solution taken for the determination of the ferrous ions (1 mL), V_3 is the final volume after complexation with phenanthroline (10 mL), l is the optical path-length of the irradiation cell (1 cm), ΔA (510 nm) is the optical difference in absorbance between the irradiated solution and the one stored in the dark, ε(510 nm) is the extinction coefficient the complex Fe(phen)$_3^{2+}$ at 510 nm (11100 L mol^{-1} cm^{-1}). The moles of Fe^{2+} formed (x) are plotted as a function of time (t). The slope of

this line was correlated to the moles of incident photons by unit of time ($q^0_{n,p}$) by the use of the following Equation 4:

$$(1)\ \Phi(\lambda) = dx/dt\ q_{n,p}^0\ [1-10^{-A(\lambda)}\ ] \qquad [Eq.\ 4]$$

where dx/dt is the rate of change of a measurable quantity (spectral or any other property), the quantum yield (Φ) for Fe^{2+} at 458 nm is 1.11,[63] $[1-10^{-A(\lambda)}]$ is the ratio of absorbed photons by the solution, and $A(\lambda)$ is the absorbance of the actinometer at the wavelength used to carry out the experiments (460 nm). The absorbance at 460 nm A(460) was measured using a UV-vis cary60-TR0 spectrophotometer in a 10 mm path quartz cuvette, obtaining an absorbance of 0.144.

$q_{n,p}^0$, which is the photon flux, was determined to be $8.49\ \times10^{-8}$ einstein s^{-1}
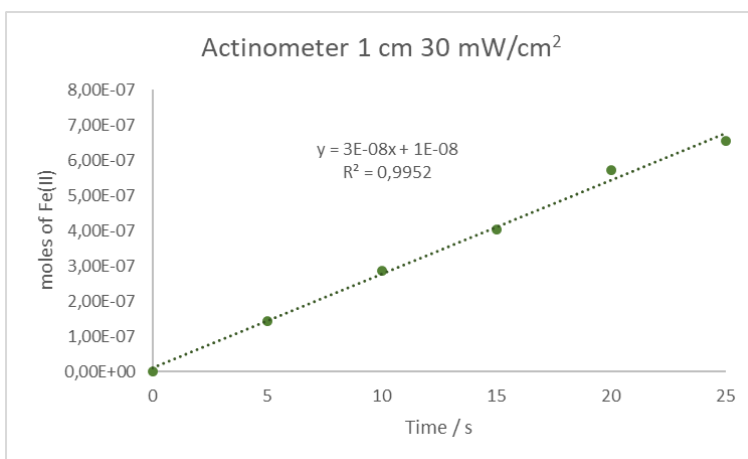
Subsequently, the photochemical reactions were performed: a screw-capped vial, fitted with a rubber septum, was charged with $[Ir(cod)Cl]_2$ (5 mg, 7.5 µmol), chiral ligand (S)-**L** (17 mg, 33.0 µmol) and anhydrous acetone (1 mL), under argon atmosphere. The resulting solution was vigorously stirred for 15 minutes and, then, transferred into a vial containing 9-((trimethylsilyl)methyl)-9H-carbazole **39** (76 mg, 300 µmol) and α-vinyl benzyl alcohol **37** (79 µL, 600 µmol), affording a yellow solution. To this solution was added TFA (24 µL, 300 µmol), and the vial was sealed with a screw-cap. The vessel was placed into a 3D-printed plastic support mounted on an aluminum block fitted with a blue high-power single LED (λ = 460 nm, irradiance = 30 mW/cm²), as controlled by an external power supply (see Figure 2.10). The reaction was stirred under visible light irradiation at ambient temperature for the time stated. Three different reactions were carried out and quenched at 10 min, 20 min and 30 min, respectively.

The moles of product **42** formed for the model reaction were determined by gas chromatography measurement (FID detector) using 1,3,5-trimethoxybenzene as internal standard. The moles of product per unit of time are related to the number of photons absorbed.

The photons absorbed are correlated to the number of incident photons by the use of Equation 1. According to this, plotting the moles of product (x) versus the moles of incident photons (q_n, $^0 \cdot dt$), the slope is equal to: $\Phi \cdot (1-10^{-A(\lambda)(460\ nm)})$, where Φ is the quantum yield to be determined and A(460 nm) is the absorption of the reaction under study. A(460 nm) was measured using a UV-vis cary60-TR0 spectrophotometer in 10 mm path quartz. An absorbance of 0.016 was determined for the model reaction mixture. The quantum yield (Φ) of the photochemical transformation was measured to be **0.14**.
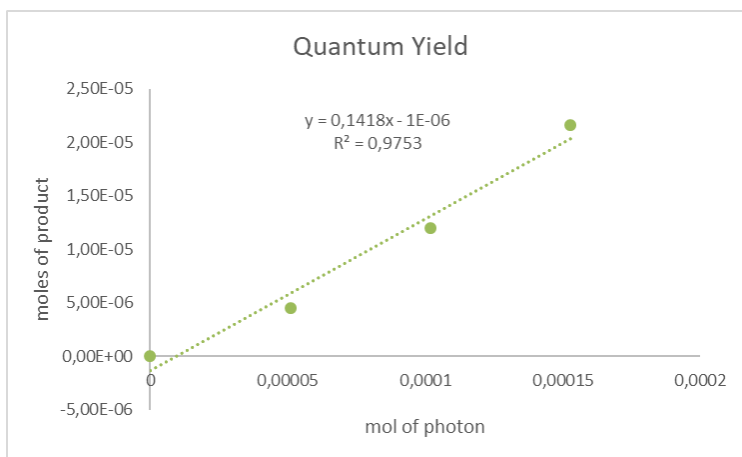
The procedure was repeated a second time to provide an akin value: quantum yield (Φ), at 460 nm of **0.13** ($R^2 = 0.916$; four points, 15 min, 20 min, 30 min and 40 min).

Quantum Yield for the Reaction between Alcohol 37 and 1,4-Dihydropyridine 41:

The actinometry measurements were performed as detailed before with modifications relative to the light intensity used, solely:

1) 1 mL of the actinometer solution was added to a screw-cap vial and placed on a single HP LED 1.5 cm away from the light source. The solution was irradiated at 460 nm (irradiance 11 mW/cm^2). This procedure was repeated 4 times, quenching the solutions after different time intervals: 5 sec, 10 sec, 15 sec, 20 sec, and 25 sec.

2) After irradiation, the actinometer solutions were removed and placed in a 10 mL volumetric flask containing 0.5 mL of 1,10-phenanthroline solution and 2 mL of buffer solution. These flasks were filled to the mark with water (HPLC grade).

3) The UV-Vis spectra of the complexed actinometer samples were recorded for each time interval. The absorbance of the complexed actinometer solution was monitored at 510 nm.
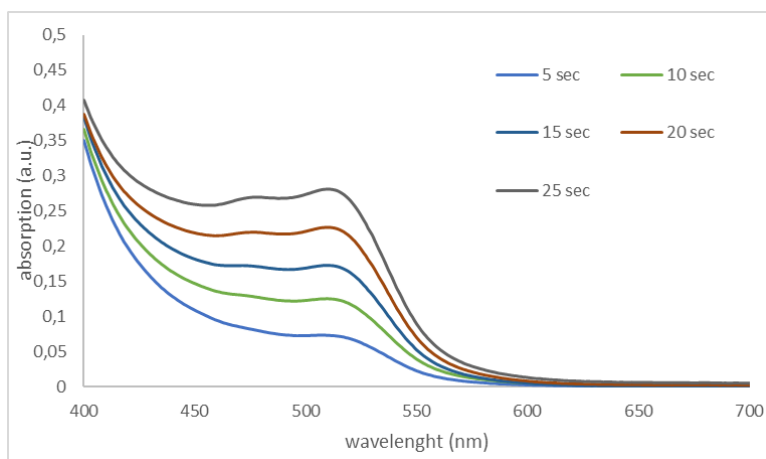
Figure 2.36. Absorbance of the complexed actinometer solutions.

The moles of Fe^{2+} formed for each sample is determined using Beers' Law (Equation 3):

$$Mols\ of\ Fe(II) = V_1 \times V_3 \times \Delta A(510\ nm)/10^3 \times V_2 \times l \times \varepsilon(510\ nm) \qquad [Eq.\ 3]$$

where V_1 is the irradiated volume (1 mL), V_2 is the aliquot of the irradiated solution taken for the determination of the ferrous ions (1 mL), V_3 is the final volume after complexation with phenanthroline (10 mL), l is the optical path-length of the irradiation cell (1 cm), ΔA (510 nm) is the optical difference in absorbance between the irradiated solution and the one stored in the dark, $\varepsilon(510\ nm)$ is the extinction coefficient the complex $Fe(phen)_3^{2+}$ at 510 nm (11100 L mol^{-1} cm^{-1}). The moles of Fe^{2+} formed (x) are plotted as a function of time (t). The slope of this line was correlated to the moles of incident photons by unit of time ($q^0_{n,p}$) by the use of the following Equation 4:

$$(1)\ \Phi(\lambda) = dx/dt\ q_{n,p}^0\ [1-10^{-A(\lambda)}\ ] \qquad [Eq.\ 4]$$

where dx/dt is the rate of change of a measurable quantity (spectral or any other property), the quantum yield (Φ) for Fe^{2+} at 458 nm is 1.11,[63] $[1-10^{-A(\lambda)}]$ is the ratio of absorbed photons by the solution, and $A(\lambda)$ is the absorbance of the actinometer at the wavelength used to carry out the experiments (460 nm). The absorbance at 460 nm A(460) was measured using a UV-vis cary60-TR0 spectrophotometer in a 10 mm path quartz cuvette, obtaining an absorbance of 0.147.

$q_{n,p}^0$, which is the photon flux, was determined to be 2.93 x10^{-8} einstein s^{-1}
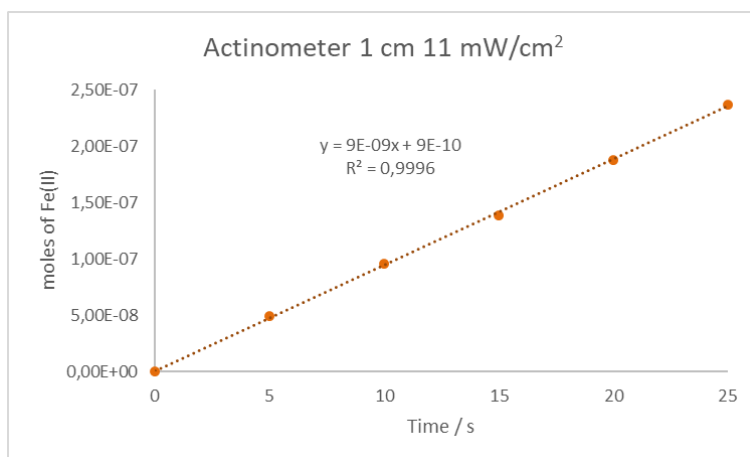
Actinometer 1 cm 11 mW/cm²

$y = 9E\text{-}09x + 9E\text{-}10$
$R^2 = 0,9996$

Subsequently, the photochemical reactions were performed: a screw-capped vial, fitted with a rubber septum, was charged with $[\text{Ir(cod)Cl}]_2$ (5 mg, 7.5 µmol), chiral ligand (*S*)-**L** (17 mg, 33.0 µmol) and anhydrous, argon sparged, acetone (1 mL), under argon atmosphere. The resulting solution was vigorously stirred for 15 minutes and, then, transferred to a vial containing diethyl 4-((9*H*-carbazol-9-yl)methyl)-2,6-dimethyl-1,4-dihydropyridine-3,5-dicarboxylate **41** (130 mg, 300 µmol) and α-vinyl benzyl alcohol **37** (79 µL, 600 µmol) under argon atmosphere, affording a yellow solution. To this solution was added TFA (24 µL, 300 µmol) and the vial was sealed with a screw-cap. The vessel was placed into a 3D-printed plastic support mounted on an aluminum block fitted with a blue high-power single LED (λ = 460 nm, irradiance = 11 mW/cm²), as controlled by an external power supply (see Figure S2). The reaction was stirred under visible light irradiation at ambient temperature for the time stated. Four different reactions were carried out and quenched at 2 min, 4 min, 6 min and 8 min, respectively.

The moles of product **42** formed for the model reaction were determined by gas chromatography measurement (FID detector) using 1,3,5-trimethoxybenzene as internal standard. The moles of product per unit of time are related to the number of photons absorbed. The photons absorbed are correlated to the number of incident photons by the use of Equation 1. According to this, plotting the moles of product (x) versus the moles of incident photons ($q_n,^{0} \cdot dt$), the slope is equal to: $\Phi \cdot (1\text{-}10^{-A(\lambda)(460 \text{ nm})})$, where Φ is the quantum yield to be determined and A(460 nm) is the absorption of the reaction under study. A(460 nm) was measured using a UV-Vis cary60-TR0 spectrophotometer in 10 mm path quartz. An absorbance of 0.043 was determined for the model reaction mixture. The quantum yield (Φ) of the photochemical transformation was measured to be **0.80**.
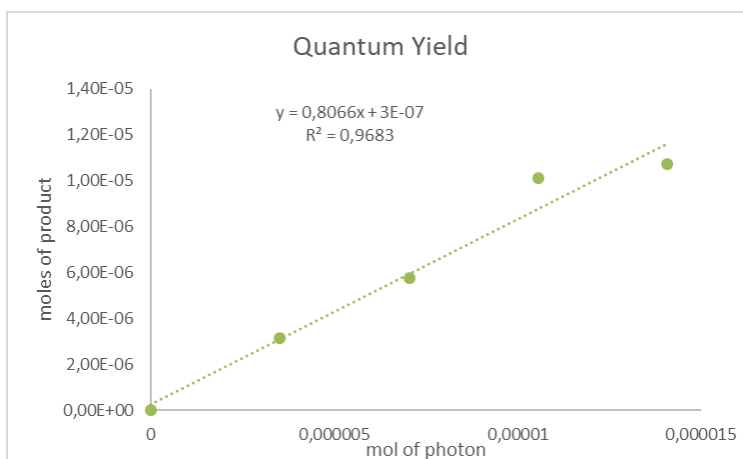
The procedure was repeated a second time to provide an akin value: quantum yield (Φ) at 460 nm of **0.66** ($R^2 = 0.98$; three points, 5 min, 10 min and 15 min).

2.8.4.6 Experiments to prove the radical generation

Experiment in the presence of TEMPO:
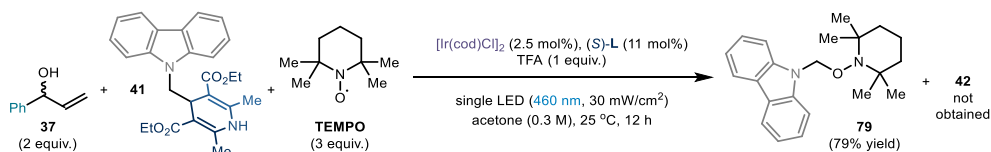
A screw-capped vial, fitted with a rubber septum, was charged with [Ir(cod)Cl]$_2$ (1.7 mg, 2.50 µmol), the chiral ligand (S)-**L** (5.6 mg, 11.0 µmol) and anhydrous, argon-sparged acetone (300 µL), under argon atmosphere. The resulting solution was vigorously stirred for 15 minutes and transferred to a Schlenk tube containing alcohol **37** (26 µL, 200 µmol), diethyl 4-((9H-carbazol-9-yl)methyl)-2,6-dimethyl-1,4-dihydropyridine-3,5-dicarboxylate **41** (43 mg, 100 µmol) and the radical scavenger TEMPO (47 mg, 300 µmol), affording a dark orange solution. TFA (7.7 µL, 100 µmol) was added to this solution and the Schlenk tube was sealed with a screw-cap. The vessel was placed into a 3D-printed plastic support mounted on an aluminum block fitted with a 460 nm high-power single LED (λ = 460 nm, irradiance = 30 mW/cm^2 as controlled by an external power supply, see Figure 2.10 for details). The reaction was stirred under visible light irradiation at ambient temperature for 12 hours, prior to removal of the solvent under reduced pressure. ^{1}H NMR analysis on the crude mixture, using mesitylene (14 µL) as the internal standard, revealed that no product **42** was formed. Purification of the crude mixture by flash column chromatography on silica gel (gradient from hexane to 20% toluene

in hexane) provided adduct **79** (26.5 mg, 79% yield, colorless needles), derived from the TEMPO trapping of the radical formed from **41**. The title compound was previously unknown.

*Characterization of compound **79***:

^{1}H NMR (400 MHz, CDCl$_3$): δ 8.08 (d, *J* = 7.5 Hz, 2H), 7.59 (d, *J* = 8.0 Hz, 2H), 7.48 (ddd, *J* = 8.0, 7.0, 1.0 Hz, 2H), 7.29 – 7.24 (m, 2H), 5.90 (s, 2H), 1.60 – 1.45 (m, 5H), 1.39 – 1.32 (m, 1H), 1.16 (s, 6H), 1.09 (s, 6H).

^{13}C NMR (101 MHz, CDCl$_3$): δ 140.8, 126.0, 123.5, 120.3, 119.8, 110.0, 78.5, 60.2, 40.0, 33.4, 20.3, 17.3.

HRMS (ESI) Exact mass calculated for C$_{22}$H$_{29}$N$_2$O [M+H]$^+$: 337.2274, found: 337.2275.

Experiment with the radical trap:
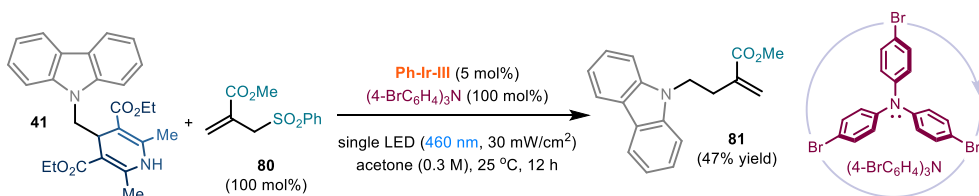
Substrate 2-((phenylsulfonyl)methyl)acrylate **80** was synthesized according to a reported procedure.[64] A Schlenk tube, fitted with a rubber septum, was charged with methyl 2-((phenylsulfonyl)methyl)acrylate **80** (24 mg, 100 μmol), diethyl 4-((9*H*-carbazol-9-yl)methyl)-2,6-dimethyl-1,4-dihydropyridine-3,5-dicarboxylate **41** (43 mg, 100 μmol), tris(4-bromophenyl)amine (TBPA, 48.2 mg, 100 μmol), and anhydrous, argon-sparged acetone (200 μL), under argon atmosphere. To this stirring mixture was added dropwise a solution of the preformed complex **Ph-Ir-III** (7.5 mg, 5 mol%) in anhydrous, argon-sparged acetone (300 μL). The Schlenk tube was sealed with a screw-cap, placed into a 3D-printed plastic support mounted on an aluminum block fitted with a 460 nm high-power single LED (λ = 460 nm, irradiance = 30 mW/cm^2 as controlled by an external power supply, see Figure S2 for details), and stirred under visible light irradiation at ambient temperature for 12 hours. The volatiles were removed under reduced pressure, and the crude mixture was purified by flash column chromatography on silica gel (*isocratic* 2% Et$_2$O in hexane) to afford compound **81** (13 mg, 47% yield) as an off-white solid. The title compound was previously unknown.

---

[64] Rouquet, G., Robert, F., Méreau, R., Castet, F., Landais, Y. "Allylsilanes in "tin-free" oximation, alkenylation, and allylation of alkyl halides" *Chem. Eur. J.* **2001**, *17*, 13904-13911.

Characterization of compound 81:

^{1}H NMR (400 MHz, CDCl$_3$): δ 8.13 – 8.04 (m, 2H), 7.49 – 7.39 (m, 4H), 7.27 – 7.19 (m, 2H), 6.11 (d, J = 1.0 Hz, 1H), 5.49 (d, J = 1.0 Hz, 1H), 4.51 – 4.44 (m, 2H), 3.80 (s, 3H), 2.84 (ddd, J = 8.5, 6.0, 1.0 Hz, 2H).

^{13}C NMR (101 MHz, CDCl$_3$): δ 167.3, 140.4, 137.0, 128.2, 125.8, 123.0, 120.5, 119.1, 108.8, 52.2, 42.4, 32.2.

HRMS (ESI) Exact mass calculated for C$_{18}$H$_{17}$NNaO$_2$ [M+Na]$^+$: 302.1151, found: 302.1153.

Experiment with the Thermal Radical Generation:
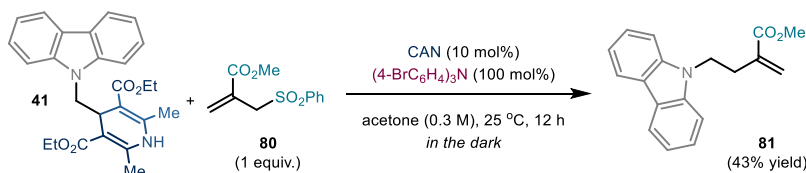
A Schlenk tube, fitted with a rubber septum, was charged with methyl 2-((phenylsulfonyl)methyl)acrylate **80** (24.0 mg, 100 μmol), diethyl 4-((9*H*-carbazol-9-yl)methyl)-2,6-dimethyl-1,4-dihydropyridine-3,5-dicarboxylate **41** (43 mg, 100 μmol), tris(4-bromophenyl)amine (TBPA, 48.2 mg, 100 μmol), and anhydrous, argon-sparged acetone (200 μL), under an argon atmosphere. To this stirring mixture was added dropwise a solution of cerium ammonium nitrate (CAN, 5.5 mg, 10.0 μmol) in anhydrous, argon-sparged acetone (300 μL). The Schlenk tube was sealed with a screw-cap, and the mixture was vigorously stirred for 12 hours in the dark. The crude mixture was filtered through a short pad of silica gel, to remove the insoluble materials, and the filtrate was concentrated under reduced pressure. Purification of the crude material by flash column chromatography on silica gel (*isocratic* 2% Et$_2$O in hexane) afforded product **81** (12 mg, 43% yield) as an off-white solid.

Thermal Radical Generation Strategy in the Asymmetric Ir-Catalyzed Cross-Coupling:
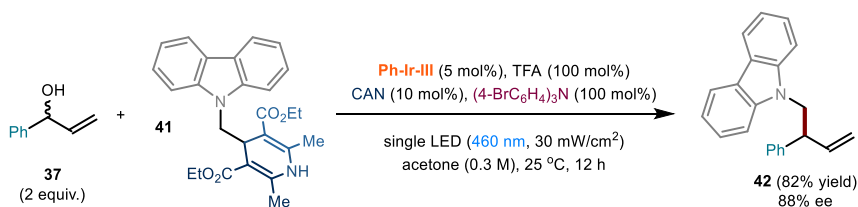
A screw-capped vial, fitted with a rubber septum, was charged with pre-formed complex **Ph-Ir-III** (7.5 mg, 5 mol%) and anhydrous, argon-sparged acetone (200 μL) under argon atmosphere. The resulting solution was transferred to a Schlenk tube containing α-vinyl benzyl alcohol **37** (26 μL, 200 μmol), diethyl 4-((9*H*-carbazol-9-yl)methyl)-2,6-dimethyl-1,4-

dihydropyridine-3,5-dicarboxylate **41** (43 mg, 100 µmol) and tris(4-bromophenyl)amine (TBPA, 48.2 mg, 100 µmol), affording a yellow solution. To this solution were sequentially added TFA (7.66 µL, 100 µmol) and a solution of cerium ammonium nitrate (CAN, 5.5 mg, 10.0 µmol) in anhydrous, argon-sparged acetone (100 µL). The Schlenk tube was sealed with a screw-cap, and placed into a 3D-printed plastic support mounted on an aluminum block fitted with a 460 nm high-power single LED (λ = 460 nm, irradiance = 30 mW/cm^2 as controlled by an external power supply). The reaction was stirred under visible light irradiation at ambient temperature for 12 hours. The crude mixture was filtered through a short pad of silica gel, to remove the insoluble materials, and the filtrate was concentrated under reduced pressure. Purification of the crude material by flash column chromatography on silica gel (*isocratic* 5% toluene in hexane) provided the enantioenriched product **42** (24.5 mg, 82% yield, 88% ee) as a colorless oil.

The same experiment was repeated in the *absence of light radiation*, by placing the reaction vessel on a stirring plate. In this case, ^{1}H NMR analysis on the crude mixture, using mesitylene (14 µL) as the internal standard, revealed substantial consumption of the 1,4-dihydropyridine radical precursor **41** (75% conversion), but product **42** was detected only in traces.
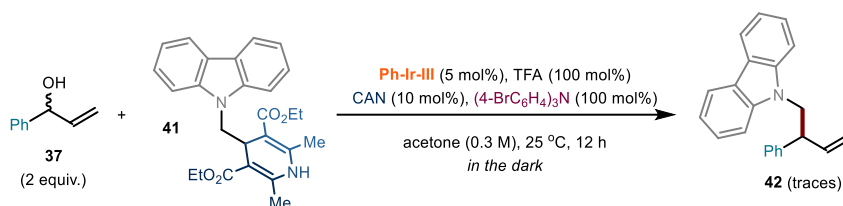
The last result suggests that the radical, generated from **41**, either does not add to the ground-state electrophilic complex **Ph-Ir-III** or, if it could, this event does not generate an organometallic species suitable for sustaining a radical chain propagation (*i.e.* oxidizing substrate **41** to reform the propagating radical).

2.8.5 X-ray Crystallographic Data

2.8.5.1 Single Crystal X-ray Diffraction Data for Product 66:

X-ray structure determination: stable colorless crystals of compound **66** were obtained by slow evaporation of a dichloromethane solution stored at 4°C.

Data Collection: Measurements were made on a Rigaku MicroMax-007HF single crystal X-ray diffractometer equipped with a Pilatus 200K area detector, a Rigaku MicroMax-007HF microfocus rotating anode with Mo$_{K\alpha}$ radiation, Confocal Max Flux optics and an Oxford Cryosystems low temperature device Cryostream 700 plus (T = -173 °C). Full-sphere data collection was used with ω and φ scans.
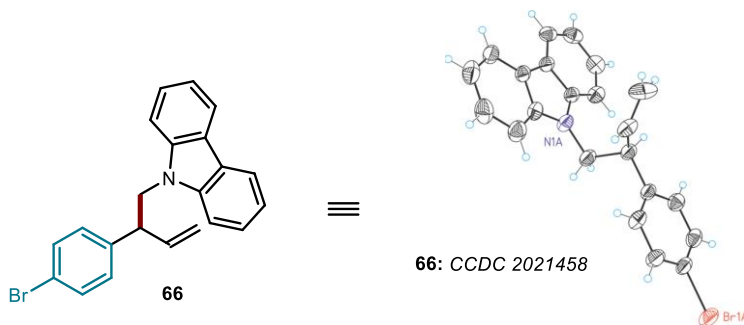
66: *CCDC 2021458*

Table 2.4. Crystal data and structure refinement for **66**. *CCDC 2021458*.

_____

Empirical formula	C22 H18 Br N
Formula weight	376.28
Temperature	296(2)K
Wavelength	0.71073 Å
Crystal system	triclinic
Space group	P 1
Unit cell dimensions	a = 8.3897(3)Å a = 96.917(3)°.
	b = 8.6780(3)Å b = 99.133(3)°.
	c = 13.8659(4)Å g = 117.516(3)°.
Volume	862.06(5) Å^3
Z	2
Density (calculated)	1.450 mg/m^3
Absorption coefficient	2.386 mm^{-1}
F(000)	384
Crystal size	0.200 x 0.100 x 0.100 mm^3
Theta range for data collection	2.714 to 32.130°.
Index ranges	-12<=h<=12,-12<=k<=12,-20<=l<=20
Reflections collected	25785
Independent reflections	11065[R(int) = 0.0255]
Completeness to theta =32.130°	94.2%
Absorption correction	Multi-scan
Max. and min. transmission	1.00 and 0.77
Refinement method	Full-matrix least-squares on F^2
Data / restraints / parameters	11065/ 63/ 472
Goodness-of-fit on F^2	0.998
Final R indices [I>2sigma(I)]	R1 = 0.0320, wR2 = 0.0814

R indices (all data)	R1 = 0.0426, wR2 = 0.0854
Flack parameter	x = -0.002(2)
Largest diff. peak and hole	0.630 and -0.248 e.$Å^{-3}$

*2.8.5.2 Single Crystal X-ray Diffraction Data for Product **67***:

X-ray structure determination: stable colorless crystals of compound **67** were obtained by slow evaporation of a dichloromethane solution stored at 4ºC.

Data Collection: Measurements were made on a Rigaku MicroMax-007HF single crystal X-ray diffractometer equipped with a Pilatus 200K area detector, a Rigaku MicroMax-007HF microfocus rotating anode with $Mo_{K\alpha}$ radiation, Confocal Max Flux optics and an Oxford Cryosystems low temperature device Cryostream 700 plus (T = -173 °C). Full-sphere data collection was used with ω and φ scans.

Table 2.5. Crystal data and structure refinement for **67**. CCDC 2021459.

Empirical formula	C22 H18 Cl N
Formula weight	331.82
Temperature	296(2)K
Wavelength	0.71073 Å
Crystal system	tetragonal
Space group	I 41
Unit cell dimensions	a = 18.4165(2)Å a = 90°.
	b = 18.4165(2)Å b = 90°.
	c = 10.6556(3)Å g = 90°.
Volume	3614.03(13) $Å^{3}$
Z	8

Density (calculated)	$1.220\ Mg/m^3$
Absorption coefficient	$0.213\ mm^{-1}$
F(000)	1392
Crystal size	$0.300\ x\ 0.300\ x\ 0.150\ mm^3$
Theta range for data collection	3.126 to 32.069°.
Index ranges	-26<=h<=27,-27<=k<=27,-15<=l<=15
Reflections collected	58409
Independent reflections	6115[R(int) = 0.0308]
Completeness to theta =32.069°	98.2%
Absorption correction	Multi-scan
Max. and min. transmission	1.00 and 0.63
Refinement method	Full-matrix least-squares on F^2
Data / restraints / parameters	6115/ 1/ 217
Goodness-of-fit on F^2	0.998
Final R indices [I>2sigma(I)]	R1 = 0.0501, wR2 = 0.1520
R indices (all data)	R1 = 0.0888, wR2 = 0.1805
Flack parameter	x =0.03(2)
Largest diff. peak and hole	0.090 and -0.188 e.Å^{-3}

Chapter III

Enantioselective Biocascade Catalysis Using a Single Multifunctional Enzyme

Target

Developing enantioselective two- and three-component cascade reactions using a single multifunctional carboligase enzyme.
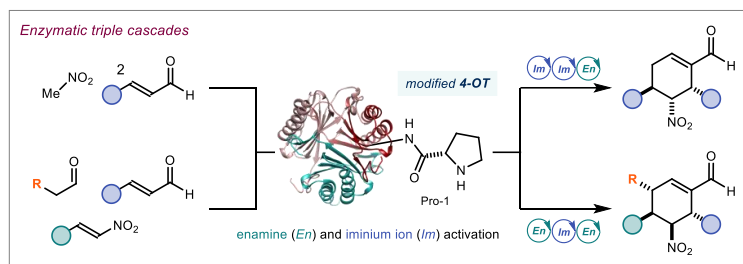
Tools

Exploiting the ability of the terminal proline residue in 4-oxalocrotonate tautomerase enzymes to catalyze reactions *via* both enamine and iminium ion activation.[1]

3.1 Introduction

Multicomponent reactions[2] are desirable in organic synthesis since they allow the construction of multiple chemical bonds in a single step, leading to the rapid formation of structurally complex and functionality dense products (Scheme 3.1).[3] Multicomponent processes in which all the reaction components are mixed from the onset and the conditions are not changed in the course of the single synthetic step are termed *domino reactions*.[4] The currently accepted definition of a *domino reaction*, proposed by Tietze in the 1990s,[5] refers to a process that involves two or more consecutive chemical transformations, usually C-C bond formation, in

---

[1] The project discussed in this chapter was conducted in collaboration with Dr. Vasilis Tseliou, Laura Kqiku, Dr. Jan Vilím, and Gianluca Simionato. The biochemical work was directed by Dr. Vasilis Tseliou and Dr. Jan Vilím, who conducted also the optimization studies. Laura Kqiku and I were involved in the synthetic work, optimization studies and investigation of the scope of the three processes. I was also involved in the mechanistic studies. Part of the work has been published in: Tseliou, V., Faraone, A., Kqiku, L., Vilím, J., Simionato, G., Melchiorre, P. "Enantioselective Biocascade Catalysis With a Single Multifunctional Enzyme", *Angew. Chem. Int. Ed.* **2022**, *61*, e202212176.

[2] Zhu, J., Bienaymé, H. "Multicomponent Reactions" Wiley-VCH, Weinheim, 2005.

[3] Pellissier, H. "Stereocontrolled Domino Reactions" *Chem. Rev.* **2013**, *113*, 442-524.

[4] Tietze, L. F., Brasche, G., Gericke K. M. (Eds.) "Domino Reactions in Organic Synthesis" Wiley-VCH, Weinheim, 2006.

[5] (a) Tietze, L. F., Beifuss, U. "Sequential Transformations in Organic Chemistry: A Synthetic Strategy with a Future" *Angew. Chem. Int. Ed.* **1993**, *32*, 131-163. (b) Tietze, L. F. "Domino Reactions in Organic Synthesis" *Chem. Rev.* **1996**, *96*, 115-136.

which each transformation occurs only as a consequence of the functionality forged in the previous step. These processes are highly atom efficient, since they incorporate most of the reactants into the final product. They also produce a low amount of chemical waste, which is desirable in terms of sustainability. In addition, they avoid energy- and time-intensive isolation of intermediates and extra steps, such as protection and deprotection of chemical functionalities. A closely related term, *cascade reactions*, is also used to define this type of processes. The words *domino* and *cascade* are used interchangeably as synonyms by Nicolaou[6] and will be used as such in the present thesis.

Asymmetric cascade reactions are processes that engage more than two substrates in the formation of enantioenriched chiral complex products.[7] The stereoinduction in these processes can be governed *via* two main strategies (Scheme 3.1): *i*) by using chiral substrates or chiral auxiliaries to induce diastereoselective transformations; *ii*) by using chiral catalysts to promote catalytic enantioselective reactions starting from achiral substrates.
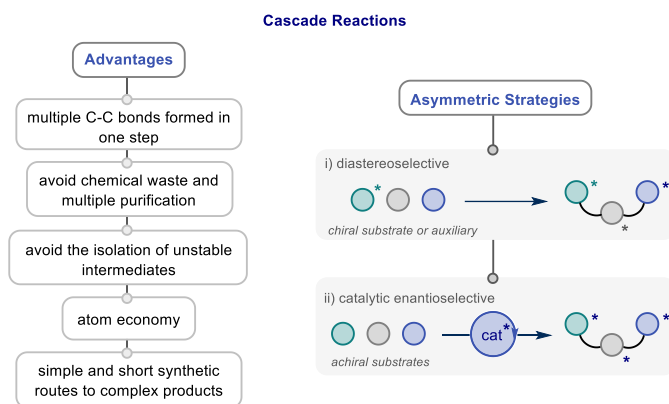
Scheme 3.1. General aspects of cascade reactions.

The catalytic strategy is considered more desirable since it avoids the installation of chiral auxiliaries into the substrates, which are not always easily available from the chiral pool. Additionally, this approach often requires additional chemical steps, i.e. the installation and the removal of the auxiliary. For an asymmetric catalytic cascade reaction to be efficient, a chiral catalyst should be readily available, be used in low quantities, and it should be capable of catalyzing each step of the transformation imparting a high degree of stereocontrol. In the

---

[6] Nicolaou, K. C., Edmonds, D. J., Bulger, P. G. "Cascade Reactions in Total Synthesis" *Angew. Chem. Int. Ed.* **2006**, *45*, 7134-7186.

[7] (a) Ramón, D. J., Yus, M. "Asymmetric Multicomponent Reactions (AMCRs): The New Frontier" *Angew. Chem. Int. Ed.* **2005**, *44*, 1602-1634. (b) De Graaff, C., Ruijter, E., Orru, R. V. A. "Recent developments in asymmetric multicomponent reactions" *Chem. Soc. Rev.* **2012**, *41*, 3969-4009.

last two decades, organocatalysis[8] has dominated the field of asymmetric catalytic cascade reactions. Several elegant strategies have been reported since the early 2000,[9] with some examples inspired by Nature through the use of naturally occurring small molecules as catalysts.[10] Despite the simplicity offered by the use of small organic molecules as catalysts, these reactions generally require high catalyst loadings,[11] or long reaction times.[10a]

Nature uses enzymes to build up molecular complexity in highly defined three-dimensional structures.[12] Due to the high specificity of enzymes in terms of catalytic activity and substrate selectivity,[13] the most common strategies adopted by Nature to assemble complex molecules *via* cascade processes rely on sophisticated multi-enzyme sequential metabolic processes.[12] In these biocascade processes, each enzyme catalyzes an individual step of the reaction sequence by means of a specific mechanism of substrate activation. However, developing novel artificial enzymatic cascade reactions is complicated by the need to combine multiple enzymes in a single sequence. In fact, ensuring compatibility between the different enzymatic systems in terms of reaction media and rates while achieving high selectivity often requires substantial protein engineering of each enzyme component. Therefore, using a single enzyme capable of driving each step of a cascade process with high stereocontrol is desirable (Scheme 3.2). This one-pot, one-catalyst system would offer a more straightforward approach to biocascades, but it requires the identification of a multifunctional enzyme able to sequentially activate substrates with different functionalities and master orthogonal mechanisms of catalysis by distinct activation modes. So far, only rare examples of multifunctional enzymes that could catalyze all the individual steps of a cascade sequence have been reported.[14] In this project, we disclosed a class of multifunctional biocatalysts, specifically carboligase enzymes,

[8] MacMillan, D. W. C. "The advent and development of asymmetric organocatalysis" *Nature* **2008**, *455*, 304-308.

[9] (a) Guillena, G., Ramón, D. J., Yus, M. "Organocatalytic enantioselective multicomponent reactions (OEMCRs)" *Tetrahedron: Asymmetry* **2007**, *18*, 693-700. (b) Enders, D., Grondal, C., Hüttl, M. R. M. "Asymmetric Organocatalytic Domino Reactions" *Angew. Chem. Int. Ed.* **2007**, *46*, 1570-1581.

[10] (a) Chowdari, N. S., Ramachary, D. B., Córdova, A., Barbas, III, C. F. "Proline-catalyzed asymmetric assembly reactions: enzyme-like assembly of carbohydrates and polyketides from three aldehyde substrates" *Tetrahedron Letters* **2002**, *43*, 9591-9595. (b) Movassaghi, M., Jacobsen, E. N. "The Simplest 'Enzyme'" *Science* **2002**, *298*, 1904-1905.

[11] List, B. "The Direct Catalytic Asymmetric Three-Component Mannich Reaction" *J. Am. Chem. Soc.* **2000**, *122*, 9336-9337.

[12] Liu, H. W. B., Begley, T. P. (Eds.) "Comprehensive Natural Products III, Third Edition" Elsevier 2020.

[13] Drauz, K., Gröger, H., May, O. (Eds.) "Enzyme Catalysis in Organic Synthesis" Wiley-VCH, Weinheim, 2012.

[14] (a) Gijsen, H. J. M, Wong, C. H. "Sequential Three- and Four-Substrate Aldol Reactions Catalyzed by Aldolases" *J. Am. Chem. Soc.* **1995**, *117*, 7585-7591; (b) Szekrenyi, A., Garrabou, X., Parella, T., Joglar, J., Bujons, J., Clapés, P. "Asymmetric Assembly of Aldose Carbohydrates from Formaldehyde and Glycolaldehyde by Tandem Biocatalytic Aldol Reactions" *Nat. Chem.* **2015**, *7*, 724-729; (c) Thorpe, T. W., Marshall, J. R., Harawa, V., Ruscoe, R. E., Cuetos, A., Finnigan, J. D., Angelastro, A., Heath, R. S., Parmeggiani, F., Charnock, S. J., Howard, R. M., Kumar, R., Daniels, D. S. B., Grogan, G., Turner, N. J. "Multifunctional Biocatalyst for Conjugate Reduction and Reductive Amination" *Nature* **2022**, *604*, 86-91.

that could promote asymmetric biocascade reactions by catalyzing each of the multiple C-C bond forming steps of the cascade sequence with high stereocontrol. The identified carboligase enzymes could, in fact, master different modes of substrate activation in a sequential fashion (Scheme 3.2). While this is an uncommon approach in biocatalysis, cascade processes in organocatalysis are traditionally designed exploiting this strategy and led to highly efficient techniques for the one-step synthesis of stereochemically dense molecules, including natural products.[15] Our work demonstrated that biocatalysis could match and even surpass in efficiency the potential of traditional organocascade catalysis.
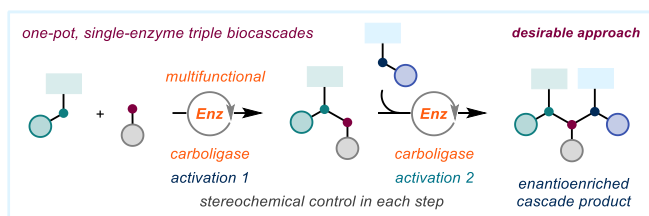
Scheme 3.2. General target of this study: multicomponent single-enzyme biocascade reactions.

3.2 Historical Background of Multicomponent Cascade Reactions

The first documented multicomponent reaction is the venerable Strecker reaction, reported by Adolf Strecker in 1850 (Scheme 3.3).[16] The reaction featured the nucleophilic addition of cyanide **3** to an imine intermediate generated upon in situ condensation of an aldehyde **1** with an amine **2**, affording versatile α-aminonitrile products **4**. This process has been largely exploited for the synthesis of unnatural amino acids.[17]
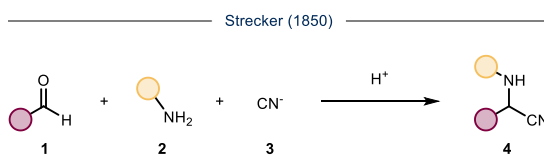
Scheme 3.3. The Strecker reaction (1850).

---

[15] Jones, S. P., Simmons, B., Mastracchio, A., MacMillan, D. W. C. "Collective synthesis of natural products by means of organocascade catalysis" *Nature* **2011**, *475*, 183-188.

[16] Strecker, A. *Justus Liebigs Ann. Chem.* **1850**, *75*, 27-45.

[17] Enders, D., Shilvock, J. P. "Some recent applications of α-amino nitrile chemistry" *Chem. Soc. Rev.* **2000**, *29*, 359-373.

Perhaps the most impactful multicomponent process was the Mannich reaction. Discovered by Carl Mannich in 1912,[18] the reaction involved a condensation between a non-enolizable aldehyde **1**, an amine **2** and an enolizable carbonyl compound **5** (Scheme 3.4a). The imine **I**, generated upon in situ condensation of amine **2** with the aldehyde **1**, underwent a nucleophilic addition from the enol tautomer **II** of the enolizable carbonyl **5**. One of the most significant applications of the Mannich reaction in natural product synthesis was reported by Robinson in 1917,[19] and is still among the most inspiring multicomponent strategies to assemble alkaloid scaffolds (Scheme 3.4b). Robinson's elegant strategy to synthesise tropinone **10** was based on a cascade reaction that featured a double Mannich/cyclization sequence followed by double decarboxylation of the intermediate under heating.
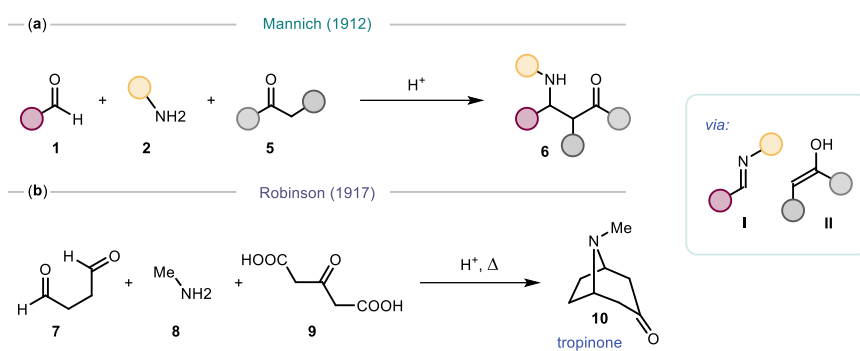
Scheme 3.4. (a) The Mannich reaction (1912); (b) the first application of a multicomponent reaction in natural product synthesis: Robinson' synthesis of tropinone (1917).

3.3 Biocatalytic Cascade Reactions

In this paragraph, general aspects of biocascade reactions will be discussed, with a focus on the few examples of cascade processes that were promoted by a single enzyme, capable of catalyzing each of the multiple steps of the transformation.

Natural and *de novo*[20] biocatalytic cascade reactions traditionally rely on the combination of multiple enzymes, each catalyzing a single step of the sequence.[21] Asymmetric biocascade processes relying on the combination of multiple enzymes (Scheme 3.5a) have acquired

[18] (a) Mannich, C., Krösche, W. *Arch. Pharm.* (Weinheim, Ger.) **1912**, *241*, 647. (b) Tramontini, M. "Advances in the Chemistry of Mannich Bases" *Synthesis* **1973**, 703-775.
[19] (a) Robinson, R. "A Synthesis of Tropinone" *J. Chem. Soc.* **1917**, *111*, 762-768. (b) Robinson, R. "A Theory of the Mechanism of the Phytochemical Synthesis of certain Alkaloids" *J. Chem. Soc.* **1917**, *111*, 876-899.
[20] France, S. P., Hepworth, L. J., Turner, N. J., Flitsch, S. L. "Constructing Biocatalytic Cascades: In Vitro and in Vivo Approaches to de Novo Multi-Enzyme Pathways" *ACS Catal.* **2017**, *7*, 710-724.
[21] Benítez-Mateos, A. I., Roura Padrosa, D., Paradisi, F. "Multistep Enzyme Cascades as a Route towards Green and Sustainable Pharmaceutical Syntheses" *Nat. Chem.* **2022**, *14*, 489-499.

enormous synthetic potential in the synthesis of complex enantioenriched scaffolds;[22] however their implementation is not trivial. For instance, ensuring compatibility between each enzymatic system, including reaction media (buffer and pH) and, when needed, enzyme cofactors is challenging. Moreover, another major challenge is to avoid unwanted transformations that may occur due to interference of multiple catalysts, as well as possible enzyme inhibition due to the accumulation of intermediates and/or products in the reaction medium.[23] Alternatively, *domino* reactions in biocatalysis have been described in which a spontaneous or a chemically-induced sequence of reactive events is triggered by the initiation of an enzyme acting as the catalyst only in the first step of the transformation (Scheme 3.5b).[24] In this case, the stereochemistry of the subsequent steps is not controlled by the enzyme.
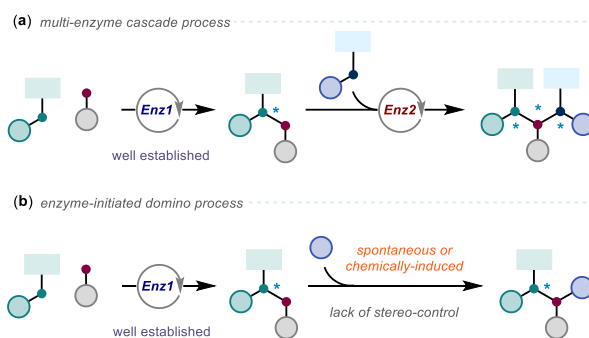
Scheme 3.5. Traditional strategies for the development of enzymatic cascade reactions: (a) multi-enzyme sequential transformations; (b) enzyme-initiated domino processes.

A desirable alternative to develop asymmetric multicomponent biocascade reactions would rely on the use of a single enzyme to drive each transformation of the multistep process, as discussed in the *Introduction* (Scheme 3.2). However, only few examples of single enzyme biocascades were reported in which the enzyme could drive each step of the transformation and impart high stereocontrol.

In the 1990's, the group of Wong described few examples of asymmetric multicomponent biocascade reactions promoted by the aldolase enzyme DERA (2-deoxy-D-ribose-5-phosphate aldolase, EC 4.1.2.4)[25] as the sole catalyst. In these reactions, two molecules of acetaldehyde **12** or propanal **13** were condensed with different aldehyde acceptors **11** to

---

[22] For a notable example developed by Merck & Co., see: Huffman, M. A. *et al.* "Design of an in vitro biocatalytic cascade for the manufacture of islatravir" *Science* **2019**, *366*, 1255-1259.

[23] Schrittwieser, J. H., Velikogne, S., Hall, M., Kroutil, W. "Artificial Biocatalytic Linear Cascades for Preparation of Organic Molecules" *Chem. Rev.* **2018**, *118*, 270-348.

[24] Mayer, S. F., Kroutil, W., Faber, K. "Enzyme-initiated domino (cascade) reactions" *Chem. Soc. Rev.* **2001**, *30*, 332-339.

[25] (b) Haridas, M., Abdelraheem, E. M. M., Hanefeld, U. "2-Deoxy-D-ribose-5-phosphate aldolase (DERA): applications and modifications" *Appl. Microbiol. Biotechnol.* **2018**, *102*, 9959-9971.

deliver complex polyketides products **15** with high stereocontrol *via* a sequence of aldol reactions (Scheme 3.6a).[26] The enzyme DERA catalyzed each step of the aldol-aldol sequence by activating the aldehyde **12** or **13** *via* formation of an enamine intermediate **III** inside the active site. The enamine activation occurred upon condensation of the carbonyl group of the aldehyde **12** or **13** with the ε-amino group of the catalytically active lysine 167 in the active site of DERA. The products of the first two aldol reactions were the linear intermediates **14**. The subsequent spontaneous hemiacetal formation that delivered products **15** was crucial to prevent over-reaction since hemiacetals were unreactive in the aldol addition.
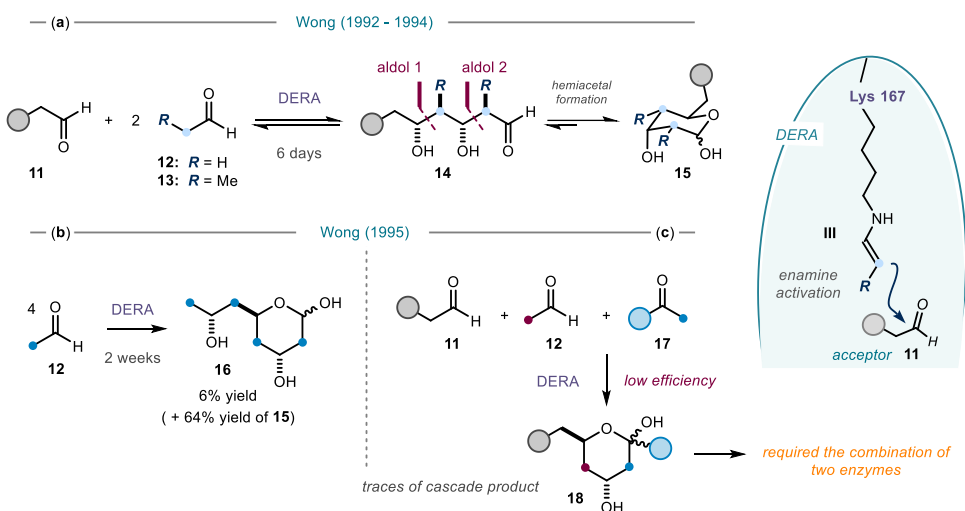
Scheme 3.6. (a) Three-component cascade assemble of polyketides via sequential aldol reactions catalyzed by DERA; (b) evidence of a triple aldol sequence for the assemble of four molecules of acetaldehyde with DERA enzyme; (c) attempts towards a hetero-multicomponent single-enzyme cascade with DERA aldolase.

In another report, the Wong group showed that up to four molecules of acetaldehyde **12** could be engaged in a domino process *via* three sequential self-aldol reactions to form the 2,4-deoxy sugar **16**, although in low yield and long reaction times (Scheme 3.6b).[27] Attempts to use DERA to react three different carbonyl compounds in a cross-aldol-aldol sequence proved unsuccessful due to low yields (Scheme 3.6c). In this case, the use of two distinct aldolase enzymes was required to obtain the target cascade product **18** in a one-pot sequence (strategy in Scheme 3.5a). In these seminal reports, the enzyme showed the ability to engage more than

[26] (a) Chen, L., Dumas, D. P., Wong, C. H. "Deoxyribose-5-phosphate Aldolase as a Catalyst in Asymmetric Aldol Condensation" *J. Am. Chem. Soc.* **1992**, *114*, 741-748; (b) Gijsen, H. J. M, Wong, C. H. "Unprecedented Asymmetric Aldol Reactions with Three Aldehyde Substrates Catalyzed by 2-Deoxyribose-5-phosphate Aldolase" *J. Am. Chem. Soc.* **1994**, *116*, 8422-8423.
[27] Gijsen, H. J. M, Wong, C. H. "Sequential Three- and Four-Substrate Aldol Reactions Catalyzed by Aldolases" *J. Am. Chem. Soc.* **1995**, *117*, 7585-7591.

two molecules of small achiral substrates to construct complex chiral compounds in multiple sequential steps. However, the multistep sequence relied on a *single and iteratively repeated activation mode* -the enamine activation-, therefore offering a simpler strategy than the ideal approach exploiting a multifunctional enzyme.

Another example of similar multicomponent asymmetric biocascade reactions catalyzed by a single enzyme was reported in 2015 by Clapés.[28] Different variants of the engineered aldolase FSA (D-fructose-6-phosphate aldolase) from *E. coli* could assemble two molecules of glycolaldehyde **20** with one molecule of a small aldehyde **19**, including formaldehyde as a simple C_1 synthon, in a sequential aldol cascade towards the synthesis of aldose sugars **22** in moderate to good yields and high stereocontrol (Scheme 3.7). In these reactions, one molecule of **20** was activated as an enamine intermediate by the catalytically active lysine residue in the enzyme FSA, whereas aldehyde **19** acted as the acceptor in the first aldol addition. In the second aldol reaction, another molecule of **20** was activated *via* formation of an enamine intermediate in the active site of FSA, whereas intermediate **21** generated from the previous step acted as the aldehyde acceptor. A final spontaneous cyclization delivered the hemiacetal products **22**.
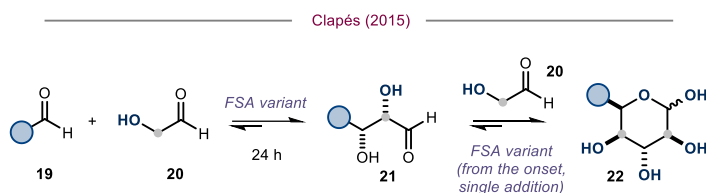
Scheme 3.7. Multicomponent aldol cascade for the synthesis of sugars mediated by engineered FSA aldolases.

Also in this example, the transformation was promoted by a single enzyme which could drive each step of the sequence but could master only the enamine activation mode, catalyzing iteratively the same type of aldol addition.

Recently, the group of Turner reported a remarkable example of a biocascade process promoted by a single multifunctional enzyme capable of driving two mechanistically distinct reactions in a domino sequence.[29] Specifically, the authors screened a large library of metagenomic imine reductases (IREDs) enzymes and identified a variant (EneIRED) capable of accepting iminium ion intermediates **25**, generated upon spontaneous condensation of

[28] Szekrenyi, A., Garrabou, X., Parella, T., Joglar, J., Bujons, J., Clapés, P. "Asymmetric Assembly of Aldose Carbohydrates from Formaldehyde and Glycolaldehyde by Tandem Biocatalytic Aldol Reactions" *Nat. Chem.* **2015**, *7*, 724-729.

[29] Thorpe, T. W., Marshall, J. R., Harawa, V., Ruscoe, R. E., Cuetos, A., Finnigan, J. D., Angelastro, A., Heath, R. S., Parmeggiani, F., Charnock, S. J., Howard, R. M., Kumar, R., Daniels, D. S. B., Grogan, G., Turner, N. J. "Multifunctional Biocatalyst for Conjugate Reduction and Reductive Amination" *Nature* **2022**, *604*, 86-91.

cyclohexenones **23** with amines **24**, in the active site. The enzyme catalyzed, sequentially, the asymmetric conjugate reduction of the C-C double bonds in iminium ions **25** (ene-reductase, EneRED, activity), followed by the asymmetric C-N double bond reduction (IRED activity) of iminium ion intermediates **26** to deliver enantioenriched chiral amines **27** with moderate to high chemo- and stereoselectivity (Scheme 3.8). The novelty of this EneIRED enzyme relied on its unusual ability to catalyze two mechanistically distinct reaction steps. Mechanistic experiments provided evidence that the C-C bond reduction (the first step) did not occur on the cyclohexenone **23** in the absence of the amine **24**. Thus, the EneIRED variant discovered showed the ability to selectively activate only iminium ion functionalities and displayed limited substrate promiscuity.
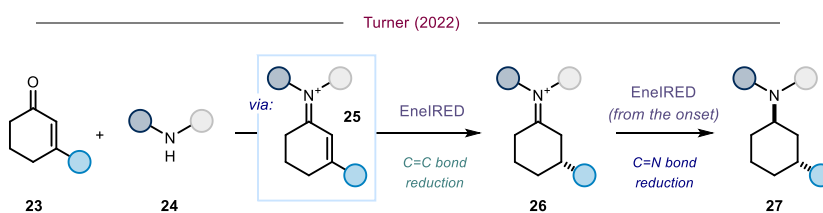
Scheme 3.8. A recently discovered multifunctional imine reductase (EneIRED) enzyme drives a sequential two-step cascade characterized by two distinct reactivities.

The examples discussed constitute the few exceptions that have been reported to date of biocascade processes driven by a single enzyme, which could catalyze each step of the transformation and control the three-dimensional arrangement of each stereocenter forged.

3.4 Organocatalytic Cascade Reactions

Following the re-discovery of organocatalysis with the two seminal contributions by List and MacMillan in the early 2000's,[30] organocatalytic transformations experienced a great development in the following two decades,[31] culminating in the Nobel Prize assignation of 2021 to MacMillan and List.[32]

In contrast to biocatalysis, organocatalysis has dominated the field of asymmetric multicomponent cascade reactions driven by a single multifunctional catalyst, capable of activating different substrates *via* divergent mechanisms.[9] The most traditional examples of

---

[30] (a) List, B., Lerner, R. A., Barbas, III, C. F. "Proline-Catalyzed Direct Asymmetric Aldol Reactions" *J. Am. Chem. Soc.* **2000**, *122*, 2395-2396; (b) Ahrendt, K. A., Borths, C. J., MacMillan, D. W. C. "New Strategies for Organic Catalysis: The First Highly Enantioselective Organocatalytic Diels-Alder Reaction" *J. Am. Chem. Soc.* **2000**, *122*, 4243-4244.

[31] Melchiorre, P., Marigo, M., Carlone, A., Bartoli, G. "Asymmetric Aminocatalysis - Gold Rush in Organic Chemistry" *Angew. Chem. Int. Ed.* **2008**, *43*, 6138-6171.

[32] Hargittai, I. "The 2021 chemistry Nobel laureates and asymmetric organocatalysis" *Struct Chem* **2022**, *33*, 303-305.

such organocascade reactions exploited the use of small secondary amine catalysts and combined the enamine and iminium ion activation modes of carbonyl substrates in the same reaction sequence. In the following paragraph, general aspects of the enamine and iminium ion activation strategies will be discussed, followed by the combination of both strategies in traditional organocascade reactions.

3.4.1 General aspects of Enamine and Iminium Ion Activation

Enamine reactivity was broadly documented by Stork in the 1950's as a powerful strategy for the stoichiometric α-alkylation and α-acylation of carbonyl compounds.[33] However, the catalytic use of enamines as nucleophilic intermediates[34] only reached its potential in the early 2000's with the seminal contribution by Barbas, III and List.[35] In this reaction, proline activated acetone **28** *via* the enamine intermediate and catalyzed the aldol addition of **28** to a substituted benzaldehyde of type **29** to deliver product **30** with moderate yield and enantiomeric excess (Scheme 3.9).
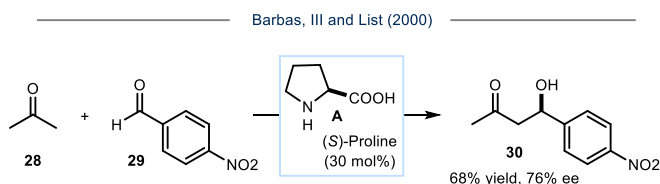
Scheme 3.9. Barbas, III and List's landmark reaction in enamine catalysis.

This landmark reaction opened up a new field in asymmetric catalysis, dominated by the use of small organic molecules, now known as organocatalysis.[36] Enamine activation is based on the ability of primary and secondary amines to condense with enolizable carbonyl compounds to generate imines or iminium ions, which upon deprotonation, deliver a nucleophilic enamine activated at the α position. In this HOMO-raising activation approach[37] (Scheme 3.10a), the energy of the highest occupied molecular orbital (HOMO) is raised relative to the starting carbonyl species.

---

[33] (a) Stork, G., Terrelland, R., Szmuszkovicz, J. "A New Synthesis of 2-Alkyl and 2-Acyl Ketones" *J. Am. Chem. Soc.* **1954**, *76*, 2029-2030. (b) Stork, G., Brizzolara, A., Landesman, H., Szmuszkovicz, J., Terrell, R. "The Enamine Alkylation and Acylation of Carbonyl Compounds" *J. Am. Chem. Soc.* **1963**, *85*, 207-222.

[34] Mukherjee, S., Yang, J. W., Hoffmann, S., List, B. "Asymmetric Enamine Catalysis" *Chem. Rev.* **2007**, *107*, 5471-5569.

[35] List, B., Lerner, R. A., Barbas, III, C. F. "Proline-Catalyzed Direct Asymmetric Aldol Reactions" *J. Am. Chem. Soc.* **2000**, *122*, 2395-2396.

[36] List, B. "The ying and yang of asymmetric aminocatalysis" *Chem. Commun.* **2006**, 819-824.

[37] Arceo, E., Melchiorre, P. "Extending the Aminocatalytic HOMO-Raising Activation Strategy: Where Is the Limit?" *Angew. Chem. Int. Ed.* **2012**, *51*, 5290-5292.
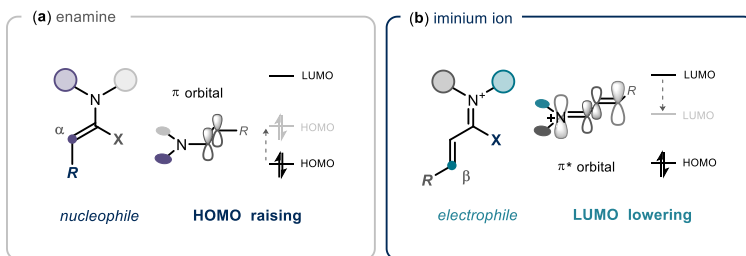
Scheme 3.10. (a) Enamine activation; (b) iminium ion activation.

The condensation of an amine with an unsaturated carbonyl compound delivers an electrophilic iminium ion species.[38] α,β-unsaturated carbonyl compounds are activated at the β position through a LUMO-lowering mechanism[39] - the lowering of the energy of the lowest unoccupied molecular orbital (LUMO) relative to the starting unsaturated carbonyl compound, upon formation of the iminium ion (also called eneiminium ion) intermediate (Scheme 3.10b).

3.4.2 Organocascade Reactions which combine Enamine and Iminium Ion Activation

An effective organocatalytic approach for the development of asymmetric multicomponent cascade reactions exploits the combination of both enamine and iminium ion activations in one-pot and in a sequential fashion. These two activation modes are usually operated by the same chiral secondary amine catalyst to activate different carbonyl substrates along the reaction sequence.[40]

Two seminal examples of organocascade processes that exploited a sequence of iminium ion and enamine activations were reported by Jørgensen[41] and MacMillan[40a] in 2005. In the first work, the diphenylprolinol-type catalyst **B**, previously reported by Hayashi and Jørgensen,[42] activated crotonaldehyde **31** towards the sulfa-Michael addition of thiol **32**, followed by

---

[38] Erkkilä, A., Majander, I., Pihko, P. M. "Iminium Catalysis" *Chem. Rev.* **2007**, *107*, 5416-5470.

[39] Ahrendt, K. A., Borths, C. J., MacMillan, D. W. C. "New Strategies for Organic Catalysis: The First Highly Enantioselective Organocatalytic Diels-Alder Reaction" *J. Am. Chem. Soc.* **2000**, *122*, 4243-4244.

[40] (a) Huang, Y., Walji, A. M., Larsen, C. H., Macmillan, D. W. C. "Enantioselective Organo-Cascade Catalysis" *J. Am. Chem. Soc.* **2005**, *127*, 15051-15053; (b) Simmons, B., Walji, A. M., MacMillan, D. W. C. "Cycle-Specific Organocascade Catalysis: Application to Olefin Hydroamination, Hydro-oxidation, and Amino-oxidation, and to Natural Product Synthesis" *Angew. Chem. Int. Ed.* **2009**,*48*, 4349-4353.

[41] Marigo, M., Schulte, T., Franzén, J., Jørgensen, K. A. "Asymmetric Multicomponent Domino Reactions and Highly Enantioselective Conjugated Addition of Thiols to α,β-Unsaturated Aldehydes" *J. Am. Chem. Soc.* **2005**, *127*, 15710-15711.

[42] (a) Marigo, M., Wabnitz, T. C., Fielenbach, D., Jørgensen, K. A. "Enantioselective Organocatalyzed α Sulfenylation of Aldehydes" *Angew. Chem. Int. Ed.* **2005**, *44*, 794-797; (b) Hayashi, Y., Gotoh, H., Hayashi, T., Shoji, M. "Diphenylprolinol Silyl Ethers as Efficient Organocatalysts for the Asymmetric Michael Reaction of Aldehydes and Nitroalkenes" *Angew. Chem. Int. Ed.* **2005**, *44*, 4212-4215.

interception of the resulting enamine with electrophilic azodicarboxylate reagent **33**, both in a one-pot sequential addition procedure or a single-addition cascade step. After reduction of the aldehydic products to the corresponding alcohols, cyclic carbamates **34** were isolated in high diastereomeric ratio and enantiomeric excess (Scheme 3.11a).
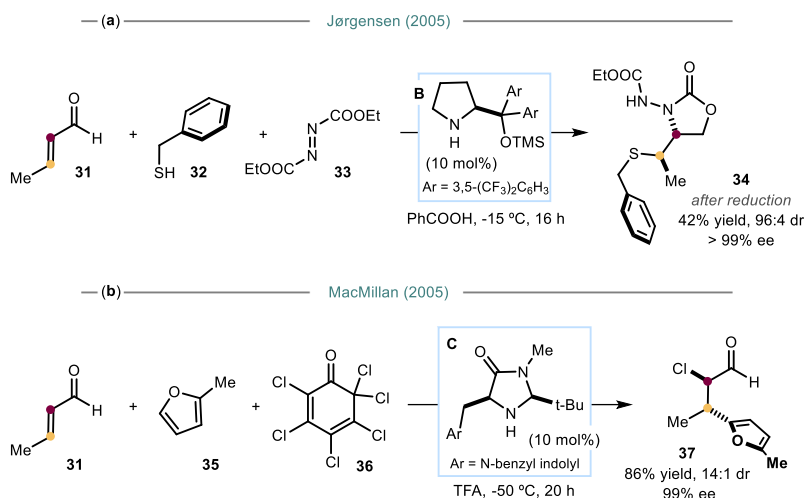
Scheme 3.11. Seminal reports on asymmetric organocatalyzed iminium ion-enamine sequence cascades by (a) Jørgensen and (b) MacMillan (2005).

In this case, the organocatalyst **B** was used to activate the enal **31** in the first step *via* iminium ion-based LUMO-lowering mechanism (Scheme 3.10b) and in the second step *via* the enamine-based HOMO-raising strategy (Scheme 3.10a). The second report by MacMillan showed that a similar three-component cascade reaction following the same iminium ion-enamine activation sequence could be performed using a heteroaromatic nucleophile such as furane **35** and an electrophilic chlorinating agent such as **36** to difunctionalize diverse α,β-unsaturated aldehydes such as crotonaldehyde **31** and obtain product **37** in high yield and enantiomeric excess (Scheme 3.11b).

An alternative strategy for organocascade reactions relies on an enamine-iminium ion sequence. The most sophisticated example of an organocatalytic triple cascade that exploited this strategy, followed by a third enamine activation step, was reported in 2006 by Enders. This study is considered one of the landmark reactions in the field of organocatalytic asymmetric multicomponent cascade reactions (Scheme 3.12).[43] In this work, linear aldehydes such as butanal **38** reacted with β-nitrostyrenes of type **39** and α,β-unsaturated aldehydes such as cinnamaldehyde **40** in the presence of the diphenylprolinol catalyst **D** to

---

[43] Enders, D., Hüttl, M. R. M., Grondal, C., Raabe, G. "Control of Four Stereocentres in a Triple Cascade Organocatalytic Reaction" *Nature* **2006**, *441*, 861-863.

deliver complex cyclohexene carbaldehydes **41** with up to four contiguous stereocenters in a highly stereoselective fashion. The products were obtained as mixtures of only two diastereomers (epimers at carbon 5) with excellent enantiomeric excess.
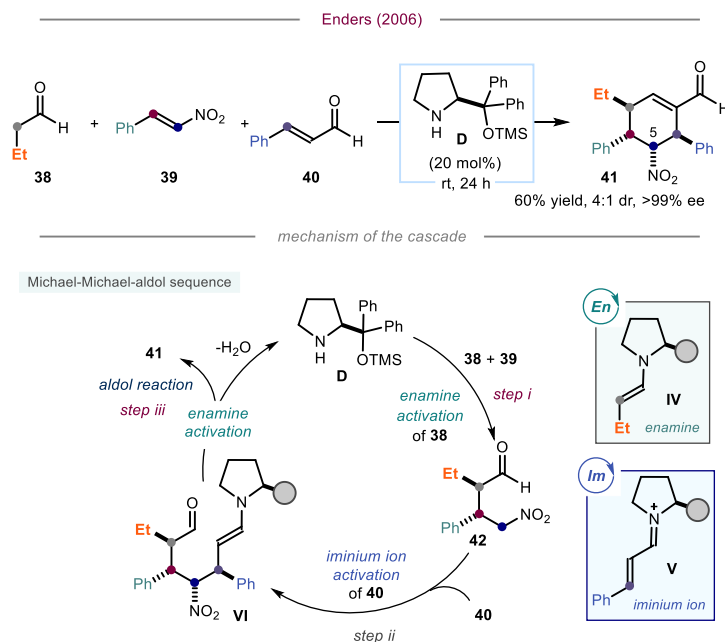
Scheme 3.12. Asymmetric three-component cascade reaction operating through a Michael-Michael-aldol sequence reported by Enders in 2006.

The mechanism of this elegant triple cascade involved the generation of the enamine intermediate **IV** upon condensation of aldehyde **38** with catalyst **D**, followed by the first Michael addition between the enamine **IV** and nitrostyrene **39** (*step i*). The second step of the cascade involved a second Michael addition between intermediate **42** and iminium ion-activated cinnamaldehyde **40** (intermediate **V**, *step ii*), ultimately delivering the enamine intermediate **VI** which underwent an intramolecular aldol condensation towards product **41** (*step iii*). Products **41** could be diversified with different substituents at carbons 4 and 6 by varying selectively the nitroalkene or the α,β-unsaturated aldehyde, respectively. Importantly, all the three steps of the Enders cascade were driven by the same organocatalyst, which activated different carbonyl compounds, an aliphatic aldehyde **38** and an enal **40**, *via* two orthogonal activation strategies, i.e. the enamine and the iminium ion intermediates, respectively.

In 2009, Enders reported a simpler but mechanistically related two-component process based on a Michael addition-Michael addition-aldol reaction cascade sequence.[44] This two-component process operated through an iminium ion-iminium ion-enamine activation sequence and allowed the synthesis of cyclohexene carbaldehydes **44** with up to three contiguous stereocenters as mixtures of only two and highly enantioenriched diastereomers (Scheme 3.13).
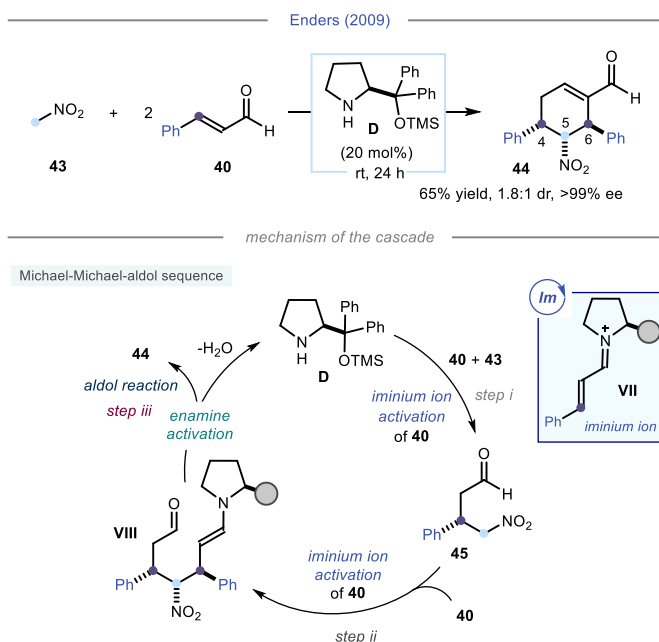
Scheme 3.13. Asymmetric two-component cascade reaction operating through a Michael-Michael-aldol sequence reported by Enders in 2009.

In the first step, the Michael addition of nitromethane **43** to cinnamaldehyde **40** activated by the diphenylprolinol catalyst **D** *via* iminium ion delivered intermediate **45** (*step i*). This intermediate was nucleophilic and underwent another Michael addition to a second equivalent of iminium ion-activated cinnamaldehyde **40** to generate the enamine intermediate **VIII** (*step ii*). A subsequent cyclization of the enamine intermediate **VIII** followed by dehydration gave product **44** (*step iii*). In this case, the cyclohexene carbaldehyde products **44** bore identical substituents on carbon 4 and 6, and diversification of the aromatic moieties in these two positions was synthetically unattainable following this single-step procedure. The two-component Enders process constituted another example of a sophisticated cascade protocol that was promoted by the same multifunctional organocatalyst **D** that catalyzed the previous

---

[44] Enders, D., Jeanty, M., Bats, J. W. "Organocatalytic Asymmetric Triple Domino Reactions of Nitromethane with α,β-Unsaturated Aldehydes" *Synlett* **2009**, *19*, 3175-3178.

triple cascade reaction shown in Scheme 3.12 and, therefore, was capable of activating different classes of substrates *via* mechanistically distinct activation strategies.

3.5 Target of the Project

Cascade reactions exploiting a single multifunctional catalyst to drive each step of the process are a powerful strategy in organocatalysis.[45] The most sophisticated examples of such transformations combined two different activation strategies, the enamine and the iminium ion activations, operated by the same catalyst in one sequence and culminating in the classic examples of the triple cascade and the two-component cascade processes reported by Enders in 2006 (Scheme 3.12)[43] and 2009 (Scheme 3.13)[44], respectively.

In contrast, biocatalytic cascade reactions exploiting a single multifunctional enzyme are less explored, and the traditional strategies rather rely on the combination of multiple enzymes, each catalyzing only one step of the sequence[23] (see *Section 3.3*). However, single-enzyme cascade processes are desirable because they would allow to overcome the challenges associated with the combination of multiple enzymes, such as the potential incompatibility of the different catalytic systems in one-pot. To date, only few examples of multifunctional enzymes have been reported that are capable to promote mechanistically different reactions in a cascade sequence and in one-pot.[29]

Due to the paucity of methods in single-enzyme driven biocascade catalysis, the aim of this project was to target such elusive asymmetric multicomponent biocascade processes. Specifically, we targeted the triple cascade reaction reported by Enders in 2006 and we aimed to implement the biocatalytic version of this elegant strategy (Scheme 3.14a). This target required the identification of a multifunctional enzyme capable of performing both enamine activation of aldehydes **46** and iminium ion activation of enals **48** in a sequential fashion to deliver complex products **49**. Specifically, we identified a class of multifunctional carboligase enzymes, the 4-oxalocrotonate tautomerase (4-OT) family, that could perform both activation strategies generating intermediates **IX** and **X**.[46] The more simple and mechanistically related two-component process reported by Enders in 2009 would serve as a testbed to prove the feasibility of 4-OT enzymes to combine enamine and iminium ion activation in a single sequence (Scheme 3.14b). Ideally, our biocatalytic protocols for the implementation of the two Enders cascade processes would match, and even surpass, the organocatalytic protocol in

---

[45] (a) Grondal, C., Jeanty, M., Enders, D. "Organocatalytic cascade reactions as a new tool in total synthesis" *Nat. Chem.* **2010**, *2*, 167-178; (b) Jones, S. P., Simmons, B., Mastracchio, A., MacMillan, D. W. C. "Collective synthesis of natural products by means of organocascade catalysis" *Nature* **2011**, *475*, 183-188.
[46] (a) Zandvoort, E., Geertsema, E. M., Baas, B.-J., Quax, W. J., Poelarends, G. J. "Bridging between Organocatalysis and Biocatalysis: Asymmetric Addition of Acetaldehyde to β-Nitrostyrenes Catalyzed by a Promiscuous Proline-Based Tautomerase" *Angew. Chem.* **2012**, *124*, 1266-1269; (b) Guo, C., Saifuddin, M., Saravanan, T., Sharifi, M., Poelarends, G. J. "Biocatalytic Asymmetric Michael Additions of Nitromethane to α,β-Unsaturated Aldehydes via Enzyme-Bound Iminium Ion Intermediates" *ACS Catal.* **2019**, *9*, 4369-4373.

terms of efficiency and selectivity for the synthesis of complex products **49** and **50**, respectively.
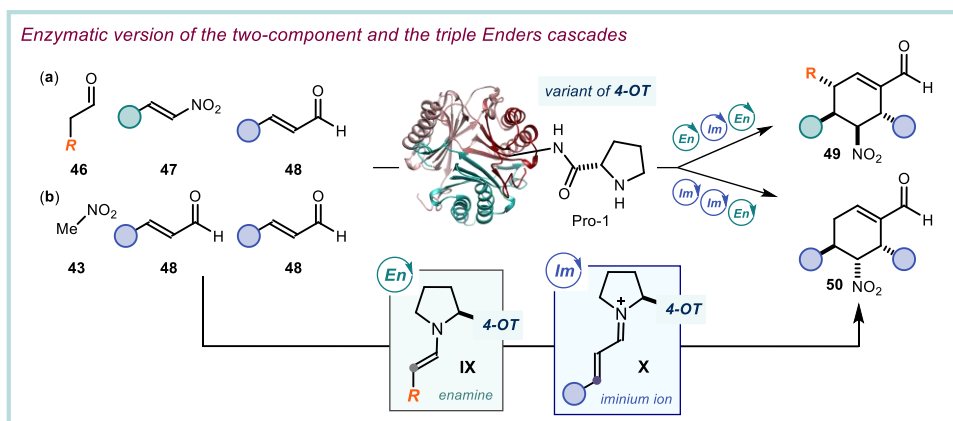
Scheme 3.14. Target of the project: enzymatic version of the Enders cascades.

In the next paragraph, the general aspects of the 4-OT family of enzymes will be discussed, followed by the previous reports on the ability of these enzymes to perform both the enamine and the iminium ion activation strategies.

3.5.1 The 4-Oxalocrotonate Tautomerase (4-OT) Family

To successfully implement the enzymatic version of one of the most sophisticated examples of organocascade catalysis, the Enders triple cascade, we needed to identify a biocatalyst with the ability to readily form enamine and iminium ion intermediates from aldehyde substrates, in analogy with the multifunctional behaviour showed by the diphenylprolinol organocatalyst **D** in Scheme 3.12 and 3.13. We were inspired by recent works of Poelarends and co-workers, who demonstrated that natural 4-oxalocrotonate tautomerases (4-OT) from *Pseudomonas putida* (Pp-4OT) and their engineered variants could be used to successfully develop a variety of non-natural carbon-carbon bond-forming processes using the catalytic mechanisms of classical organocatalysis with high stereocontrol.[47] 4-OT (4-oxalocrotonate tautomerase, EC 5.3.2.X) is a subgroup of the tautomerase superfamily.[48] 4-OT from the soil bacterium *Pseudomonas putida* (Pp-4-OT, EC 5.3.2.6)[48] is an enzyme involved in the microbial degradation of aromatic hydrocarbons to intermediates of the Krebs cycle which in Nature

---

[47] (a) Miao, Y., Rahimi, M., Geertsema, E. M., Poelarends, G. J. "Recent developments in enzyme promiscuity for carbon-carbon bond-forming reactions" *Curr. Opin. Chem. Biol.* **2015**, *25*, 115-123. For a review, see: (b) Xu, G., Poelarends, G. J. "Unlocking New Reactivities in Enzymes by Iminium Catalysis" *Angew. Chem. Int. Ed.* **2022**, *61*, e202203613.

[48] Davidson, R., Baas, B. J., Akiva, E., Holliday, G. L., Polacco, B. J., LeVieux, J. A., Pullara, C. R., Zhang, Y. J., Whitman, C. P., Babbitt, P. C. "A Global View of Structure-Function Relationships in the Tautomerase Superfamily" *J. Biol. Chem.* **2018**, *293*, 2342-2357.

catalyzes the isomerization of 4-oxalocrotonate **51** to 2-oxo-3-hexene-1,6-dioate **53** through the intermediate 2-hydroxymuconate **52** (Scheme 3.15a).
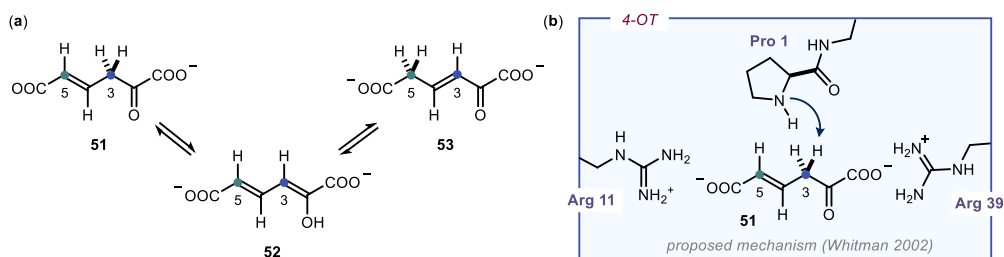
Scheme 3.15. (a) Natural reactivity of the Pp-4-OT enzyme: the isomerization of 4-oxalocrotonate; (b) proposed mechanism.[49]

The structure of this enzyme was elucidated in 1992[50] and later confirmed by X-ray crystallography as a homohexamer composed of six short monomers of 62 amino acid residues each (Figure 3.1).[51] The monomers present a β-α-β structure that starts on the N-terminus with a β-sheet β-1, followed by an α-helix α-1, then a small 3_{10} helix followed by a second β-sheet β-2 and ends with two small β-3 and β-4 strands on the C-terminus (Figure 3.1a).[49] Two monomers couple to form a dimer where the β strands and the α helices are arranged in an anti-parallel way (Figure 3.1b). Three dimers interact to form the hexamer *via* non-covalent interactions between the β strands of a dimer and the C-terminal β hairpins of another dimer. Each dimer exposes the regions composed of the 4 anti-parallel β sheets towards the centre of the hexameric structure, thus creating a hydrophobic cavity (Figure 3.1c).

[49] Whitman, C. P. "The 4-Oxalocrotonate Tautomerase Family of Enzymes: How Nature Makes New Enzymes Using a β-α-β Structural Motif" *Arch. Biochem. Biophys.* **2002**, *402*, 1-13.

[50] Chen, L. H., Kenyon, G. L., Curtin, F., Harayama, S., Bembenek, M. E., Hajipour, G., Whitman, C. P. "4-Oxalocrotonate Tautomerase, an Enzyme Composed of 62 Amino Acid Residues per Monomer" *J. Biol. Chem.* **1992**, *267*, 17716-17721.

[51] Subramanya, H. S., Roper, D. I., Dauter, Z., Dodson, E. J., Davies, G. J., Wilson, K. S., Wigley, D. B. "Enzymatic Ketonization of 2-Hydroxymuconate: Specificity and Mechanism Investigated by the Crystal Structures of Two Isomerases" *Biochemistry* **1996**, *35*, 792-802.
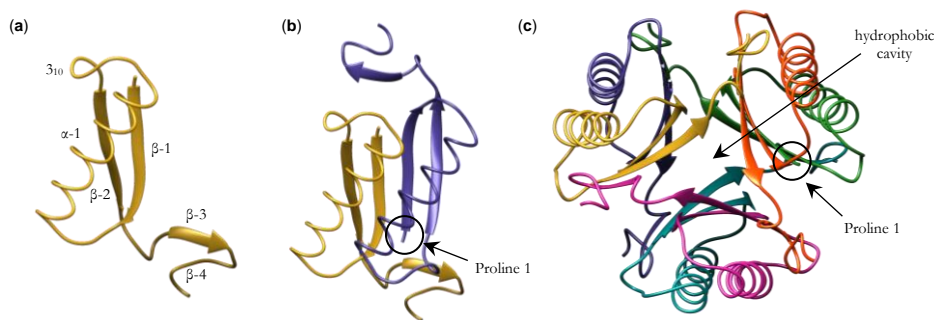
Figure 3.1. Crystal structure of the (a) monomer, (b) dimer, (c) hexamer of 4-oxalocrotonate tautomerase isolated from *Pseudomonas sp. CF600*: reported by Subramanya et al. in 1996 (*PDB 1OTF*).[51] All structures were plotted by UCSF Chimera 1.15.

The catalytic activity of the enzyme is exerted by the proline residue in the N-terminal position 1, for which its conjugate acid has a measured pK_a as low as 6.4 inside the active site (for comparison, the pK_a of the free amino acid is approximately 10.6).[52] Since this residue exists preferentially as the neutral non-protonated form at physiological pH, it behaves as a general base in the isomerization of its natural substrate *via* abstraction of *pro-R* proton in carbon 3 of **51** (Scheme 3.15b), and as an acid *via* protonation of carbon 5 in **52**.[49] Cationic residues, including arginine 11, from the anti-parallel monomer of the dimer, and arginine 39, from a second dimeric structure, were found to be essential for the stabilization of the carboxylic groups in **51** and for the build-up of the negative charge generated during deprotonation to give intermediate **52**. Overall, the active site is located at the interface of two adjacent dimers and benefits from the amino acid residues of three different monomers. Cooperation of the three residues Pro-1, Arg-11 and Arg-39 is essential for the catalytic activity of 4-OT.

In 2011, the group of Poelarends reported a novel promiscuous activity[53] of the 4-OT enzyme as a catalyst in the aldol condensation of acetaldehyde **12** with benzaldehyde **54** to yield cinnamaldehyde **40**, which required long reaction times of up to 14 days (Scheme 3.16).[54] The authors proposed the formation of the enamine intermediate **XI** in the active site of 4-OT upon condensation of acetaldehyde **12** with the catalytically active residue proline 1, in analogy with the well-known organocatalytic methods that exploit the enamine activation operated by the free amino acid proline.[10,30a] The nucleophilic enamine **XI** generated in the active site of 4-OT reacted with benzaldehyde **54** to give an oxyanion intermediate bearing a negative

---

[52] Czerwinski, R. M., Harris, T. K., Massiah, M. A., Mildvan, A. S., Whitman, C. P. "The Structural Basis for the Perturbed PKa of the Catalytic Base in 4-Oxalocrotonate Tautomerase: Kinetic and Structural Effects of Mutations of Phe-50" *Biochemistry* **2001**, *40*, 1984-1995.

[53] Bornscheuer, U. T., Kazlauskas, R. J. "Catalytic Promiscuity in Biocatalysis: Using Old Enzymes to Form New Bonds and Follow New Pathways" *Angew. Chem. Int. Ed.* **2004**, *43*, 6032-6040.

[54] Zandvoort, E., Baas, B. J., Quax, W. J., Poelarends, G. J. "Systematic Screening for Catalytic Promiscuity in 4-Oxalocrotonate Tautomerase: Enamine Formation and Aldolase Activity" *ChemBioChem* **2011**, *12*, 602-609.

charge, which was stabilized by the arginine residue 11. Protonation of this intermediate and subsequent hydrolysis furnished product **40**. This work demonstrated that the proline 1 residue in 4-OT enzymes could activate aldehyde **12** via the formation of an enamine intermediate **XI**.
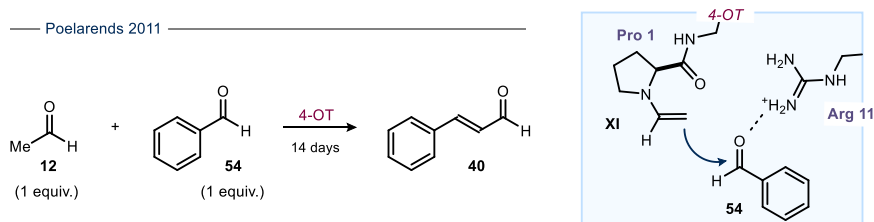
Scheme 3.16. Novel promiscuous activity of 4-OT tautomerase as an aldolase catalyst.

The formation of the enamine intermediate in the active site of 4-OT was confirmed by its direct observation in the structure of the enzyme obtained by crystallographic X-ray analysis. Crystals of the enzyme were obtained after incubation of 4-OT with acetaldehyde.[55] The authors also showed that substrates other than acetaldehyde, such as longer chain aldehydes or small ketones, could form the enamine intermediate of type **XI** with residue Pro-1.[54]

Beside the 4-OT's promiscuous activity as both an aldolase and a retro-aldolase enzyme,[56] the same group reported shortly after the activity of the 4-OT tautomerase as a "Michaelase" catalyst in the addition of acetaldehyde **12** to *trans*-β-nitrostyrene **39** to generate the GABA-analogue (γ-aminobutyric acid derivative) precursor (*S*)-**45** with good stereoinduction (Scheme 3.17).[57] Importantly, we recognized that this reaction was the *step i* of the Enders triple cascade illustrated in Scheme 3.12 when butanal **38** was substituted with acetaldehyde **12**. This first step delivered intermediate **45** which was the product of the *step i* of the Enders two-component process illustrated in Scheme 3.13.

[55] Poddar, H., Rahimi, M., Geertsema, E. M., Thunnissen, A. M. W. H., Poelarends, G. J. "Evidence for the Formation of an Enamine Species during Aldol and Michael-Type Addition Reactions Promiscuously Catalyzed by 4-Oxalocrotonate Tautomerase" *ChemBioChem* **2015**, *16*, 738-741.

[56] Zandvoort, E., Geertsema, E. M., Quax, W. J., Poelarends, G. J. "Enhancement of the Promiscuous Aldolase and Dehydration Activities of 4-Oxalocrotonate Tautomerase by Protein Engineering" *ChemBioChem* **2012**, *13*, 1274-1277.

[57] Zandvoort, E., Geertsema, E. M., Baas, B.-J., Quax, W. J., Poelarends, G. J. "Bridging between Organocatalysis and Biocatalysis: Asymmetric Addition of Acetaldehyde to β-Nitrostyrenes Catalyzed by a Promiscuous Proline-Based Tautomerase" *Angew. Chem.* **2012**, *124*, 1266-1269.

Scheme 3.17. Novel promiscuous activity of 4-OT as a "Michaelase" catalyst.

Mechanistically, proline 1 residue was proposed to condense with **12** to generate intermediate **XI**. The nucleophilic enamine **XI** subsequently reacted with electrophilic β-nitrostyrene **39**, stabilized by non-covalent interactions with arginine 11, to produce the new C-C bond. Diversely substituted aromatic *trans*-β-nitrostyrenes,[58] aliphatic nitroalkenes[59] and longer chain aldehydes[60] were successfully engaged in the Michael addition to generate highly enantioenriched γ-nitroaldehydes. Furthermore, a systematic mutability campaign of 4-OT conducted by investigating all possible single point mutations along the 62 amino acid sequence of the enzyme monomers revealed the greater influence of residue Arg-39 over Arg-11 in directing the binding of the substrate inside the active site of 4-OTs.[61] This was most likely involved in the protonation step of the nitronate intermediate following the addition of **XI** to **39**. The mutability campaign also delivered two new 4-OT mutants (A33D and M45Y/F50A) with enhanced "Michaelase" activity and high stereoselectivity for the antipodal product (*R*)-**45** in the addition of acetaldehyde to nitrostyrene derivatives of type **39**.[61]

After demonstrating the capability of the 4-OT tautomerase to activate aldehydes *via* the formation of an enamine intermediate with Pro-1 in the active site, in 2019 the authors demonstrated that a variant of 4-OT displaying a single mutation in the amino acid sequence could activate α,β-unsaturated aldehyde **40** *via* the formation of an iminium ion intermediate

[58] Miao, Y., Tepper, P. G., Geertsema, E. M., Poelarends, G. J. "Stereochemical Control of Enzymatic Carbon-Carbon Bond-Forming Michael-Type Additions by 'Substrate Engineering'" *Eur. J. Org. Chem.* **2016**, *32*, 5350-5354.

[59] Kunzendorf, A., Saifuddin, M., Poelarends, G. J. "Enantiocomplementary Michael Additions of Acetaldehyde to Aliphatic Nitroalkenes Catalyzed by Proline-Based Carboligases" *ChemBioChem* **2022**, *23*, 15-17.

[60] Miao, Y., Geertsema, E. M., Tepper, P. G., Zandvoort, E., Poelarends, G. J. "Promiscuous Catalysis of Asymmetric Michael-Type Additions of Linear Aldehydes to β-Nitrostyrene by the Proline-Based Enzyme 4-Oxalocrotonate Tautomerase" *ChemBioChem* **2013**, *14*, 191-194.

[61] Van Der Meer, J. Y., Poddar, H., Baas, B. J., Miao, Y., Rahimi, M., Kunzendorf, A., Van Merkerk, R., Tepper, P. G., Geertsema, E. M., Thunnissen, A. M. W. H., Quax, W. J., Poelarends, G. J. "Using Mutability Landscapes of a Promiscuous Tautomerase to Guide the Engineering of Enantioselective Michaelases" *Nat. Commun.* **2016**, *7:10911*, 1-16.

XII by condensation with proline 1 (Scheme 3.18).[62] Specifically, the F50A mutant of 4-OT catalyzed the addition of nitromethane **43** to cinnamaldehyde **40** activated *via* eneiminium ion **XII** by Pro-1 to generate γ-nitroaldehyde (*R*)-**45** in high yield and enantiopurity. The mutation of the phenylalanine 50 with an alanine residue was proposed to favour the hydrolysis of the enamine intermediate resulting from the addition of **43** to **XII** and the subsequent product release. In fact, this mutation opened up a new cavity for water molecules,[56] rendering the active site less hydrophobic but without altering the pK_a of proline 1. The mutation also improved the enantioselectivity of the reaction to 98% ee (for comparison, the product with wild-type 4-OT was obtained only in 35% yield and 72% ee when a large excess of **43** was employed). Importantly, we recognized that this reaction was the *step i* of the Enders two-component process illustrated in Scheme 3.13.
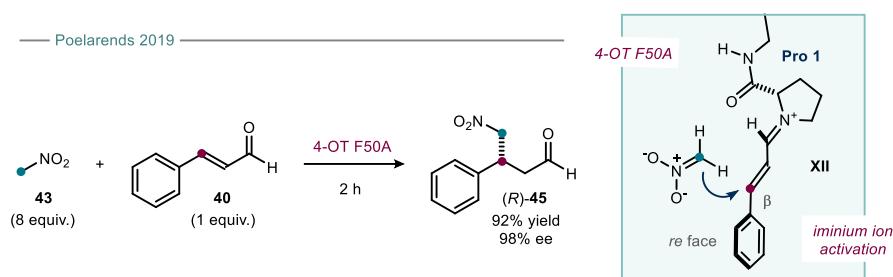
Scheme 3.18. Iminium ion activation in a 4-OT mutant.

These findings proved that 4-OT enzymes are capable of performing both the enamine and the iminium ion activation of carbonyl substrates by condensation with the catalytically active terminal proline. These activation modes are straightforward strategies in organocatalysis but uncommon in the active site of an enzyme. Recent reports from the same authors revealed that the iminium ion activation mode in 4-OT variants can be exploited with different nucleophiles, including peroxides and halogenated malonates, to efficiently perform epoxidation[63] and cyclopropanation[64] reactions, respectively.

Overall, 4-OT tautomerases proved highly promiscuous enzymes with the ability to activate different classes of substrates (linear aliphatic aldehydes and α,β-unsaturated aldehydes) *via* both enamine and iminium ion activation and to catalyze different types of reactions such as

---

[62] Guo, C., Saifuddin, M., Saravanan, T., Sharifi, M., Poelarends, G. J. "Biocatalytic Asymmetric Michael Additions of Nitromethane to α,β-Unsaturated Aldehydes via Enzyme-Bound Iminium Ion Intermediates" *ACS Catal.* **2019**, *9*, 4369-4373.

[63] Xu, G., Crotti, M., Saravanan, T., Kataja, K. M., Poelarends, G. J. "Enantiocomplementary Epoxidation Reactions Catalyzed by an Engineered Cofactor-Independent Non-Natural Peroxygenase" *Angew. Chem. Int. Ed.* **2020**, *59*, 10374-10378.

[64] Kunzendorf, A., Xu, G., Saifuddin, M., Saravanan, T., Poelarends, G. J. "Biocatalytic Asymmetric Cyclopropanations via Enzyme-Bound Iminium Ion Intermediates" *Angew. Chem. Int. Ed.* **2021**, *60*, 24059-24063.

Michael addition and aldol reactions. These reactions are the key steps of the triple cascade and two-component cascade processes reported by Enders, that are the target of this work.[43,44] Therefore, we identified 4-OT enzymes as the best multifunctional catalysts to test in order to develop a biocatalytic version of the Enders cascade reactions.

3.6 Results and Discussion

3.6.1 Preliminary Results and Optimization

At the onset of our investigation, we decided to test the ability of 4-OT enzymes as multifunctional catalysts in biocascade processes targeting the two-component reaction reported by Enders in 2009 (Scheme 3.13).[44] The enzymatic version of this process is illustrated in Scheme 3.19. The reaction combined nitromethane **43** and cinnamaldehyde **40** to afford tri-substituted cyclohexene carbaldehyde **44** bearing three contiguous stereogenic centers. The mechanism of this process relied on a sequence of Michael-Michael-aldol reactions (in analogy with the organocatalytic mechanism illustrated in Scheme 3.13). Enal **40** would be initially activated by the 4-OT enzyme through the generation of the iminium ion intermediate **XII** in Scheme 3.18, followed by subsequent Michael addition of **43** to **XII**. The Michael product **45** generated in the first step would undergo a second Michael addition from its nucleophilic carbon bearing the nitro group to another intermediates **XII**. A final aldol cyclization and dehydration step would afford product **44**.
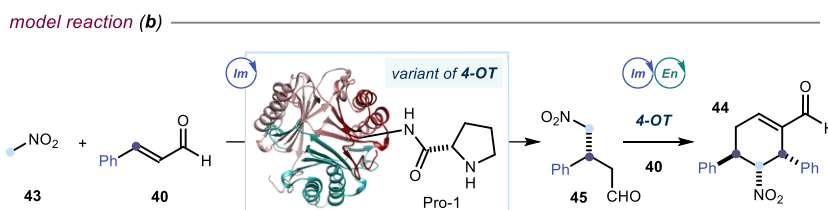
Scheme 3.19. Model reaction: enzymatic version of the cascade reaction reported by Enders in 2009.

We selected this two-component cascade as a testbed for our real goal, which was to develop the more complex triple cascade reported by Enders in 2006 (Scheme 3.13).[43] Our choice was informed by different observations: first, 4-OTs have been reported to promote the Michael addition of nitromethane **43** to cinnamaldehyde **40**,[62] which is the first step in the two-component process. In addition, the resulting Michael product **45** is the same intermediate of the second step of the Enders triple cascade. In fact, the second and the third steps of the two-component cascade process follow the exact same mechanism of the more complex triple cascade; therefore this reaction offered a simplified testbed for our studies.

We started our investigation testing the activity of the wild-type Pp-4OT from *Pseudomonas putida*[48] in the iminium ion activation of **40**. The gene encoding for this enzyme was cloned,

encoded by the pET20b plasmids, the enzyme expressed in *E. coli* BL21(DE3) competent cells and purified following a reported procedure.[54] We tested first the formation of Michael product **45** by incubation of Pp-4-OT (200 μM, 4 mol%) with cinnamaldehyde **40** (5 mM) and nitromethane **43** (50 mM) for 24 h in 500 μL of 50 mM KPi (potassium phosphate) buffer pH 6.5 containing 10% DMSO at 30 ℃ (Table 3.1, entry 1). Pleasingly, we observed the formation of product (*R*)-**45** in 44% yield and 99% ee and traces of the cascade product **44**. This indicated the feasibility of our hypothesis, but that further optimization of the catalyst and/or reaction conditions was needed to promote the cascade process towards the formation of the desired product **44**.

Table 3.1. Initial screening to test the activity of different 4-OT variants in the iminium ion activation of cinnamaldehyde.[a]

entry	enzyme (loading)	equiv. **43**	yield **45** (%)	ee **45** (%)[b]	yield **44** (%)	dr **44**[c]	ee **44** (%)[c]
1	**Pp**-4OT (4 mol%)	10	44	99	<5	nd	nd
2	**Ps**-4OT (4 mol%)	10	38	37	0	nd	nd
3	**MI**-4OT (4 mol%)	10	41	12	0	nd	nd
4	**Tb**-4OT (4 mol%)	10	27	22	0	nd	nd
5	**DERA-MA** (4 mol%)	10	50	99	0	nd	nd
6	**Pp**-4OT (4 mol%)	1	13	99	49	>20:1	96
7	**Ps**-4OT (4 mol%)	1	22	37	7	nd	nd
8	**MI**-4OT (4 mol%)	1	12	12	6	nd	nd
9	**Tb**-4OT (4 mol%)	1	18	22	6	nd	nd
10	**DERA-MA** (4 mol%)	1	38	99	7	nd	nd
11	-	1	0	nd	0	nd	nd

[a]Reactions performed on a 2.5 μmol scale (5 mM) at 30 °C. Analytical yields of **45** and **44** determined by GC-FID analysis (calibration using mesitylene as internal standard) and by HPLC analysis (calibration using 1,3,5-methoxybenzene as internal standard). [b]Enantiomeric excess (ee) value determined by UPC[2] analysis. [c]Diastereomeric ratio (dr) and enantiomeric excess (ee) measured by HPLC analysis. nd = not determined; KPi = potassium phosphate.

To improve the reactivity of the cascade process, we tested other 4-OT enzymes. We used PSI-BLAST,[65] an iterative search method for protein sequence similarity, to identify new enzymes sharing >75% of sequence similarity with Pp-4OT. All the enzymes selected retained

[65] Altschul, S. F., Madden, T. L., Schäffer, A. A., Zhang, J., Zhang, Z., Miller, W., Lipman, D. J. "Gapped BLAST and PSI-BLAST: A new generation of protein database search programs" *Nucleic Acids Res.* **1997**, *25*, 3389-3402.

the N-terminal proline 1 because of this residue's critical catalytic role. A collection of 4-OT enzymes, including Ml-4OT from *Marinobacter lipolyticus* SM19 (NCBI: txid1318628, 85.7% sequence similarity with Pp-4OT), Tb-4OT from *Thiolapillus brandeum* (NCBI: txid1076588, 79.4% sequence similarity) and Ps-4OT from *Pseudomonas sagittaria* (NCBI: txid1135990, 93.7% sequence similarity), was cloned, expressed, and purified with the same procedure used for Pp-4OT. Incubation of these variants with 5 mM of cinnamaldehyde **40** and 50 mM of nitromethane **43** under the same conditions as in entry 1 delivered product **45** with less efficiency and enantiocontrol. In this case, no cascade product **44** was observed (Table 3.1, entries 2-4). We then focused on an engineered variant of deoxyribose-phosphate aldolase DERA (DERA-MA), which was reported recently to outperform Pp-4OT enzyme in the iminium ion-mediated addition of nitromethane **43** to cinnamaldehyde **40**.[66] After successful expression and purification of the DERA-MA variant according to the reported procedure,[66] a 10:1 ratio of nitromethane **43** and cinnamaldehyde **40** (5 mM) was incubated with 4 mol% of DERA-MA in 50 mM KPi buffer (pH 6.5, 10% DMSO, 30 ºC for 24 hours). The Michael addition product (*R*)-**45** was obtained in 50% yield and 99% ee. However, the target cascade product **44** was not formed at all (Table 3.1, entries 5). Once tested the ability of the 4-OT variants and DERA-MA to activate **40** and catalyze the Michael addition to form **45**, we sought to increase the formation of cascade product **44** by adjusting the stoichiometry of substrates **43**:**40** from 10:1 to a 1:1 ratio. This choice was motivated by the need of cinnamaldehyde to react twice; therefore, its relative increase in concentration could facilitate the cascade sequence. We tested again all the available enzymes under these conditions. Pleasingly, Pp-4OT gave 49% of cascade product **44** with excellent diastereo- and enantioselectivity (>20:1 dr, 96% ee), together with intermediate **45** in 13% yield (Table 3.1, entry 6). The other variants delivered **45** in poor yields while only traces of cascade product **44** were detected (Table 3.1, entries 7-9). Under these conditions, DERA-MA offered only traces of the cascade product **44**, demonstrating the inability to further react intermediate **45** (Table 3.1, entry 10). A control experiment without the enzyme did not lead to products **45** or **44** (Table 3.1, entry 11). Authentic samples of cascade product **44** were prepared using the Enders procedure[44] and used to determine the analytical yields in Table 3.1.

Comparison between the organocatalytic and the enzymatic processes revealed that 4-OT catalyzes the formation of the diastereomer of **44** that was the minor isomer formed under the Enders organocascade, which delivered a 1.8:1 dr (Scheme 3.13). The excellent diastereoselectivity of the enzymatic process clearly outperformed the organocatalytic protocol while providing complementary access to a poorly accessible diastereomer with exquisite enantiopurity.

[66] Kunzendorf, A., Xu, G., van der Velde, J. J. H., Rozeboom, H. J., Thunnissen, A. W. H., Poelarends, G. J. "Unlocking Asymmetric Michael Additions in an Archetypical Class I Aldolase by Directed Evolution" *ACS Catal.* **2021**, *11*, 13236-13243.

3.6.2 Construction of fused 4-OT variants

Based on these results, we selected Pp-4OT for further structural modification. We envisioned that inserting a polyhistidine-tag (His-Tag) in the amino acid sequence would allow us to simplify the purification of Pp-4OT and deliver more pure catalyst by applying metal ion affinity chromatography purification. Moreover, the His-tagged enzyme may offer great opportunities for immobilization and application in organic solvents when elevated concentrations of reactants are required. The His-Tag technology is based on the binding of the imidazole moiety from histidine residues on peptides to metal ions (such as nickel) immobilized on a chromatographic column.[67] Previous studies indicated that His-Tag installed on the C-terminus of 4-OT enzymes was detrimental for their catalytic activity.[68] Therefore, we decided to include it in the internal sequence. We looked at a naturally fused 4-OT from *Burkholderia lata* (PDB 6BLM),[48] which shares 59% sequence similarity with Pp-4OT, to design a tandem 4-OT by fusing the C-terminus of a monomer in Pp-4OT with the N-terminus of a second monomer (see *Section 3.5.1* for a detailed description of 4-OTs structure). The designed fused enzyme would be characterized by three subunits rather than a hexameric structure. The idea of a fused enzyme was informed by both the existence of this structural arrangement in the evolutionary history of the tautomerase superfamily[48] and by recent studies by Poelarends, who reported a tandem-fused 4-OT showing increased catalytic activity in the iminium ion activation of cinnamaldehyde **40**.[69] The fused enzyme would allow us to expand the space available for genetic manipulations and for the insertion of an internal His-Tag. Therefore, in order to construct the fused enzyme, we inserted the linker sequence GAGGSL between the C-terminus of a monomer and the N-terminus of a second monomer of Pp-4OT (all the sequences are reported in the *Experimental Section*). This flexible glycine-rich linker consisting of six amino acid residues is similar to the GAPPSL linker found in the naturally fused enzyme. The proline residues were substituted with glycine since it offers increased flexibility when constructing artificial fusions.[70] We also removed the last three residues (VRR) in the sequence of Pp-4OT to further increase the flexibility of the linker while matching the length of the naturally fused 4-OT from *Burkholderia lata* (127 amino acids). The resulting Pp-4OT-F$_1$ enzyme was successfully expressed and tested in the model cascade process under the reaction conditions of entry 5 in Table 3.1. The fused variant maintained its catalytic activity and delivered cascade product **x** in a slightly increased yield

[67] Porath, J. "Immobilized Metal Ion Affinity Chromatography" *Protein Expr. Purif.* **1992**, *3*, 263-281.
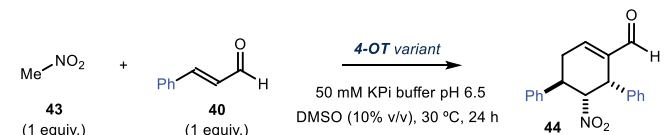
[68] Lukesch, M. S., Pavkov-Keller, T., Gruber, K., Zangger, K., Wiltschi, B. "Substituting the Catalytic Proline of 4-Oxalocrotonate Tautomerase with Non-Canonical Analogues Reveals a Finely Tuned Catalytic System" *Sci. Rep.* **2019**, *9*, 1-9.

[69] Xu, G., Kunzendorf, A., Crotti, M., Rozeboom, H. J., Thunnissen, A. M. W. H., Poelarends, G. J. "Gene Fusion and Directed Evolution to Break Structural Symmetry and Boost Catalysis by an Oligomeric C-C Bond-Forming Enzyme" *Angew. Chem. Int. Ed.* **2022**, *61*. DOI: e20211397.

[70] Caparco, A. A., Bommarius, A. S., Champion, J. A. "Effect of Peptide Linker Length and Composition on Immobilization and Catalysis of Leucine Zipper-Enzyme Fusion Proteins" *AIChE J.* **2018**, *64*, 2934-2946.

of 55% compared to the unfused counterpart and with excellent diastereomeric ratio and enantiomeric excess (Table 3.2, entry 1).

Table 3.2. Screening of fused 4-OT variants in the model biocascade process.[a]

entry	enzyme (loading)	yield **44** (%)	dr **44**	ee **44** (%)
1	**Pp**-4OT-**F$_1$** (4 mol%)	55	>20:1	99
2	**Pp**-4OT-**F$_2$** (4 mol%)	8	nd	nd
3	**Pp**-4OT-**F$_3$** (4 mol%)	57	>20:1	99

[a]Reactions performed on a 2.5 μmol scale (5 mM) at 30 °C. Analytical yields of **44** determined by GC-FID analysis (calibration using mesitylene as internal standard); dr and ee of **44** measured by HPLC analysis. nd = not determined; KPi = potassium phosphate.

Since the fused variant Pp-4OT-F$_1$ was fully functional, we simulated a homology model with YASARA software to predict the enzyme's structure and better evaluate where to include the His-Tag (Figure 3.2). We targeted loop regions of the enzyme exposed to the aqueous environment. In particular, we designed Pp-4OT-F$_2$, which carries a His-Tag at positions 57-62, close to the GAGGSL linker; Pp-4OT-F$_3$, containing a His-Tag at positions 12-17, the loop connecting β1 to α1; and Pp-4OT-F$_4$, which carries a C-terminal His-Tag at positions 130-135, which is the most common strategy for His-Tag insertion in protein sequences. All fused His-tagged Pp-4OTs were successfully expressed and purified in one step using Nickel affinity chromatography with yields of 45-50 mg gr^{-1} of cell pellet (details of the procedure and purity of the proteins are provided in the *Experimental Section*). We tested the new variants in our model reaction and found that Pp-4OT-F$_2$ delivered product **44** in only 8% yield (Table 3.2, entry 2), whereas Pp-4OT-F$_3$ offered an improvement compared to the previous variants, affording **44** in 57% yield and with perfect stereoselectivity in favor of the same stereoisomer afforded by unfused Pp-4OT (Table 3.2, entry 3). The Pp-4OT-F$_4$ enzyme, instead, could not be tested in any biocatalytic reaction due to immediate precipitation after purification, in accordance with the reports about the loss of activity for the C-terminal histidine-tagged unfused 4-OT.[68] Figure 3.2 offers a visual comparison between the crystal structure of wild-type Pp-4OT (PDB: 4x19)[55] and the homology model of fused Pp-4OT-F$_3$ enzyme containing a His-Tag, which was selected as the best performing multifunctional enzyme.
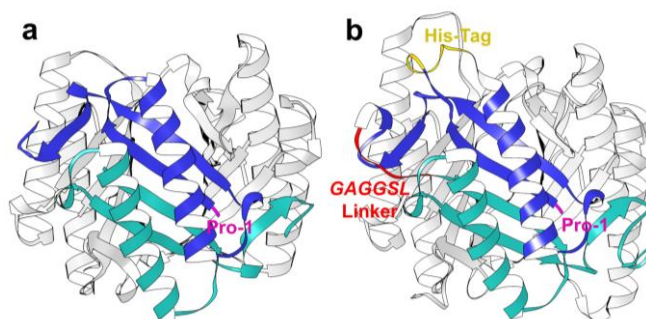
Figure 3.2. (a) Crystal structure of wild type Pp-4OT (PDB: 4X19); (b) homology model of Pp-4OT-F₃ created with YASARA structure. UCSF Chimera software was used for visualization.

The crystal structure of Pp-4OT shows the homo-hexameric three-dimensional space arrangement of the enzyme, where each monomer (blue or green in Figure 3.2) displays a β1-α-β2 structure. The homology model created for Pp-4OT-F₃ predicts the location of the His-Tag in the loop connecting the β1 and the α1 of each of the three subunits, in position 12-17 (shown in yellow in Figure 3.2). The His-Tag is far in space from the proline 1 residue (shown in magenta in Figure 3.2) and therefore should not affect its catalytic activity. The linker connecting the N-terminus (shown in green) with the C-terminus (shown in blue) of the two original monomers creates a loop (position 67-72) highlighted in red in Figure 3.2.
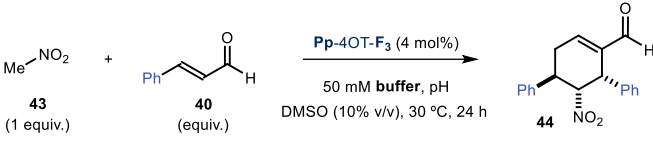
3.6.3 Optimization Studies

Based on our results, we decided to attempt further optimization of the model reaction using the best performing enzyme Pp-4OT-F₃ to promote the transformation. The catalyst loading and the reaction time were investigated (results listed in Table 3.3). Increasing the catalyst loading from 4 mol% to 5 mol% did not improve the efficiency of the process (entry 3 compared to entry 2 in Table 3.3), whereas lowering the loading to 2 mol% delivered product **44** in slightly lower yield (44% compared to 57% yield, entry 1 and 2, respectively).

Table 3.3. Screening of the catalyst loading and the reaction time in the model biocascade process.[a]

entry	x	time (h)	yield **44** (%)	dr **44**	ee **44** (%)
1	2 mol%	24	44	>20:1	99
2	4 mol%	24	57	>20:1	99
3	5 mol%	24	49	>20:1	99
4	4 mol%	6	40	>20:1	99
5	4 mol%	16	45	>20:1	99
6	4 mol%	48	58	>20:1	99

[a]Reactions performed on a 2.5 μmol scale (5 mM) at 30 °C. Analytical yields of **44** determined by GC-FID analysis (calibration using mesitylene as internal standard); dr and ee of **44** measured by HPLC analysis. KPi = potassium phosphate.
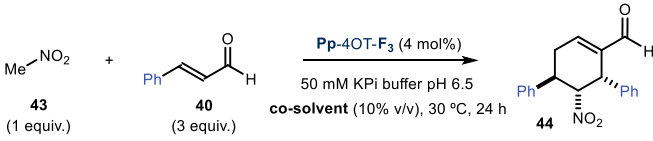
We extended the reaction time to 48 hours but the efficiency of the process did not significantly improve (entry 6 in Table 3.3), whereas shorter reaction times of 6 and 16 hours resulted in lower yield (40 and 45%, respectively, entry 4 and 5). Therefore, 4 mol% of catalyst and 24 hours of reaction time were selected for the next round of optimization. The effect of the reaction medium (buffer and pH) and the stoichiometry of the reaction were investigated (Table 3.4). Higher pH of 7.5 gave significantly reduced yield, and further increasing the pH to 9 totally impeded the formation of product **44** (entries 1 and 2). Increasing the equivalents of cinnamaldehyde **40** was beneficial for the cascade process and the optimal conditions were found when 3 equivalents of **40** were employed, delivering the product **44** in 80% yield and perfect stereocontrol (entry 5). A further increase to 4 equivalents did not offer any significant improvement (entry 6).

Table 3.4. Screening of the buffer, the pH and the equivalents of cinnamaldehyde in the model biocascade process.[a]

entry	equiv. of **40**	buffer (pH)	yield **44** (%)	dr **44**	ee **44** (%)
1	1	NaH₂PO₄ (7.5)	29	11:1	99
2	1	NaH₂PO₄ (9)	<5	nd	nd
3	1	KPi (6.5)	57	>20:1	99
4	2	KPi (6.5)	60	>20:1	99
5	3	KPi (6.5)	80	>20:1	99
6	4	KPi (6.5)	81	>20:1	99

[a]Reactions performed on a 2.5 μmol scale (5 mM) at 30 °C. Analytical yields of **44** determined by GC-FID analysis (calibration using mesitylene as internal standard); dr and ee of **44** measured by HPLC analysis. nd = not determined; KPi = potassium phosphate.

The conditions in entry 5 of Table 3.4 were selected for further screenings. We investigated the effect of the co-solvent in the reaction mixture (Table 3.5), and found that DMF and EtOH performed similarly to DMSO, providing the cascade product in 80% and 75% yield, respectively (entries 2 and 3). The reaction also tolerates other alcohols, such as ethylene glycol (EG) and MeOH, although the product was obtained in slightly reduced yield (71 and 69% respectively, entries 4 and 5).

Table 3.5. Screening of solvents in the model biocascade process.[a]


entry	co-solvent	yield **44** (%)	dr **44**	ee **44** (%)
1	DMSO	80	>20:1	99
2	DMF	80	>20:1	99
3	EtOH	75	>20:1	99
4	EG	71	>20:1	99
5	MeOH	69	>20:1	99

[a]Reactions performed on a 2.5 μmol scale (5 mM) at 30 °C. Analytical yields, dr and ee of **44** determined by HPLC analysis (calibration using 1,3,5-trimethoxybenzene as internal standard). KPi = potassium phosphate; EG = ethylene glycol.

In all cases, product **44** was obtained in excellent stereocontrol as a highly enantioenriched single diastereomer. Therefore, the conditions in entries 1 or 2 were selected to evaluate the scope of the biocascade process.

3.6.4 Scope of the two-component biocascade

A survey of the enals that successfully participated in the biocascade process with nitromethane **43** is shown in Figure 3.3. The analytical yields of products **50** were obtained after performing instrumental calibrations using authentic product samples prepared according to the procedures described in the *Experimental Section*. In most cases, the organocatalytic Enders procedure[44] for the preparation of the authentic product samples was not suitable since it afforded the cascade product as a mixture of several diastereomers and only in trace amounts. Therefore, most samples for calibration were obtained by running a semi-preparative enzymatic reaction on milligrams scale as described in *Section 3.6.5*. We found that Pp-4OT-F$_3$ accepts in the active site different *ortho-*, *meta-* or *para-* substituted cinnamaldehydes **48**, adorned with both electron-rich and electron-poor substituents, delivering the corresponding cascade products **50a**-**h** in high yields (from 44 to 89%), good to excellent diastereoselectivity (dr from 3:1 to >20:1) and complete enantioselectivity in all cases (>99% ee). Cinnamaldehydes bearing *para*-fluoro- and *meta*-methoxy substitution performed best, affording products **50a** and **50b** in 89% and 88% yield, respectively, with total stereocontrol. *Ortho*-methyl-cinnamaldehyde afforded product **50c** in 63% and 9:1 dr, which could be improved to 77% yield by using EtOH as co-solvent, although with slightly lower diastereoselectivity (dr of 7:1). O*rtho*-chloro substituted-cinnamaldehyde gave product **50e** in 44% yield and 3:1 dr, result which could not be improved by changing the co-solvent. *Meta*-bromo and *meta*-chloro substituted-cinnamaldehydes gave products **50d** and **50f** in 73% and 68% yield, respectively. In this case, the yield of product **50f** could be improved to 84% yield by using DMF as co-solvent, although with lower diastereocontrol (from >20:1 to 10:1 dr). Finally, a 2-furyl α,β-unsaturated aldehyde was also accepted by Pp-4OT-F$_3$, affording the cascade product **50h** in 20% yield and 3:1 dr. Aliphatic enals failed to deliver the cascade product, while substituted nitroalkanes remained unreacted. Other nucleophiles, such as malonates, were tested in the biocascade process but proved unsuccessful.
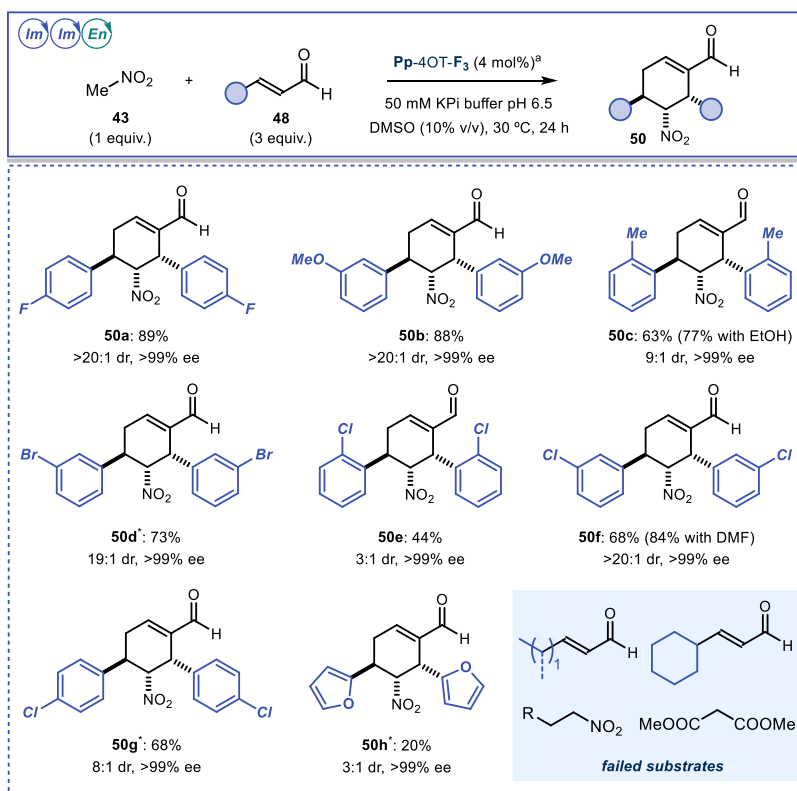
Figure 3.3. Scope of the enals that can participate in the biocascade process. [a]Reactions performed on a 2.5 μmol scale (5 mM) at 30 °C over 24 h. Analytical yields of **50** determined as an average of two runs by HPLC analysis (calibration using 1,3,5-trimethoxybenzene as internal standard); dr and ee of **50** measured by HPLC analysis. *Reactions run with DMF as co-solvent.

3.6.5 Semi-preparative enzymatic cascade reactions

To assess the scalability of the method and characterize products **50** after isolation, we performed some of the cascade processes on a semi-preparative scale (150 μmol of substrate **43**) using 30 mL of buffer solution and *E. coli* cell-free-extracts (CFE) containing ~75 mg of enzyme, that corresponds approximately to 2.5 mg enzyme mL^{-1} of reaction (~3 mol% of catalyst loading). Using the unpurified enzyme from the cell-free extracts, products **44** and **50a** were isolated as single stereoisomers in 61% yield (28 mg) and 88% yield (46 mg), respectively, after purification by column chromatography (results in Figure 3.4). The increased scale of reaction allowed us to obtain single crystals of the major stereoisomer of product **50e**, which permitted to unambiguously assign the relative and absolute configuration by X-ray crystallographic analysis.[71] Through-space ^{1}H NMR analysis confirmed the structure

---

[71] Data have been deposited at the Cambridge Crystallographic Data Centre, under deposition number CCDC2190489.

of the minor stereoisomer of **50e** as the epimer at the carbon 5 bearing the nitro group (experiments described in the *Experimental Section*). In general, products **50** were isolated with moderate yields and good to excellent diastereoselectivity (products **50b**-**f**, Figure 3.4), with the exception of **50h**, for which a 1:1 mixture of diastereomers was obtained.
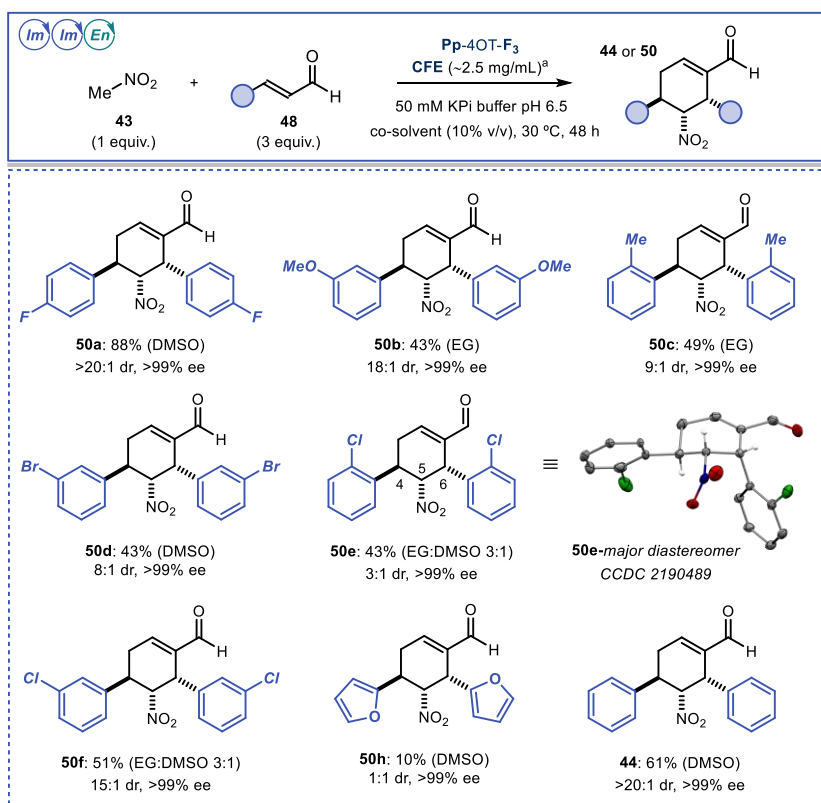

Figure 3.4. Scope of the semi-preparative scale biocascade process. [a]Reactions performed on a 150 μmol scale (5 mM) at 30 °C over 48 h in 30 mL of reaction volume with cell-free-extract containing Pp-4OT-F$_3$ (2.5 mg mL^{-1}) and the co-solvent or mixture of co-solvents indicated in parenthesis. Isolated yields of **44** and **50** determined after column chromatography; dr and ee of **44** and **50** measured by HPLC analysis. CFE = cell-free extracts.

3.6.6 Alternative sequential double-enzyme cascade process

Up to this point, both the C(4) and C(6) substituents of the cascade products were identical, since these substituents came from the same cinnamaldehyde substrate **48**. To achieve products bearing different substituents, two different cinnamaldehyde reactants would have to be used. However, differentiation of these two reactants by the same enzyme would require the ability of the biocatalyst to selectively activate the two different enals **48** in each of the two sequential iminium ion steps of the cascade. This target was also not achievable using organocatalysis (Scheme 3.13),[44] since there was no possibility for the chiral diphenylprolinol

catalyst to differentiate and specifically regulate the different steps of the cascade sequence. A sequential biocascade process involving the combination of two enzymes in sequence might provide a solution. Specifically, we aimed to identify an enzyme able to stop after the first step of the biocascade, which was the Michael addition of nitromethane **43** to an enal **48**. After completion of the first step, a different enal **48'** would be added, together with the variant Pp-4OT-F₃, allowing for reaction of intermediate **55** towards the formation of non-symmetric cascade products **56** (Figure 3.5). This idea was based on our observation that DERA-MA could effectively promote the step of the iminium-ion-mediated Michael addition of nitromethane **43** to cinnamaldehyde **40** to afford intermediate (R)-**45**, without being able to form the cascade product **44** (see entry 10 in Table 3.1). This sequential enzymatic cascade was successfully implemented by combining the action of DERA-MA and Pp-4OT-F₃ (Figure 3.5). Once nitromethane **43** and cinnamaldehyde **40** were incubated for 5 hours with 4 mol% of DERA-MA and intermediate **45** was selectively generated, the sequential addition of Pp-4OT-F₃ and a different enal **48'** led to the target non-symmetric cascade products **56**. This process could be applied to different substituted cinnamaldehydes **48'**. We obtained products **56a-c** bearing three contiguous stereocenters in good yields (45 to 74%), with excellent diastereoselectivity (13:1 to >20:1 dr) and always in near perfect enantioselectivity (>99% ee).
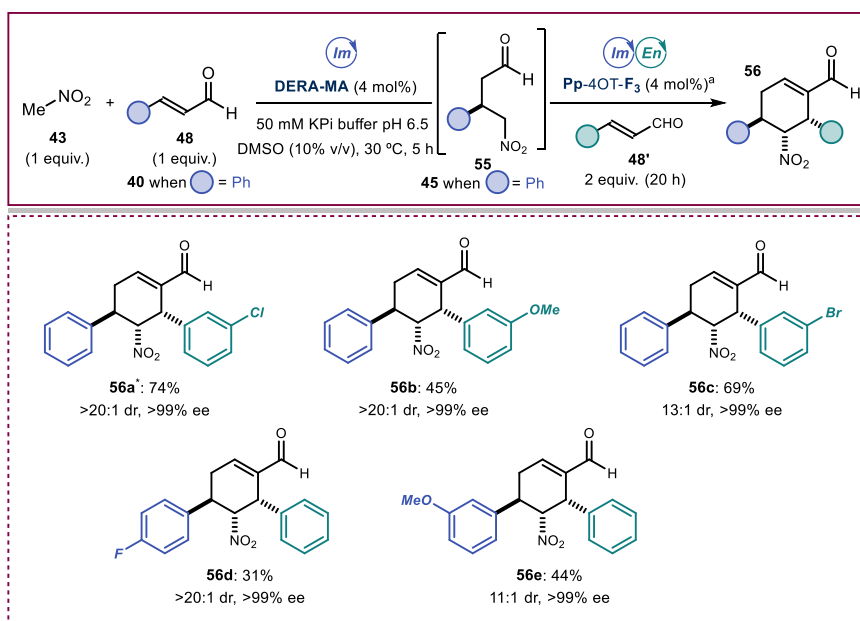

Figure 3.5. Scope of the sequential one-pot two-enzyme cascade for the synthesis of non-symmetric products **56**. ᵃReactions performed on a 2.5 μmol scale of **43** (5 mM) at 30 °C in two steps; first step performed in the presence of DERA-MA (4 mol%), enal **48** (5 mM) and **43** (5 mM) for 5 h; second step performed by adding in situ 2 equivalents of a different enal **48'** (10 mM)

together with Pp-4OT-F$_3$ (4 mol%) and run for additional 20 h. Analytical yields of **56**
determined as an average of two runs by HPLC analysis (calibration using 1,3,5-
trimethoxybenzene as internal standard); dr and ee of **56** measured by HPLC analysis.
*Reactions run with DMF as co-solvent.

When substituted cinnamaldehydes **48a** and **48b** were used in the first step and
cinnamaldehyde **40** in the second step of the sequential cascade, we obtained products **56d**
and **56e** in moderate yields and good to excellent diastereocontrol (Figure 3.5). The analytical
yields of products **56** were calculated after performing instrumental calibrations using
authentic product samples prepared according to the procedures reported in the *Experimental
Section*. Racemic samples of products **56** were obtained by a two-step organocatalytic
procedure employing racemic mixtures of a diphenylprolinol organocatalyst, which required
isolation and purification of **55**. Semi-preparative scale enzymatic synthesis of products **56**
was performed using Pp-4OT-F$_3$ as the only catalyst starting from the enal **48** and enantiopure
intermediate **55** in a 3:1 ratio, as described in the *Experimental Section*.

### 3.6.7 Studies for the development of the Enders triple cascade

After we disclosed the potential of 4-OTs as multifunctional catalysts in biocascade reactions
and successfully employed them to develop the enzymatic two-component cascade process,
we next focused on our real target: the development of a biocatalytic version of the Enders
triple cascade[43] reported in 2006 (Scheme 3.20).
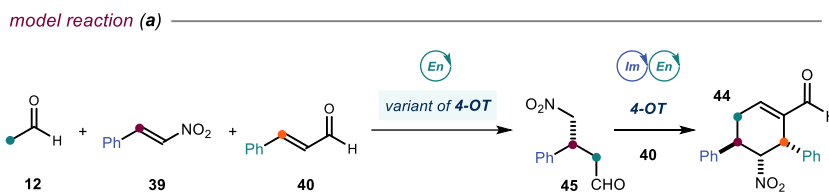
Scheme 3.20. Model reaction: enzymatic version of the triple cascade reported by Enders in 2006.

We reasoned that the Pp-4OT-F$_3$ enzyme, which successfully catalyzed the two-component
biocascade, could also promote the Enders triple cascade process by promoting the reaction
between acetaldehyde **12**, nitrostyrene **39**, and cinnamaldehyde **40**. This process would start
with the enamine activation of acetaldehyde **12**, followed by Michael addition of the enamine
intermediate to nitrostyrene **39**. Our hypothesis was motivated by previous studies showing
that 4-OT-based enzymes could promote the enamine-catalyzed Michael addition of
acetaldehyde **12** to nitrostyrene **39**.[57] The intermediate **45** thus generated is the same
intermediate arising from the first step of the two-component reaction discussed above.
Therefore, we expected that Pp-4OT-F$_3$ would further accept intermediate **45** and enable the
same iminium ion-enamine sequence as in the two-component process, thus leading to
cascade product **44** starting from different substrates. All the available 4-OT variants were

first tested in the model reaction illustrated in Scheme 3.20 between acetaldehyde **12**, β-nitrostyrene **39** and cinnamaldehyde **40**. The enzymes (4 mol%) were incubated with **39** (1.25 µmol, 2.5 mM), **12** (4-10 equiv.) and **40** (3-4 equiv.) in 50 mM KPi buffer (pH 6.5, 10% DMSO, 30 ºC for 24 hours to 3 days, Scheme 3.21). However, in all cases no cascade product **44** was detected.
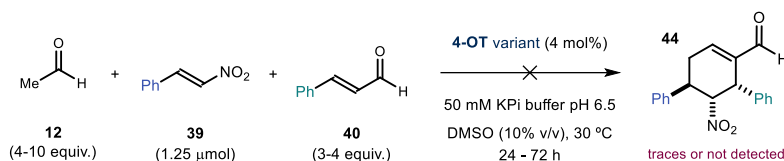
Scheme 3.21. Attempts for the enzymatic Enders triple cascade.

We then focused on Pp-4OT-F$_3$, which was the best performing multifunctional enzyme in the two-component process. We confirmed the ability of this enzyme to drive the enamine-mediated addition of acetaldehyde **12** to nitrostyrene **39**. When **12** (10 equiv.) was incubated with **39** (2.5 mM) and Pp-4OT-F$_3$ (4 mol%), the Michael product (*S*)-**45** was obtained in 37% yield and 81% ee (Scheme 3.22a). However, Pp-4OT-F$_3$ proved unsuccessful to promote the triple cascade reaction, although product **45** is the same intermediate generated in the first step of the two-component cascade. Looking for a possible explanation for this lack of reactivity, we realized that Pp-4OT-F$_3$ catalyzed the addition of acetaldehyde **12** to nitrostyrene **39** affording intermediate **45** with an (*S*) absolute configuration (Scheme 3.22a), whereas the same enzyme catalyzed the addition of nitromethane **43** to cinnamaldehyde **40** leading to the opposite enantiomer (*R*) of the same intermediate **45** (Scheme 3.22b). We questioned whether the absolute configuration of intermediate **45** was crucial for the cascade process to proceed. In fact, this intermediate should be accepted in the active site of the enzyme and further react with iminium ion-activated cinnamaldehyde **40** in the second step of the triple cascade. Enzymes generally display an exceptional selectivity for the activation of chiral substrates and, therefore, we hypothesized that an extreme case of matched-mismatched effect could be responsible for the inability of Pp-4OT-F$_3$ to drive the triple cascade, in which intermediate (*S*)-**45** rather than (*R*)-**45** is generated in the first step of the process. To test this possibility, we prepared authentic samples of enantiopure (*S*) and (*R*) products **45**, which were then subjected to the second part of the cascade in the presence of cinnamaldehyde **40**. Indeed, when intermediate (*S*)-**45** prepared in 97% ee (1.5 equiv.) was incubated with cinnamaldehyde **40** (5 mM) and Pp-4OT-F$_3$ (4 mol%), only traces of the cascade product **44** were obtained (Scheme 3.22c). In contrast, an authentic sample of (*R*)-**45** prepared in 99% ee provided the cascade product **44** in 62% yield and complete diastereo- and enantioselectivity (Scheme 3.22d), in accordance with the result in Table 3.2. Control experiments without enzyme

confirmed the necessity of the catalyst to drive both the first and the second step of the cascade process.
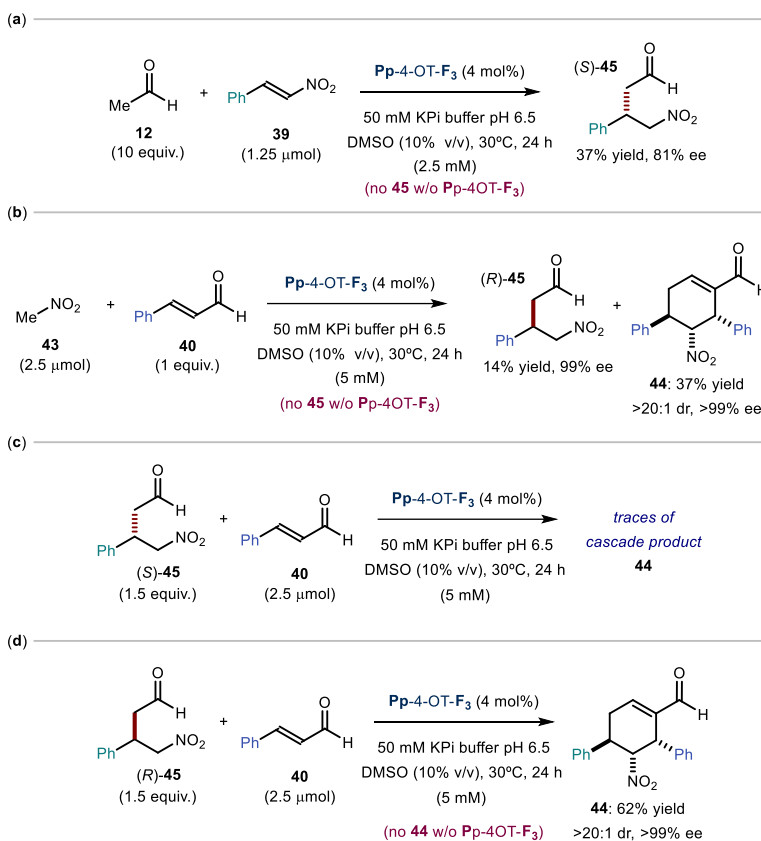

Scheme 3.22. Mechanistic experiments for the development of the enzymatic triple cascade.

These results indicated that Pp-4OT-F$_3$ could readily accommodate in the active site only (R)-**45** in a productive position for the Michael addition to iminium ion-activated cinnamaldehyde **40**, whereas the (S) enantiomer would not be accommodated productively. Similar matched/mismatched scenarios, in which a single bifunctional catalyst governs a highly enantioselective first step in a cascade process but is mismatched for the second step, have been described in organocatalytic multicomponent reactions.[72]

[72] (a) Varga, S., Jakab, G., Drahos, L., Holczbauer, T., Czugler, M., Soós, T. "Double Diastereocontrol in Bifunctional Thiourea Or-ganocatalysis: Iterative Michael-Michael-Henry Sequence Regu-lated by the Configuration of Chiral Catalysts" *Org. Lett.* **2011**, *13*, 5416-5419; (b) Varga, S., Jakab, G., Csámpai, A., Soós, T. "Iterative Coupling of Two Different Enones by Nitromethane Using Bi-functional Thiourea Organocatalysts. Stereocontrolled Assembly of Cyclic and Acyclic Structures" *J. Org. Chem.* **2015**, *80*, 8990-8996.

To understand the preference of Pp-4OT-F$_3$ towards (R)-**45**, docking studies were performed using the software YASARA Structure. Both enantiomers of intermediate **45** were modelled into the active site of Pp-4OT-F$_3$. We considered the interactions between **45** and the iminium ion intermediate from cinnamaldehyde **40** bound to proline 1. We found two possible binding poses for both (R)-**45** and (S)-**45** (Figure 3.6). For a productive binding pose, the optimal distance between the reacting γ-carbon of **45** and the β-carbon of the iminium ion should be around 3.6 Å (the sum of the van der Waals radii).[73] For (S)-**45**, all the binding poses found showed an interatomic distance greater than 6 Å, indicating a non-productive interaction of this enantiomer (Figure 3.6b shows one of the energetically more favored binding poses of (S)-**45**). In contrast, the energetically more favored binding pose of (R)-**45** showed a distance of 3.4 Å, suitable for a productive reaction (Figure 3.6a). Intermediate **45** was stabilized in the active site of Pp-4OT-F$_3$ by the residue R46 (arginine 46, corresponding to the arginine 39 in the wild-type 4-OT, see *Section 3.5.1* for discussion on the importance of this residue) through non-covalent interactions between the positively charged amino acid and the negatively charged oxygen atoms of the nitro group.
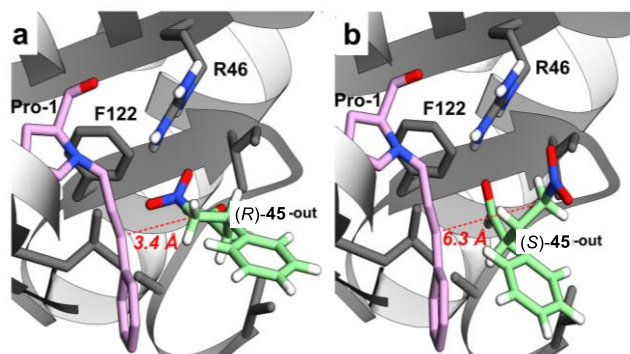

Figure 3.6. (a) Docking of (R)-**45** in the active site of Pp-4OT-F$_3$, binding energy: 4.00 Kcal mol^{-1}; (b) docking of (S)-**45** in the active site of Pp-4OT-F$_3$, binding energy: 4.31 kcal mol^{-1}. The iminium ion is shown in purple while intermediate **45** is in green. The dashed red line shows the distance between the two reactive carbons for C-C bond formation. All docking simulations were performed with YASARA Structure. UCSF Chimera software was used for visualization.

Once understood the reason for the lack of reactivity of (S)-**45**, we thought to identify a variant of 4-OT that could promote the addition of acetaldehyde **12** to β-nitrostyrene **39** delivering the right (R) enantiomer of **45** to react further in the cascade process.[72] Previous studies have shown that mutations M45Y and F50A in wild-type 4-OT allowed the preparation of (R)-**45** starting from acetaldehyde **12** and β-nitrostyrene **39**.[61] We hypothesized that the introduction of these mutations in our fused F$_3$ variant may reverse the configuration of intermediate **45** in

[73] Rowland, R. S., Taylor, R. "Intermolecular Nonbonded Contact Distances in Organic Crystal Structures: Comparison with Distances Expected from van Der Waals Radii" *J. Phys. Chem.* **1996**, *100*, 7384-7391.

the first step of the cascade process. Since positions 45 and 50 in wild-type 4-OT are located between the end of β-2 and the final β hairpin, they are far away from the active proline 1 that belongs to the same amino acid sequence. However, they are close to the proline 1 of the pairing monomer. As a consequence, installation of these mutations on the second half of the fused F$_3$ variant was carried out, and as such, the mutations M45Y and F50A became M117Y and F122A (sequence reported in the *Experimental Section*). The resulting variant Pp-4OT-F$_3$$^{M117Y/F122A}$ was successfully expressed and purified using the same experimental procedure adapted for Pp-4OT-F$_3$. When we incubated Pp-4OT-F$_3$$^{M117Y/F122A}$ (4 mol%) with acetaldehyde **12** (10 equiv.) and β-nitrostyrene **39** (1.25 µmol, 2.5 mM) in 50 mM KPi buffer (pH 6.5, 10% DMSO, 30 °C for 24 hours), product (*R*)-**45** was observed in 10% yield and 85% ee (Scheme 3.23a).
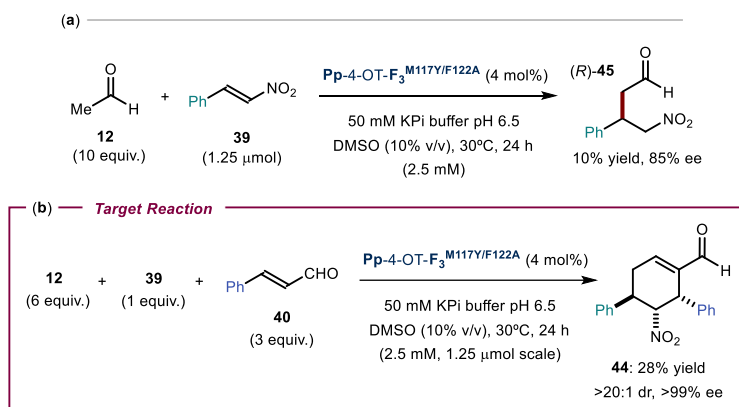
Scheme 3.23. (a) Michael addition between **12** and **39** driven by the M117Y/F122A variant of the fused 4-OT. (b) Successful implementation of the target reaction: triple cascade enabled by the M117Y/F122A variant of the fused 4-OT.

Gratifyingly, when the new variant (4 mol%) was incubated with acetaldehyde **12** (6 equiv.), β-nitrostyrene **39** (1.25 µmol, 2.5 mM) and cinnamaldehyde **40** (3 equiv.), the new enzyme effectively promoted the triple cascade, leading to product **44** in 28% yield and with complete stereocontrol (Scheme 3.23b). Increasing the equivalents of acetaldehyde **12** to 10 proved detrimental for the reaction outcome, leading to product **44** in less than 10% yield. These findings indicated that the new variant Pp-4OT-F$_3$$^{M117Y/F122A}$ produced the right (*R*) enantiomer of intermediate **45** and could promote the triple cascade reaction by accepting this enantiomer and catalyzing the Michael addition of (*R*)-**45** to cinnamaldehyde **40** as postulated.

3.6.8 Scope of the three-component cascade

Once we assessed the capability of the new variant Pp-4OT-F$_3$$^{M117Y/F122A}$ to promote the Enders triple cascade, we investigated the compatibility of different substrates **46**, **47** and **48**

in the three-component protocol (results in Figure 3.7). Using butanal **38** (4 equiv.) as the aldehyde with β-nitrostyrene **39** and cinnamaldehyde **40**, the cascade product **41** was obtained in 50% yield, 3.7:1 dr and >99% ee. In this case, the major stereoisomer of the enzymatic reaction had the same relative configuration of the major diastereomer obtained in the organocatalytic Enders protocol with comparable selectivity (4:1 dr).[43] An increased enzyme loading of 6 mol % resulted in 64% yield of **41**. The enzyme also accepted substituted β-nitrostyrene derivatives **47** and cinnamaldehydes **48**, affording the corresponding products **49a** and **49b** in moderate yields and diastereoselectivity (Figure 3.7). Furthermore, the reaction could also be scaled up to a 150 µmol scale (30 mL reaction volume) using the *E. coli* cell-free-extracts containing approximately 2.5 mg mL^{-1} of Pp-4OT-F$_3$[M117Y/F122A], delivering product **49b** in 23% yield after column chromatography. Our method for the enzymatic synthesis of product **41** matched the organocatalytic protocol in efficiency and stereoselectivity.[43]
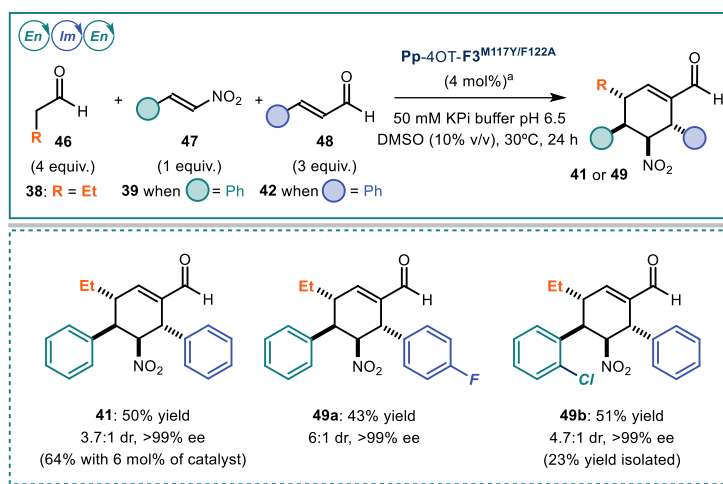
Figure 3.7. Scope of the three-component enzymatic cascade. [a]Reactions performed on a 1.25 µmol scale of nitrostyrene **47** (2.5 mM) for 24 hours at 30°C. Analytical yields of products **41** or **49** are given as an average of two runs and determined by HPLC analysis (calibration using 1,3,5-trimethoxybenzene as the internal standard). The dr and ee of **41** or **49** were measured via chiral HPLC or UPC² analysis. The yield in parenthesis refers to the isolated product for the reaction on a 150 µmol scale.

Finally, longer-chain alkyl aldehydes **46** resulted in very low yields, whereas alkyl substituted Michael acceptors were not tolerated, in analogy with the organocatalytic protocol reported by Enders. A survey of low yielding or unsuccessful substrates is provided in Figure 3.8.
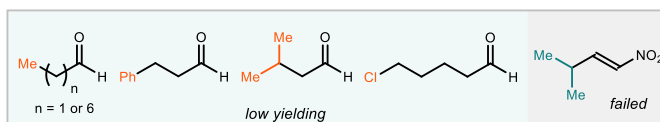
Figure 3.8. Survey of unsuccessful substrates in the triple biocascade.

3.6.9 Deuterium labelling experiment

The control experiments in the absence of catalyst described in Table 3.1 and Scheme 3.22 proved the necessity of the enzyme to catalyze both the first step (iminium ion in the two-component or enamine in the triple cascade) and the second step (iminium ion in both methods) of the cascade processes. However, the pre-aldol condensation intermediate **XV** (Scheme 3.25) could not be isolated, and therefore subjection of this intermediate to an enzyme-free environment was not possible. To probe the role of Pp-4OT-F$_3$ in the aldol step of both cascade reactions, a deuterium labelling experiment was conducted by incubation of β-deuterated cinnamaldehyde **40** (5 mM) and (R)-**45** (1.1 equiv.) with *E. coli* cell-free-extracts (CFE) containing ~2.5 mg mL^{-1} of the enzyme on a 158 µmol scale (Scheme 3.24). Product **d-44** was isolated in 34% yield with complete incorporation of the deuterium atom at carbon 6.
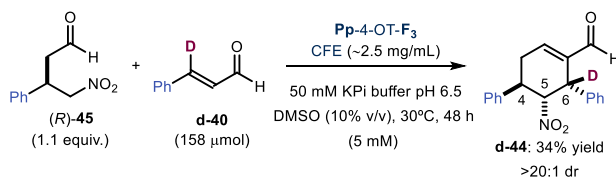
Scheme 3.24. Deuterium labelling experiment on a semi-preparative scale. CFE = cell-free extracts.

If the pre-aldol enamine intermediate **XIV** (Scheme 3.25a) generated upon Michael addition of (R)-**45** to **d-40** underwent hydrolysis to intermediate **XV** and subsequent spontaneous aldol cyclization took place outside the active site, the resulting product **d-44** would contain the deuterium label at both C(4) and C(6), since either aldehyde may undergo aldol addition via *path i* or *path ii* (Scheme 3.25b). Since the deuterium incorporation in product **44** occurred completely on C(6), the aldol cyclization likely took place inside the active site of the catalyst and was driven by the enzyme-bound enamine **XIV**.
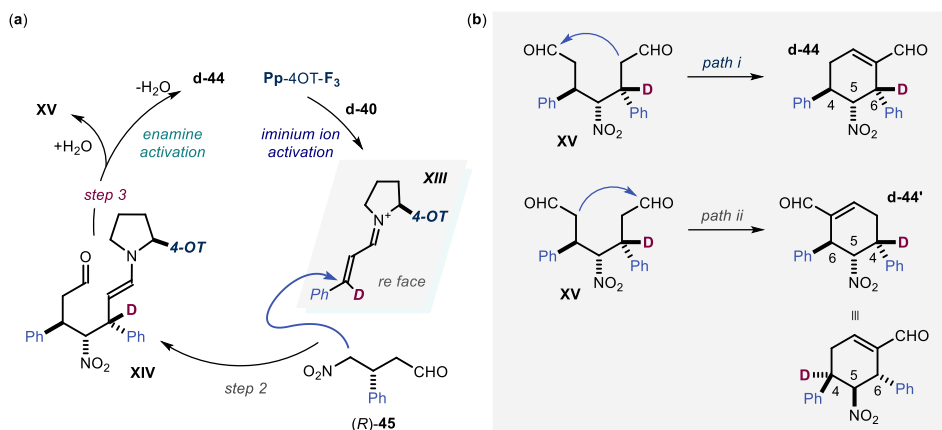
Scheme 3.25. (a) Mechanism of the reaction between intermediate (*R*)-**45** and deuterated cinnamaldehyde **d-40**; (b) possible mechanisms for the spontaneous aldol cyclization of intermediate **XV**.

3.7 Conclusions

In conclusion, we have developed rare examples of asymmetric multicomponent biocascade processes promoted by a single multifunctional enzyme capable of catalyzing each step of the sequence in one-pot and one step. Asymmetric multicomponent cascade reactions promoted by a single multifunctional catalyst are common strategies in organocatalysis for the synthesis of highly enantioenriched molecules. The most sophisticated example of an organocascade process is the Enders triple cascade reported in 2006, which exploits the combination of enamine and iminium ion activation of carbonyl substrates. We targeted this reaction by identifying a suitable class of enzymes, 4-OTs, that are capable of performing both enamine and iminium ion activations. We designed genetically modified multifunctional variants of 4-OT enzymes to catalyze the triple cascade reported by Enders in 2006, as well as a mechanistically similar but synthetically more simple two-component cascade reaction reported by Enders in 2009. We found that, in some cases, the biocatalytic strategy could complement and even outperform the organocatalytic methods in efficiency and stereoselectivity. Mechanistic experiments allowed us to overcome the initial poor reactivity in the enzymatic triple cascade and to identify mutations that were crucial for the development of this biocascade process. We also targeted the synthesis of synthetically more challenging products **56** bearing different substituents on carbon C(4) and C(6), that were unattainable with the organocatalytic procedure. We also designed a mechanistically different double-enzyme tandem process to access this class of compounds, showing the higher versatility of the enzymatic cascade strategy compared to the organocatalytic approach.

3.8 Experimental Section

3.8.1 General Information

The NMR spectra are available in the published manuscript[1] and are not reported in the present dissertation.

The NMR spectra were recorded at 300 MHz, 400 MHz, and 500 MHz for ^{1}H, at 75 MHz, 101 MHz and 125 MHz for ^{13}C, at 376 MHz for ^{19}F and at 162 and 202 MHz for ^{31}P. The chemical shifts (δ) for ^{1}H and ^{13}C are given in ppm relative to residual signals of the solvents (CHCl$_3$ @ 7.26 ppm ^{1}H NMR, 77.16 ppm ^{13}C NMR; DMSO @ 2.54 ppm ^{1}H NMR, 40.45 ppm ^{13}C NMR). Coupling constants (J) are given in Hz, and are quoted to the nearest 0.5 Hz. The following abbreviations are used to indicate the multiplicity: s, singlet; d, doublet; t, triplet; q, quartet; sext, sextet; hept, heptuplet; m, multiplet. Additionally, signals can be described as broad (br) and apparent (app).

High-resolution mass spectra (HRMS) were obtained from the ICIQ High Resolution Mass Spectrometry Unit on MicroTOF Focus and Maxis Impact (Bruker Daltonics) with electrospray ionization. Optical rotations were measured on a Polarimeter Jasco P-1030 and are reported as follows: $[\alpha]_D^T$ (c in g per 100 mL, solvent).

Cell growing and enzyme expression were performed in a standard INFORS-HT multitron incubator with an orbital of 50 mm. Cells lysis was performed with a Thermo Fisher ultrasonicator 120 W. Centrifugation was performed with a Thermo Fisher SORVALL ST16R centrifuge equipped with different rotors. When applicable, enzyme concentration was determined using a Nanodrop^{TM} One from Thermo Fisher Scientific. The optical density (OD) was measured in a Cell Density Meter Model 40 from Thermo Fisher. LB broth was sterilized with a 75 L Autoclave Sterilmatic (AE-75-DRY) from Thermo Fisher. Biocatalytic transformations on the analytical scale were performed in a 1.5 mL Thermoshaker from Thermo Scientific equipped with a temperature control. Mini-PROTEAN^{TM} SDS-Acrylamide Electrophoresis equipment was purchased from BIO-RAD.

General Procedures. Biochemical reactions were set up in standard 2 mL Eppendorf tubes under air. Synthesis and HPLC grade solvents were used as purchased. Anhydrous solvents were taken from a commercial SPS solvent dispenser. Chromatographic purification of products was accomplished using force-flow chromatography (FC) on silica gel (230-400 mesh). For thin layer chromatography (TLC) analyses throughout this work, Merck precoated TLC plates (silica gel 60 GF$_{254}$, 0.25 mm) were employed. UV light was used as the visualizing agent, and either an ethanol solution of phosphomolybdic acid or basic aqueous potassium permanganate (KMnO$_4$), and heat served as developing agents. Organic solutions were concentrated under reduced pressure on a Büchi rotary evaporator (in vacuo at 40 ℃, ~5 mbar).

Determination of Enantiomeric Purity. HPLC analyses on chiral stationary phase were performed on an Agilent 1200 series HPLC, using Daicel Chiralpak IB-3 and IC-3 column. UPC^2 analyses on chiral stationary phases were performed on a Waters ACQUITY® UPC^2 instrument, using Daicel Chiralpak IC-3 chiral column. For each compound, the exact conditions for the analysis are specified within the characterization section. HPLC/UPC^2 traces were compared to the mixtures of the two enantiomers prepared by running the reactions under the conditions specified in the reference compounds synthesis.

Materials. HisTrap^{TM} HP chromatography columns for enzyme purification were purchased from Cytiva. HiTrap^{TM} DEAE FF columns for ion exchange chromatography were purchased from GE Healthcare. PD-10 columns containing Sephadex^{TM} G-25 M for buffer exchange were purchased from Cytiva. LB Broth powder was purchased from Nzytech. Customized genes encoding for the enzymes used in this study were purchased from GenScript. BL21(DE3) competent cells were purchased from New England BioLabs$_{Inc}$. Coomassie R250 powder was purchased from BIO-RAD. Protein ladders and standard markers were purchased from BIO-RAD. Commercial grade reagents and solvents were purchased at the highest commercial quality from Sigma Aldrich or Alfa Aesar and used as received, unless otherwise stated. Cinnamaldehyde was purchased from Sigma Aldrich, distilled prior to use and stored in a closed vial under argon at -20 ℃. Butanal was purchased from Sigma Aldrich, distilled prior to use and stored at -20℃.

3.8.2 Enzyme Preparation

For heterologous expression of all enzymes, *E. coli* BL21(DE3) (New England BioLabs, NEB) was used as host organism. All enzymes except of DERA-MA were cloned in pET20b vector between NdeI and XhoI. DERA-MA was cloned in pET26b vector with a C-terminus His-Tag and without the pelB signal peptide. Transformations were performed at 42 ˚C for 10 seconds according to the standard protocol (NEB). For expression of all enzymes except of DERA-MA the following protocol was used: 400 mL of LB medium, supplemented with ampicillin (100 μg mL^{-1}) were inoculated with 7 mL of pre-culture. The cells were allowed to grow at 37 °C until an OD$_{600}$ of 0.7-1 was reached. Expression of the enzymes were performed by inducing the main cultures with 1 mM of isopropyl β-D-1-thiogalactopyranoside (IPTG) and cultures were grown overnight at 37 °C with shaking at 170 rpm. The next day, the cells were harvested by centrifugation (4.700 g, 20 min, 4 °C), resuspended in 10 mM NaH$_2$PO$_4$ pH 8 and lysed by ultrasonication. For DERA-MA, 400 mL of LB medium, supplemented with kanamycin (50 μg mL^{-1}) were inoculated with 7 mL of pre-culture and cells were grown at 37 °C until the OD$_{600}$ was between 0.7-1. Expression of the enzyme was performed by the addition of 0.1 mM IPTG and cultures were grown overnight at 25 °C with shaking at 170 rpm. The cells were harvested by centrifugation (4.700 g, 20 min, 4 °C), resuspended in lysis buffer (50 mM KH$_2$PO$_4$, 300 mM NaCl, 10 mM imidazole, pH 8.0) and lysed by

ultrasonication. For protein purification of Pp-4OT, Ps-4OT, Ml-4OT and Tb-4OT the lysate was centrifuged (18.000 rpm, 50 min, 4 °C) and filtered through a 0.45 μm filter. After that, 1.5 M of $(NH_4)_2SO_4$ was added into the supernatant which was stirred for 6 h. Protein solution was centrifuged (12.000 g, 20 min, 4 °C) and the supernatant was dialyzed overnight against the 10 mM NaH_2PO_4 pH 8. Dialyzed sample was loaded into a column containing DEAE sepharose (GE Healthcare) for an anion exchange chromatography when Pp-4OT, Ps-4OT and Ml-4OT enzymes were purified. For Tb-4OT the dialyzed sample was loaded into a HiTrap^{TM} CM FF column (Cytiva) for cation exchange. The column was pre-equilibrated with 10 column volumes (CV) of 10 mM NaH_2PO_4 pH before loading of the protein. After the loading of the enzymatic solutions, the column was washed with 3 CV using the loading buffer and the elution was performed with the same buffer supplemented with 90 mM Na_2SO_4. Elution fractions were collected and analyzed by SDS-PAGE. Fractions containing the enzyme were combined and concentrated using centricon with 6-8 kDa cutoff. Buffer exchange was performed with PD-10 desalting columns (cytiva). The protein concentration was determined using Biuret assay. For His-Tagged Pp-4OT-F_{2-4} and DERA-MA, protein purification was performed by Ni-NTA affinity chromatography using pre-packed Ni-NTA HisTrap FF columns (GE Healthcare) according to the manufacturer's instructions. First the cell pellet was resuspended in lysis buffer (50 mM KH_2PO_4, 300 mM NaCl, 10 mM imidazole, pH 8.0). After sonication the enzyme solution was filtrated with a 0.45 μm filter and loaded into the column which has been previously equilibrated with lysis buffer. After loading of the filtered lysate, the column was washed with sufficient amounts of washing buffer (50 mM KH_2PO_4, 300 mM NaCl, 25 mM imidazole, pH 8.0), and bound protein was recovered with elution buffer (50 mM KH_2PO_4, 300 mM NaCl, 300 mM imidazole, pH 8.0). The process of purification was monitored with SDS-PAGE and fractions containing pure protein were pooled and dialyzed overnight against potassium phosphate buffer (50 mM, pH 6.5). Protein solutions were concentrated, and the concentration was determined either spectrophotometrically using the extinction coefficient at 280 nm or the Biuret assay. Typically, a protein yield of 50 mg per gram of cell culture was obtained. All amino acid sequences of the enzymes are shown in Table 3.6. The purity of the enzymes was verified by SDS-PAGE (Figure 3.9).

Table 3.6. The amino acid sequences of the enzymes used in this study.

Enzyme	Amino acid sequence
Pp-4OT	PIAQIHILEGRSDEQKETLIREVSEAISRSLDAPLTSVRVIITEMAKGHFGIG GELASKVRR
Ml-4OT	PIAQINIMEGRSDEQKEALIVEVTAAISRALDAPEQNIRVLIQELPRQNWGIA GQSAKKLGR
Ps-4OT	PIAHVQIMEGRSDEQKEAMIREVSEALARTLDSPLDRVRVLITEVPKSHWGIA GEPASKVR
Tb-4OT	PFAQISILEGRSDEKKAELIREVTEAIHRSLGAPREAIRVALYEVKKTEWGIG GETAKKLGR
Pp-4OT-F$_1$	PIAQIHILEGRSDEQKETLIREVSEAISRSLDAPLTSVRVIITEMAKGHFGIG GELASK**GAGGSL**PIAQIHILEGRSDEQKETLIREVSEAISRSLDAPLTSVRVI ITEMAKGHFGIGGELASKVRR
Pp-4OT-F$_2$	PIAQIHILEGRSDEQKETLIREVSEAISRSLDAPLTSVRVIITEMAKGHFGIG GEL**HHHHHH**GSLPIAQIHILEGRSDEQKETLIREVSEAISRSLDAPLTSVRVI ITEMAKGHFGIGGELASKVRR
Pp-4OT-F$_3$	PIAQIHILEGA**HHHHHH**GSDEQKETLIREVSEAISRSLDAPLTSVRVIITEMA KGHFGIGGELASK**GAGGSL**PIAQIHILEGRSDEQKETLIREVSEAISRSLDAP LTSVRVIITEMAKGHFGIGGELASKVRR
Pp-4OT-F$_4$	PIAQIHILEGRSDEQKETLIREVSEAISRSLDAPLTSVRVIITEMAKGHFGIG GELASK**GAGGSL**PIAQIHILEGRSDEQKETLIREVSEAISRSLDAPLTSVRVI ITEMAKGHFGIGGELASKVRRLG**HHHHHH**
Pp-4OT-F$_3$$^{M117Y/F122A}$	PIAQIHILEGAHHHHHHGSDEQKETLIREVSEAISRSLDAPLTSVRVIITEMA KGHFGIGGELASKGAGGSLPIAQIHILEGRSDEQKETLIREVSEAISRSLDAP LTSVRVIITE**Y**AKGH**A**GIGGELASKVRR
DERA-MA	MTDLKASSLRALKLMDLSTLNGDYTDEKVIALCHQAKTPVGNTAAISIYPRSI PIARKTLKEQGTPEIRIATVTNFPHGNDDIDIALAETRAAIAYGADEVDVVFP YRALMAGNEQVGFDLVKACKEACAAANVLLKVIIESGELKDEALIRKASEISI KAGADFIKTSTGLVAVNATPESARIMMEVIRDMGVEKSVGFKVTGGARTAEDA QKYLAIADELFGADWADARHYRFGASGLLASLLKALGHGDGKSASSYLEHHHH HH

Genetic alterations of Pp-4OT variants with respect to the wild type enzyme are shown in bold. Ml-4OT is from *Marinobacter lipolyticus* SM19 (NCBI:[74] txid1318628), Tb-4OT is from *Thiolapillus brandeum* (NCBI: txid1076588) Ps-4OT is from *Pseudomonas sagittaria* (NCBI: txid1135990).

[74] Schoch, C. L., Ciufo, S., Domrachev, M., Hotton, C. L., Kannan, S., Khovanskaya, R., Leipe, D., McVeigh, R., O'Neill, K., Robbertse, B., Sharma, S., Soussov, V., Sullivan, J. P., Sun, L., Turner, S., Karsch-Mizrachi, I. "NCBI Taxonomy: A Comprehensive Update on Curation, Resources and Tools" Database 2020, 2020.
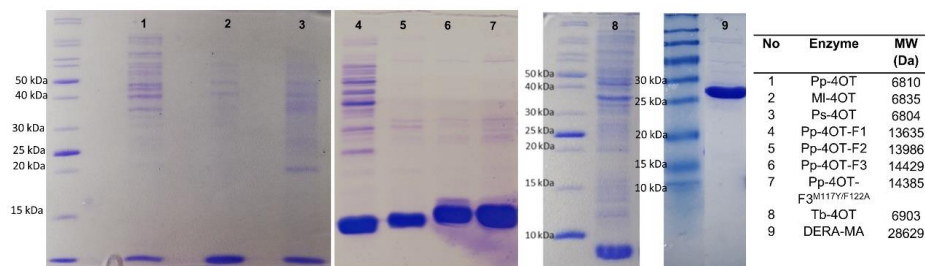
Figure 3.9. Purity of enzymes used in this study.

3.8.3 Substrate Synthesis

GP1 – General Procedure for the Synthesis of Enals 48
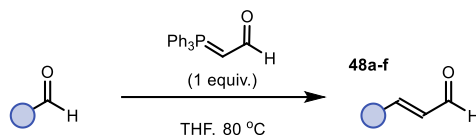
The general procedure for the synthesis of the enals **48** was adapted from a reported procedure.[75] A suspension of (triphenylphosphoranylidene)acetaldehyde (1 equiv.) and the corresponding aldehyde (1 equiv.) in anhydrous THF (0.35 M) was refluxed overnight at 80 ºC until complete conversion of the aldehyde was inferred by TLC analysis. The resulting mixture was cooled down to ambient temperature and dried under reduced pressure. Purification of the crude material by flash column chromatography on silica gel provided the enal products **48a-f** and **d-40**.

(*E*) 3-(4-fluorophenyl)acrylaldehyde (48a)
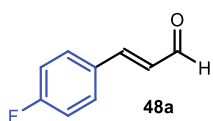
Prepared according to *GP1*, using 4-fluorobenzaldehyde (760 µL, 7.10 mmol) and (triphenylphosphoranylidene)acetaldehyde (2.2 g, 7.70 mmol) in THF (20 mL). The crude mixture was purified by flash column chromatography (isocratic 10% EtOAc in hexane) to afford product **48a** (456 mg, 43% yield) as a yellow liquid. The product was stored at -20 ºC under an argon atmosphere. The characterization of the title compound was consistent with the data available in the literature.[76]

---

[75] Zu, L., Zhang, S., Xie, H., Wang, W. "Catalytic Asymmetric oxa-Michael-Michael Cascade for Facile Construction of Chiral Chromans via an Aminal Intermediate" *Org. Lett.* **2009**, *11*, 1627-1630.

[76] Huang, H., Yu, C., Li, X., Zhang, Y., Zhang, Y., Chen, X., Mariano, P. S., Xie, H., Wang, W. "Synthesis of Aldehydes by Organocatalytic Formylation Reactions of Boronic Acids with Glyoxylic Acid" *Angew. Chem. Int. Ed.* **2017**, *56*, 8201-8205.

^{1}H NMR (500 MHz, CDCl$_3$): δ 9.69 (d, J = 7.7 Hz, 1H), 7.61 – 7.53 (m, 2H), 7.45 (d, J = 16.0 Hz, 1H), 7.17 – 7.09 (m, 2H), 6.65 (dd, J = 16.0, 7.6 Hz, 1H).

^{19}F NMR (471 MHz, CDCl$_3$): δ -107.7.

^{13}C NMR (126 MHz, CDCl$_3$): δ 193.6, 164.6 (d, $J_{C\text{-}F}$ = 253.2 Hz), 151.4, 130.6 (d, $J_{C\text{-}F}$ = 8.7 Hz), 130.5 (d, $J_{C\text{-}F}$ = 3.3 Hz), 128.5 (d, $J_{C\text{-}F}$ = 2.3 Hz), 116.5 (d, $J_{C\text{-}F}$ = 22.1 Hz).

(*E*) 3-(3-methoxyphenyl)acrylaldehyde (48b)
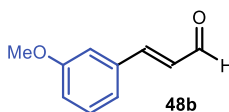
Prepared according to *GP1*, using 3-methoxybenzaldehyde (600 μL, 4.92 mmol) and (triphenylphosphoranylidene)acetaldehyde (2.25 g, 7.38 mmol, 1.5 equiv.) in THF (10 mL). The crude mixture was purified by flash column chromatography (isocratic 10% EtOAc in hexane) to afford product **48b** (310 mg, 39% yield) as a yellow oil. The product was stored at -20 ºC. The characterization of the title compound was consistent with the data available in the literature.[76]

^{1}H NMR (400 MHz, CDCl$_3$): δ 9.71 (d, J = 7.8 Hz, 1H), 7.45 (d, J = 15.9 Hz, 1H), 7.35 (t, J = 7.9 Hz, 1H), 7.16 (d, J = 7.6 Hz, 1H), 7.08 (t, J = 2.1 Hz, 1H), 7.00 (dd, J = 8.3, 2.5 Hz, 1H), 6.71 (dd, J = 15.9, 7.7 Hz, 1H), 3.85 (s, 3H).

^{13}C NMR (101 MHz, CDCl$_3$): δ 193.8, 160.2, 152.8, 135.5, 130.2, 129.0, 121.4, 117.2, 113.4, 55.5.

(*E*) 3-(2-methylphenyl)acrylaldehyde (48c)
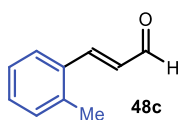
Prepared according to *GP1*, using 2-methylbenzaldehyde (810 μL, 7.00 mmol) and (triphenylphosphoranylidene)acetaldehyde (2.13 g, 7.00 mmol) in THF (20 mL). The crude mixture was purified by flash column chromatography (isocratic 5% EtOAc in hexane) to afford product **48c** (321 mg, 31% yield) as a pale yellow oil. The product was stored at -20ºC. The characterization of the title compound was consistent with the data available in the literature.[77]

^{1}H NMR (500 MHz, CDCl$_3$): δ 9.73 (d, J = 7.7 Hz, 1H), 7.78 (d, J = 15.8 Hz, 1H), 7.64 – 7.50 (m, 1H), 7.37 – 7.30 (m, 1H), 7.28 – 7.23 (m, 2H), 6.67 (dd, J = 15.8, 7.7 Hz, 1H), 2.48 (s, 3H).

^{13}C NMR (126 MHz, CDCl$_3$): δ 194.0, 150.4, 138.1, 133.0, 131.2, 131.2, 129.8, 127.0, 126.8, 19.9.

---

[77] Liu, J., Zhu, J., Jiang, H., Wang, W., Li, J. "Pd-catalyzed cascade Heck-Saegusa: direct synthesis of enals from aryl iodides and allyl alcohol" *Chem. Commun.* **2010**, *46*, 415-417.

### (*E*) 3-(3-bromophenyl)acrylaldehyde (48d)
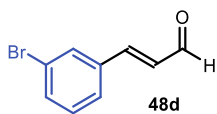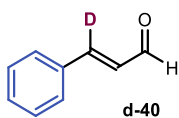
Prepared according to *GP1*, using 3-bromobenzaldehyde (900μL, 7.7 mmol) and (triphenylphosphoranylidene)acetaldehyde (2.35 g, 7.7 mmol) in THF (22 mL). The crude mixture was purified by flash column chromatography (isocratic 10% EtOAc in hexane) to afford product **48d** (894 mg, 55% yield) as a yellow solid. The product was stored at -20°C. The characterization of the title compound was consistent with the data available in the literature.[78]

¹H NMR (400 MHz, CDCl₃): δ 9.71 (d, *J* = 7.6 Hz, 1H), 7.71 (t, *J* = 1.8 Hz, 1H), 7.57 (ddd, *J* = 8.0, 2.0, 1.0 Hz, 1H), 7.52 – 7.47 (m, 1H), 7.40 (d, *J* = 16.0 Hz, 1H), 7.31 (t, *J* = 7.9 Hz, 1H), 6.70 (dd, *J* = 16.0, 7.6 Hz, 1H).

¹³C NMR (101 MHz, CDCl₃): δ 193.4, 150.8, 136.2, 134.1, 131.4, 130.8, 129.8, 127.0, 123.4.

(*E*) 3-(2-chlorophenyl)acrylaldehyde (48e)
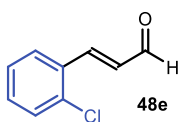
Prepared according to *GP1*, using 2-chlorobenzaldehyde (800 μL, 7.10 mmol) and (triphenylphosphoranylidene)acetaldehyde (2.16 g, 7.10 mmol) in THF (20 mL). The crude mixture was purified by flash column chromatography (isocratic 10% EtOAc in hexane) to afford product **48e** (579 mg, 49% yield) as a pale yellow solid. The product was stored at -20°C. The characterization of the title compound was consistent with the data available in the literature.[76]

¹H NMR (500 MHz, CDCl₃): δ 9.77 (d, *J* = 7.7, 1H), 7.94 (d, *J* = 16.0 Hz, 1H), 7.67 (dd, *J* = 7.7, 1.8 Hz, 1H), 7.51-7.43 (m, 1H), 7.41-7.29 (m, 2H), 6.71 (dd, *J* = 16.1, 7.7 Hz, 1H).

¹³C NMR (126 MHz, CDCl₃): δ 193.7, 148.1, 135.4, 132.2, 132.1, 130.7, 130.5, 128.0, 127.5.

(*E*) 3-(3-chlorophenyl)acrylaldehyde (48f)
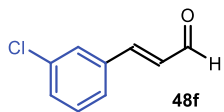
Prepared according to *GP1*, using 3-chlorobenzaldehyde (560 μL, 4.98 mmol) and (triphenylphosphoranylidene)acetaldehyde (1.52 g, 4.98 mmol) in THF (15 mL). The crude mixture was purified by flash column chromatography (isocratic 10% EtOAc in hexane) to afford product **48f** (472 mg, 56% yield) as a yellow solid. The product was stored at -20 °C. The characterization of the title compound was consistent with the data available in the literature.[76]

¹H NMR (500 MHz, CDCl₃): δ 9.72 (d, *J* = 7.6 Hz, 1H), 7.55 (t, *J* = 1.9 Hz, 1H), 7.47-7.35 (m, 4H), 6.71 (dd, *J* = 16.0, 7.5 Hz, 1H).

¹³C NMR (126 MHz, CDCl₃): δ 193.4, 150.9, 135.9, 135.3, 131.2, 130.5, 129.8, 128.4, 126.5.

[78] Zhang, X., Jiang, G., Lei, S., Shan, X., Qu, J., Kang, Y. "Iron-Catalyzed α,β-Dehydrogenation of Carbonyl Compounds" *Org. Lett.* **2021**, *23*, 1611-1615.
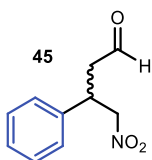
(*E*) cinnamaldehyde-3-d (d-40)

Prepared according to *GP1*, using benzaldehyde-d_1 (500 μL, 4.92 mmol) and (triphenylphosphoranylidene)acetaldehyde (2.25 g, 7.30 mmol) in THF (12 mL). The crude mixture was purified by flash column chromatography (isocratic 10% EtOAc in hexane) to afford product **d-40** (110 mg, 16% yield) as a yellow liquid. The product was stored at -20 °C. The characterization of the title compound was consistent with the data available in the literature.[79]

^{1}H NMR (300 MHz, CDCl$_3$): δ 9.72 (d, *J* = 7.8 Hz, 1H), 7.63 – 7.52 (m, 2H), 7.49 – 7.39 (m, 3H), 6.73 (dt, J_{H-H} = 7.7, J_{H-D} = 2.4 Hz, 1H).

^{13}C NMR (75 MHz, CDCl$_3$): δ 193.9, 134.1, 131.4, 129.3, 129.1, 128.7, 128.6.

GP2 – General Procedure for the Synthesis of Intermediates 45 and 55a-b
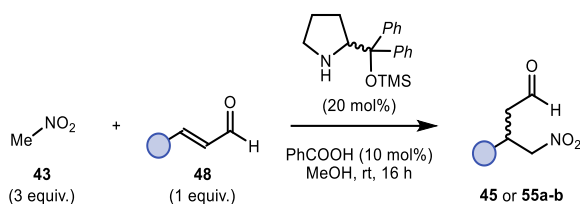
The general procedure for the synthesis of the intermediates **45** and **55** was adapted from a reported procedure.[80] To a solution of benzoic acid (20 mol%) in MeOH (0.5 M) were added an approximately 1:1 (*R*) and (*S*) mixture of the diphenylprolinol TMS ether as the organocatalyst (10 mol%), the corresponding enal **48** (1 equiv.) and nitromethane **43** (3 equiv.). After stirring the reaction at room temperature for 16 hours, the resulting mixture was quenched with saturated aqueous NaHCO$_3$ and extracted twice with ethyl acetate. The combined organic extracts were dried over anhydrous MgSO$_4$, filtered and concentrated under reduced pressure. Purification of the crude material by flash column chromatography on silica gel provided the corresponding compounds as racemic mixtures.

4-nitro-3-phenyl-butanal (45)

Prepared according to *GP2*, using cinnamaldehyde **40** (465 μL, 3.70 mmol) and nitromethane **43** (600 μL, 11.1 mmol) in MeOH (7.4 mL). The crude mixture was purified by flash column chromatography (gradient from 10 to 20% EtOAc in hexane) to afford product **45** (290 mg, 40% yield) as a

[79] Chavhan, S. W., Cook, M. J. "Silicon-Directed Rhenium-Catalyzed Allylic Carbaminations and Oxidative Fragmentations of γ-Silyl Allylic Alcohols" *Chem. Eur. J.* **2014**, *20*, 4891-4895.

[80] Gotoh, H., Ishikawa, H., Hayashi, Y. "Diphenylprolinol Silyl Ether as Catalyst of an Asymmetric, Catalytic, and Direct Michael Reaction of Nitroalkanes with α,β-Unsaturated Aldehydes" *Org.Lett.* **2007**, *9*, 5307-5309.

yellow liquid. The product was stored at -20 ºC. The characterization of the title compound was consistent with the data available in the literature.[80]

^{1}H NMR (500 MHz, CDCl$_3$): δ 9.70 (t, J = 1.1 Hz, 1H), 7.38 – 7.31 (m, 2H), 7.31 – 7.27 (m, 1H), 7.25 – 7.20 (m, 2H), 4.71 – 4.58 (m, 2H), 2.94 (ddd, J = 6.9, 3.1, 1.1 Hz, 2H).

^{13}C NMR (101 MHz, CDCl$_3$): δ 199.1, 138.3, 129.3 (2C), 128.3 (2C), 127.5, 79.5, 46.5, 38.1.

4-nitro-3-(4-fluorophenyl)-butanal (55a)
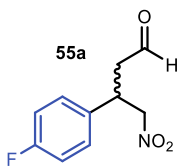
Prepared according to *GP2*, using 4-fluorocinnamaldehyde **48a** (60.1 mg, 0.40 mmol) and nitromethane **43** (65 µL, 1.20 mmol) in MeOH (800 µL). The crude mixture was purified by flash column chromatography (isocratic 30% EtOAc in hexane) to afford product **55a** (32 mg, 38% yield) as a yellow liquid. The product was stored at -20ºC. The characterization of the title compound was consistent with the data available in the literature.[81]

^{1}H NMR (400 MHz, CDCl$_3$): δ 9.70 (t, J = 1.0 Hz, 1H), 7.26 – 7.16 (m, 2H), 7.11 – 6.96 (m, 2H), 4.67 (app dd, J = 12.6, 6.9 Hz, 1H), 4.58 (app dd, J = 12.5, 7.9 Hz, 1H), 4.07 (p, J = 7.2 Hz, 1H), 2.94 (dd, J = 7.1, 1.0 Hz, 2H).

^{19}F NMR (376 MHz, CDCl$_3$): δ -113.81.

^{13}C NMR (101 MHz, CDCl$_3$): δ 198.6, 162.5 (d, J_{C-F} = 246.3 Hz), 134.1 (d, J_{C-F} = 3.4 Hz), 129.2 (d, J_{C-F} = 8.2 Hz), 116.3 (d, J_{C-F} = 21.6 Hz), 46.7, 37.4.

4-nitro-3-(3-methoxyphenyl)-butanal (55b)
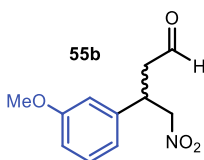
Prepared according to *GP2*, using 3-methoxycinnamaldehyde **48b** (65 mg, 0.40 mmol) and nitromethane **43** (65 µL, 1.20 mmol) in MeOH (800 µL). The crude mixture was purified by flash column chromatography (isocratic 30% EtOAc in hexane) to afford product **55b** (29 mg, 32% yield) as a yellow liquid. The product was stored at -20ºC. The characterization of the title compound was consistent with the data available in the literature.[82]

^{1}H NMR (400 MHz, CDCl$_3$): δ 9.71 (t, J = 1.1 Hz, 1H), 7.31 – 7.22 (m, 1H), 6.82 (dtd, J = 7.0, 3.5, 3.0, 1.4 Hz, 2H), 6.76 (t, J = 2.1 Hz, 1H), 4.71 – 4.56 (m, 2H), 4.04 (q, J = 7.3 Hz, 1H), 3.80 (s, 3H), 2.94 (ddd, J = 6.9, 4.1, 1.1 Hz, 2H).

[81] Chen, W., Fang, H., Xie, K., Oestreich, M. "The Cyclohexa-2,5-dienyl Group as a Placeholder for Hydrogen: Organocatalytic Michael Addition of an Acetaldehyde Surrogate" *Chem. Eur. J.* **2020**, *26*, 15126-15129.

[82] Zu, L., Xie, H., Li, H., Wang, J., Wang, W. "Highly Enantioselective Organocatalytic Conjugate Addition of Nitromethane to α,β-Unsaturated Aldehydes: Three-Step Synthesis of Optically Active Baclofen" *Adv. Synth. Catal.* **2007**, *349*, 2660-2664.

^{13}C NMR (101 MHz, CDCl$_3$): δ 198.9, 160.2, 139.8, 130.5, 119.6, 113.8, 113.3, 79.5, 55.4, 46.5, 38.2.

*Synthesis and Characterization of Enantiopure Intermediates 45*

(*R*) and (*S*)-**45** were prepared following the general procedure *GP2* using, respectively, the (*R*) or (*S*) enantiomer of the diphenylprolinol TMS ether as the organocatalyst.

(*R*)-4-nitro-3-phenyl-butanal (45)
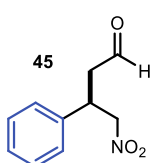
Prepared according to *GP2*, using cinnamaldehyde **40** (126 μL, 1.00 mmol), nitromethane **43** (161 μL, 3.00 mmol) and (*R*)-2-(diphenyl((trimethylsilyl)oxy)methyl)pyrrolidine (32 mg, 100 μmol) in MeOH (2 mL). The crude mixture was purified by flash column chromatography (gradient from 10 to 20% EtOAc in hexane) to afford product **45** (122 mg, 60% yield, >99% ee) as a yellow liquid. The enantiomeric ratio was determined by UPC^2 analysis on a Daicel Chiralpak IG-3 column: isocratic CO$_2$/i-PrOH 97:3, flow rate 2 mL/min, λ = 210 nm: τ_{minor} = 5.5 min, τ_{major} = 6.2 min. The product was stored at -20 ºC. The characterization of the title compound was consistent with the data available in the literature.[80]

(*S*)-4-nitro-3-phenyl-butanal (45)
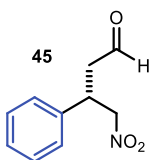
Prepared according to *GP2*, using cinnamaldehyde **40** (126 μL, 1.00 mmol), nitromethane **43** (161 μL, 3.00 mmol) and (S)-2-(diphenyl((trimethylsilyl)oxy)methyl)pyrrolidine (32 mg, 100 μmol) in MeOH (2 mL). The crude mixture was purified by flash column chromatography (gradient from 10 to 20% EtOAc in hexane) to afford product **45** (96 mg, 50% yield, 97% ee) as a yellow liquid. The enantiomeric ratio was determined by UPC^2 analysis on a Daicel Chiralpak IG-3 column: isocratic CO$_2$/i-PrOH 97:3, flow rate 2 mL/min, λ = 210 nm: τ_{major} = 5.5 min, τ_{minor} = 6.2 min. The product was stored at -20ºC. The characterization of the title compound was consistent with the data available in the literature.[80]

(*R*)-**55a** and (*R*)-**55b** were prepared following the general procedure *GP2* using, the (*R*) enantiomer of the diphenylprolinol TMS ether as the organocatalyst.

3.8.4 Synthesis of Reference Compounds

GP3 – General Procedure for the Organocatalyzed Synthesis of Reference Compounds 44 and 50
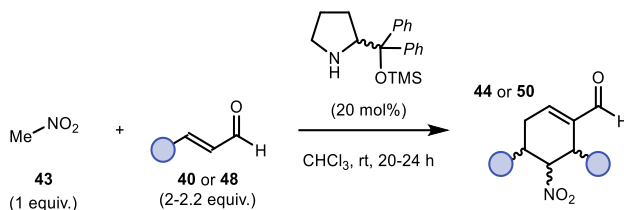
Racemic compounds **44** and **50** were synthesized following a reported literature procedure.[44] To a 10 mL screw-cup vial were added, in sequence, an approximately 1:1 (*R*) and (*S*) mixture of the diphenylprolinol TMS ether as the organocatalyst (20 mol%), the corresponding enal **40** or **48** (2.2 equiv.), if solid, and chloroform (1 M). To the resulting mixture were added nitromethane **43** (1 mmol, 1 equiv.) and the corresponding enal **40** or **48** (2.2 equiv.), if liquid, under argon atmosphere. The reaction mixture was stirred at ambient temperature for 20 to 24 hours. The crude mixture was diluted with dichloromethane and washed with water. The combined organic extracts were dried over anhydrous MgSO$_4$, filtered and concentrated under reduced pressure. Purification of the crude material by flash column chromatography on silica gel provided the corresponding reference compounds **44** or **50** as mixtures of two main diastereomers. The relative configuration of the two main diastereomers were assigned by comparison with the reported data for compound **44**.[44] These diastereomers are the same obtained in the biocatalytic semi-preparative scale reactions described below and were used for the determination of the diastereomeric ratio and the enantiomeric excess of the products obtained in both semi-preparative and analytical scale biocatalytic reactions.

4,6-bis-(4-chlorophenyl)-5-nitrocyclohex-1-ene carbaldehyde (50g)
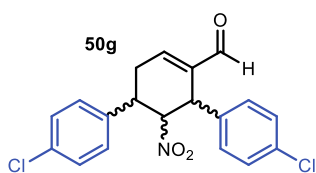
Prepared according to *GP3*, using nitromethane **43** (54 µL, 1.00 mmol), the racemic diphenylprolinol catalyst (65 mg, 200 µmol) and 4-chlorocinnamaldehyde **48g** (333 mg, 2.00 mmol) in anhydrous chloroform (1 mL). The crude mixture was purified by flash column chromatography (gradient from 10 to 30% EtOAc in hexane) to afford product **50g** as a mixture of two diastereomers ***d₁*** and ***d₂*** (240 mg, 64% yield, 1:1.4 dr ***d₁***:***d₂***) as orange solids. The enantiomers were separated by HPLC analysis on a Daicel Chiralpak IB-3 column: isocratic 100% hexane for 2 min; gradient from 100% hexane to 90:10 hexane/*i*-PrOH for 8 min; gradient from 90:10 to 70:30 hexane/*i*-PrOH for 2 min; isocratic hexane/*i*-PrOH 70:30 for 23 min, flow rate 1.0 mL/min, λ = 215 nm: ***d₁***: τ = 24 min and τ = 25 min; ***d₂***: τ = 18 min and τ = 19 min. The relative configurations were assigned by comparison with compound **44**.

<u>^{1}H NMR</u> (**50g-d_1**, 400 MHz, CDCl$_3$): δ 9.57 (s, 1H), 7.40 – 7.33 (m, 3H), 7.32 – 7.22 (m, 2H), 7.21 – 7.11 (m, 2H), 7.03 – 6.95 (m, 2H), 4.86 (dd, J = 3.3, 2.0 Hz, 1H), 4.50 (s, 1H), 3.32 (ddd, J = 9.7, 5.8, 3.3 Hz, 1H), 3.28 – 3.14 (m, 1H), 2.90 (dt, J = 19.9, 5.3 Hz, 1H).

<u>^{13}C NMR</u> (**50g-d_1**, 101 MHz, CDCl$_3$): δ 191.5, 150.2, 138.0, 137.3, 136.2, 134.3, 134.2, 129.6 (2C), 129.4 (2C), 129.3 (2C), 128.8 (2C), 90.9, 42.5, 37.0, 28.0.

<u>HRMS (ESI)</u> Exact mass calculated for **50g-d_1**, C$_{19}$H$_{15}$Cl$_2$NNaO$_3$ [M+Na]$^+$: 398.0321, found: 398.0315.

<u>^{1}H NMR</u> (**50g-d_2**, 400 MHz, CDCl$_3$): δ 9.53 (s, 1H), 7.37 – 7.24 (m, 5H), 7.19 – 7.09 (m, 2H), 7.10 – 6.99 (m, 2H), 5.21 (dd, J = 12.4, 5.8 Hz, 1H), 4.69 (d, J = 5.9 Hz, 1H), 3.55 (ddd, J = 12.4, 10.8, 6.5 Hz, 1H), 3.11 (ddd, J = 20.9, 6.5, 4.6 Hz, 1H), 2.64 (ddt, J = 20.9, 10.8, 2.2 Hz, 1H).

<u>^{13}C NMR</u> (**50g-d_2**, 101 MHz, CDCl$_3$): δ 190.6, 148.0, 139.9, 138.3, 134.8, 133.8, 133.7, 129.9 (2C), 129.4 (2C), 129.2 (2C), 128.7 (2C), 89.1, 42.0, 37.4, 35.2.

<u>HRMS (ESI)</u> Exact mass calculated for **50g-d_1**, C$_{19}$H$_{15}$Cl$_2$NNaO$_3$ [M+Na]$^+$: 398.0321, found: 398.0315.

Reference compounds **44**, **50b-f** and **50h** were synthesized using the general procedure *GP3*. The main diastereomers obtained for these compounds using the general procedure above are the same diastereomers obtained in the biocatalytic semi-preparative scale reactions detailed below. Therefore, their full characterization is provided below.

GP4 – General Procedure for the Organocatalyzed Synthesis of Reference Compounds 56
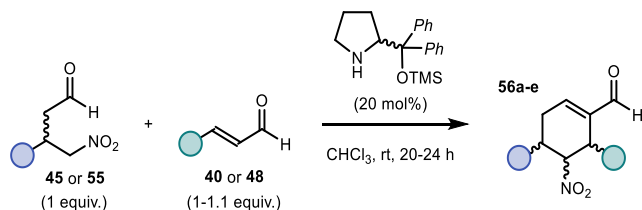
To a 10 mL screw-cup vial were added, in sequence, the intermediate **45** or **55** (1.0 equiv.), an approximately 1:1 (*R*) and (*S*) mixture of the diphenylprolinol TMS ether as the organocatalyst (20 mol%) and chloroform (1 M). To the resulting mixture was added the corresponding enal **40** or **48** (1-1.1 equiv.) under argon atmosphere. The reaction mixture was stirred at ambient temperature for 20 to 24 hours. The crude mixture was diluted with dichloromethane and washed with water. The combined organic extracts were dried over anhydrous MgSO$_4$, filtered and concentrated under reduced pressure. Purification of the crude material by flash column chromatography on silica gel provided the corresponding reference compounds **56** as mixtures of two main diastereomers. The relative configurations of the two main diastereomers were assigned by comparison with compound **44**. These diastereomers

are the same obtained in the biocatalytic semi-preparative scale reactions detailed below. Therefore, the full characterization of compounds **56a-e** is provided further below. The isolated products **56** were used for the determination of the diastereomeric ratio and the enantiomeric excess of the products obtained in both semi-preparative and analytical scale biocatalytic reactions.

GP5 – General Procedure for the Organocatalyzed Synthesis of Reference Compounds 41 or 50
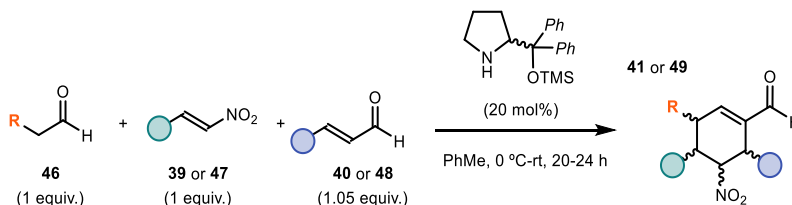
Reference compounds **41** and **49** were synthesized following a reported literature procedure.[43] To a 10 mL screw-cup vial were added, in sequence, an approximately 1:1 (*R*) and (*S*) mixture of the diphenylprolinol TMS ether as the organocatalyst (20 mol%), the corresponding trans-β-nitrostyrene **39** or **47** (1 mmol, 1 equiv.), the corresponding enal **40** or **48** (1.05 equiv.), if solid, and anhydrous toluene (1.25 M). To the resulting mixture were added at 0ºC the aliphatic aldehyde **46** (1 equiv.) and the corresponding enal **40** or **48** (1.05 equiv.), if liquid, under argon atmosphere. The reaction mixture was allowed to reach the ambient temperature for approximately 1 hour and left stirring for additional 20 to 24 hours. The crude mixture was concentrated under reduced pressure. Purification of the crude material by flash column chromatography on silica gel provided the corresponding reference compounds **41** and **49** as mixtures of two main diastereomers. The relative configurations of the two main diastereomers were assigned by comparison with the reported data for compound **41**.[43,83]

3-ethyl-5-nitro-4,6-diphenylcyclohex-1-ene carbaldehyde (41)
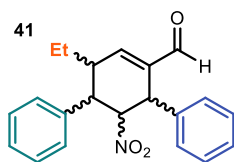
Prepared according to *GP5*, using trans-β-nitrostyrene **39** (106 mg, 710 µmol), the (*R*) and (*S*) mixture of the diphenylprolinol catalyst (46 mg, 142 µmol), butanal **38** (64 µL, 710 µmol) and cinnamaldehyde **40** (94 µL, 746 µmol) in anhydrous toluene (600 µL). The crude mixture was purified by flash column

chromatography (gradient from 10 to 30% EtOAc in hexane) to afford product **41** as a mixture of two diastereomers d_1 and d_2 (197 mg, 60% yield, 3:1 dr d_1:d_2) as yellow solids. The enantiomers were separated by HPLC analysis on a Daicel Chiralpak IB-3 column: isocratic

[83] Jia, Y., Mao, Z., Wanga, R. "Asymmetric triple cascade organocatalytic reaction in water: construction of polyfunctional cyclohexene building blocks having multiple stereocenters" *Tetrahedron: Asymmetry* **2011**, *22*, 2018-2023.

100% hexane for 5 min; gradient from 100% hexane to 95:5 hexane/*i*-PrOH for 10 min; gradient from 95:5 to 80:20 hexane/*i*-PrOH for 5 min; isocratic hexane/*i*-PrOH 80:20 for 10 min, flow rate 1.0 mL/min, $\lambda = 215$ nm: d_1: $\tau = 16$ min and $\tau = 19$ min; d_2: $\tau = 24$ min and $\tau = 29$ min. The relative and absolute configurations were assigned by comparison with the data reported in the literature.[43,83]

<u>^{1}H NMR</u> (**41-d_1**, 400 MHz, CDCl$_3$): δ 9.62 (s, 1H), 7.47 – 7.15 (m, 9H), 7.06 – 6.96 (m, 2H), 4.89 (dd, $J = 3.5, 1.8$ Hz, 1H), 4.47 (s, 1H), 3.38 – 3.28 (m, 1H), 3.06 (dd, $J = 10.5, 3.5$ Hz, 1H), 1.77 (dqd, $J = 13.8, 7.6, 4.1$ Hz, 1H), 1.55 – 1.40 (m, 1H), 1.07 (t, $J = 7.5$ Hz, 3H).

<u>^{13}C NMR</u> (**41-d_1**, 101 MHz, CDCl$_3$): δ 192.0, 154.4, 138.9, 137.9, 137.4, 129.3 (2C), 129.2 (2C), 128.2, 128.1 (2C), 127.9 (2C), 127.0, 92.7, 43.2, 42.9, 38.3, 25.2, 10.8.

<u>^{1}H NMR</u> (**41-d_2**, 400 MHz, CDCl$_3$): δ 9.54 (s, 1H), 7.37 – 7.20 (m, 6H), 7.20 – 7.15 (m, 2H), 7.14 – 7.06 (m, 3H), 5.28 (dd, $J = 12.4, 5.9$ Hz, 1H), 4.69 – 4.63 (m, 1H), 3.27 (dd, $J = 12.4, 10.2$ Hz, 1H), 2.70 (dddq, $J = 10.3, 8.4, 4.3, 1.9$ Hz, 1H), 1.78 (dqd, $J = 13.9, 7.6, 4.1$ Hz, 1H), 1.51 (ddd, $J = 13.8, 8.0, 7.1$ Hz, 1H), 1.09 (t, $J = 7.5$ Hz, 3H).

<u>^{13}C NMR</u> (**41-d_2**, 101 MHz, CDCl$_3$): δ 191.2, 152.0, 139.6, 139.0, 137.9, 135.4, 128.9 (2C), 128.8 (2C), 128.7 (2C), 128.5, 127.8, 127.0, 90.3, 45.8, 43.0, 42.7, 24.7, 11.0.

3-ethyl-6-(4-fluorophenyl)-5-nitro-4-phenylcyclohex-1-ene carbaldehyde (49a)
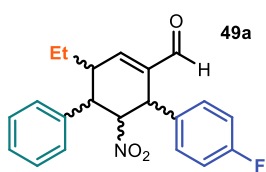
Prepared according to *GP5*, using trans-β-nitrostyrene **39** (75 mg, 500 µmol), the (*R*) and (*S*) mixture of the diphenylprolinol catalyst (46 mg, 140 µmol), butanal **38** (54 µL, 600 µmol) and 4-fluoro-cinnamaldehyde **48a** (79 mg, 525 µmol) in anhydrous toluene (400 µL). The crude mixture was purified by flash column chromatography (gradient from 10 to 30% EtOAc in hexane) to afford product **49a** as a mixture of several compounds with d_1 as the main diastereomer and traces amount of d_2 (29 mg, 16% yield for **49a-d_1**) as a yellow oil. The enantiomers were separated by HPLC analysis on a Daicel Chiralpak IB-3 column: isocratic 100% hexane for 2 min; gradient from 100% hexane to 90:10 hexane/*i*-PrOH for 8 min; gradient from 90:10 to 80:20 hexane/*i*-PrOH for 2 min; isocratic hexane/*i*-PrOH 80:20 for 23 min, flow rate 1.0 mL/min, $\lambda = 215$ nm: $\tau = 11$ min, $\tau = 12$ min. The relative and absolute configurations were assigned by comparison with compound **41**.

<u>^{1}H NMR</u> (**49a-d_1**, 400 MHz, CDCl$_3$): δ 9.60 (s, 1H), 7.33 (dd, $J = 2.7, 0.9$ Hz, 1H), 7.31 – 7.27 (m, 3H), 7.23 – 7.14 (m, 2H), 7.14 – 7.02 (m, 2H), 7.05 – 6.96 (m, 2H), 4.83 (dd, $J = 3.5, 1.9$ Hz, 1H), 4.44 (s, 1H), 3.38 – 3.26 (m, 1H), 3.03 (dd, $J = 10.4, 3.5$ Hz, 1H), 1.85 – 1.69 (m, 1H), 1.47 (dt, $J = 13.7, 7.4$ Hz, 1H), 1.06 (t, $J = 7.4$ Hz, 3H).

<u>^{19}F NMR</u> (**49a-d_1**, 376 MHz, CDCl$_3$): δ -114.13.

<u>^{13}C NMR</u> (**49a-d_1**, 101 MHz, CDCl$_3$): δ 192.0, 162.4 (d, J_{C-F} = 247.4 Hz), 154.6, 137.9, 137.2, 134.7, 129.7 (d, J_{C-F} = 8.2 Hz), 129.3, 128.3, 127.9, 116.3 (d, J_{C-F} = 21.7 Hz), 92.6, 43.0, 42.4, 38.4, 25.3, 10.9.

<u>HRMS (ESI)</u> Exact mass calculated for **49a-d_1**, C$_{21}$H$_{20}$FNNaO$_3$ [M+Na]$^+$: 376.1319, found: 376.1319.

<u>^{1}H NMR</u> (**49a-d_2**, 400 MHz, CDCl$_3$): δ 9.54 (s, 1H), 7.32 – 7.20 (m, 3H), 7.20 – 7.14 (m, 2H), 7.11 (d, J = 2.6 Hz, 1H), 7.09 – 6.97 (m, 4H), 5.26 (dd, J = 12.4, 5.9 Hz, 1H), 4.63 (d, J = 5.9 Hz, 1H), 3.21 (dd, J = 12.4, 10.2 Hz, 1H), 2.74 – 2.65 (m, 1H), 1.77 (dtd, J = 15.1, 7.6, 4.2 Hz, 1H), 1.48 (dd, J = 14.4, 7.3 Hz, 1H), 1.08 (t, J = 7.5 Hz, 3H).

<u>^{19}F NMR</u> (**49a-d_2**, 376 MHz, CDCl$_3$): δ -113.8.

<u>^{13}C NMR</u> (**49a-d_2**, 101 MHz, CDCl$_3$): δ 190.9, 164.0, 152.1, 139.4, 138.6, 131.0, 130.1 (d, J_{C-F} = 8.2 Hz), 128.9, 128.0, 127.8, 115.8 (d, J_{C-F} = 21.5 Hz), 90.0, 45.6, 42.8, 41.8, 24.1, 10.8.

The synthesis of the reference compound **49b** using the general procedure *GP5* only afforded a mixture of several diastereomers in traces amount. Further attempts to synthesize these compounds were not undertaken since the amount obtained was in general sufficient for HPLC detection and chiral separation of the desired diastereomers.
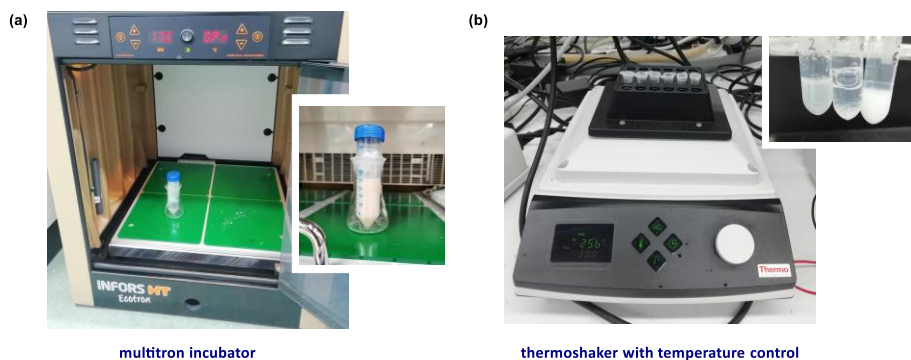
3.8.5 Semi-Preparative Scale Biocatalytic Reactions

GP6 – General Procedure for the Semi-Preparative Scale Enzymatic Synthesis of Enantiopure Products 44 or 50
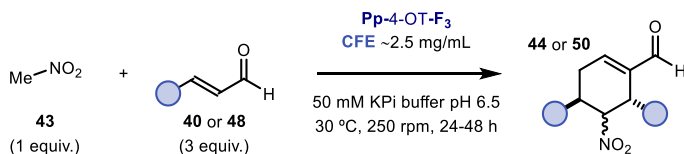

In typical procedure for the Pp-4-OT-F$_3$-catalyzed biosynthesis of compounds **44** or **50** on a semi-preparative scale, 1.5 g of *E. coli* cells containing the overexpressed Pp-4OT-F$_3$ enzyme were resuspended in 27 mL of 50 mM KPi buffer pH 6.5 and sonicated for 20 min. The lysate was cleared by centrifugation for 20 min at 4ºC and the supernatant collected and used without further purification. In a 50 mL Falcon tube a solution of nitromethane **43** (0.15 mmol, final concentration of 5 mM) and enal **40** or **48** (0.45 mmol, final concentration of 15 mM) in DMSO was added to the supernatant to reach the final volume of 30 mL (10% v/v DMSO/water buffer). The reaction mixture was shaken in an incubator at 30 ºC and 250 rpm for 24 to 48 hours (see Figure 3.10a). The crude mixture was quenched with 1 mL of 1M HCl and extracted twice with 30 mL of ethyl acetate. The combined organic extracts were dried over anhydrous MgSO$_4$, filtered and concentrated under reduced pressure. Purification of the

crude material by flash column chromatography on silica gel provided the corresponding enantiopure reference compounds.

Figure 3.10. (a) Set-up for the semi-preparative scale enzymatic reactions (150 μmol scale); (b) set-up for the analytical scale enzymatic reactions (2.50 μmol scale).

(4*R*,5*R*,6*S*)-5-nitro-4,6-diphenylcyclohex-1-ene carbaldehyde (44)
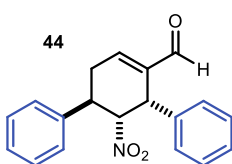
Prepared according to *GP6*, using nitromethane **43** (8.2 uL, 150 μmol) and cinnamaldehyde **40** (57 μL, 450 μmol) as the substrates in DMSO as solvent. The crude mixture was purified by flash column chromatography (gradient from 10 to 30% EtOAc in hexane) to afford product **44** as a major diastereomer d_1 and traces of a second diastereomer d_2 (28 mg, 61% yield, >20:1 dr d_1:d_2, >99% ee) as a white solid. The enantiomeric excess was determined by HPLC analysis on a Daicel Chiralpak IB-3 column: isocratic 100% hexane for 2 min; gradient from 100% hexane to 90:10 hexane/*i*-PrOH for 8 min; gradient from 90:10 to 70:30 hexane/*i*-PrOH for 2 min; isocratic hexane/*i*-PrOH 70:30 for 23 min, flow rate 1.0 mL/min, λ = 215 nm: τ_{major} = 26 min, τ_{minor} = 29 min; $[\alpha]_D^{26}$ = +373 (c = 0.0012, CH$_2$Cl$_2$, >99% ee). The relative and absolute configurations were assigned by comparison with compound **50e** and the data reported in the literature.[44]

<u>1H NMR</u> (**44-d_1**, 500 MHz, CDCl$_3$): δ 9.52 (s, 1H), 7.35 – 7.16 (m, 8H), 7.15 – 7.07 (m, 3H), 5.27 (dd, *J* = 12.4, 5.8 Hz, 1H), 4.71 (d, *J* = 5.8 Hz, 1H), 3.61 (ddd, *J* = 12.4, 10.7, 6.6 Hz, 1H), 3.11 (ddd, *J* = 21.0, 6.6, 4.6 Hz, 1H), 2.66 (dddd, *J* = 21.0, 10.7, 2.9, 1.8 Hz, 1H).

<u>13C NMR</u> (**44-d_1**, 126 MHz, CDCl$_3$): δ 190.8, 148.1, 140.2, 140.1, 135.3, 129.1, 128.9, 128.7, 128.6, 127.8, 127.3, 89.3, 42.7, 37.9, 35.5.

<u>HRMS (ESI)</u> Exact mass calculated for **44-d_1**, C$_{19}$H$_{17}$NNaO$_3$ [M+Na]$^+$: 330.1101, found: 330.1097.

^{1}H NMR (**44-d_2**, 500 MHz, CDCl$_3$): δ 9.60 (s, 1H), 7.41 – 7.35 (m, 3H), 7.35 – 7.21 (m, 6H), 7.09 – 7.01 (m, 2H), 4.97 (dd, J = 3.3, 1.8 Hz, 1H), 4.54 (s, 1H), 3.43 – 3.35 (m, 1H), 3.28 (ddt, J = 20.1, 11.3, 2.4 Hz, 1H), 2.91 (dt, J = 20.0, 5.3 Hz, 1H).

^{13}C NMR (**44-d_2**, 126 MHz, CDCl$_3$): δ 191.8, 150.5, 138.9, 138.2, 138.1, 129.4, 129.1, 128.2, 128.1, 127.4, 91.3, 43.3, 37.3, 28.0.

(4R,5R,6S)- 4,6-bis-(4-fluorophenyl)-5-nitrocyclohex-1-ene carbaldehyde (50a)
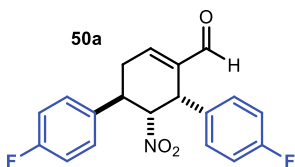
Prepared according to *GP6*, using nitromethane **43** (8.2 uL, 150 µmol) and 4-fluorocinnamaldehyde **48a** (68 mg, 450 µmol) as the substrates in DMSO as solvent. The crude mixture was purified by flash column chromatography (gradient from 10 to 50% EtOAc in hexane) to afford product **50a** as a single diastereomer (46 mg, 88% yield, >99% ee) as colorless crystals. The enantiomeric excess was determined by HPLC analysis on a Daicel Chiralpak IB-3 column: isocratic 100% hexane for 2 min; gradient from 100% hexane to 90:10 hexane/i-PrOH for 8 min; gradient from 90:10 to 80:20 hexane/i-PrOH for 2 min; isocratic hexane/i-PrOH 80:20 for 23 min, flow rate 1.0 mL/min, λ = 215 nm: τ$_{minor}$ = 25 min, τ$_{major}$ = 26 min; $[α]_D^{26}$ = +310 (c = 0.0012, CH$_2$Cl$_2$, >99% ee). The relative and absolute configurations were assigned by comparison with compound **50e**.

^{1}H NMR (400 MHz, CDCl$_3$): δ 9.53 (s, 1H), 7.26 – 6.91 (m, 9H), 5.21 (dd, J = 12.4, 5.8 Hz, 1H), 4.70 (d, J = 6.2 Hz, 1H), 3.65 – 3.49 (m, 1H), 3.11 (ddd, J = 21.0, 6.5, 4.6 Hz, 1H), 2.65 (ddt, J = 21.1, 10.9, 2.4 Hz, 1H).

^{19}F NMR (376 MHz, CDCl$_3$): δ -113.5, -114.4.

^{13}C NMR (101 MHz, CDCl$_3$): δ 190.6, 162.8 (d, J_{C-F} = 247.9 Hz), 161.1 (d, J_{C-F} = 246.8 Hz), 147.8, 140.0, 135.4 (d, J_{C-F} = 3.2 Hz), 130.9 (d, J_{C-F} = 3.3 Hz), 130.2 (d, J_{C-F} = 8.3 Hz), 128.8 (d, J_{C-F} = 8.1 Hz), 116.0 (d, J_{C-F} = 20 Hz), 115.8 (d, J_{C-F} = 20 Hz), 89.2, 41.8, 37.1, 35.2.

HRMS (ESI) Exact mass calculated for C$_{19}$H$_{15}$F$_2$NNaO$_3$ [M+Na]$^+$: 366.0912, found: 366.0911.

(4R,5R,6S)- 4,6-bis-(3-methoxyphenyl)-5-nitrocyclohex-1-ene carbaldehyde (50b)
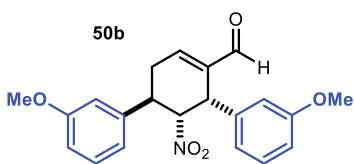
Prepared according to *GP6*, using nitromethane **43** (8.2 uL, 150 µmol) and 3-methoxycinnamaldehyde **48b** (73 mg, 450 µmol) as the substrates in ethylene glycol as solvent. The crude mixture was purified by flash column chromatography (gradient from 10 to 30% EtOAc in hexane) to afford product **50b** as the major diastereomer **d_1** and traces of **d_2** (24 mg, 43% yield, 18:1 dr **d_1:d_2**, >99% ee) as a white solid. The enantiomeric excess was determined by HPLC analysis on a Daicel Chiralpak IB-3 column: isocratic 100% hexane for 2 min; gradient from

100% hexane to 90:10 hexane/*i*-PrOH for 8 min; gradient from 90:10 to 40:60 hexane/*i*-PrOH for 2 min; isocratic hexane/*i*-PrOH 40:60 for 23 min, flow rate 1.0 mL/min, λ = 215 nm: τ_{major} = 27 min, τ_{minor} = 23 min; $[\alpha]_D^{26}$ for **50b-*d₁*** = +314 (c = 0.0010, CH$_2$Cl$_2$, >99% ee). The relative and absolute configurations were assigned by comparison with compound **50e**.

<u>^{1}H NMR</u> (**50b-*d₁***, 400 MHz, CDCl$_3$): δ 9.51 (s, 1H), 7.22 (dt, *J* = 12.8, 8.1 Hz, 2H), 7.11 – 7.05 (m, 1H), 6.84 (ddd, *J* = 8.3, 2.6, 0.9 Hz, 1H), 6.80 – 6.73 (m, 2H), 6.73 – 6.66 (m, 2H), 6.64 – 6.59 (m, 1H), 5.23 (dd, *J* = 12.4, 5.8 Hz, 1H), 4.67 (d, *J* = 5.8 Hz, 1H), 3.78 (s, 3H), 3.76 (s, 3H), 3.59 (ddd, *J* = 12.4, 10.6, 6.5 Hz, 1H), 3.09 (ddd, *J* = 21.0, 6.4, 4.7 Hz, 1H), 2.63 (dddd, *J* = 21.0, 10.6, 2.9, 1.9 Hz, 1H).

<u>^{13}C NMR</u> (**50b-*d₁***, 126 MHz, CDCl$_3$): δ 190.9, 160.1, 159.7, 148.1, 141.8, 140.1, 136.8, 130.2, 129.8, 121.2, 119.3, 115.2, 113.6, 113.1, 112.9, 89.1, 55.4, 55.3, 42.6, 37.92, 35.5.

<u>HRMS (ESI)</u> Exact mass calculated for **50b-*d₁***, C$_{21}$H$_{21}$NNaO$_5$ [M+Na]$^+$: 390.1312, found: 390.1311.

<u>^{1}H NMR</u> (**50b-*d₂***, 500 MHz, CDCl$_3$): δ 9.58 (s, 1H), 7.34 (dd, *J* = 4.8, 2.8 Hz, 1H), 7.29 (t, *J* = 7.9 Hz, 1H), 7.21 (t, *J* = 8.0 Hz, 1H), 6.88 – 6.78 (m, 4H), 6.65 (dd, *J* = 7.7, 1.7 Hz, 1H), 6.60 (t, *J* = 2.2 Hz, 1H), 4.97 (dd, *J* = 3.3, 1.8 Hz, 1H), 4.50 (s, 1H), 3.81 (s, 3H), 3.75 (s, 3H), 3.36 (ddd, *J* = 11.3, 6.0, 3.3 Hz, 1H), 3.24 (ddt, *J* = 20.0, 11.4, 2.3 Hz, 1H), 2.89 (dt, *J* = 20.1, 5.5 Hz, 1H).

<u>^{13}C NMR</u> (**50b-*d₂***, 126 MHz, CDCl$_3$): δ 191.8, 160.2, 160.0, 150.5, 140.5, 139.7, 138.1, 130.4, 130.1, 120.4, 119.6, 114.5, 113.9, 112.9, 112.7, 91.1, 55.4, 43.2, 37.4, 28.0.

(4*R*,5*R*,6*S*)- 4,6-bis-(2-tolyl)-5-nitrocyclohex-1-ene carbaldehyde (50c)
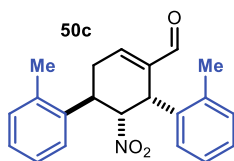
Prepared according to *GP6*, using nitromethane **43** (8.2 uL, 150 µmol) and 2-methylcinnamaldehyde **48c** (66 mg, 450 µmol) as the substrates in ethylene glycol as solvent. The crude mixture was purified by flash column chromatography (gradient from 10 to 30% EtOAc in hexane) to afford product **50c** as a mixture of two diastereomers *d₁* and *d₂* (27 mg, 49% yield, 9:1 dr *d₁*:*d₂*, >99% ee) as white solids. The enantiomeric excess was determined by HPLC analysis on a Daicel Chiralpak IB-3 column: isocratic 100% hexane for 2 min; gradient from 100% hexane to 90:10 hexane/*i*-PrOH for 8 min; gradient from 90:10 to 80:20 hexane/*i*-PrOH for 2 min; isocratic hexane/*i*-PrOH 80:20 for 23 min, flow rate 1.0 mL/min, λ = 215 nm: τ_{major} = 27 min, τ_{minor} = 25 min; $[\alpha]_D^{26}$ for **50c-*d₁*** = +389 (c = 0.0009, CH$_2$Cl$_2$, >99% ee). The relative and absolute configurations were assigned by comparison with compound **50e**.

<u>^{1}H NMR</u> (**50c-*d₁***, 500 MHz, CDCl$_3$): δ 9.47 (s, 1H), 7.20 – 7.13 (m, 5H), 7.13 – 7.10 (m, 2H), 7.10 – 7.03 (m, 2H), 5.36 (dd, *J* = 12.4, 5.8 Hz, 1H), 5.16 (d, *J* = 5.6 Hz, 0H), 4.18 (ddd, *J* =

12.6, 10.6, 6.4 Hz, 1H), 3.07 (ddd, J = 21.0, 6.4, 4.6 Hz, 1H), 2.58 (ddt, J = 21.0, 10.7, 2.4 Hz, 1H), 2.40 (s, 3H), 2.32 (s, 3H).

^{13}C NMR (**50c-d_1**, 126 MHz, CDCl$_3$): δ 191.0, 147.5, 141.7, 138.6, 138.2, 136.9, 134.0, 131.4, 131.1, 128.0, 128.0, 127.4, 127.0, 125.6, 88.8, 37.6, 34.5, 19.8, 19.4.

HRMS (ESI) Exact mass calculated for **50c-d_1**, C$_{21}$H$_{21}$NNaO$_3$ [M+Na]$^+$: 358.1419, found: 358.1414.

^{1}H NMR (**50c-d_2**, 500 MHz, CDCl$_3$): δ 9.62 (s, 1H), 7.45 (dd, J = 4.8, 2.4 Hz, 1H), 7.32 – 7.29 (m, 1H), 7.25 (td, J = 7.4, 1.4 Hz, 1H), 7.21 – 7.14 (m, 4H), 7.12 – 7.09 (m, 1H), 7.03 (dd, J = 7.6, 1.4 Hz, 1H), 4.69 (s, 1H), 4.63 (dd, J = 3.0, 1.1 Hz, 1H), 3.69 (ddd, J = 12.0, 5.7, 3.0 Hz, 1H), 3.36 (ddt, J = 20.1, 12.0, 2.3 Hz, 1H), 2.79 (dt, J = 20.1, 5.4 Hz, 1H), 2.53 (s, 3H), 1.68 (s, 3H).

^{13}C NMR (**50c-d_2**, 126 MHz, CDCl$_3$): δ 192.0, 151.2, 138.7, 136.9, 136.3, 135.9, 135.7, 131.7, 131.2, 128.2, 128.0, 126.8, 126.8, 126.4, 126.3, 88.0, 40.2, 33.0, 27.5, 19.5, 18.6.

HRMS (ESI) Exact mass calculated for **50c-d_2**, C$_{21}$H$_{21}$NNaO$_3$ [M+Na]$^+$: 358.1414, found: 358.1418.

(4R,5R,6S)- 4,6-bis-(3-bromophenyl)-5-nitrocyclohex-1-ene carbaldehyde (50d)
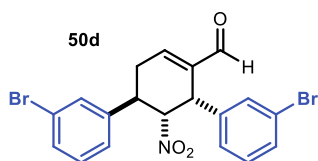
Prepared according to *GP6*, using nitromethane **43** (8.2 uL, 150 µmol) and 3-bromocinnamaldehyde **48d** (95 mg, 450 µmol) as the substrates in DMSO as solvent. The crude mixture was purified by flash column chromatography (gradient from 10 to 30% EtOAc in hexane) to afford product **50d** as a mixture of two diastereomers d_1 and d_2 (30 mg, 43% yield, 8:1 dr d_1:d_2, >99% ee) as white solids. The enantiomeric excess was determined by HPLC analysis on a Daicel Chiralpak IB-3 column: isocratic 100% hexane for 2 min; gradient from 100% hexane to 90:10 hexane/i-PrOH for 8 min; gradient from 90:10 to 70:30 hexane/i-PrOH for 2 min; isocratic hexane/i-PrOH 70:30 for 23 min, flow rate 1.0 mL/min, λ = 215 nm: d_1: $τ_{major}$ = 24 min, $τ_{minor}$ = 28 min; d_2: $τ_{minor}$ = 17 min, $τ_{major}$ = 20 min; $[α]_D^{26}$ for **50d-d_1** = +349 (c = 0.0011, CH$_2$Cl$_2$, >99% ee). The relative and absolute configurations were assigned by comparison with compound **50e**.

^{1}H NMR (**50d-d_1**, 500 MHz, CDCl$_3$): δ 9.51 (s, 1H), 7.45 (ddd, J = 8.1, 1.9, 1.0 Hz, 1H), 7.41 – 7.33 (m, 2H), 7.23 – 7.09 (m, 5H), 7.04 (dt, J = 7.8, 1.4 Hz, 1H), 5.20 (dd, J = 12.4, 5.9 Hz, 1H), 4.66 (dd, J = 5.8, 1.7 Hz, 1H), 3.52 (ddd, J = 12.5, 10.7, 6.5 Hz, 1H), 3.11 (ddd, J = 21.0, 6.6, 4.6 Hz, 1H), 2.63 (ddt, J = 21.0, 10.7, 2.4 Hz, 1H).

^{13}C NMR (**50d-d_1**, 126 MHz, CDCl$_3$): δ 190.5, 148.1, 142.1, 139.6, 137.4, 131.9, 131.2, 131.2, 130.8, 130.7, 130.5, 127.7, 125.9, 123.2, 123.0, 88.8, 42.1, 37.7, 35.2.

HRMS (ESI) Exact mass calculated for **50d-d_1**, $C_{19}H_{15}Br_2NNaO_3$ [M+Na]$^+$: 485.9311, found: 485.9308.

^{1}H NMR (**50d-d_2**, 500 MHz, CDCl$_3$): δ 9.59 (s, 1H), 7.48 (ddd, J = 8.0, 2.0, 1.1 Hz, 1H), 7.42 (ddd, J = 8.0, 2.0, 1.0 Hz, 1H), 7.40 – 7.35 (m, 1H), 7.34 (t, J = 1.9 Hz, 1H), 7.31 – 7.24 (m, 1H), 7.23 – 7.15 (m, 3H), 7.03 – 6.98 (m, 1H), 4.91 (dd, J = 3.2, 1.9 Hz, 1H), 4.52 (s, 1H), 3.35 – 3.19 (m, 2H), 2.93 (dt, J = 19.7, 5.2 Hz, 1H).

^{13}C NMR (**50d-d_2**, 126 MHz, CDCl$_3$): δ 191.5, 150.3, 141.0, 140.0, 137.7, 131.6, 131.5, 131.0, 131.0, 130.7, 130.7, 126.9, 126.0, 123.6, 123.2, 90.5, 42.8, 37.0, 27.8.

HRMS (ESI) Exact mass calculated for **50d-d_2**, $C_{19}H_{15}Br_2NNaO_3$ [M+Na]$^+$: 485.9311, found: 485.9308.

(4R,5R,6S)- 4,6-bis-(2-chlorophenyl)-5-nitrocyclohex-1-ene carbaldehyde (50e)
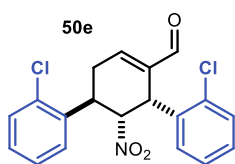
Prepared according to *GP6*, using nitromethane **43** (8.2 uL, 150 µmol) and 2-chlorocinnamaldehyde **48e** (75 mg, 450 µmol) as the substrates in ethylene glycol:DMSO 3:1 as solvent mixture. The crude mixture was purified by flash column chromatography (gradient from 10 to 30% EtOAc in hexane) to afford product **50e** as a mixture of two diastereomers *d_1* and *d_2* (24 mg, 43% yield, 3:1 dr *d_1:d_2*, >99% ee) as white solids. The enantiomeric excess was determined by HPLC analysis on a Daicel Chiralpak IB-3 column: isocratic 100% hexane for 2 min; gradient from 100% hexane to 90:10 hexane/*i*-PrOH for 8 min; gradient from 90:10 to 70:30 hexane/*i*-PrOH for 2 min; isocratic hexane/*i*-PrOH 70:30 for 23 min, flow rate 1.0 mL/min, λ = 215 nm: *d_1*: τ$_{major}$ = 25 min, τ$_{minor}$ = 33 min; *d_2*: τ$_{minor}$ = 17 min, τ$_{major}$ = 20 min; [α]$_D^{26}$ for **50e-d_1** = +261 (c = 0.0018, CH$_2$Cl$_2$, >99% ee). Crystals of derivatives **50e-d_1**, suitable for X-ray diffraction analysis, were obtained upon slow evaporation of a CH$_2$Cl$_2$ solution of the title compound. This enabled the unambiguous determination of the absolute and relative stereochemical configurations for product **50e-d_1**. NMR conformational studies detailed below further confirmed the relative configuration of compounds **50e-d_1** and **50e-d_2**.

^{1}H NMR (**50e-d_1**, 500 MHz, CDCl$_3$): δ 9.52 (s, 1H), 7.44 – 7.39 (m, 1H), 7.40 – 7.35 (m, 1H), 7.31 – 7.19 (m, 5H), 7.16 (td, J = 7.3, 3.0 Hz, 2H), 5.61 – 5.42 (m, 2H), 4.44 – 4.27 (m, 1H), 3.22 (ddd, J = 20.9, 6.2, 4.6 Hz, 1H), 2.74 – 2.55 (m, 1H).

^{13}C NMR (**50e-d_1**, 126 MHz, CDCl$_3$): δ 190.5, 148.0, 140.7, 136.7, 136.2, 134.2, 133.2, 130.6, 130.4, 129.7, 129.5, 129.1, 127.9, 126.7, 86.9, 37.8, 35.4, 33.1.

HRMS (ESI) Exact mass calculated for **50e-d_1**, $C_{19}H_{15}Cl_2NNaO_3$ [M+Na]$^+$: 398.0321, found: 398.0322.

^{1}H NMR (**50e-d_2**, 500 MHz, CDCl$_3$): δ 9.62 (s, 1H), 7.49 (dd, J = 7.7, 1.6 Hz, 1H), 7.43 (dd, J = 5.2, 2.5 Hz, 1H), 7.37 – 7.15 (m, 6H), 7.06 (dd, J = 7.5, 1.9 Hz, 1H), 5.06 (dd, J = 3.1, 1.2

Hz, 1H), 5.00 (s, 1H), 3.84 (ddd, J = 12.3, 5.5, 2.9 Hz, 1H), 3.18 (ddt, J = 19.8, 12.3, 2.3 Hz, 1H), 2.78 (dt, J = 19.8, 5.3 Hz, 1H).

^{13}C NMR (**50e-d_2**, 126 MHz, CDCl$_3$): δ 191.4, 150.7, 138.3, 135.4, 135.0, 134.3, 133.7, 130.4, 130.1, 129.4, 129.2, 128.8, 128.0, 127.3, 127.1, 85.9, 40.1, 34.2, 26.6.

<u>HRMS (ESI)</u> Exact mass calculated for **50e-d_2**, C$_{19}$H$_{15}$Cl$_2$NNaO$_3$ [M+Na]$^+$: 398.0321, found: 398.0328.

(4*R*,5*R*,6*S*)-4,6-bis-(3-chlorophenyl)-5-nitrocyclohex-1-ene carbaldehyde (50f)
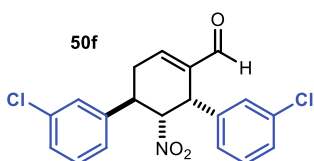
Prepared according to *GP6*, using nitromethane **43** (8.2 uL, 150 µmol) and 3-chlorocinnamaldehyde **48f** (75 mg, 450 µmol) as the substrates in ethylene glycol:DMSO 3:1 as solvent mixture. The crude mixture was purified by flash column chromatography (gradient from 10 to 30% EtOAc in hexane) to afford product **50f** as a mixture of two diastereomers *d_1* and *d_2* (29 mg, 51% yield, 15:1 dr *d_1*:*d_2*, >99% ee) as white solids. The enantiomeric excess was determined by HPLC analysis on a Daicel Chiralpak IB-3 column: isocratic 100% hexane for 2 min; gradient from 100% hexane to 90:10 hexane/*i*-PrOH for 8 min; gradient from 90:10 to 70:30 hexane/*i*-PrOH for 2 min; isocratic hexane/*i*-PrOH 70:30 for 23 min, flow rate 1.0 mL/min, λ = 215 nm: *d_1*: τ_{major} = 23 min, τ_{minor} = 26 min; *d_2*: τ_{minor} = 17 min, τ_{major} = 19 min; $[\alpha]_D^{26}$ for **50f-d_1** = +268 (c = 0.0010, CH$_2$Cl$_2$, >99% ee). The relative and absolute configurations were assigned by comparison with compound **50e**.

^{1}H NMR (**50f-d_1**, 400 MHz, CDCl$_3$): δ 9.54 (s, 1H), 7.36 – 7.19 (m, 5H), 7.18 – 6.98 (m, 4H), 5.24 (dd, J = 12.4, 5.9 Hz, 1H), 4.70 (dd, J = 5.5, 1.7 Hz, 1H), 3.56 (ddd, J = 12.4, 10.7, 6.5 Hz, 1H), 3.14 (ddd, J = 21.0, 6.5, 4.6 Hz, 1H), 2.73 – 2.58 (m, 1H).

^{13}C NMR (**50f-d_1**, 101 MHz, CDCl$_3$): δ 190.4, 148.0, 141.7, 139.5, 137.1, 134.9, 134.7, 130.4, 130.1, 128.9, 128.3, 128.1, 127.6, 127.1, 125.3, 88.7, 42.0, 37.6, 35.0.

<u>HRMS (ESI)</u> Exact mass calculated for **50f-d_1**, C$_{19}$H$_{15}$Cl$_2$NNaO$_3$ [M+Na]$^+$: 398.0321, found: 398.0317.

^{1}H NMR (**50f-d_2**, 500 MHz, CDCl$_3$): δ 9.61 (s, 1H), 7.42 – 7.15 (m, 7H), 7.08 (d, J = 2.1 Hz, 1H), 6.98 (dt, J = 7.0, 1.8 Hz, 1H), 4.94 (dd, J = 3.2, 1.9 Hz, 1H), 4.55 (s, 1H), 3.38 – 3.22 (m, 2H), 2.95 (dt, J = 19.8, 5.2 Hz, 1H).

^{13}C NMR (**50f-d_2**, 126 MHz, CDCl$_3$): δ 191.3, 150.2, 140.6, 139.7, 137.6, 135.2, 134.9, 130.6, 130.3, 128.5, 128.4, 128.0, 127.7, 126.3, 125.4, 90.4, 42.6, 36.9, 27.6.

<u>HRMS (ESI)</u> Exact mass calculated for **50f-d_2**, C$_{19}$H$_{15}$Cl$_2$NNaO$_3$ [M+Na]$^+$: 398.0321, found: 398.0333.

(4R,5R,6S)- 4,6-bis-(2-furyl)-5-nitrocyclohex-1-ene carbaldehyde (50h)
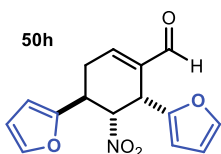
Prepared according to *GP6*, using nitromethane **43** (8.2 uL, 150 µmol) and (E)-3-(furan-2-yl)acrylaldehyde **48h** (55 mg, 450 µmol) as the substrates in DMSO as solvent. The crude mixture was purified by flash column chromatography (gradient from 10 to 30% EtOAc in hexane) to afford product **50h** as a mixture of two diastereomers d_1 and d_2 (4.3 mg, 10% yield, 1:1 dr d_1:d_2, >99% ee) as brown oils. The enantiomeric excess of **50h-d_1** was determined by HPLC analysis on a Daicel Chiralpak IB-3 column: isocratic 100% hexane for 2 min; gradient from 100% hexane to 90:10 hexane/*i*-PrOH for 8 min; isocratic hexane/*i*-PrOH 90:10 for 25 min, flow rate 1.0 mL/min, λ = 215 nm: d_1: $τ_{major}$ = 27 min, $τ_{minor}$ = 26 min; d_2: τ = 16 min. The enantiomeric excess of **50h-d_2** was determined by HPLC analysis on a Daicel Chiralpak IC-3 column: isocratic 100% hexane for 2 min; gradient from 100% hexane to 90:10 hexane/*i*-PrOH for 8 min; gradient from 90:10 to 40:60 hexane/*i*-PrOH for 2 min; isocratic hexane/*i*-PrOH 40:60 for 23 min, flow rate 1.0 mL/min, λ = 215 nm: $τ_{major}$ = 19 min, $τ_{minor}$ = 20 min; $[α]_D^{26}$ for **50h-d_1** = +145 (c = 0.0008, CH$_2$Cl$_2$, >99% ee). The relative and absolute configurations were assigned by comparison with compound **50e**.

^{1}H NMR (**50h-d_1**, 500 MHz, CDCl$_3$): δ 9.50 (s, 1H), 7.35 (dd, *J* = 1.9, 0.8 Hz, 1H), 7.30 (dd, *J* = 1.9, 0.8 Hz, 1H), 7.04 – 6.99 (m, 1H), 6.29 (ddd, *J* = 16.9, 3.2, 1.8 Hz, 2H), 6.17 (ddd, *J* = 10.0, 3.2, 0.8 Hz, 2H), 5.08 (dd, *J* = 12.1, 5.5 Hz, 1H), 4.79 (dd, *J* = 5.3, 1.6 Hz, 1H), 4.00 (ddd, *J* = 12.1, 10.4, 6.6 Hz, 1H), 3.07 (ddd, *J* = 20.9, 6.6, 4.6 Hz, 1H), 2.83 (dddd, *J* = 20.9, 10.4, 3.0, 1.8 Hz, 1H).

^{13}C NMR (**50h-d_1**, 126 MHz, CDCl$_3$): δ 190.4, 152.2, 148.3, 148.1, 143.6, 142.3, 137.8, 110.9, 110.7, 110.3, 107.7, 86.6, 36.5, 33.0, 31.9.

HRMS (ESI) Exact mass calculated for **50h-d_1**, C$_{15}$H$_{13}$NNaO$_5$ [M+Na]$^+$: 310.0686, found: 310.0682.

^{1}H NMR (**50h-d_2**, 500 MHz, CDCl$_3$): δ 9.56 (s, 1H), 7.37 (dd, *J* = 14.7, 1.9 Hz, 2H), 7.17 (t, *J* = 3.8 Hz, 1H), 6.32 (td, *J* = 3.6, 1.8 Hz, 2H), 6.17 (d, *J* = 3.3 Hz, 1H), 6.10 (d, *J* = 3.4 Hz, 1H), 5.36 (dd, *J* = 3.4, 1.9 Hz, 1H), 4.68 (s, 1H), 3.64 (ddd, *J* = 10.4, 7.1, 3.4 Hz, 1H), 3.07 – 2.89 (m, 2H).

^{13}C NMR (**50h-d_2**, 126 MHz, CDCl$_3$): δ 191.4, 151.8, 150.8, 149.2, 143.0, 142.5, 136.8, 110.9, 110.6, 109.0, 107.0, 84.7, 36.3, 33.0, 26.8.

HRMS (ESI) Exact mass calculated for **50h-d_2**, C$_{15}$H$_{13}$NNaO$_5$ [M+Na]$^+$: 310.0686, found: 310.0682.

GP7 – General Procedure for the Semi-Preparative Scale Enzymatic Synthesis of Enantiopure Compounds 56
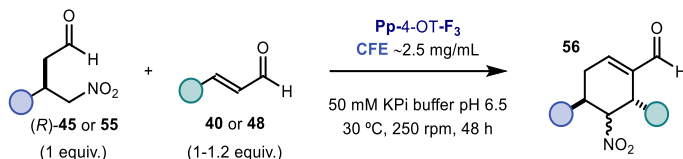
In typical procedure for the Pp-4-OT-F$_3$-catalyzed biosynthesis of compounds **56** on a semi-preparative scale, 1.5 g of *E. coli* cells containing the overexpressed Pp-4OT-F$_3$ enzyme were resuspended in 27 mL of 50 mM KPi buffer pH 6.5 and sonicated for 20 min. The lysate was cleared by centrifugation (20 min, 4°C) and the supernatant collected and used without further purification. In a 50 mL Falcon tube a solution of intermediate **45** or **55** (0.12 mmol, final concentration of 5 mM) and enal **40** or **48** (0.12-0.14 mmol, final concentration of 5-6 mM) in DMSO was added to the supernatant to reach the final volume of 25 mL (10% v/v DMSO/water buffer). The reaction mixture was shaken in an incubator at 30 °C and 250 rpm for 48 hours (see Figure 3.10a). The crude mixture was quenched with 1 mL of 1M HCl and extracted twice with 30 mL of ethyl acetate. The combined organic extracts were dried over anhydrous MgSO$_4$, filtered and concentrated under reduced pressure. Purification of the crude material by flash column chromatography on silica gel provided the corresponding enantiopure reference compounds **56**.

(4R,5R,6S)-6-(3-chlorophenyl)-5-nitro-4-phenylcyclohex-1-ene carbaldehyde (56a)
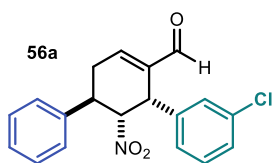
Prepared according to *GP7*, using intermediate (*R*)-**45** (23 mg, 120 µmol) and 3-chlorocinnamaldehyde **48f** (28 mg, 145 µmol) as the substrates in DMSO as solvent. The crude mixture was purified by flash column chromatography (gradient from 10 to 20% EtOAc in hexane) to afford product **56a** as diastereomer *d₁*

and traces amount of *d₂* (16 mg, 38% yield, 12:1 dr *d₁*:*d₂*, >99% ee) as a white solid. The enantiomeric excess was determined by HPLC analysis on a Daicel Chiralpak IC-3 column: isocratic 100% hexane for 2 min; gradient from 100% hexane to 90:10 hexane/*i*-PrOH for 8 min; gradient from 90:10 to 70:30 hexane/*i*-PrOH for 2 min; isocratic hexane/*i*-PrOH 70:30 for 40 min, flow rate 0.5 mL/min, λ = 215 nm: τ$_{major}$ = 30 min, τ$_{minor}$ = 29 min; $[\alpha]_D^{26}$ for **56a-d₁** = +380 (c = 0.0010, CH$_2$Cl$_2$, >99% ee). The relative and absolute configurations were assigned by comparison with compound **50e**.

^{1}H NMR (**56a-d₁**, 500 MHz, CDCl$_3$): δ 9.52 (s, 1H), 7.35 – 7.27 (m, 3H), 7.27 – 7.21 (m, 2H), 7.22 – 7.18 (m, 2H), 7.16 – 7.13 (m, 1H), 7.06 (t, *J* = 1.9 Hz, 1H), 7.01 (dt, *J* = 7.5, 1.5 Hz, 1H), 5.26 (dd, *J* = 12.4, 5.9 Hz, 1H), 4.67 (d, *J* = 5.9 Hz, 1H), 3.56 (ddd, *J* = 12.4, 10.7, 6.5 Hz, 1H), 3.13 (ddd, *J* = 21.0, 6.5, 4.6 Hz, 1H), 2.67 (dddd, *J* = 21.1, 10.7, 2.9, 1.9 Hz, 1H).

^{13}C NMR (**56a-d_1**, 126 MHz, CDCl$_3$): δ 190.7, 148.7, 139.7, 139.7, 137.4, 134.7, 130.2, 129.2, 128.9, 128.5, 127.9, 127.3, 89.1, 42.2, 37.9, 35.4.

HRMS (ESI) Exact mass calculated for **56a-d_1**, C$_{19}$H$_{16}$ClNNaO$_3$ [M+Na]$^+$: 364.0711, found: 364.0716.

^{1}H NMR (**56a-d_2**, 400 MHz, CDCl$_3$): δ 9.59 (s, 1H), 7.39 (m, 1H), 7.36 – 7.26 (m, 5H), 7.22 – 7.10 (m, 2H), 7.06 (m, 2H), 4.94 (dd, J = 3.2, 2.0 Hz, 1H), 4.50 (d, J = 2.0 Hz, 1H), 3.36 (ddd, J = 11.1, 5.5, 3.2 Hz, 1H), 3.27 (dddd, J = 19.8, 11.0, 2.8, 1.8 Hz, 1H), 2.94 (dt, J = 19.7, 5.5 Hz, 1H).

^{13}C NMR (**56a-d_2**, 101 MHz, CDCl$_3$): δ 191.7, 151.0, 141.0, 137.7, 137.7, 135.2, 130.6, 129.1, 128.5, 128.3, 128.2, 127.4, 126.5, 90.9, 42.8, 37.5, 28.0.

HRMS (ESI) Exact mass calculated for **56a-d_2**, C$_{19}$H$_{16}$ClNNaO$_3$ [M+Na]$^+$: 364.0711, found: 364.0715.

(4R,5R,6S)-6-(3-methoxyphenyl)-5-nitro-4-phenylcyclohex-1-enecarbaldehyde(56b)
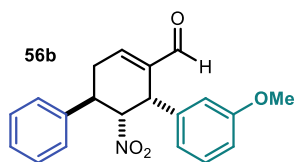
Prepared according to *GP7*, using intermediate (*R*)-**45** (23 mg, 120 µmol) and 3-methoxycinnamaldehyde **48b** (23 mg, 120 µmol) as the substrates in DMSO as solvent. The crude mixture was purified by flash column chromatography (gradient from 10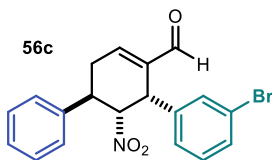 to 30% EtOAc in hexane) to afford product **56b** as a single diastereomer (12 mg, 30% yield, >99% ee) as a colorless oil. The enantiomeric excess was determined by UPC^2 analysis on a Daicel Chiralpak IC-3 column: isocratic 100% CO$_2$ for 1 min; gradient CO$_2$/MeOH from 100% CO$_2$ to 60:40 over 5 minutes, curve 6, flow rate 2 mL/min, λ = 210: τ_{major} = 4.2 min and τ_{minor} = 4.7 min; $[\alpha]_D^{26}$ = +311 (c = 0.00085, CH$_2$Cl$_2$, >99% ee). The relative and absolute configuration were assigned by comparison with compound **50e**.

^{1}H NMR (500 MHz, CDCl$_3$): δ 9.52 (s, 1H), 7.32 – 7.26 (m, 2H), 7.25 – 7.17 (m, 4H), 7.12 – 7.08 (m, 1H), 6.84 (ddd, J = 8.3, 2.6, 0.9 Hz, 1H), 6.71 – 6.67 (m, 1H), 6.62 (t, J = 2.1 Hz, 1H), 5.24 (dd, J = 12.4, 5.8 Hz, 1H), 4.67 (d, J = 5.8 Hz, 1H), 3.79 (s, 3H), 3.62 (ddd, J = 12.4, 10.7, 6.6 Hz, 1H), 3.09 (ddd, J = 21.0, 6.5, 4.7 Hz, 1H), 2.64 (dddd, J = 21.0, 10.6, 2.9, 1.8 Hz, 1H).

^{13}C NMR (126 MHz, CDCl$_3$): δ 190.9, 159.8, 148.1, 140.2, 136.8, 129.9, 129.1, 127.8, 127.4, 121.3, 115.2, 113.2, 89.3, 55.4, 42.6, 37.9, 35.5.

HRMS (ESI) Exact mass calculated for C$_{20}$H$_{19}$NNaO$_4$ [M+Na]$^+$: 360.1206, found: 360.1209.

(4R,5R,6S)-6-(3-bromophenyl)-5-nitro-4-phenylcyclohex-1-ene carbaldehyde (56c)

Prepared according to *GP7*, using intermediate (*R*)-**45** (23 mg, 120 µmol) and 3-bromocinnamaldehyde **48d** (30 mg, 120 µmol) as the substrates in DMSO as solvent. The crude mixture was purified by flash column chromatography (gradient from 10 to 20% EtOAc in hexane) to afford product **56c** as diastereomer *d_1*

and traces amount of *d_2* (15 mg, 32% yield, >20:1 dr *d_1*:*d_2*, >99% ee) as a white solid. The enantiomeric excess was determined by HPLC analysis on a Daicel Chiralpak IC-3 column: isocratic 100% hexane for 2 min; gradient from 100% hexane to 90:10 hexane/*i*-PrOH for 8 min; gradient from 90:10 to 70:30 hexane/*i*-PrOH for 2 min; isocratic hexane/*i*-PrOH 70:30 for 23 min, flow rate 1.0 mL/min, λ = 215 nm: τ_{major} = 18 min and τ_{minor} =19 min; $[\alpha]_D^{26}$ = +297 (c = 0.0013, CH₂Cl₂, >99% ee). The relative and absolute configuration were assigned by comparison with compound **50e**.

¹H NMR (**56c-*d_1***, 500 MHz, CDCl₃): δ 9.52 (s, 1H), 7.44 (ddd, *J* = 7.9, 2.0, 1.0 Hz, 1H), 7.33 – 7.27 (m, 2H), 7.26 – 7.17 (m, 5H), 7.17 – 7.13 (m, 1H), 7.05 (dt, *J* = 7.8, 1.4 Hz, 1H), 5.25 (dd, *J* = 12.4, 6.0 Hz, 1H), 4.65 (dd, *J* = 6.0, 1.7 Hz, 1H), 3.55 (ddd, *J* = 12.4, 10.7, 6.5 Hz, 1H), 3.13 (ddd, *J* = 20.7, 6.5, 4.6 Hz, 1H), 2.66 (dddd, *J* = 21.1, 10.7, 2.9, 1.9 Hz, 1H).

¹³C NMR (**56c-*d_1***, 126 MHz, CDCl₃): δ 190.7, 148.7, 139.7, 139.7, 137.7, 131.8, 131.3, 130.5, 129.2, 128.0, 127.8, 127.3, 123.0, 89.1, 42.2, 37.9, 35.4.

HRMS (ESI) Exact mass calculated for **56c-*d_1***, $C_{19}H_{16}BrNNaO_3$ [M+Na]⁺: 408.0206, found: 408.0218.

¹H NMR (**56c-*d_2***, 400 MHz, CDCl₃): δ 9.59 (s, 1H), 7.46 (ddd, *J* = 7.9, 2.0, 1.1 Hz, 1H), 7.40 (m, 1H), 7.37 – 7.26 (m, 4H), 7.20 (m, 1H), 7.09 – 7.04 (m, 2H), 4.94 (dd, *J* = 3.2, 1.9 Hz, 1H), 4.49 (s, 1H), 3.39 – 3.32 (m, 1H), 3.32 – 3.22 (m, 1H), 2.94 (dt, *J* = 19.2, 4.9 Hz, 1H).

¹³C NMR (**56c-*d_2***, 101 MHz, CDCl₃): δ 191.6, 151.0, 141.3, 137.7, 137.7, 131.4, 131.1, 130.9, 129.2, 128.3, 127.4, 127.0, 123.5, 91.0, 42.7, 37.5, 28.0.

(4R,5R,6S)-4-(4-fluorophenyl)-6-5-nitro-6-phenylcyclohex-1-enecarbaldehyde(56d)
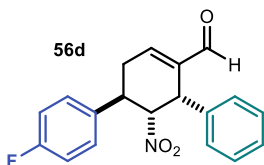
Prepared according to *GP7*, using intermediate (*R*)-**65a** (38 mg, 180 µmol) and cinnamaldehyde **40** (24 mg, 180 µmol) as the substrates in DMSO as solvent. The crude mixture was purified by flash column chromatography (isocratic 30% EtOAc in hexane) to afford product **56d** as a single diastereomer (30 mg, 51% yield,

>99% ee) as a white solid. The enantiomeric excess was determined by HPLC analysis on a Daicel Chiralpak IC-3 column: isocratic 100% hexane for 2 min; gradient from 100% hexane to 70:30 hexane/*i*-PrOH for 8 min; isocratic hexane/*i*-PrOH 70:30 for 40 min, flow rate 1.0 mL/min, λ = 215 nm: τ_{major} = 18 min and τ_{minor} = 20 min; $[\alpha]_D^{26}$ = +285 (c = 0.0019, CH₂Cl₂,

>99% ee). The relative and absolute configuration were assigned by comparison with compound **50e**.

^{1}H NMR (400 MHz, CDCl$_3$): δ 9.51 (s, 1H), 7.31 (dt, J = 4.1, 1.6 Hz, 3H), 7.20 – 7.13 (m, 2H), 7.10 (ddt, J = 6.1, 4.4, 2.0 Hz, 3H), 7.01 – 6.93 (m, 2H), 5.20 (dd, J = 12.4, 5.8 Hz, 1H), 4.73 – 4.66 (m, 1H), 3.60 (ddd, J = 12.4, 10.7, 6.5 Hz, 1H), 3.09 (ddd, J = 21.0, 6.5, 4.6 Hz, 1H), 2.62 (dddd, J = 21.0, 10.7, 2.9, 1.8 Hz, 1H).

^{19}F NMR (376 MHz, CDCl$_3$): δ -114.2.

^{13}C NMR (101 MHz, CDCl$_3$): δ 190.8, 162.2 (d, $J_{C\text{-}F}$ = 246.6 Hz), 147.9, 140.1, 135.8 (d, $J_{C\text{-}F}$ = 3.3 Hz), 135.1, 129.0 (d, $J_{C\text{-}F}$ = 8.2 Hz), 128.9, 128.7, 128.6, 116.0 (d, $J_{C\text{-}F}$ = 21.6 Hz), 89.5, 42.7, 37.2, 35.4.

HRMS (ESI) Exact mass calculated for C$_{19}$H$_{16}$FNNaO$_3$ [M+Na]$^+$: 348.1006, found: 348.1011.

(4*R*,5*R*,6*S*)-4-(3-methoxyphenyl)-5-nitro-6-phenylcyclohex-1-enecarbaldehyde(56e)
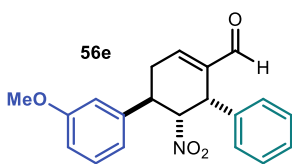
Prepared according to *GP7*, using intermediate (*R*)-**55b** (78 mg, 350 μmol) and cinnamaldehyde **40** (53 μL, 420 μmol) as the substrates in DMSO as solvent. The crude mixture was purified by flash column chromatography (gradient from 10 to 30% EtOAc in hexane) to afford product **56e** as a major diastereomer *d$_1$* and traces amount of *d$_2$* (24.5 mg, 21 % yield, 10:1 dr *d$_1$*:*d$_2$*, >99% ee) as a colorless oil. The enantiomeric excess was determined by HPLC analysis on a Daicel Chiralpak IC-3 column: isocratic 100% hexane for 2 min; gradient from 100% hexane to 90:10 hexane/*i*-PrOH for 8 min; gradient from 90:10 to 70:30 hexane/*i*-PrOH for 2 min; isocratic hexane/*i*-PrOH 70:30 for 40 min, flow rate 0.5 mL/min, λ = 215 nm: *d$_1$*: τ$_{major}$ = 23 min, τ$_{minor}$ = 24 min; *d$_2$*: τ$_{major}$ = 22 min, τ$_{minor}$ = 28 min; [α]$_D^{26}$ for **56e-*d$_1$*** = +260 (c = 0.0009, CH$_2$Cl$_2$, >99% ee). The relative and absolute configuration were assigned by comparison with compound **50e**.

^{1}H NMR (**56e-*d$_1$***, 500 MHz, CDCl$_3$): δ 9.52 (s, 1H), 7.34 – 7.29 (m, 3H), 7.20 (t, J = 8.0 Hz, 1H), 7.13 – 7.09 (m, 3H), 6.80 – 6.73 (m, 2H), 6.73 – 6.70 (m, 1H), 5.25 (dd, J = 12.4, 5.8 Hz, 1H), 4.70 (dt, J = 5.7, 1.3 Hz, 1H), 3.76 (s, 3H), 3.58 (ddd, J = 12.4, 10.6, 6.5 Hz, 1H), 3.11 (ddd, J = 21.0, 6.6, 4.7 Hz, 1H), 2.65 (dddd, J = 21.1, 10.7, 2.9, 1.8 Hz, 1H).

^{13}C NMR (**56e-*d$_1$***, 126 MHz, CDCl$_3$): δ 190.9, 160.1, 148.1, 141.79, 140.2, 135.3, 130.2, 128.9, 128.7, 128.6, 119.3, 113.6, 112.9, 89.2, 55.4, 42.7, 37.9, 35.5.

HRMS (ESI) Exact mass calculated for **56e-*d$_1$***, C$_{20}$H$_{19}$NNaO$_4$ [M+Na]$^+$: 360.1206, found: 360.1213.

^{1}H NMR (**56e-*d$_2$***, 500 MHz, CDCl$_3$): δ 9.59 (s, 1H), 7.39 – 7.34 (m, 2H), 7.34 – 7.29 (m, 1H), 7.26 – 7.17 (m, 4H), 6.80 (ddd, J = 8.2, 2.6, 0.9 Hz, 1H), 6.66 – 6.61 (m, 1H), 6.59 (t, J = 2.2 Hz, 1H), 4.96 (dd, J = 3.2, 1.8 Hz, 1H), 4.53 (s, 1H), 3.75 (s, 3H), 3.35 (ddd, J = 11.3, 5.8, 3.3 Hz, 1H), 3.28 (dt, J = 11.3, 2.3 Hz, 0H), 2.90 (dt, J = 19.9, 5.2 Hz, 1H).

^{13}C NMR (**56e-*d*$_2$**, 126 MHz, CDCl$_3$): δ 191.8, 160.0, 150.5, 139.7, 138.9, 138.2, 130.1, 129.4, 128.2, 128.1, 119.6, 113.9, 112.8, 91.2, 55.4, 43.3, 37.3, 28.1.

Deuterium labelling experiment
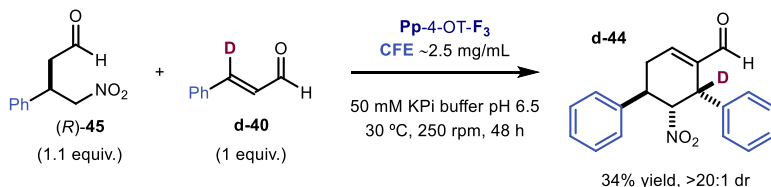
The experimental procedure *GP7* was followed using intermediate (*R*)-**45** (32 mg, 168 µmol) and cinnamaldehyde-3-d **d-40** (21 mg, 158 µmol) as the substrates in DMSO as co-solvent in KPi buffer pH 6.5. The crude mixture was analyzed by ^{1}H NMR spectroscopy and purified by flash column chromatography (gradient from 10 to 30% EtOAc in hexane) to afford product **d-44** as a *single* diastereomer (18 mg, 34% yield) as a yellow oil. The product was obtained has a >99% deuterium incorporation on carbon C6.

^{1}H NMR (300 MHz, CDCl$_3$): δ 9.47 (s, 1H), 7.42 – 6.93 (m, 11H), 5.22 (d, *J* = 12.4 Hz, 1H), 3.56 (ddd, *J* = 12.4, 10.7, 6.5 Hz, 1H), 3.06 (ddd, *J* = 21.0, 6.6, 4.6 Hz, 1H), 2.60 (ddd, *J* = 21.0, 10.7, 2.8 Hz, 1H).

^{13}C NMR (75 MHz, CDCl$_3$): δ 190.9, 148.2, 140.1, 135.2, 129.1 (2C), 128.9 (2C), 128.7, 128.6, 127.8, 127.3 (2C), 89.2, 42.4 (t), 37.9, 35.5.

Synthesis of (3R,4R,5S,6S)- 4-(2-chlorophenyl)-3-ethyl-5-nitro-4-phenylcyclohex-1-ene carbaldehyde (49b)
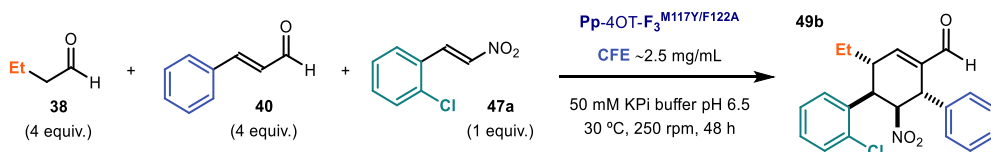
In a 50 mL Falcon tube 1.5 g of *E. coli* cells containing the overexpressed Pp-4OT-F$_3$$^{M117Y/F122A}$ were resuspended in 27 mL of 50 mM KPi buffer pH 6.5 and sonicated for 20 min. The lysate was cleared by centrifugation for 20 min at 4ºC and the supernatant collected and used without further purification. A solution of trans-2-chloro-β-nitrostyrene **47a** (27 mg, 150 µmol) and cinnamaldehyde **40** (76 µL, 600 µmol) in DMSO (3 mL) was added to the supernatant (10% v/v DMSO/water buffer). To this mixture, butanal **38** (64 µL, 600 µmol) was added and the reaction mixture was shaken in an incubator at 30 ºC and 250 rpm for 48 hours (see Figure 3.10a). The crude mixture was quenched with 1 mL of 1M HCl and extracted twice with 30 mL of ethyl acetate. The combined organic extracts were dried over anhydrous MgSO$_4$, filtered and concentrated under reduced pressure. Purification of the crude material by flash column chromatography (gradient from 10 to 30% EtOAc in hexane)

afforded product **49b** as a mixture of two main diastereomers d_1 and d_2 (13 mg, 23%, 3.8:1 dr d_1:d_2) as colorless oils. The enantiomers were separated by HPLC analysis on a Daicel Chiralpak IB-3 column: isocratic 100% hexane for 2 min; gradient from 100% hexane to 90:10 hexane/*i*-PrOH for 8 min; gradient from 90:10 to 80:20 hexane/*i*-PrOH for 2 min; isocratic hexane/*i*-PrOH 80:20 for 23 min, flow rate 1.0 mL/min, $\lambda = 215$ nm: d_1: $\tau_{minor} = 12$ min and $\tau_{major} = 14$ min; d_2: $\tau_{minor} = 17$ min and $\tau_{major} = 21$ min; $[\alpha]_D^{26}$ for **49b-d_1** = -31 (c = 0.0012, CH$_2$Cl$_2$, >99% ee). The relative and absolute configurations were assigned by comparison with compound **43** and the data reported in the literature for similar structures.[43,84]

<u>^{1}H NMR</u> (**49b-d_1**, 400 MHz, CDCl$_3$): δ 9.64 (s, 1H), 7.44 – 7.14 (m, 10H), 4.92 (dd, $J = 3.2$, 1.4 Hz, 1H), 4.55 (s, 1H), 3.75 (dd, $J = 11.3$, 3.2 Hz, 1H), 3.41 – 3.30 (m, 1H), 1.74 (dqd, $J = 15.0$, 7.6, 3.9 Hz, 1H), 1.55 – 1.39 (m, 1H), 1.04 (t, $J = 7.5$ Hz, 3H).

<u>^{13}C NMR</u> (**49b-d_1**, 101 MHz, CDCl$_3$): δ 192.0, 154.2, 138.4, 138.0, 134.7, 134.4, 130.3, 129.2, 129.1 (2C), 128.14 (2C), 128.08, 128.06, 127.5, 90.1, 43.2, 38.0, 37.3, 24.7, 10.5.

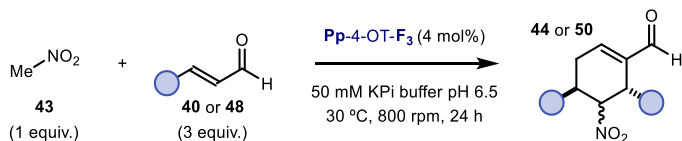<u>HRMS (ESI)</u> Exact mass calculated for **49b-d_1**, C$_{21}$H$_{20}$ClNNaO$_3$ [M+Na]$^+$: 392.1024, found: 392.1032.

<u>^{1}H NMR</u> (**49b-d_2**, 400 MHz, CDCl$_3$): δ 9.58 (s, 1H), 7.41 – 7.07 (m, 10H), 5.26 (dd, $J = 12.3$, 5.8 Hz, 1H), 4.72 (d, $J = 5.7$ Hz, 1H), 4.16 (dd, $J = 12.3$, 10.3 Hz, 1H), 2.71 – 2.61 (m, 1H), 1.78 (dqd, $J = 14.9$, 7.3, 4.1 Hz, 1H), 1.68 – 1.46 (m, 1H), 1.15 (t, $J = 7.4$ Hz, 3H).

<u>^{13}C NMR</u> (**49b-d_2**, 126 MHz, CDCl$_3$): δ 190.9, 151.4, 139.4, 137.4, 136.3, 134.2, 130.0, 128.7 (2C), 128.54 (2C), 128.51 (2C), 127.6, 126.1, 90.0, 46.8, 42.9, 37.8, 30.9, 24.1, 11.2.

3.8.6 Analytical Scale Biocatalytic Reactions

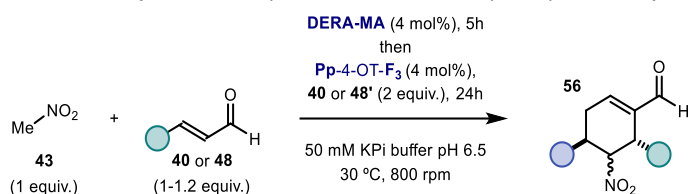*GP8 – General Procedure for the Analytical Scale Biocatalytic Synthesis of Compounds 44 and 50*

A stock solution of nitromethane **43** (2.50 µmol, final concentration of 5 mM) and a stock solution of the corresponding enal **40** or **48** (7.50 µmol, final concentration of 15 mM) in the selected organic solvent were added to an Eppendorf tube containing the purified enzyme Pp-4-OT-F$_3$ (200 µmol, 0.04 equiv.) in KPi buffer pH 6.5 to reach the final volume of 500 µL. The reaction mixture was shaken at 800 rpm in a thermoshaker (see Figure 3.10b) at 30 ºC for

---

[84] Enders, D., Hüttl, M. R. M., Raabe, G., Bats, J. W. "Asymmetric Synthesis of Polyfunctionalized Mono-, Bi-, and Tricyclic Carbon Frameworks via Organocatalytic Domino Reactions" *Adv. Synth. Catal.* **2008**, *350*, 267-279.
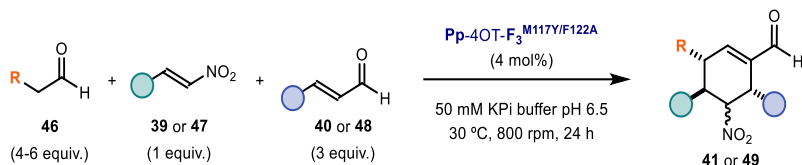
24 hours. The crude mixture was quenched with 50 µL of 1M HCl and extracted with 600 µL ethyl acetate containing 5 mM of the internal standard 1,3,5-trimethoxybenzene. The organic extract was dried over anhydrous MgSO$_4$, filtered and analyzed by HPLC chromatography on Daicel Chiralpak IB-3 and IC-3 columns. Calibration curves, not reported in the present dissertation, were obtained using the previously synthesized reference compounds **44** and **50** and 1,3,5-trimethoxybenzene as the internal standard. The HPLC data for the analytical scale reactions were fit in the equation to determine the analytical yield and diastereomeric ratio of the enantiopure products reported in Figure 3.3. The enantiomeric excess of products **44** and **50** was determined by HPLC analysis by comparison with the (*R*) and (*S*) mixture of the corresponding authentic samples prepared as described earlier.

GP9 – General Procedure for the Analytical Scale Biocatalytic Synthesis of Compounds 56

A stock solution of nitromethane **43** (2.50 µmol, final concentration of 5 mM) and a stock solution of the corresponding enal **40** or **48** (2.50 µmol, final concentration of 5 mM) in the selected organic solvent were added to an Eppendorf tube containing the purified enzyme DERA-MA (200 µmol, 0.04 equiv.) in KPi buffer pH 6.5. The reaction mixture was shaken at 800 rpm in a thermoshaker (see Figure 3.10b) at 30ºC for 5 hours. Purified enzyme Pp-4-OT-F$_3$ (200 µmol, 0.04 equiv.) and the second enal **40** or **48'** (5.00 µmol, final concentration of 10 mM) were added to the reaction mixture which was left stirring for additional 20 hours. The crude mixture was quenched with 50 µL of 1M HCl and extracted with 600 µL ethyl acetate containing 5 mM of the internal standard 1,3,5-trimethoxybenzene. The organic extract was dried over anhydrous MgSO$_4$, filtered and analyzed by HPLC chromatography on Daicel Chiralpak IB-3 and IC-3 columns and UPC^2 chromatography on Daicel Chiralpak IC-3 column. Calibration curves, not reported in the present dissertation, were obtained using the previously synthesized reference compounds **56** and 1,3,5-trimethoxybenzene as the internal standard. The HPLC data for the analytical scale reactions were fit in the equation to determine the analytical yield of the enantiopure products **56** shown in Figure 3.5. The diastereomeric ratio was determined by HPLC or UPC^2. The enantiomeric excess of products **56** was determined by HPLC analysis by comparison with the (*R*) and (*S*) mixture of the corresponding authentic samples prepared as described earlier.

GP10 – General Procedure for the Analytical Scale Biocatalytic Synthesis of Compounds 43 and 50


A stock solution of trans-β-nitrostyrene **39** or **47** (1.25 µmol, final concentration of 2.5 mM) and a stock solution of the corresponding enal **40** or **48** (3.75 µmol, final concentration of 7.5 mM) in DMSO were added to an Eppendorf tube containing the purified protein Pp-4OT-F$_3$$^{M117Y/F122A}$ (100 µmol, 0.04 equiv.) in KPi buffer pH 6.5 to reach the final volume of 500 µL. A stock solution of the corresponding aldehyde **46** (5.00-7.50 µmol, final concentration of 10-15 mM) in DMSO was added to this mixture and the reaction tube was shaken at 800 rpm in a thermoshaker (see Figure 3.10b) at 30 ºC for 24 hours. The crude mixture was quenched with 50 µL of 1M HCl and extracted once with 600 µL ethyl acetate containing 5 mM of the internal standard 1,3,5-trimethoxybenzene. The organic extract was dried over anhydrous MgSO$_4$, filtered and analyzed by HPLC chromatography on Daicel Chiralpak IB-3 column. Calibration curves, not reported in the present dissertation, were obtained using the previously synthesized reference compounds **41** and **49** and 1,3,5-trimethoxybenzene as the internal standard. The HPLC data for the analytical scale reactions were fit in the equation to determine the analytical yield and diastereomeric ratio of the enantiopure products reported in Scheme 3.28b and Figure 3.7. The enantiomeric excess of products **41** and **49** was determined by HPLC analysis by comparison with the (*R*) and (*S*) mixture of the corresponding authentic samples prepared as described earlier.

3.8.7 NMR Conformational Studies

The relative and absolute configurations of compound **50e-d_1** were unambiguously determined by X-ray crystallographic analysis (detailed below). The relative configuration was further confirmed by nuclear Overhauser enhancement (NOESY) spectroscopy. The relative configuration of compound **50e-d_2** was assigned as the one of the epimer of compound **50e-d_1** at the carbon bearing the nitro group by NOESY.
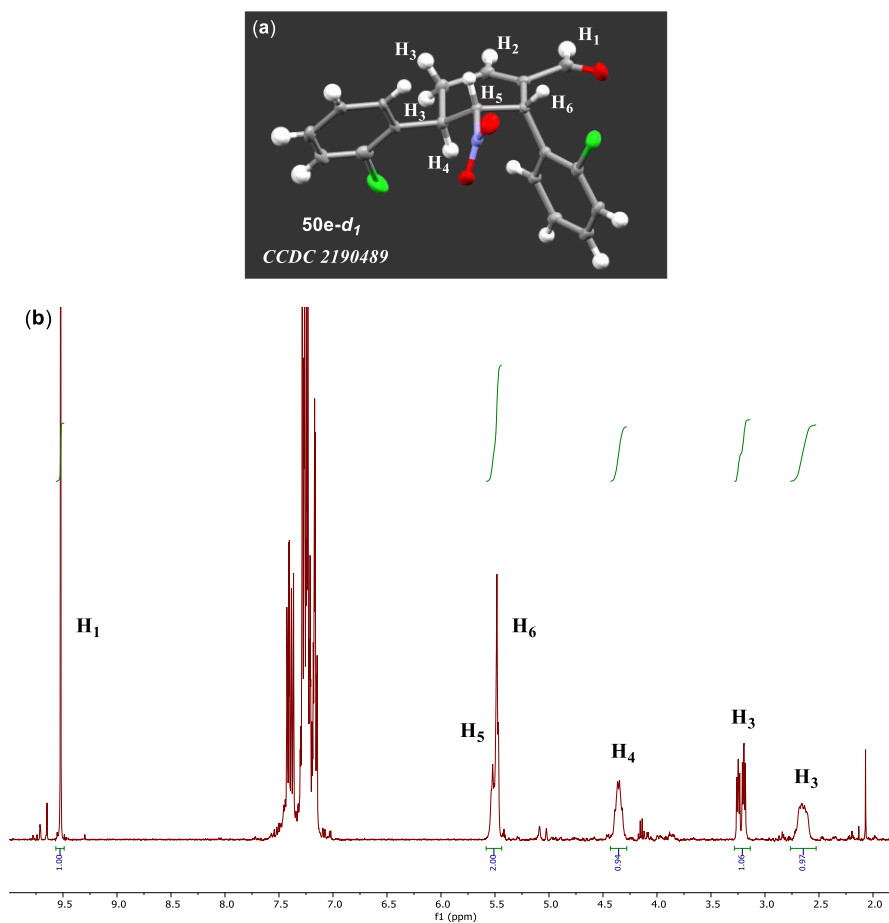
Figure 3.11. (a) Crystal structure of the major diastereomer of **50e**; (b) ^{1}H NMR of the major diastereomer of **50e** in CDCl$_3$.
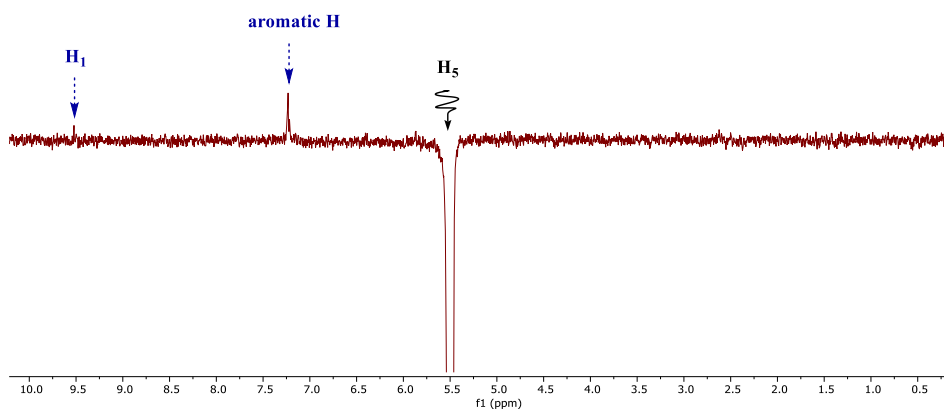
Figure 3.12. NOESY experiment of **50e-*d₁*** in CDCl₃.

NOESY experiment of 50e-*d₁* in CDCl₃: Weak Nuclear Overhauser Effects (NOE) are detected when H$_5$ is selectively irradiated at 5.50 ppm only for aromatic protons of the vicinal phenyl ring and the aldehydic proton H$_1$ (this correlation is very weak). The correlation is not observed with H$_4$ due to their *trans* axial relative spatial arrangement. The correlation with H$_6$ is not observed due to signal overlap.
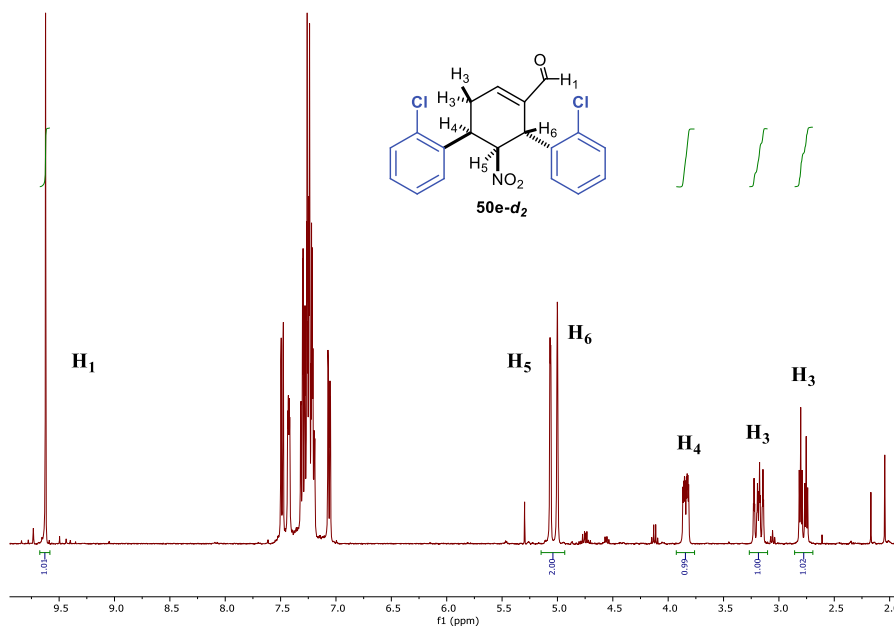

Figure 3.13. ¹H NMR and structure of the minor diastereomer of **50e** in CDCl₃.
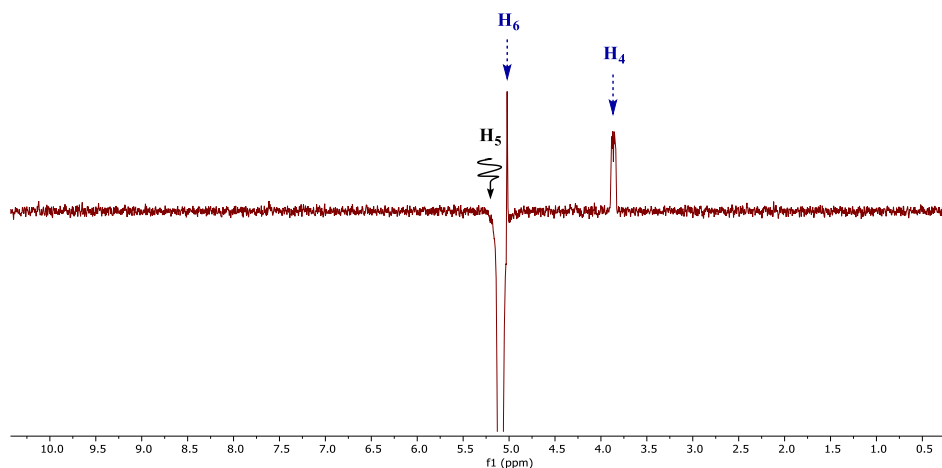
Figure 3.14. NOESY experiment of **50e-d_2** in CDCl₃.

NOESY experiment of 50e-d_2 in CDCl₃: Strong Nuclear Overhauser Effects (NOE) are detected when H_5 is selectively irradiated at 5.09 ppm for the vicinal H_6, which is in 1-2 spatial arrangement relative to H_5, and for the vicinal H_4, which is also in 1-2 spatial arrangement relative to H_5. The correlation with the vicinal proton H_4 is absent in the NOE spectra of previously analyzed diastereomer **50e-d_1** due to a *trans* axial relative spatial arrangement between H_4 and H_5. This suggests a *cis* spatial arrangement between H_4 and H_5 in compound **50e-d_2**. The relative configuration of compound **50e-d_2** has been assigned as the one corresponding to the epimer of **50e-d_1** at the carbon bearing the nitro group. This is in accordance with the relative configuration observed for the minor diastereomer (**44-d_2**) detected in the biocatalytic synthesis of model compound **44**, confirmed by data reported in the literature,[44] and with an (*R*)-configured intermediate of type **55** leading to both products **50e-d_1** and **50e-d_2**.

3.8.8 Computational Studies

The generation of homology models was carried out using the YASARA structure[85] homology model building protocol,[86] which involves multi-template structural model generation. Since the linear amino acid sequence of the target protein was the only given input, the possible templates were identified by running 3 PSI-BLAST[65] iterations to extract a position specific

[85] Krieger, E., Koraimann, G., Vriend, G. "Increasing the precision of comparative models with YASARA NOVA-a self-parameterizing force field" *Proteins* **2002**, *47*, 393-402.
[86] Venselaar, H., Joosten, R., Vroling, B., Baakman, C., Hekkelman, M., Krieger, E., Vriend, G. "Homology modelling and spectroscopy, a never-ending love story" *Eur. Biophys. J.* **2010**, *39*, 551-563.

scoring matrix (PSSM) from UniRef90,[87] and then searching the PDB for a match with an E-value below the homology modeling cutoff 0.005. A maximum of 5 templates were allowed. To aid alignment correction and loop modeling, a secondary structure prediction for the target sequence had to be obtained. This was achieved by running PSI-BLAST to create a target sequence profile and feeding it to the PSI-Pred[88] secondary structure prediction algorithm. For each of the found templates, models were built. Either a single model per template was generated, when the alignment was certain, or a number of alternative models were generated, when the alignment was ambiguous. A maximum of 100 conformations per loop were explored. A maximum of 10 residues were added to the termini. Finally, YASARA tried to combine the best parts of the generated models to obtain a hybrid model, with the intension of increasing the accuracy beyond each of the contributors. The quality of the models was evaluated by use of Z-score.[89] A Z-score describes how many standard deviations the model quality is away from the average high-resolution X-ray structure. The overall Z-scores for all models have been calculated as the weighted averages of the individual Z-scores. The overall score thus captures the correctness of backbone- (Ramachandran plot) and side-chain dihedrals, as well as packing interactions. All in silico modifications were performed using YASARA structure as software with AMBER 03 as force field.[90] After the introduction of a mutation or modification, the energy of the system was minimized following a three-step protocol that enables the adjustment of the model structure without creating any possible unwanted deformation. In step one, only the atoms constituting the mutated amino acid residue were subjected to energy minimization. In step two, the process for energy minimization was repeated by including all the atoms of the amino acid residues that are located within 6 Å distance from the mutated residue. In step three, the energy of the overall structure was minimized.

The molecular dockings were performed using Autodock Vina as tool incorporated into YASARA. The enzyme was used in its reactive binding pose with the cinnamaldehyde bound (Figure 3.15) generating the iminium ion intermediate. The simulation box was placed around the active site of the enzyme 10 Å. 25 VINA docking runs of each ligand to the receptor were run. After clustering the 25 runs, two distinct complex conformations were found for each

[87] Suzek, B. E., Huang, H., McGarvey, P., Mazumder, R., Wu, C. H. "UniRef: comprehensive and non-redundant UniProt reference clusters" *Bioinformatics* **2007**, *23*, 1282-1288.

[88] Jones, D. T. "Protein secondary structure prediction based on position-specific scoring matrices" *J. Mol. Biol.* **1999**, *292*, 195-202.

[89] (a) Laskowski, R. A., MacArthur, M. W., Moss, D. S., Thornton, J. M. "PROCHECK: a program to check the stereochemical quality of protein structures" *J. Appl. Crystallogr.* **1993**, *26*, 283-291; (b) Hooft, R. W., Vriend, G., Sander, C., Abola, E. E. "Errors in protein structures" *Nature* **1996**, *381*, 272.

[90] Oostenbrink, C., Villa, A., Mark, A. E., van Gunsteren, W. F. "A biomolecular force field based on the free enthalpy of hydration and solvation: the GROMOS force-field parameter sets 53A5 and 53A6" *J. Comput. Chem.* **2004**, *25*, 1656-1676.

docking. Results were sorted by binding energy (more positive energies indicate stronger binding). The resulted models were inspected visually.
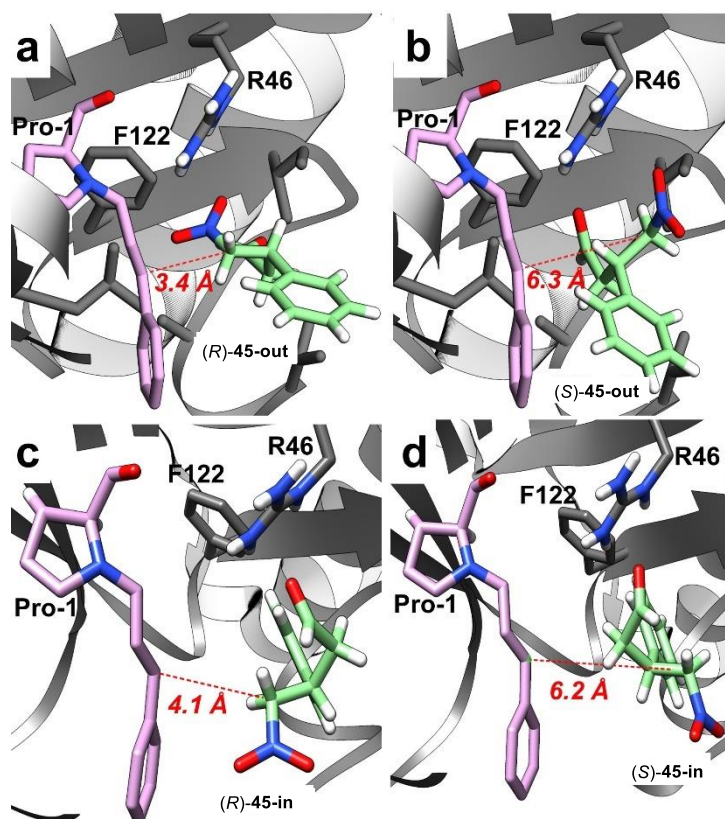

Figure 3.15. Dockings in the active site of Pp-4OT-F$_3$ of: (a) (R)-**45** in the (R)-**45-out** binding pose (calculated binding energy of 4.00 kcal mol^{-1}); (b) (S)-**45** in the (S)-**45-out** binding pose (calculated binding energy of 4.31 kcal mol^{-1}); (c) (R)-**45** in the (R)-**45-in** binding pose (calculated binding energy of 4.56 kcal mol^{-1}); (d) (S)-**45** in the (S)-**45-in** binding pose (calculated binding energy of 4.50 kcal mol^{-1}). The iminium ion of the Pro-1 with cinnamaldehyde **40** is shown in purple and ligands in green. The dashed red line shows the distance between the two reactive carbons for C-C bond formation. R46 is shown because it stabilizes the ligands in the active site of the enzymes. All dockings were performed with YASARA structure. UCSF Chimera 1.11 was used for visualization.

3.8.9 X-ray Crystallographic Data

Single Crystal X-ray Diffraction Data for Product 50e-d₁

X-ray structure determination: stable colorless crystals of compound **50e-*d₁*** were obtained by slow evaporation of a dichloromethane/hexane mixture at room temperature.

Data Collection: Measurements were made on a Rigaku MicroMax-007HF single crystal X-ray diffractometer equipped with a Pilatus 200K area detector, a Rigaku MicroMax-007HF microfocus rotating anode with Mo$_{K\alpha}$ radiation, Confocal Max Flux optics and an Oxford Cryosystems low temperature device Cryostream 700 plus (T = -173 °C). Full-sphere data collection was used with ω and φ scans.

50e-*d₁*   ≡   **50e-*d₁*: CCDC 2190489**
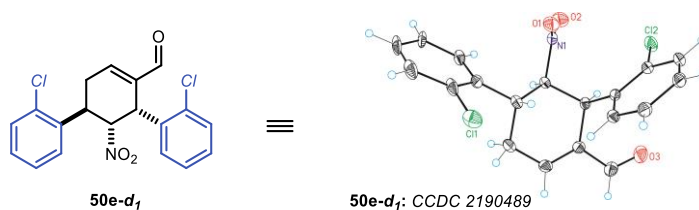
Table 3.7. Crystal data and structure refinement for **50e-*d₁*.** *CCDC2190489.*

_____

Empirical formula	C19 H15 Cl2 N O3
Formula weight	376.22
Temperature	100(2)K
Wavelength	0.71073 Å
Crystal system	orthorhombic
Space group	P 21 21 21
Unit cell dimensions	$\alpha = 8.67030(10)$Å $\alpha = 90°.$
	$\beta = 11.79300(10)$Å $\beta = 90°.$
	$\gamma = 16.8130(2)$Å $\gamma = 90°.$
Volume	1719.11(3) Å^3
Z	4
Density (calculated)	1.454 Mg/m^3
Absorption coefficient	0.396 mm^{-1}
F(000)	776
Crystal size	0.200 x 0.150 x 0.100 mm^3
Theta range for data collection	2.423 to 30.938°.
Index ranges	-12<=h<=12,-16<=k<=17,-24<=l<=23
Reflections collected	29724
Independent reflections	5183[R(int) = 0.0199]
Completeness to theta =30.938°	96.6%

Absorption correction	Multi-scan
Max. and min. transmission	1.00 and 0.84
Refinement method	Full-matrix least-squares on F^2
Data / restraints / parameters	5183/ 215/ 277
Goodness-of-fit on F^2	1.003
Final R indices [I>2sigma(I)]	R1 = 0.0226, wR2 = 0.0644
R indices (all data)	R1 = 0.0233, wR2 = 0.0648
Flack parameter	x =0.018(8)
Largest diff. peak and hole	0.267 and -0.161 e.$\mathring{A}^{-3}$

Chapter IV

General Conclusions

During my doctoral studies, I have explored novel asymmetric transformations using traditional catalysts repurposed to acquire mechanistically new catalytic functions. In chapter II, visible light excitation proved valuable to divert the established polar reactivity of a traditional chiral (η^3-allyl)iridium(III) complex. This iridium complex is an electrophile in the ground state, useful for allylic substitution reactions, but turns into a strong photooxidant in the excited state. This novel catalytic function was used to trigger the single electron oxidation of radical precursors and promote an enantioselective alkyl-alkyl cross-coupling reaction with allylic alcohols. This process, which did not proceed at all in the dark, enabled the synthesis of highly enantioenriched chiral homoallylic amino-based scaffolds, including biologically relevant fragments. Mechanistic studies confirmed the essential role of the iridium organometallic complex as competent photooxidant and active catalytic center.

In chapter III, I focused on the structural modifications of tautomerase (4-OT) enzymes, which were previously reported to activate aldehydes and enals via enamine or the iminium ion formation, respectively. This work enabled the identification of two enzymatic variants that served to drive mechanistically novel biocascade transformations. These new variants acted as multifunctional enzymes capable of performing the two activation modes (enamine and iminium ion activations) in a sequential fashion under the same reaction conditions and in a single synthetic step. The biocascade granted access to complex cyclohexene carbaldehydes products in high yields, diastereomeric ratio and enantiomeric excess. The single-enzyme biocascade processes were inspired by classic organocatalytic cascade reactions reported by Enders, which were the most sophisticated domino processes reported in organocatalysis. Our methods revealed that biocatalysis could match and, in some cases, even surpass the traditional organocatalytic approaches in terms of efficiency and stereoselectivity.

UNIVERSITAT
ROVIRA i VIRGILI